Syracuse University

SURFACE

Dissertations - ALL

8-2014

Development and Application of Explicitly Correlated Wave Function Based Methods for the Investigation of Optical Properties of Semiconductor Nanomaterials

Jennifer Mary Elward
Syracuse University

Follow this and additional works at: https://surface.syr.edu/etd

Part of the Chemistry Commons

Recommended Citation

Abstract

Semiconductor nanoparticles, or quantum dots (QDs), are well known to have very unique optical and electronic properties. These properties can be controlled and tailored as a function of several influential factors, including but not limited to the particle size and shape, effect of composition and heterojunction as well as the effect of ligand on the particle surface. This customizable nature leads to extensive experimental and theoretical research on the capabilities of these quantum dots for many application purposes. However, in order to be able to understand and thus further the development of these materials, one must first understand the fundamental interaction within these nanoparticles. In this thesis, I have developed a theoretical method which is called electron-hole explicitly correlated Hartee-Fock (eh-XCHF). It is a variational method for solving the electron-hole Schrodinger equation and has been used in this work to study electron-hole interaction in semiconductor quantum dots. The method was benchmarked with respect to a parabolic quantum dot system, and ground state energy and electron-hole recombination probability were computed. Both of these properties were found to be in good agreement with expected results. Upon successful benchmarking, I have applied the eh-XCHF method to study optical properties of several quantum dot systems including the effect of dot size on exciton binding energy and recombination probability in a CdSe quantum dot, the effect of shape on a CdSe quantum dot, the effect of heterojunction on a CdSe/ZnS quantum dot and the effect of quantum dot-biomolecule interaction within a CdSe-firefly Luciferase protein conjugate system. As metrics for assessing the effect of these influencers on the electron-hole interaction, the exciton binding energy, electron-hole recombination probability and the average electron-hole separation distance have been computed. These excitonic properties have been found to be strongly infuenced by the changing composition of the particle. It has also been found through this work that the explicitly correlated method performs very well when computing these properties as it provides a feasible computational route to compare to both experimental and other theoretical results.

Development and Application of Explicitly Correlated Wave Function Based Methods for the Investigation of Optical Properties of Semiconductor Nanomaterials

by

Jennifer Mary Elward

B.S., Chemistry Misericordia University (2009)

Submitted to the Department of Chemistry
in partial fulfillment of the requirements for the degree of

Doctor of Philosophy in Chemistry

at the

Syracuse University

August 2014

Acknowledgement

First and foremost, I would like to express my sincerest gratitude and appreciation to my advisor, Dr. Ari Chakraborty for his unwaivering support and unlimited guidance and motivation over the extent of my research career at Syracuse University. I am forever grateful to have had an advisor that has believed in me from the beginning, that has been patient and willing to teach when I didn't understand, that has instilled the drive and inspiration to become the best scientist that I can be and who has taught me to not be afraid to question both what I understand and what I dont understand. Since the beginning of my time at Syracuse, Ari has given me the skills set that I need to not only guide my PhD study, but to move on to the next phase of my career. For that I am grateful.

I would like to thank the members of my PhD committee including, Professor Joseph Chaiken, Professor Jerry Goodisman, Professor Bruce Hudson, Professor Tara Kahan, and Professor Jennifer Schwarz for their presence and support during the process of this dissertation and defense. Special thanks to Professor Chaiken and Professor Goodisman for their support, guidance and helpful insight throughout my time at Syracuse. I would also like to thank Professor Mat Maye for insightful discussions and support throughout the years.

I also thank my group members in the Chakraborty group; Mike Bayne, Ben Ellis, Jeremy Scher and Chris Blanton. I thank them for their camraderie, their insightful discussions, their thought provoking questions, programming tips and finally for making the lab experience nothing short of memorable. I also thank them for loving black coffee as much as I do, Santos forever.

I would like to thank all of the REU's, undergraduates and high school students that I have had the pleasure of working with and mentoring over the years, including, Barbara Thallinger, Jacob Hoffman, Johannes Hoja, Ben Kaplan, Saurav Goyal, Amiya Quidley and Nick Drogo. They have taught me the value of instilling knowl-

edge in others as well as the trials and tribulations that are associated therein.

I thank my friend and former roommate Rabeka Alam, for being the experimentalist to my theoretician and for being the best friend one can have. I would also like to thank Rabeka for being there during times of success and equal times of failure and for living room discussions on the theory of quantum dots.

Last, but certainly not least, I would like to greatly acknowedge my family including my parents, my brother Mike and my boyfriend Eric. My brother for his constant reminder to never give up. To Eric for his never ending positivity and for always believing in me. To my parents, for their support throughout my entire graduate school career has been unending. They have given me the means to become who I am today. For all of the struggles that I have been through as well as the successes, they have been by my side through all of it. I am very fortunate to have such supportive role models in my life and I cannot put into words how appreciative I am for that. *Also - Dad, thanks for teaching me algebra in 8th grade, it really helped out in the long run and mom, aren't you glad you now know what a Hamiltonian is? :].

Contents

List of Figures

List of Tables

Chapter 1

Introduction and background on quantum dot systems

Over the past several decades there has been increasing experimental and theoretical research with respect to particles confined to the nanoscale dimension [11]. Specifically, when a semiconductor material is confined to dimensions that are that small, they display unique optical and electronic properties that are very highly tunable [12]. These nanoscale size particles are referred to as quantum dots (QDs) [13, 14, 15, 16]. A quantum dot is generally in the size range of 1-20 nanometers (nm) and can be of differing shapes, though generally spherical [11, 12, 17, 18, 19, 20]. The nanoparticle can also be rod-like [21, 22, 23, 24], pyramidal [25, 26, 27, 28] and so on. Changing the shape [29, 30, 31, 11], size [32, 33, 34], and other influential factors can modify the optical properties of the nanocrystal. Due to this customization capability, these quantum dots find extensive experimental application and theoretical research interest.

In order to understand the application of quantum dots, one must first understand the generation and dissociation of the electron-hole pair or exciton. When light strikes a semiconductor material, an electron is excited from the valence band to
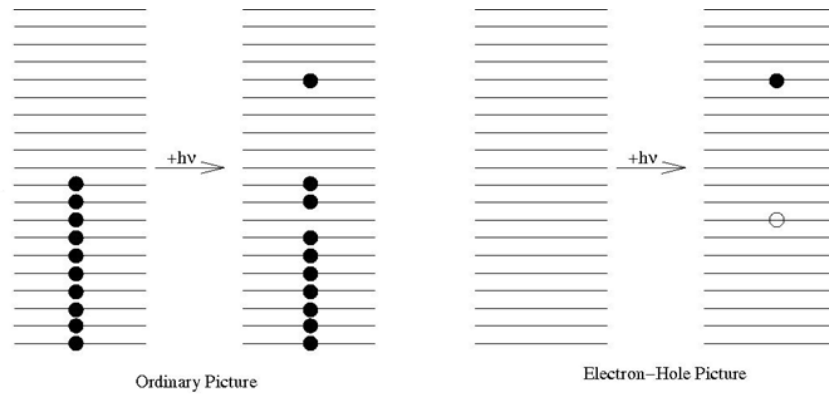
Figure 1-1: Electron-hole pair picture.

the conduction band. This electronic excitation in QDs can be represented via the quasiparticle representation which describes the formation of the exciton. This representation provides a viable route for the theoretical treatment of excitonic systems.

The goal of the work presented within this thesis is to develop a computationally efficient theoretical method which can accurately compute the optical properties of semiconductor quantum dot systems. The details of the work performed are described in the following chapters. The introduction is organized as follows, in section 1.1 the factors that influence the optical properties and electron-hole interaction within quantum dots are presented, in section 1.2 the experimental outlets for the application of quantum dots are discussed followed by the theoretical treatment of electron-hole correlation in quantum dots in section 1.3. The theoretical details of the method developed in this work is given in section 2.1. Finally, the excitonic properties of interest are discussed in section 1.4 .

2
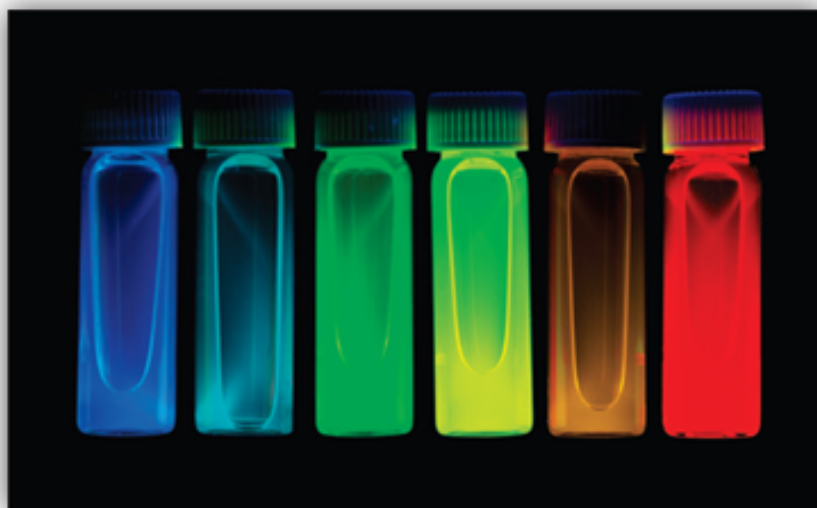
Figure 1-2: CdSe quantum dots of increasing size.

1.1 Influential factors on quantum dot properties

1.1.1 Particle size

Changing particle size is one of the direct routes for modifying the exciton dissociation in quantum dots. As shown in Figure 1-2 [35], all vials within the figure are of CdSe quantum dot material of differing size. Based on the size of the quantum dot, they fluoresce at different wavelengths [11]. Therefore, it is evident that the particle size can directly affect the optical properties . Studies on CdSe quantum dots have shown that the exciton binding energy changes as a function of dot size [3, 2, 4, 36, 37, 1, 5, 6, 7]. The exciton binding energy is defined as the energy it takes to separate an electron-hole pair and is discussed in section 1.4. In addition to modifying the exciton binding energy, the dot size also has strong influence on Auger recombination[38, 39] , multiple exciton generation [40, 41, 42, 43] , and blinking effects [44, 45, 46] within QDs. For example, Ghosh et al. have generated "giant" CdSe/ZnS core/shell quantum dots in order to study the effect of dot size and shell

growth on the ability to suppress blinking within QDs [46]. Lin et al. have also studied the effect of dot size on multi-exciton generation (MEG) rates within CdSe quantum dots [42]. In recent work, Alam et al. have studied effects of both particle shape and size on bioluminescence resonance energy transfer (BRET) between firefly luciferase protein and QDs and both the size and shape were found to be strong influencers of energy transfer capability. Size effects are discussed in detail in chapter 5 .

1.1.2 Particle shape

In addition to particle size, the nanocrystal shape also plays a large role in the tunability of the optical properties. Quantum dots are generally thought of as sphere-like particles, however, their shape can be modified and extended to resemble an ellipsoid , a rod-like structure or even greatly extended to nanowire dimensions. Changing the shape of the nanoparticle directly influences the spatial confinement of the electron and hole within the quantum dot [47, 48, 49, 50, 51, 52, 25, 53]. In experimental study, Li and coworkers have found that modifying the aspect ratio of a rod-like nanoparticle can greatly modify the optical properties of the system [52]. Wang et al. have found that in InP quantum rods the confinement can be modified at small aspect ratios, where the nanoparticle goes from 3D to 2D confinement around an aspect ratio of three [48]. It has also been found that the particle shape can be used to both control and optimize energy transfer between QDs and related charge acceptors. In work performed by Alam et al. they have shown that quantum rods have optimum energy acceptor characteristics with respect to bioluminescence resonance energy transfer (BRET) from core/shell nanoparticles to firefly Luciferase protein [54]. Additionally, quantum rods have also been found to be efficient at the dissociation of multiexcitons compared to spherical quantum dots by Zhu et al. [50]. When the particle size is confined in extreme, such as a nanowire , it has been found that this extreme confinement benefits applications like solid state lighting. In that respect, Quian et al.

have used core/shell nanowires to generate efficient multi-color light emitting diodes [55]. Studying the shape of nanoparticles is often difficult due to the inherent volume constraint. One may be able to change the shape of the particle, but if volume is not conserved a direct comparison of the optical properties cannot be easily drawn. Therefore, isovolumetric transformation is necessary in order to be able to demonstrate the true effect of shape. An overview of the effect of shape on CdSe quantum dots via isovolumetric transformation is discussed in chapter 7.

1.1.3   Heterojunction effects

One of the most prominent methods to modify optical properties and induce exciton dissociation is to introduce a heterojunction into the system [56, 57, 45, 58, 59, 60]. With respect to quantum dots, a core of a certain diameter is often modified by the addition of a shell of a differing material. When the dot diameter is modified by growth of shell , the alignment and band structure of the particle changes and introduces new features into the electronic structure of the material. These can then be classified as one of three types, a type I, type II or quasi-type II heterojunction [61]. Based on the type of heterojunction exhibited, the particle's optical properties can be modified. Additionally, the optical and charge transfer properties can be modified extensively by changing the shell thickness of the nanoparticle. Zhu et al. have shown that based on the thickness of the shell the charge transfer capability of the particle can be greatly modified in a CdSe/ZnS system [62]. Abdellah and coworkers have also found that an optimal shell thickness exists for electron transfer to ZnO nanoparticles, this specific application has possible application within solar cell materials due to the ability to control the charge transfer via shell thickness [63]. Hole transfer from core/shell quantum dots has also been investigated by Xu and coworkers, and they have found that there is a strong dependence on shell thickness for hole transfer as well [64]. Hamada and coworkers have found that coupling TiO_2

material with core/shell CdSe/ZnS core/shell quantum dots has shown to greatly decrease the blinking characteristic within the core/shell dot due to the coupling with the electron acceptor of TiO_2 [65]. This is very good for applications in which consistent emission is desired. In 2009, Jin and coworkers also found that coupling core/shell quantum dots with TiO_2 has been found to greatly increase the electron transfer rate as compared to other materials [66].

Therefore as described above, the optical properties of quantum dots can be modified extensively by the introduction of a heterojunction. In chapter 6, the effect of heterojunction and increasing shell thickness within a CdSe/ZnS quantum dot is discussed in detail and through the study of optical properties like exciton binding energy , electron hole recombination probability and average electron-hole separation the effect of heterojunction on the QDs is presented.

1.1.4   Ligand effects in QDs

The effect of ligand on exciton dissociation within quantum dots is an area of considerable research interest. The type of ligand chosen, whether it is an organic based ligand or a biological molecule can strongly effect the charge separation and the optical properties [67, 30, 68, 69]. The optical properties are highly sensitive to the local chemical environment. Therefore, changing the surrounding ligand can strongly affect the optical characteristics. The effects of protein corona formation on quantum dot surfaces are presented in chapter 8 and the firefly Luciferase protein corona formation on the optical signature of a CdSe quantum dot is investigated.

However, ligands also have an effect on properties such as Auger recombination , where Sippel and coworkers have found that the type of ligand surrounding the quantum dot has an effect on the rate of Auger recombination. They have studied a CdSe quantum dot and found that the use of a hexanedithiol capping ligand causes the Auger recombination to be slowed [70]. Zhang et al. have found that you can

control the type of ligand used in order to target different types of cells which has application in biological labeling and tracking as discussed in the following section [71]. Frederick et al. have studied the effect of ligand on several quantum dots. They find that the type of ligand chosen can strongly affect the dissociation of charge carriers , their findings have application in solid state materials [72].

1.2 Applications of quantum dots

1.2.1 Quantum dots for solar energy applications

Quantum dots find application in many experimental outlets due to their versatility and highly tunable properties. One of the most prominent applications is the use of QDs in light harvesting applications like solar cells [73, 34, 74]. Quantum dots are ideal for this application due to their ability to facilitate exciton dissociation and charge transfer which can increase solar cell efficiency depending on the type of quantum dot used within the cell. For example, Chang et al. have used PbS quantum dots coupled with CdS thin film to generate a solar cell with efficiency of nearly 3.5% [75]. Willis et al. have also used a PbS QD based solar cell coupled with ZnO . They have found that doping the ZnO material causes the capability for charge extraction to increase [76]. Santra et al. have used an approach where a solar cell is layered with CdSeS quantum dots with varying band gaps. This layering of QDs allows for efficiency of around 3% [77]. In an effort to further increase efficiency, Santra et al. have doped quantum dots to boost efficiency to 5% [78]. There have also been alternative methods for using quantum dots for light harvesting applications, wherein Genovese et al. in 2012 have developed a solar paint consisting of CdS, CdSe and TiO_2 nanoparticles. Although the efficiency of this new material is not as high as other approaches, at only 1%, it does provide a new route for generating light harvesting materials that can be improved upon in the future [79]. In a study in

2013, Abdellah and coworkers have found that core/shell CdSe/ZnS quantum dots have the capability to facilitate the charge transfer necessary to make an efficient light harvesting device. They have also found that there is an optimal ZnS shell thickness for electron transfer to ZnO nanoparticles [63].

In 2012, Ehrler et al. studied a hybrid organic/inorganic solar cell using PbS nanocrystals. They find that multi-exciton generation helps to increase the charge transfer rate within the cell [80]. Salant et al. have found that changing the shape of the nanoparticle helps to increase the charge transfer rates. It was found that rods performed the best for charge transfer due to their elongated shape [81]. Pan et al. have utilized a core/shell QD coupled with TiO_2. The specific inverted type-I core/shell system coupled with the electron acceptor allowed for recorded efficiency of up to 5.32% [82]. Many times QDs are coupled with charge accepting materials in order to increase the performance of solar cells, however, in recent work by Tang and coworkers, they have developed a fully quantum dot based solar cell with no coupling material. The efficiency for this cell was said to be 5.4%, therefore, showing an alternative approach to better the performance of quantum dot based solar cells.

1.2.2 Quantum dots as key role in energy transfer applications

Quantum dots can also facilitate energy transfer processes very well. For example, Hupp and coworkers have found that coupling a CdSe quantum dot with a metal organic framework (MOF) increased the energy transfer capability. The study reports that the coupling of the QD with the MOF has shown an increase in electron transfer of nearly 50% [83]. Algar et al. have found that a quantum dot based scaffolding approach works best for sensing of biomolecules based on its fluorescence resonance energy transfer (FRET) capability [84].

In keeping with energy producing applications of quantum dots, Zhao et al. have used CdSe QDs for photocatalytic H_2 evolution at the QD/solution interface. What

they have found within this work sheds light on the ability to use the quantum confinement effects found within nanocrystals to control the reduction of protons and thus control the energetics of Hydrogen generation [85]. Huang et al. have also found that it is possible to facilitate the mechanism by which Hydrogen is generated via charge separation in core/shell quantum dots, where the effect of the heterojunction is very important [86]. The effect of heterojunction on quantum dots is discussed in detail in chapter 6. In 2012, Ye et al. have shown that it is possible to couple Pd based QDs with TiO_2 in order to achieve efficient Hydrogen generation [87].

1.2.3 Light emitting devices

In tandem with solar cells, quantum dots have also found application in light emitting devices or LEDs [88, 89]. The tunability of quantum dots can help to tune the performance of QDs for light emitting purposes. Specifically, Jun and coworkers have used QDs in combination with a silica based structure in order to construct highly efficient quantum dot based light emitting diodes. The silica ensures that the QD retains its properties throughout the process of conversion to LED [89].

1.2.4 Role of quantum dots within biological applications

One of the other prominent applications of quantum dots is in biological applications, as they are often used for detection and tracking purposes. For example, Zhang and coworkers in 2013 have utilized quantum dots for the labeling and tracking of various viruses [90]. Wang et al. have used QDs to target disease and certain biomolecules. Specifically, they have been able to develop a quantum dot barcode approach for targeting Hepatitis-B [91]. Draz and coworkers have also coupled QDs with gold nanoparticles in order to make use of the plasmon resonance between the particles, specifically this approach was again used to test for Hepatitis B. However, the method is not necessarily limited and can be used to test for other biomolecules as well [92].

The shape of quantum dots has played a role in biological applications, in a study by Smith et al. in 2012 they have compared the effect of nanoparticle shape on cancer detection in cells [93]. The effect of ligand is again very imporant in biological applications. Zhang et al. have found that they have the ability to control the type of ligand on an Ag_2S quantum dot in order to be able to target various types of cells [71]. In 2012, Liu and coworkers have shown that single particle QDs can track the influenza virus. This technology was also used to show the step by step process of virus infection using quantum dots [94].

1.2.5 Quantum dots for detection purposes

Closely related to biological applications, recently QDs have been used for the detection of pH . Ji et al. have studied the use of core/shell CdSe/ZnS quantum dots in pH depedent chemical systems. Within their study, the QDs can interact with different types of electron transfer based materials depending on the pH of the system. Therefore, by tuning the pH, the charge transfer properties of the system can be tuned. They have also found that the recombination dynamics of the electron and hole were effected by the change in the pH of the system [95]. Mattoussi and coworkers have also found that CdSe/ZnS quantum dots can be stabilized at extreme pH by the type of ligands used within the system. These have been found to be stable even at extreme pH [96]. The effect of pH dependence on a QD-dopamine system has also been investigated by Ji et al. in 2012 [95].

In addition to the biological detection that QDs are often used for, they can also be employed for other, more general signal detection purposes. For example, Diaz et al. have used a photoswitchable quantum dot based method in order to improve signal detection capability [97]. Padilha and coworkers have used semiconductor QDs for detection purposes in order to detect x-ray and gamma rays based on high energy excitation behavior [98]. In recent work by Zhou et al., they have used CdTe quan-

tum dots as a nanothermometer due to the lattice dilation of the QD material [99]. Quantum dots also show possible application in the field of flourescence microscopy, Schwartz and coworkers have used QDs for their stability at low excitation repetition rates and thus due to the stability it is possible that they can be used within fluorescence microscopy [100].

1.2.6 Unique applications of QDs

Quantum dots also find many unique applications that provide new research interest and increasing research capabilities for both experimental and theoretical outlets. For example, Yang et al. have used QDs for application within Lithium ion batteries , where a ZnO particle was coated with Carbon in the battery. This method has shown increased electrochemical capabilities [101]. Luther et al. have used a method in which they control the stoichiometry of a quantum dot (specifically, PbS and PbSe) which can be tuned specifically to display either n or p type behavior [102].

1.3 Theoretical treatment of electron-hole correlation in quantum dots

As the experimental understanding of quantum dots and their various applications advances, the need for accurate and computationally efficient theoretical methods increases as well. Theoretical treatment of quantum dots is crucial as it allows for prediction of the optical properties of nanoparticles. It is apparent in some cases that we are able to predict with theory what may be experimentally difficult to prepare. In order to understand and thus be able to study properties of QDs, one must first understand the role of electron-hole correlation .

1.3.1 Experimental and theoretical importance of electron-hole correlation

Electron-hole correlation plays a central role in understanding and interpretation of optical properties of a wide variety of materials [103, 104, 105, 106, 107]. The role of electron-hole correlation has been investigated both experimentally and theoretically for a large number of systems including predicting excitonic ground state in quantum dots [108], light emission from quantum wires[109, 110], optical response of metal clusters[111], excitonic effects in graphene [112], radiative lifetimes in carbon nanotubes [113], excitonic states in polymers [114] and luminescence of quantum dots [115]. Accurate treatment of electron-hole correlation in computational studies can predict shapes of absorption spectra and biexciton formation in quantum dots[108]. Electron-hole correlation also has a strong influence on electron-hole recombination probability in photoactive materials. Eh-recombination plays an important role in the field of photovoltaics[116, 117, 118, 119, 120, 121] , photocatalysis[122, 123, 124, 125] , light emitting devices [126] , and electroluminescence [115]. For light-harvesting applications, it is desirable to design materials with low probability of eh-recombination. In certain TiO2-based photoactive materials, the eh-recombination causes reduction in the quantum yield[123], however, the photocatalytic activity can be enhanced by chemical modification of the material inhibiting of eh-recombination [124]. In photocatalytic nanocrystals, shape of the nanocrystal was found to influence eh-recombination and synthetic modifications of the shape of the nanocrystal can be made to suppress eh-recombination and design highly efficient photocatalysts [125]. Suppressing eh-recombination has also received attention in the field of dye-sensitized solar cells research. Chemical modifications such as addition of alkyl chains [127] and designing new metal centered complexes [120] have been carried out to enhance light-harvesting capabilities by reducing eh-recombination. In a related application, Bose-Einstein condensation of excitons was also found to be strongly influenced by the

eh-recombination probability and exciton lifetime [128]. In semiconductor quantum dots, eh-recombination can be reduced by introducing a core/shell heterostructure . This is generally achieved by using a core material whose valence and conduction bands are either higher or lower than those of the shell material [16, 129, 130]. As a consequence, one of the charge carriers (electron or hole) is mostly confined to the core, while the other charge carrier is confined to the shell. The core/shell structure induces spatial separation between electrons and holes which reduces eh-recombination[131]. Dissociation of electron-hole pair generates charge carriers and increases the quantum yield of the photocurrent generation processes. Consequently, it is important to have accurate theoretical and computational techniques for accurate calculation of electron-hole binding energies and recombination probabilities .

1.3.2 Computational treatment of electron-hole correlation in quantum dots

Computational treatment of electron-hole interaction can be carried out using various techniques including, one and two particle Green's function method [132, 133, 134] effective mass approximation (EMA) , [135] configuration-interaction (CI) [136, 137, 138, 139, 140, 141], coupled cluster (CC)[142], quantum Monte Carlo (QMC) method ,[143, 144, 145, 146] and density functional theory (DFT) [147, 148, 149]. A detailed review of various computational techniques has been presented by Sundholm and coworkers [150] The many-body pseudopotential theory for excitons in quantum dots [3, 151, 39] has been developed by Franceschetti et al. that uses CI scheme to solve the electron-hole Schrodinger equation . This method has been successfully used for studying a wide range of problems including charge carrier multiplicity [152], lifetime and recombination energies of excitons[153, 154] and Auger scattering and recombination in quantum dots [155, 155]. Sundholm and coworkers have also used CI for calculation of lifetime and binding energies [156, 157]. Accurate description of the

two-particle cusp plays an important role both in electron-electron and electron-hole systems. In electronic systems, the importance of electron-electron cusp has been demonstrated in a large number of studies [158, 159, 160] and is typically included in the calculation by either by using a Jastrow correlation function [158, 159, 161] or by explicitly correlated R12 scheme [160]. The nature of electron-hole correlation is very different from electron-electron correlation typically encountered for the ground state calculations in many-electron systems because the particles involved are oppositely charged. As a consequence of the attractive Coulomb interaction , the quality of the electron-hole wave function at small inter-particle distances is very important. This has important consequence on the calculation of electron-hole (eh) recombination probability , P_{eh}. The lifetime of the generated electron-hole pair is inversely proportional to the P_{eh} and serves as an important metric to assess the photovoltaic properties of quantum dots [162]. Since P_{eh} is the "on-top" probability of electrons and holes, an accurate description of the electron-hole wave function at small electron-hole distances is extremely important. One of the ways to achieve this is by introducing an explicit eh-inter-particle distance term in the approximation to the many-body wave function . This is generally done by introducing a Jastrow factor in the electron-hole wave function and solving the electron-hole Schrodinger equation using QMC techniques. Shumway and Ceperley have performed QMC calculations for exciton-exciton scattering [163]. Zhu and Hybertsen have also applied QMC for treating electron-hole correlation using variational Monte Carlo [144].

1.3.3 Current challenges associated with theoretical treatment of quantum dots

As the knowledge and understanding of quantum dots and their theoretical treatment advances, one of the relevant issues that needs to be addressed is the treatment of larger quantum dot systems. All electron treatment of these types of QDs is

prohibitive in general, although methods like DFT are able to treat up to for example, $Cd_{33}Se_{33}$, but beyond small diameters, treatment of quantum dots becomes difficult. Therefore it is readily apparent that theoretical methods are needed that do not find restriction in treating large quantum dots up to and surpassing 20 nm in dot diameter.

An additional challenge associated with current theoretical treatment of quantum dots is the changing morphology. If the aspect ratio of a quantum dot is modified to a shape much like a nanowire or nanorod, it could mean particle sizes of up to hundreds of nanometers. Therefore, a method that is general and computationally efficient enough to treat these large nanoparticles is of utmost importance as these longer morphologies have seen great application in light emitting devices such as solid state lighting and for energy transfer purposes as discussed in section 1.2.

The theoretical treatment of large quantum dot systems is motivated by experimental systems where large nanoparticles are of importance. For example, in work by Klimov and coworkers, they have chosen a small CdSe core of about 2 nm in diameter and have grown a shell on the core QD so that the diameter increases to nearly 20 nm [38]. Alam and coworkers have grown CdSe/ZnS core/shell nanorods that are used for bioluminescence resonance energy transfer in a nanoparticle-protein conjugate system. These nanorods deviate from typical spherical quantum dot structure [54]. As an interesting metric, Figure 1-3 shows the number of atoms in a CdSe quantum dot system as a function of particle diameter. Smaller CdSe diameters contain a managable number of atoms, the smallest diameter of 1.25 nm has the chemical formula $Cd_{20}Se_{19}$, with only 39 atoms total. However, it is clear that as the diameter increases the number of particles within the QD goes up considerably. At 20 nm in diameter, the chemical formula becomes $Cd_{74608}Se_{74837}$, where the total number of atoms is greater than 140,000. Therefore, it is clear that theoretical methods that are general and extendable in nature are necessary for the accurate treatment of these nanoparticle systems. The explicitly correlated Hartree-Fock (XCHF) method

15
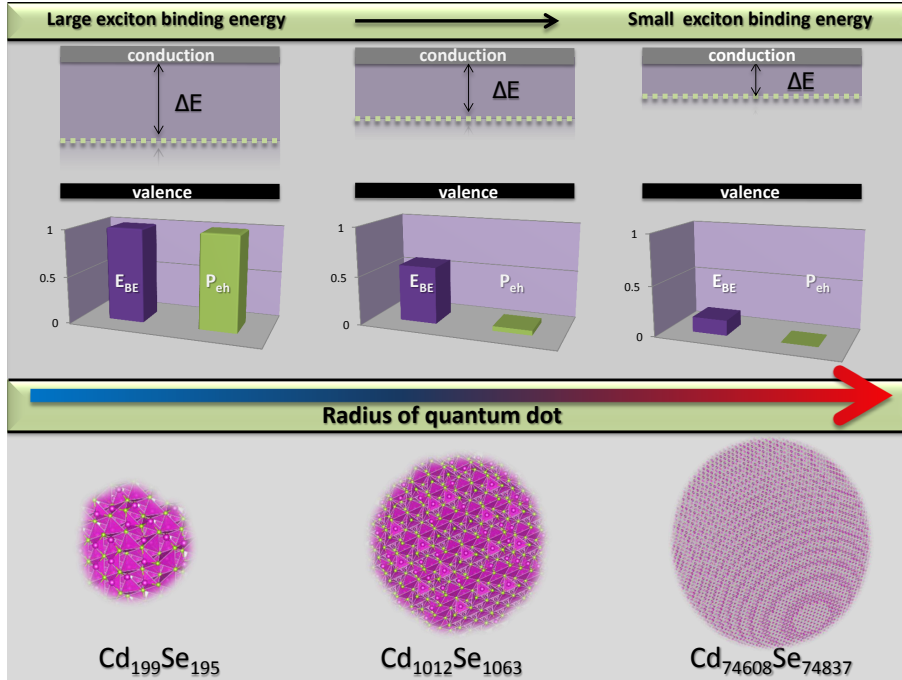
Figure 1-3: Number of CdSe atoms as a function of dot size. Full details about calculations shown are presented in chapter 5.

is presented as the given solution to address the growing need to treat these types of systems. The theoretical details of the XCHF method are presented in the following chapter, and the extension of the XCHF method to study quantum dot systems is given in chapter 5.

1.4 Properties of interest in quantum dot systems

In order to be able to study the optical properties of quantum dot systems, the following properties have been computed in varying capacities. The hallmark of the listed properties is that they rely heavily on electron-hole interaction and can give insight into the generation and dissociation of excitons . They are also highly sensitive to the modification of the characteristics of the quantum dot system, such as changing the size as discussed in chapter 5, heterojunction in chapter 6, shape in chapter 7 and ligand in chapter 8.

16

1.4.1 Exciton binding energy

Exciton binding energy (E_{BE}) in the simplest definition is defined as the energy it takes to dissociate an electron-hole pair. Being able to study the binding energy of a system is inherent in understanding the properties of the generation and dissociation of the electron-hole pair. The binding energy is of both experimental and theoretical importance. Experimentally, binding energy is defined in Figure 1-4. Computationally, the binding energy is defined as the non-interacting exciton
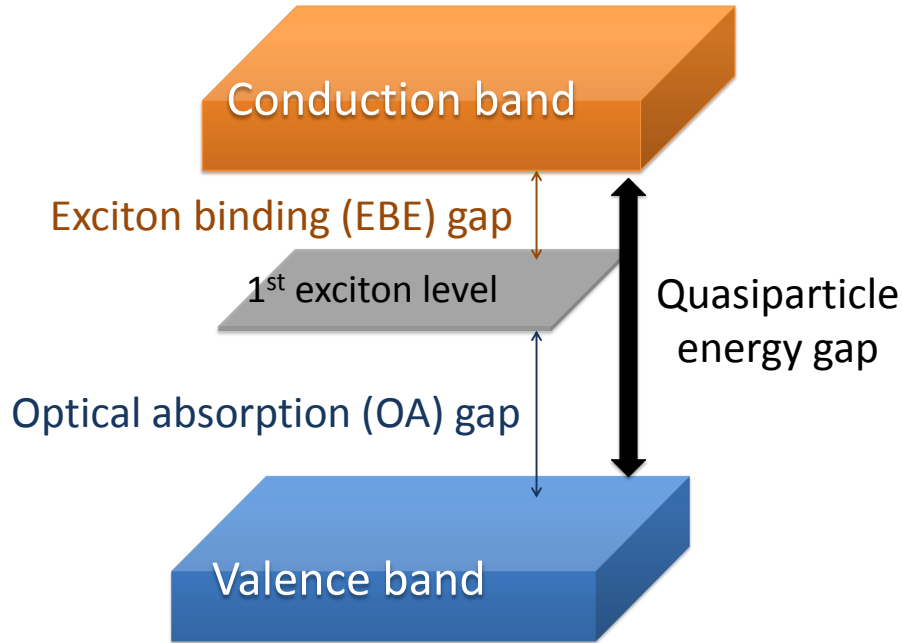
Figure 1-4: The relationship between optical energy gap, quasiparticle gap, and exciton binding energy .

energy less the interacting exciton energy as shown below.

$$E_{\text{BE}} = E_{\text{non-interacting}} - E_{\text{exciton}} \tag{1.1}$$

17
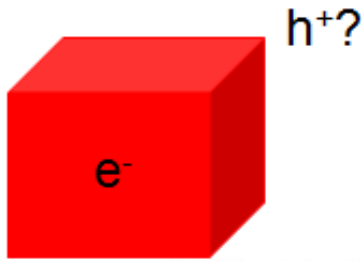
Figure 1-5: Recombination probability of an hole within a finite volume around an electron.

1.4.2 Electron-hole recombination probability

Recombination probability (P_{eh}) is defined as the probability of finding a hole within a finite cube of volume around an electron. If the hole is found within this cube of volume, the particles are likely to recombine due to the Coulomb attraction felt between them,

$$P_{eh} = \frac{1}{N_e N_h} \int d\mathbf{r}_e \int_{\mathbf{r}_e - \frac{\Delta}{2}}^{\mathbf{r}_e + \frac{\Delta}{2}} d\mathbf{r}_h \ \rho_{eh}(\mathbf{r}_e, \mathbf{r}_h). \tag{1.2}$$

Because the recombination probability is able to predict the recombining of the electron and hole within a quantum dot, it is of importance for applications where charge recombination should be suppressed or heightened. Therefore, recombination probability can be studied as a function of various influential factors within quantum dot systems to find optimal conditions for particle separation or recombination. One of the caveats of the recombination probability is that it is very heavily dependent on the form of the electron-hole wave function. If the form of the wave function is not accurate enough, it can very easily negatively effect the recombination probability.

This is displayed in both chapter 2 and chapter 5. A simple pictorial representation of recombination probability is given in Figure 1-5.

1.4.3   Average electron-hole separation

An additional metric for studying electron-hole interaction is average electron-hole separation as shown below,

$$\langle r_{\mathrm{eh}} \rangle = \langle \Psi_{\mathrm{eh-XCHF}} || \mathbf{r}_{\mathrm{e}} - \mathbf{r}_{\mathrm{h}} || \Psi_{\mathrm{eh-XCHF}} \rangle. \tag{1.3}$$

The average electron-hole separation will give insight into the spatial distance between the particles . This property is especially relevant to understand the effect of including a heterojunction in a quantum dot system. The potential felt by the particles changes considerably, so it is likely that the spatial separation between the electron and hole will change as a function of core and shell potential. It is also heavily effected by the particle size within quantum dot systems as increasing the size of the particle increases the effective volume that the particles have to reside in.

Chapter 2

Development and Benchmarking of Explicitly Correlated Hartree-Fock (XCHF) Method

2.1 Method developed: Electron-hole explicitly correlated Hartree-Fock

In the present work, I present an explicitly correlated Hartree-Fock (eh-XCHF) method for treating electron-hole correlation . The eh-XCHF method is a variational method where a geminal function [164, 165] is used to incorporate explicit eh-distance in the wave function. The explicitly correlated method using geminal functions has been successfully used to study electron-electron[166], electron-proton [167, 168, 169] and electron-positron [170] interactions in chemical systems. The eh-XCHF formulation presented here is different from earlier methods in its requirement to correctly account for electron-hole exchange interaction. This is especially important for studying optical properties of nanomaterials where eh-exchange interaction is enhanced [171, 172, 173, 104, 174, 175, 176, 177]. Electron-hole exchange interaction plays

an important role [173, 151, 178] in understanding optical properties of nanomaterials including, dark exciton states,[173, 178, 179, 172, 180] fine structure of excitons [181, 182], effect on spin relaxation [183, 184], and generation of trions in carbon nanotubes [185, 186]. In this work, the key equations of the eh-XCHF method are derived for a general many-electron many-hole system and benchmark calculations are performed on parabolic quantum dot . The parabolic quantum dot system [187, 188, 189] has been a test bed for investigation of electron-hole interaction in confined systems including investigation of electron-phonon coupling [190], third harmonic generation [191], effect of impurities on exciton binding energies [192], dipole-allowed optical transitions [193], biexciton formation [194], exciton trapping [187], and spin-orbit interactions in quantum dots [195]. The system consists of two charged particles in an external potential. The motion of the two charged particles is correlated and the interaction between them is described by the Coulomb potential . The 1-body external potential is described by three-dimensional harmonic oscillator term. This model system has been studied for investigation of both electron-electron and electron-hole correlation. For applications in electronic structure theory, the two charged particles have identical charges of 1 and the system is known as the Hooke's atom . It has been used for investigating electron-electron correlation using wave function , density-matrix and density functional based methods [196, 197, 198]. We use the parabolic quantum dot system to perform rigorous assessment of the eh-XCHF method for treating electron-hole correlation. In addition to eh-XCHF calculations, we have also performed Hartree-Fock (HF) and explicitly correlated full configuration interaction (R12-FCI) calculations on the model system. Comparison of ground state energy and recombination probability between all the three methods has been carried out to evaluate accuracy of the eh-XCHF method. The theoretical method is outlined in the section below and the results from benchmark calculations described above are given in Chapter 2 along with the computational details of the eh-XCHF method and

benchmark R12-FCI calculation.

2.1.1 Theoretical details of eh-XCHF method

The explicitly correlated ansatz for the wave function is defined as

$$\Psi_{\mathrm{xc}} = (1 + \hat{G})\Phi_0^{\mathrm{eh}} \tag{2.1}$$

where Φ_0^{eh} is the reference electron-hole wave function . Typically, the reference wave function can be chosen as the product of electron and hole Slater determinants $\Phi_0^{\mathrm{eh}} = \Phi_{\mathrm{SD}}^{\mathrm{e}}\Phi_{\mathrm{SD}}^{\mathrm{h}}$. Electron-hole exchange interaction can be included by replacing the product in the above expression by the Grassmann or wedge product[199, 200, 201, 202] between the electron and hole functions, $\Phi_0^{\mathrm{eh}} = \Phi_{\mathrm{SD}}^{\mathrm{e}} \wedge \Phi_{\mathrm{SD}}^{\mathrm{h}}$. Both forms have been successfully used in computational investigation of electron-hole pairs. The selection of one form over the other is system specific and should be made on a case-by-case basis. This topic has also been discussed in a review of computational techniques by Sundholm and coworkers [203]. The derivation of the eh-XCHF method presented below does not make any *a priori* assumption about the form of the reference wave function and is capable of handling both forms on the same footing. The geminal operator $\hat{G}$ is two-body operator that depends on the coordinates of both the electrons and the holes and is defined as:

$$G(\mathbf{r}^{\mathrm{e}}, \mathbf{r}^{\mathrm{h}}) = \sum_i^{N_{\mathrm{e}}} \sum_j^{N_{\mathrm{h}}} g(\mathbf{r}_i^{\mathrm{e}}, \mathbf{r}_j^{\mathrm{h}}) \tag{2.2}$$

where $g(\mathbf{r}_i^{\mathrm{e}}, \mathbf{r}_j^{\mathrm{h}})$ depends on the electron-hole inter-particle distance and is expressed as a linear combination of Gaussian functions,

$$g(\mathbf{r}_i^{\mathrm{e}}, \mathbf{r}_j^{\mathrm{h}}) = \sum_{k}^{N_{\mathrm{g}}} b_k e^{-\gamma_k |\mathbf{r}_i^{\mathrm{e}} - \mathbf{r}_j^{\mathrm{h}}|^2}. \tag{2.3}$$

The expansion coefficients b_k and the width parameter γ_k are parameters used for defining the geminal function. The geminal parameters and the constituting electron and hole orbitals are determined variationally by minimizing the expectation value of the Hamiltonian .

$$E = \frac{\langle \Psi_{\mathrm{xc}} | H | \Psi_{\mathrm{xc}} \rangle}{\langle \Psi_{\mathrm{xc}} | \Psi_{\mathrm{xc}} \rangle} \tag{2.4}$$

Interaction between the electrons and the holes are described by an effective many-body Hamiltonian which can be described by the following general expression: [105, 144, 204, 205, 206]

$$H = T_{\mathrm{e}} + V_{\mathrm{e}}^{\mathrm{ext}} + V_{\mathrm{ee}} + T_{\mathrm{h}} + V_{\mathrm{h}}^{\mathrm{ext}} + V_{\mathrm{hh}} + V_{\mathrm{eh}} \tag{2.5}$$

where,

$$T_{\mathrm{e}} = \frac{-\hbar^2}{2m_{\mathrm{e}}} \int d\mathbf{r}^{\mathrm{e}} \hat{\psi}^{\dagger}(\mathbf{r}^{\mathrm{e}}) \nabla^2 \hat{\psi}(\mathbf{r}^{\mathrm{e}})$$

$$T_{\mathrm{h}} = \frac{-\hbar^2}{2m_{\mathrm{h}}} \int d\mathbf{r}^{\mathrm{h}} \hat{\psi}^{\dagger}(\mathbf{r}^{\mathrm{h}}) \nabla^2 \hat{\psi}(\mathbf{r}^{\mathrm{e}})$$

$$V_{\mathrm{e}}^{\mathrm{ext}} = \int d\mathbf{r}^{\mathrm{e}} \hat{\psi}^{\dagger}(\mathbf{r}^{\mathrm{e}}) v_{\mathrm{e}}^{\mathrm{ext}} \hat{\psi}(\mathbf{r}^{\mathrm{e}})$$

$$V_{\mathrm{h}}^{\mathrm{ext}} = \int d\mathbf{r}^{\mathrm{h}} \hat{\psi}^{\dagger}(\mathbf{r}^{\mathrm{h}}) v_{\mathrm{h}}^{\mathrm{ext}} \hat{\psi}(\mathbf{r}^{\mathrm{h}}) \qquad (2.6)$$

$$V_{\mathrm{ee}} = \int d\mathbf{r}_1^{\mathrm{e}} d\mathbf{r}_2^{\mathrm{e}} \hat{\psi}^{\dagger}(\mathbf{r}_1^{\mathrm{e}}) \hat{\psi}^{\dagger}(\mathbf{r}_2^{\mathrm{e}}) r_{\mathrm{ee}}^{-1} \hat{\psi}(\mathbf{r}_2^{\mathrm{e}}) \hat{\psi}(\mathbf{r}_1^{\mathrm{e}})$$

$$V_{\mathrm{hh}} = \int d\mathbf{r}_1^{\mathrm{h}} d\mathbf{r}_2^{\mathrm{h}} \hat{\psi}^{\dagger}(\mathbf{r}_1^{\mathrm{h}}) \hat{\psi}^{\dagger}(\mathbf{r}_2^{\mathrm{h}}) r_{\mathrm{hh}}^{-1} \hat{\psi}(\mathbf{r}_2^{\mathrm{h}}) \hat{\psi}(\mathbf{r}_1^{\mathrm{h}})$$

$$V_{\mathrm{eh}} = - \int d\mathbf{r}^{\mathrm{e}} d\mathbf{r}^{\mathrm{h}} \hat{\psi}^{\dagger}(\mathbf{r}^{\mathrm{e}}) \hat{\psi}^{\dagger}(\mathbf{r}^{\mathrm{h}}) r_{\mathrm{eh}}^{-1} \hat{\psi}(\mathbf{r}^{\mathrm{h}}) \hat{\psi}(\mathbf{r}^{\mathrm{h}})$$

To facilitate the actual evaluation of the expectation value , it is advantageous to introduce the following congruently transformed operators [207, 208]

$$\begin{aligned} \tilde{H} &= (1+G)^{\dagger} H (1+G) \\ \tilde{S} &= (1+G)^{\dagger} (1+G). \end{aligned} \qquad (2.7)$$

Using the above equations, the energy expression can be written as:

$$E = \frac{\langle \Phi_0^{\mathrm{eh}} | \tilde{H} | \Phi_0^{\mathrm{eh}} \rangle}{\langle \Phi_0^{\mathrm{eh}} | \tilde{S} | \Phi_0^{\mathrm{eh}} \rangle} \qquad (2.8)$$

This expression allows us to evaluate the energy in terms of matrix element of the transformed operators in Slater determinant basis. Since evaluation of matrix elements involving Slater determinants can be done using Slater-Condon rules , this transformation provides a convenient route to the computation of the matrix elements. In the present work, the transformed operators will be expressed in second quantization representation. The action of creation and annihilation operators is well known and is used to simplify the energy expression. Since the geminal operator is

Hermitian, the transformed Hamiltonian is written as

$$\begin{aligned}
\tilde{S} &= (1+G)(1+G) \\
&= 1 + 2G + GG
\end{aligned}$$

(2.9)

$$\begin{aligned}
\tilde{H} &= (1+G)H(1+G) \\
&= H + GH + HG + GHG
\end{aligned}$$

(2.10)

The expression of the transformed operator in field operator representation is achieved in two steps. In the first step, the product of the operators is expanded as a sum of 1-particle, 2-particle,..., N-particle operators. The expanded versions of the transformed operators are described in the following equations. In the second step, the N-particle operators are written in second-quantized notation. It is important to preserve the sequence of the steps, since converting the operators first to second-quantized form and then taking the product will be identical to steps mentioned above only in the limit of infinite basis [209]. This topic has been discussed in great detail with examples by Helgaker, Jorgensen, and Olsen [209].

The expressions for the transformed operators are given as:

$$\begin{aligned}
\tilde{S} &= 1 + 2G + GG \\
&= 1 + 2\sum_{i=1}^{N_e}\sum_{i'=1}^{N_h} g(i,i') + \left[\sum_{i=1}^{N_e}\sum_{i'=1}^{N_h} g(i,i')\right]\left[\sum_{j=1}^{N_e}\sum_{j'=1}^{N_h} g(j,j')\right] \\
&= 1 + \sum_{i=1}^{N_e}\sum_{i'=1}^{N_h} O_1(i,i') + \frac{1}{2!}\sum_{i\neq j}^{N_e}\sum_{i'=1}^{N_h} O_2(i,j,i') + \frac{1}{2!}\sum_{i}^{N_e}\sum_{i'\neq j}^{N_h} O_3(i,i',j') \\
&+ \frac{1}{2!2!}\sum_{i\neq j}^{N_e}\sum_{i'\neq j}^{N_h} O_4(i,j,i',j')
\end{aligned}$$

(2.11)

25

$$
\begin{aligned}
G(T_{\mathrm{e}} + V_{\mathrm{e}}^{\mathrm{ext}})G \;\; &= \left[\sum_{i=1}^{N_{\mathrm{e}}} \sum_{i'=1}^{N_{\mathrm{h}}} g(i,i') \right] \left[\sum_{k=1}^{N_{\mathrm{e}}} -\frac{\hbar^2}{2m_{\mathrm{e}}} \nabla_k^2 + v_{\mathrm{e}}^{\mathrm{ext}}(k) \right] \left[\sum_{j=1}^{N_{\mathrm{e}}} \sum_{j'=1}^{N_{\mathrm{h}}} g(j,j') \right] \\
&= \sum_{i=1}^{N_{\mathrm{e}}} \sum_{i'=1}^{N_{\mathrm{h}}} O_5(i,i') + \frac{1}{2!} \sum_{i=1}^{N_{\mathrm{e}}} \sum_{i' \neq j}^{N_{\mathrm{h}}} O_6(i,i',j') \\
&\quad + \frac{1}{2!} \sum_{i \neq j}^{N_{\mathrm{e}}} \sum_{i'=1}^{N_{\mathrm{h}}} O_7(i,j,i') + \frac{1}{2!2!} \sum_{i \neq j}^{N_{\mathrm{e}}} \sum_{i' \neq j}^{N_{\mathrm{h}}} O_8(i,j,i',j') \\
&\quad + \frac{1}{3!} \sum_{i \neq j \neq k}^{N_{\mathrm{e}}} \sum_{i'=1}^{N_{\mathrm{h}}} O_9(i,i') + \frac{1}{3!2!} \sum_{i \neq j \neq k}^{N_{\mathrm{e}}} \sum_{i' \neq j}^{N_{\mathrm{h}}} O_{10}(i,j,k,i',j')
\end{aligned}
\tag{2.12}
$$

$$
\begin{aligned}
G(T_{\mathrm{e}} + V_{\mathrm{e}}^{\mathrm{ext}}) + (T_{\mathrm{e}} + V_{\mathrm{e}}^{\mathrm{ext}})G \;\; &= \left[\sum_{i=1}^{N_{\mathrm{e}}} \sum_{i'=1}^{N_{\mathrm{h}}} g(i,i') \right] \left[\sum_{k=1}^{N_{\mathrm{e}}} -\frac{\hbar^2}{2m_{\mathrm{e}}} \nabla_k^2 + v_{\mathrm{e}}^{\mathrm{ext}}(k) \right] \\
&\quad + \left[\sum_{i=1}^{N_{\mathrm{e}}} -\frac{\hbar^2}{2m_{\mathrm{e}}} \nabla_i^2 + v_{\mathrm{e}}^{\mathrm{ext}}(i) \right] \left[\sum_{i=1}^{N_{\mathrm{e}}} \sum_{i'=1}^{N_{\mathrm{h}}} g(i,i') \right] \\
&= \sum_{i=1}^{N_{\mathrm{e}}} \sum_{i'=1}^{N_{\mathrm{h}}} \sum_{k=1}^{N_{\mathrm{e}}} g(i,i') \left[-\frac{\hbar^2}{2m_{\mathrm{e}}} \nabla_k^2 + v_{\mathrm{e}}^{\mathrm{ext}}(k) \right] + \left[-\frac{\hbar^2}{2m_{\mathrm{e}}} \nabla_k^2 + v_{\mathrm{e}}^{\mathrm{ext}}(k) \right] g(i,i') \\
&= \sum_{i=1}^{N_{\mathrm{e}}} \sum_{i'=1}^{N_{\mathrm{h}}} O_{11}(i,i') + \frac{1}{2!} \sum_{i \neq j}^{N_{\mathrm{e}}} \sum_{i'=1}^{N_{\mathrm{h}}} O_{12}(i,j,i')
\end{aligned}
\tag{2.13}
$$

$$
\begin{aligned}
GV_{\mathrm{ee}}G \;\; &= \left[\sum_{i=1}^{N_{\mathrm{e}}} \sum_{i'=1}^{N_{\mathrm{h}}} g(i,i') \right] \left[\frac{1}{2} \sum_{k \neq l}^{N_{e}} r_{kl}^{-1} \right] \left[\sum_{j=1}^{N_{\mathrm{e}}} \sum_{j'=1}^{N_{\mathrm{h}}} g(j,j') \right] \\
&= \frac{1}{2!} \sum_{i \neq j}^{N_{\mathrm{e}}} \sum_{i'=1}^{N_{\mathrm{h}}} O_{13}(i,j,i') + \frac{1}{2!2!} \sum_{i \neq j}^{N_{\mathrm{e}}} \sum_{i' \neq j'}^{N_{\mathrm{h}}} O_{14}(i,j,i',j') \\
&\quad + \frac{1}{3!} \sum_{i \neq j \neq k}^{N_{\mathrm{e}}} \sum_{i'=1}^{N_{\mathrm{h}}} O_{15}(i,j,k,i') + \frac{1}{3!2!} \sum_{i \neq j \neq k}^{N_{\mathrm{e}}} \sum_{i' \neq j}^{N_{\mathrm{h}}} O_{16}(i,j,k,i',j') \\
&\quad + \frac{1}{4!} \sum_{i \neq j \neq k \neq l}^{N_{\mathrm{e}}} \sum_{i'=1}^{N_{\mathrm{h}}} O_{17}(i,j,k,l,i') + \frac{1}{4!2!} \sum_{i \neq j \neq k}^{N_{\mathrm{e}}} \sum_{i' \neq j'}^{N_{\mathrm{h}}} O_{18}(i,j,k,l,i',j')
\end{aligned}
\tag{2.14}
$$

$$GV_{\text{ee}} + V_{\text{ee}}G = \left[\sum_{i=1}^{N_{\text{e}}}\sum_{i'=1}^{N_{\text{h}}} g(i,i')\right]\left[\frac{1}{2}\sum_{k\neq l}^{N_e} r_{kl}^{-1}\right] + \left[\frac{1}{2}\sum_{i\neq j}^{N_e} r_{ij}^{-1}\right]\left[\sum_{i=1}^{N_{\text{e}}}\sum_{i'=1}^{N_{\text{h}}} g(i,i')\right]$$
$$= \frac{1}{2!}\sum_{i\neq j}^{N_{\text{e}}}\sum_{i'=1}^{N_{\text{h}}} O_{19}(i,j,i') + \frac{1}{3!}\sum_{i\neq j\neq k}^{N_{\text{e}}}\sum_{i'=1}^{N_{\text{h}}} O_{20}(i,j,k,i') \tag{2.15}$$

$$GV_{\text{eh}}G = \left[\sum_{i=1}^{N_{\text{e}}}\sum_{i'=1}^{N_{\text{h}}} g(i,i')\right]\left[\sum_{kk'}^{N_e} r_{kk'}^{-1}\right]\left[\sum_{j=1}^{N_{\text{e}}}\sum_{j'=1}^{N_{\text{h}}} g(j,j')\right] = \sum_{ijk}^{N_{\text{e}}}\sum_{i'j'k'}^{N_{\text{h}}} g(i,i')r_{kk'}^{-1}g(j,j')$$
$$= \sum_{i}^{N_{\text{e}}}\sum_{i'}^{N_{\text{h}}} O_{21}(i,i') + \frac{1}{2!}\sum_{i}^{N_{\text{e}}}\sum_{i'\neq j}^{N_{\text{h}}} O_{22}(i,i',j') + \frac{1}{3!}\sum_{i}^{N_{\text{e}}}\sum_{i'\neq j\neq k}^{N_{\text{h}}} O_{23}(i,i',j',k')$$
$$+ \frac{1}{2!}\sum_{i\neq j}^{N_{\text{e}}}\sum_{i'}^{N_{\text{h}}} O_{24}(i,j,i') + \frac{1}{2!2!}\sum_{i\neq j}^{N_{\text{e}}}\sum_{i'\neq j}^{N_{\text{h}}} O_{25}(i,j,i',j') + \frac{1}{2!3!}\sum_{i\neq j}^{N_{\text{e}}}\sum_{i'\neq j\neq k}^{N_{\text{h}}} O_{26}(i,j,i',j',k')$$
$$+ \frac{1}{3!}\sum_{i\neq j\neq k}^{N_{\text{e}}}\sum_{i'}^{N_{\text{h}}} O_{27}(i,j,k,i') + \frac{1}{3!2!}\sum_{i\neq j\neq k}^{N_{\text{e}}}\sum_{i'\neq j}^{N_{\text{h}}} O_{28}(i,j,k,i',j') + \frac{1}{3!3!}\sum_{i\neq j\neq k}^{N_{\text{e}}}\sum_{i'\neq j\neq k}^{N_{\text{h}}} O_{29}(i,j,k,i',j',k')$$
$$\tag{2.16}$$

The expression for the hole operators are obtained in a similar fashion.

It is important to note that the transformed operators $O_\alpha, \alpha = 1, \ldots, 29$ must be completely symmetric when operated on by the permutation operators of the symmetric group, $\S_n$. For a general operator of the form $O_\alpha(1, \ldots M, 1, \ldots M')$ that couples M number of electrons with M' number of holes, the complete symmetric condition is satisfied by the following relationship,

$$\mathcal{P}_k\mathcal{P}_{k'}O_\alpha(1, \ldots M, 1', \ldots, M') = O_\alpha(1, \ldots M, 1', \ldots, M') \qquad k = 1, \ldots M!; k' = 1, \ldots, M'!$$
$$\tag{2.17}$$

where $\mathcal{P}_k$ and $\mathcal{P}_k'$ are permutation operators in the symmetric group S_M and $S_{M'}$, respectively.

The general expression for an N-particle operator in second-quantization and field operator notation is well known. The general expression of a many-body operator

that couples M and M' electrons and holes, respectively, is represented in terms of electron and hole field operators as:

$$\Omega_\alpha = \int d(1) \ldots d(M) d(1') \ldots d(M')$$
$$\hat{\psi}^\dagger(1) \ldots \hat{\psi}^\dagger(M) \hat{\psi}^\dagger(1') \ldots \hat{\psi}^\dagger(M') O_\alpha(1, \ldots, M, 1', \ldots, M') \hat{\psi}(M') \ldots \hat{\psi}(1') \hat{\psi}(M) \ldots \hat{\psi}(1)$$

$$(2.18)$$

The explicitly correlated wave function is obtained variationally by minimizing the total energy with respect to the electron and hole molecular orbitals and the parameters in the geminal operator . Minimizing the total energy with respect to the electron and hole molecular orbitals $\{\chi_i^e, \chi_i^h\}$ results in the following set of Fock equations :

$$f^e \chi_i^e = \varepsilon_i^e \chi_i^e$$
$$f^h \chi_i^h = \varepsilon_i^h \chi_i^h \qquad\qquad (2.19)$$

where the electron and hole Fock operators can be defined as:

$$f^e = -\frac{\hbar^2}{2m_e} \nabla_e^2 + v_e^{ext} + v_e^{eff}[\{\chi_i^h\}]$$
$$f^h = -\frac{\hbar^2}{2m_h} \nabla_h^2 + v_h^{ext} + v_h^{eff}[\{\chi_i^e\}] \qquad\qquad (2.20)$$

The single-particle operator v_e^{eff} includes all the terms arising from the geminal expression and is equal to the Hartree-Fock potential v_e^{HF} in the limiting case of $G = 0$. The electronic Fock operator depends on the hole molecular orbitals, and both electron and hole Fock equations are solved self-consistently till convergence is achieved. The molecular orbitals are represented as a linear combination of atomic orbitals and the expansion coefficients are determined variationally. The integrals

28

Table 2.1: Material parameters for the CdSe quantum dots used in the electron-hole Hamiltonian

Property	Value (Atomic units) [138]
m_e	0.13
m_h	0.38
ϵ	6.2

over atomic orbital involving the geminal function are well known and were calculated using the procedure described by Boys and Persson [210].

The eh-XCHF method is general and can be used to study both single component and multi-component systems. It has been benchmarked with respect to the Hooke's atom in chapter 2, electron-hole pair in a parabolic confining potential in chapter 2 and the Helium atom in chapter 4 to showcase the versatility of the method. The eh-XCHF method is also used for the development of an adiabatic connection curve towards the development of an electron-hole correlation functional for use in electron-hole multi-component density functional theory, the details of this implementation are given in chapter 9.

After successful benchmarking of the eh-XCHF method with respect to these simple systems, the method was applied to study electron-hole interaction within nanoparticles. To study these systems, the effective electron-hole Hamiltonian was applied and full details for each system of interest are given in chapter 5, chapter 6, chapter 7, and chapter 8. However, it is important to note that there are several material-specific parameters that are taken into account so as to denote the material that makes up the nanoparticle. These parameters include effective mass of both the electron and hole as well as dielectric constant . The dielectric constant controls the screening between the electron and hole particles as per the specific material. It is essential that material parameters are very carefully chosen. A table of example parameters for a CdSe system is given in Table 2.1. It is also important to note that all dielectric constants within this work were chosen to be consistent among size of

particles.

2.2   Details of eh-XCHF calculation

The form of the wave function used in the present calculation is defined to be of the form:

$$\Psi(\mathbf{x}_1, \mathbf{x}_2) = \Psi_\alpha(\mathbf{r}_1, \mathbf{r}_2)\Psi_{\text{spin}}(\omega_1, \omega_2) \qquad \alpha = \text{HF}, \text{R12} - \text{FCI}, \text{eh} - \text{XCHF} \qquad (2.21)$$

where particles 1 and 2 have opposite spins and $\Psi_{\text{spin}}(\omega_1, \omega_2)$ is antisymmetric . The Hamiltonian for the benchmark system is defined as:

$$H_\lambda = -\frac{1}{2m}\nabla_1^2 - \frac{1}{2m}\nabla_2^2 + \frac{1}{2}kr_1^2 + \frac{1}{2}kr_2^2 + \lambda\frac{1}{|\mathbf{r}^{\text{e}} - \mathbf{r}^{\text{h}}|} \qquad (2.22)$$

where $m_{\text{e}} = m_{\text{h}} = m = 1\text{a.u.}$, k is the force constant and all quantities are in atomic units . For the present calculations the force constant was set to $k = 1/4$. A scaling parameter λ was introduced to scale the magnitude of the Coulomb interaction between the two particles. The Coulomb interaction between the two particles is represented by λr_{12}^{-1} where, $\lambda = +1$ if charges are identical and $\lambda = -1$ if the particles are oppositely charged. For the electron-hole system the scaling parameter was set to $\lambda = -1$.

The explicitly correlated Hartree-Fock (eh-XCHF) method was used to calculate the ground state energy and electron-hole recombination probability . Gaussian-type orbitals (GTO) were used for the calculations and the coefficient used in the GTO basis are presented in Table 3.1. All the GTOs were centered at the minimum of the parabolic potential . The FCI calculations for the two-electron Hooke's atom

have been carried out earlier by Matito and coworkers and the method for generating even-tempered GTO basis defined earlier was used in the present work. Issues related to linear dependencies were resolved by performing canonical orthogonalization. The implementation of the computer program was checked by reproducing the FCI results obtained by Matito et al.

Since, eh-XCHF is an explicitly correlated method, a fair and accurate comparison was obtained by performing an explicitly correlated full-configuration interaction calculation using Slater-type orbitals (STOs) . To emphasize this fact, the FCI method used in this work is labeled as (R12-FCI) and is described in the following subsection. The analytical results for the two-electron Hooke's atoms with $k = 1/4$ is well known [211, 212] and was used to benchmark the R12-FCI implementation. The R12-FCI energy of 2.00074 Hartree was obtained for the Hooke's atom which was in good agreement with the exact analytical result of 2.0 Hartree.

2.3   Details of the R12-FCI calculation

The R12-FCI calculation was performed by transforming the 6D Hamiltonian described to a 1D radial Hamiltonian . This was done by first separating out the center-of-mass coordinate followed by transforming into spherical polar coordinates . Defining the relative and center-of-mass coordinates as:

$$
\begin{aligned}
\mathbf{R} &= \frac{\mathbf{r}_1 + \mathbf{r}_2}{2} \\
\mathbf{r} &= \mathbf{r}_1 - \mathbf{r}_2
\end{aligned}
\tag{2.23}
$$

The total Hamiltonian can be written as

$$H = H_{\mathrm{R}} + H_{\mathrm{r}}$$

$$H_{\mathrm{R}} = -\frac{1}{2M}\nabla_{\mathrm{R}}^2 + \frac{1}{2}M\omega^2 R^2 \qquad (2.24)$$

$$H_{\mathrm{r}} = -\frac{1}{2\mu}\nabla_{\mathrm{r}}^2 + \frac{1}{2}\mu\omega^2 r^2 + \lambda\frac{1}{r}$$

where $M = m_1 + m_2$ and $\mu = m_1 m_2 M^{-1}$. The total wave function is defined as:

$$
\begin{aligned}
H\Psi &= E\Psi \\
H_{\mathrm{R}}\Phi_{\mathrm{R}} &= E_{\mathrm{R}}\Phi_{\mathrm{R}} \\
H_{\mathrm{r}}\Phi_{\mathrm{r}} &= E_{\mathrm{r}}\Phi_{\mathrm{r}} \qquad (2.25)\\
\Psi &= \Phi_{\mathrm{R}}\Phi_{\mathrm{r}} \\
E &= E_{\mathrm{R}} + E_{\mathrm{r}}
\end{aligned}
$$

The center-of-mass Hamiltonian is a 3D harmonic oscillator whose eigenvalues and eigenfunctions are known analytically and is equal to $3\hbar\omega$ for the ground state. The Hamiltonian associated with the relative coordinate was transformed into spherical polar coordinates, and the radial equation for $l = 0$ is given as:

$$\left[-\frac{\hbar^2}{2\mu}\left(\frac{\partial^2}{\partial r^2} + \frac{2}{r}\frac{\partial}{\partial r} \right) + \frac{1}{2}\mu\omega^2 r^2 + \lambda\frac{1}{r} \right]\chi(r) = E_r\chi(r) \qquad \text{for } l = 0 \qquad (2.26)$$

The 1D radial Schrodinger equation was solved by expanding the radial wave function as a linear combination of Slater-type orbitals and performing configuration interaction calculation

Table 2.2: STO basis used in the R12-FCI calculations

N	Exponent
0	5.8600×10^{-1}
1	5.8600×10^{-1}
2	5.8600×10^{-1}
0	1.5172
1	1.5172
2	1.5172
0	3.9279
1	3.9279
2	3.9279
0	1.0169×10^{1}
1	1.0169×10^{1}
2	1.0169×10^{1}
0	2.6328×10^{1}
1	2.6328×10^{1}
2	2.6328×10^{1}

$$\chi(r) = \sum_i c_i \phi_i^{\text{STO}}$$

$$\phi^{\text{STO}}(r) = r^n e^{-\alpha r}$$

(2.27)

Ground state energy was obtained by minimizing both the expansion coefficients $\{c_i\}$ and the STO exponent $\{\alpha_i\}$. The STO basis functions used for the R12-FCI

Table 2.3: GTO basis used in HF and eh-XCHF calculations

Type	Exponent
S	2.500×10^{-1}
S	2.3721×10^{-1}
S	3.5522×10^{-1}
S	5.3193×10^{-1}
S	7.9655×10^{-1}
S	1.1928
S	1.7862
S	2.6748
S	4.0054
S	1.6442×10^{-1}

calculations are listed in Table 2.2.

The radial equation can be solved analytically for the limiting cases of $\lambda = 0$ and $\omega = 0$. The R12-FCI method can be systematically improved by addition of more basis functions and will reproduce the exact ground state energy in the limit of infinite basis functions. The R12-FCI calculation with the STO basis presented in Table 2.2 was found to reproduce the analytical energies.

2.4 Results and Discussion

2.4.1 Correlation energy from HF and R12-FCI calculations

The Hartree-Fock theory plays an important role in electronic structure theory. The Hartree-Fock wave function is used as a zeroth order wave function for post-HF calculations such as perturbation theory and configuration interaction calculations. For application of the HF wave function as a reference wave function in electron-hole systems it is very important to investigate the quality of the mean-field approximation versus highly accurate calculations. In the present work, a comparison study of the quality of the mean-field approximation for electron-hole and electron-electron system was carried out by performing a series of HF and R12-FCI calculations. The calculations were performed for H_λ and the coupling parameter λ was varied from $\lambda = -1, \ldots, +1$. For each value of λ the difference between the HF and R12-FCI energies was computed using the following expression,

$$\Delta E(\lambda) = \frac{E_{\text{HF}}(\lambda) - E_{\text{R12-FCI}}(\lambda)}{E_{\text{R12-FCI}}(\lambda)} \times 100. \qquad (2.28)$$

The difference between the HF and R12-FCI energies is used as a metric to analyze the quality of mean field approximation for electron-electron versus electron-hole
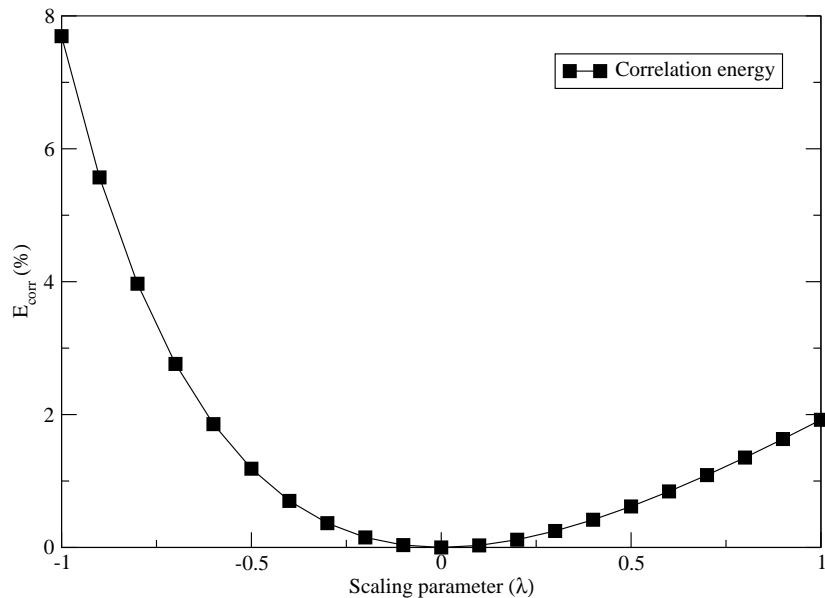
Figure 2-1: Relative difference between that HF and R12-FCI energies as a function of the Coulomb scaling parameter.

system. The result of the computed ΔE as a function of λ is presented in . It is seen that plot is not symmetric with respect to the coupling parameter.

This implies that the HF approximation is worse for the electron-hole system as compared to an electron-electron system. It was found that the electron-hole is larger than the electron-electron system by a factor of 4. This large difference in the quality of the mean field approximation for identical and oppositely charged particles can be attributed to the Coulomb interaction term in the Hamiltonian . Because of the Coulomb hole in the electron-electron system, there is a reduced probability of finding another electron in the vicinity of the first electron. For the electron-hole system the situation is reversed and there is an enhanced probability of finding an oppositely charged particle in the vicinity of the first one. This can be seen clearly by deriving the Kato cusp condition for the 2-particle density. The Kato cusp condition

for the ground state wave function for the electron-electron and electron-hole system is defined as [213]

$$\Psi_{ee}(r_{12}) = \Psi_{ee}(r_{12} = 0) \left[1 + \frac{1}{2}r_{12} + O(r_{12}^2) \right] \qquad (2.29)$$

where we have assumed that the ground state is a S state. Using the above expression, the 2-particle density can be defined as

$$\rho_{ee}(r_{12}) = \rho_{ee}(r_{12} = 0) \left[1 + r_{12} + O(r_{12}^2) \right] \qquad (2.30)$$

$$\rho_{eh}(r_{12}) = \rho_{eh}(r_{12} = 0) \left[1 - r_{12} + O(r_{12}^2) \right] \qquad (2.31)$$

The above equations indicate that the probability density of finding two electrons increases with increasing r_{12} at small inter-particle separation. This is indicative of a Coulomb hole. For the electron-hole system, the probability density of finding an electron-hole pair decreases at small inter-particle separation which indicates a local enhancement of the 2-particle density in the vicinity of the cusp. Since $\rho_{ee}(r_{12})/\rho_{ee}(0) > 1$ and $\rho_{eh}(r_{12})/\rho_{eh}(0) < 1$ at small inter-particle separation, the quality of the eh-wave function at short range, and the electronic wave function at intermediate range, is important for obtaining accurate results. Similar conclusion for the electronic wave function has been reported earlier by Prendergast et al. [214].

The Kato cusp condition is generally satisfied by incorporating Slater-type orbital (STO) functions that depend on r_{eh},

36

$$e^{-\varsigma r_\text{eh}} = 1 - \varsigma r_\text{eh} + O(r^2). \tag{2.32}$$

In this present work, Gaussian type geminal (GTG) functions were used to describe the form of the wave function at small inter-particle distances,

$$e^{-\varsigma r_\text{eh}} \simeq \sum_{k}^{N_g} b_k e^{-\gamma_k r_\text{eh}^2}, \tag{2.33}$$

where $\{b_k, \gamma_k\}$ are variational parameters. The GTG function was introduced by Boys for explicitly including R12 term in the electronic wave function. The necessary integrals involved in the implementation of the GTG function are have well-known analytical expressions and have been derived earlier by Boys [165] and Persson et al.[210]. The STO is expanded as a linear combination of Gaussian function to avoid computation of integrals involving STOs. This is a general strategy to avoid computation of atomic orbital (AO) integrals using STO and has been used successfully in the field of basis set development [215] and GTG calculations [166, 216].

However, we stress that the expansion in Equation 2.33 is approximate and is not capable of describing the eh-cusp exactly since the Gaussian functions have zero first derivative at the cusp. The description of the electron-hole cusp can be systematically improved by performing post-SCF explicit R12 calculations. In the present work, the expansion coefficients are obtained variationally by minimizing the total energy . However, pre-computed values of the expansion coefficients and GTG functions can also be used in the above expression.

2.4.2 Energy and recombination probability from eh-XCHF calculations

The eh-XCHF calculations were performed only for the electron-hole system and Hamiltonian for the system was obtained by setting $k = 1/4$ in Equation 2.22. The total eh-XCHF wave function for the system is defined as:

$$\Psi_{\text{xc}}(\mathbf{x}^{\text{e}}, \mathbf{x}^{\text{h}}) = \left[1 + G(\mathbf{r}^{\text{e}}, \mathbf{r}^{\text{h}})\right] \Phi^{\text{e}}(\mathbf{r}^{\text{e}})\Phi^{\text{h}}(\mathbf{r}^{\text{h}})\Psi_{\text{spin}}(\omega^{\text{e}}, \omega^{\text{h}}) \tag{2.34}$$

where Ψ_{spin} is anti-symmetric and the electron and the hole have opposite spins. Gaussian-type orbitals (GTO) were used to describe the spatial component of the wave function and are defined in Table 3.1. The number of parameters N_g in the geminal expansion were incrementally increased until convergence was achieved with respect to energy. At each value of N_g the set of geminal parameters $\{b_k, \gamma_k\}$ were determined variationally. The energies and recombination probability from the eh-XCHF calculation are compared with HF and R12-FCI calculations and results are plotted in Figure 2-2 and Figure 2-3, respectively,

as a function of N_g. The $N_g = 0$ in the plot represents the HF solution since the eh-XCHF calculation reduces to HF in the limit of G = 0. The value of N_g was systematically increased and convergence with respect to the total energy was achieved at $N_g = 7$. The geminal parameters were optimized in a sequential process and parameters optimized for $N_g - 1$ step were kept fixed. As a result, for the N_g step, all parameters from the previous step $\{b_i, \gamma_i; i = 1, \ldots, N_g - 1\}$ were kept fixed and only $\{b_i, \gamma_i; i = N_g\}$ was variationally optimized. The list of optimized geminal parameters are listed in Table 3.2. The HF energy was found to be higher that the R12-FCI energy by 0.0648 Hartree (1.76 eV). The best eh-XCHF energy with $N_g = 7$ is 0.8407 Hartree and is higher than the R12-FCI energy by 0.02 eV. From Figure 2-2,
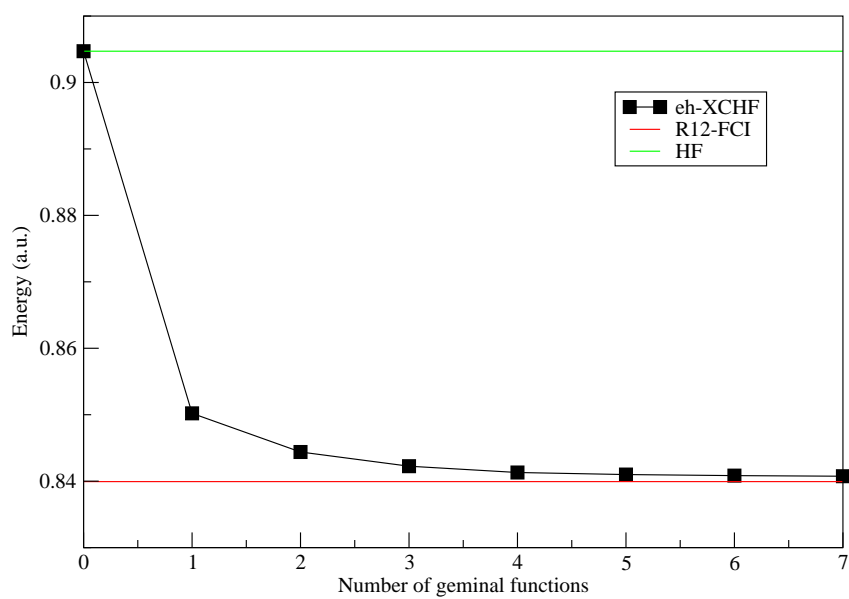
Figure 2-2: Convergence of the ground state energy as a function of number of geminal parameters.
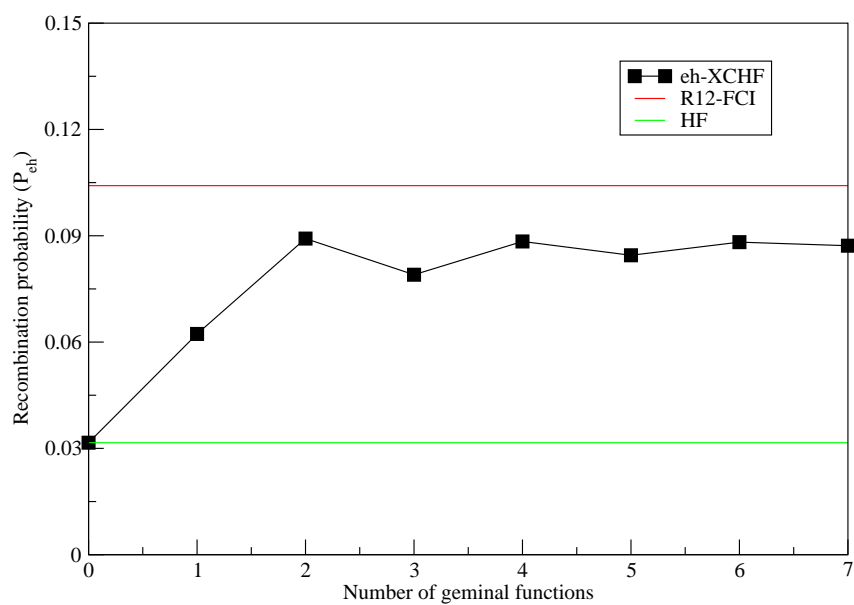
Figure 2-3: Comparison of the electron-hole recombination enhancement factor from the eh-XCHF calculation with HF and R12-FCI results.

Table 2.4: Optimized geminal parameters

k	b_k	γ_k
1	1.2100	0.3500
2	0.4640	3.9600
3	0.5800	0.0900
4	0.2270	1.9000
5	0.2800	0.1000
6	0.1028	1.6700
7	-0.1020	0.3500

it is seen that the eh-XCHF wave function can be systematically improved by addition of geminal parameters. The eh-XCHF energy for $N_g = 1$ is lower than the HF energy by 0.0545 Hartree (1.48 eV).

This shows the importance of improving the short-range description of the electron-hole wave function that is missing in the mean-field approximation. The form of the geminal function with $N_g = 7$ is plotted as the function of inter-particle distance and is presented in Figure 2-4. An exponential function of the form $e^{-\varsigma r_{eh}}$ is fitted to the geminal function and also shown in Figure 2-4. The width parameter from the exponential fit was found to be $\varsigma = 0.5605$ which is close to the theoretical exact value of 0.5 from the Kato cusp condition [213] .

The quality of the electron-hole wave function can also be analyzed by computing either the electron-hole recombination rate or the associated recombination probability . Both of these quantities are computed from the electron-hole density matrix and is sensitive to accurate treatment of electron-hole correlation . The general expression for electron-hole density matrix for arbitrary number of excitons has been derived earlier by Corni and coworkers [156] for studying transitions from (N+1) to (N) excitonic states [156, 157]. In a separate study, van der Horst et al. used electron-hole distance probability distribution function [217] to analyze excitonic wave function in conjugated polymers obtained using the Bethe-Salpeter method. The electron-hole distance probability distribution function (in atomic uints) is defined as [217]
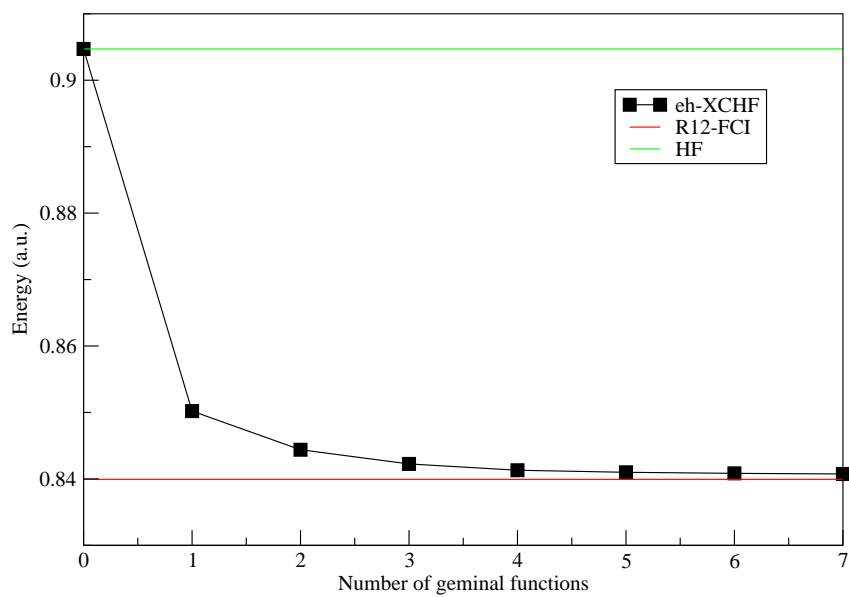
Figure 2-4: Comparison of the geminal function with the fitted exponential function and R12-FCI wave function. The geminal function has been scaled so that the geminal and the R12-FCI curves can be plotted in the same figure.

$$P_{\text{eh}}^{\alpha} = \frac{\langle \Psi_{\alpha} | \delta(\mathbf{r}^{\text{e}} - \mathbf{r}^{\text{h}}) | \Psi_{\alpha} \rangle}{\langle \Psi_{\alpha} | \Psi_{\alpha} \rangle} \qquad \alpha = \text{HF}, \text{R12} - \text{FCI}, \text{XCHF} \qquad (2.35)$$

and was used for analyzing HF, R12-FCI, and eh-XCHF wave functions. Since we are interested in comparison of the correlated wave functions with respect to the mean-field approximation, we also defined the eh-recombination enhancement factor η which is obtained from the P_{eh} using the following expression,

$$\eta^{\alpha} = \frac{P_{\text{eh}}^{\alpha}}{P_{\text{eh}}^{\text{HF}}} \qquad \alpha = \text{HF}, \text{R12} - \text{FCI}, \text{XCHF} \qquad (2.36)$$

Results from eh-XCHF calculations with $N_g = 0, \ldots, 7$ together with the HF and R12-FCI results are presented in Figure 2-3. It is seen, that the recombination probability converges as a function of geminal parameters. On comparison of results from the three methods, it is seen that HF calculation severely underestimates the recombination probability by a factor of three for both the eh-XCHF and R12-FCI methods. The recombination probability is very sensitive to form of the wave function at small electron-hole inter-particle distances. The ground state energies and the eh-recombination enhancement factor for HF, R12-FCI, and eh-XCHF are summarized in Table 2.5. The results in this table highlight the challenging aspect of computation of accurate recombination probability. The energy from the eh-XCHF wave function is higher than the benchmark by 0.1%. In contrast, the eh-recombination probability is lower by 16%.

It is seen in Figure 2-2 that the eh-XCHF energy is converged with respect to number of GTG functions. Analogous to the conventional electronic structure theory, the converged eh-XCHF method can be systematically improved using perturbation theory and configuration interaction [140] calculation using the eh-XCHF as

Table 2.5: Comparison of calculated ground state energy and electron-hole recombination enhancement factor from HF, R12-FCI, and eh-XCHF calculations for the parabolic quantum dot. The Hamiltonian for the dot was defined by setting $k = 1/4$ in the Equation 2.22.

Method	Energy	η
HF	0.9047	1
R12-FCI	0.8399	3.29
eh-XCHF	0.8407	2.76

the reference wave function. This approach of successive improvement of a correlated reference wave function is also analogous to a typical diffusion Monte Carlo (DMC) calculation where correlated wave function from variational Monte Carlo (VMC) is used as a starting point for a more accurate calculation.

In general, it will not be possible to perform R12-FCI calculation for any given system due to the lack of a spherically symmetric potential and numerical cost associated with using Slater-type orbitals. The eh-XCHF formulation on the other hand is a general purpose method that does not require any a priori assumption about the potential and utilizes GTO as opposed to STO as basis functions. The use of Gaussian type geminal functions in the eh-XCHF method allows analytical evaluation of the AO integrals.61,108. In electronic structure theory, the resolution of identity (RI) method [218, 219] has been used successfully for integral evaluation with GTG [220, 221, 222, 223]. The RI method will be used in the eh-XCHF calculation for fast evaluation of many-particle integrals involving geminal functions. The eh-XCHF benchmark calculations presented here are the first in a series of calculations on various electron-hole systems. Future work using the eh-XCHF method involves investigation of effect of shell thickness on electron-hole recombination in CdSe/ZnS multilayered quantum dots and replacing HF by eh-XCHF wave function as the zeroth order reference wave function in post-SCF schemes such as MP2 and CI methods [141].

2.5 Conclusions about eh-XCHF method

The explicitly correlated Hartree-Fock method for a general many-electron many-hole system is presented and was used for calculation of ground state energy and electron-hole recombination probability. The eh-XCHF method is general technique for solving the electron-hole Schrodinger equation and can be applied to a large variety of electron-hole system by appropriate selection of the quasi-particle masses and the external potential terms in the effective electron-hole Hamiltonian. In the present work, the eh-XCHF method was applied to the parabolic quantum dot system which consists of an interacting electron-hole pair confined by the three-dimensional parabolic potential. Ground state energy and electron-hole recombination probabilities were computed and the results were found to be in good agreement with the highly accurate explicitly correlated full configuration interaction calculations. Hartree-Fock calculation was also performed and the HF wave function was found to severely underestimate the electron-hole recombination probability. The accuracy of the HF wave function was compared for both electron-electron and electron-hole system and it was found that the HF approximation is worse for the electron-hole system. The results from these calculations highlight the importance of accuracy of the form of the electron-hole wave function at small inter-particle distances for electron-hole systems and the capability of eh-XCHF method to successfully address this issue.

Chapter 3

Development of Explicitly Correlated Configuration Interaction

3.1 Motivation for the development of explicitly correlated configuration interaction

The understanding the dynamics of electron-hole pair has become crucial for advances in the field of semiconductor materials . Electron-hole correlation has shown to be important for understanding optical processes in a wide variety of materials including quantum dots, [224, 4, 225, 131] carbon nanotubes,[226, 227, 228, 229] solar cells, [230, 231] biomaterials, [232, 233, 234, 235] and photocatalysts. [236, 237]. There are various approaches to study electron-hole interaction including effective mass approximation,[150] configuration interaction (CI),[157, 156, 238, 154, 153, 108, 162] quantum Monte Carlo (QMC), [239, 240, 163, 241, 242, 144, 145] and many-body Green's function approach .[132] These methods have been used to investigate various properties of quantum dots including exciton binding energy , recombination rates , and exciton lifetimes . The physics of the electron-hole pair is very different from the electron-electron interaction found in electronic structure theory.

The electron and hole are oppositely charged and therefore experience an attractive Coulomb potential . As a consequence, the quality of the eh-wave function at small inter-particle distances becomes important for accurate description of the electron-hole interaction. Typically, this is addressed by accurate description of the electron-hole cusp and can be incorporated by using Jastrow functions in a QMC calculation.[239, 240, 163, 241, 242, 144, 145, 243]. However, such correlation functions are complicated mathematical functions and one has to resort to a numerical procedure such as Monte Carlo to calculate the integrals involved in the energy calculation.

In the present work, the explicitly correlated configuration interaction (XCCI) method is presented for solving the electron-hole Schrodinger equation . The core strategy of the XCCI method is to perform a CI calculation using an explicitly correlated reference wave function . The XCCI method shares features that are present in conventional CI and QMC methods. Like conventional CI, the XCCI method is also variational and is based on a CI expansion. However, unlike the conventional CI method which uses the mean-field (Hartree-Fock) wave function as the reference wave function, the XCCI method uses an explicitly correlated reference wave function. Both XCCI and variational Monte Carlo (VMC) methods use explicitly correlated wave functions and in both methods the wave function is an explicit function of the electron-hole interparticle distance r_{eh}. In VMC this is typically achieved by using a Jastrow correlation function. In the XCCI method, Gaussian-type geminal (GTG)[164] functions are used for including r_{eh}. The principle reason for using GTG as opposed to Slater-type functions or Jastrow functions is that integrals involving GTG are known analytically[210] and are much faster to compute than integrals involving Slater and Jastrow functions.

The remainder of the article is organized as follows. The derivation of the XCCI method for a general many-electron many-hole system is presented in Sec. 3.2. Bench-

mark calculations were performed on parabolic quantum dot system and the details of the calculations are discussed in Sec.9.2. The results from the XCCI method were compared with FCI and the highly accurate R12-FCI calculations and are discussed in Sec. 9.3.

3.2 Theoretical and computational details of XCCI method

The underlying idea of the XCCI method is to perform CI calculation using a correlated zeroth-order wave function . In the XCCI method, the zeroth order correlated wave function is obtained from the electron-hole explicitly correlated Hartree-Fock (eh-XCHF) method.[9, 244, 168] The derivation of the eh-XCHF method has been described earlier and only a brief summary is presented here. The eh-XCHF wave function ansatz obtained by multiplying the mean-field (Hartree-Fock) wave function with an explicitly correlated function

$$\Psi_{\text{XCHF}} = G\Phi_{\text{e}}\Phi_{\text{h}} \tag{3.1}$$

where G is a Gaussian-type geminal (GTG) function which is defined as

$$G(\mathbf{r}^{\text{e}}, \mathbf{r}^{\text{h}}) = \sum_{i=1}^{N_{\text{e}}} \sum_{j=1}^{N_{\text{h}}} \sum_{k=1}^{N_{\text{g}}} b_k \exp[-\gamma_k r_{ij}^2] \tag{3.2}$$

The GTG function depends of the r_{eh} term and is responsible for introduction of electron-hole inter-particle distance dependence in the the eh-XCHF wave function. The coefficients b_k and γ_k are expansion coefficients which are obtained variationally . The Φ_{e} and Φ_{h} are electron and hole Slater determinants . The XCHF wave function is obtained variationally by minimizing the total energy with respect to the electron

and hole spin-orbitals $\{\chi_i^e, \chi_i^h\}$ and the geminal expansion coefficient

$$E_{\text{XCHF}} = \min_{\substack{b_k, \gamma_k \\ \chi_i^e, \chi_i^h}} \frac{\langle \Psi_{\text{XCHF}} | H | \Psi_{\text{XCHF}} \rangle}{\langle \Psi_{\text{XCHF}} | \Psi_{\text{XCHF}} \rangle} \tag{3.3}$$

Using the eh-XCHF wave function as the zeroth-order reference wave function , the XCCI wave function is defined by the following CI expansion,

$$\Psi_{\text{XCCI}} = c_0 \Psi_{\text{XCHF}} + \sum_{ia} \sum_{i'a'} c_{ii'}^{aa'} G \Phi_{\text{e}i}^{\ a} \Phi_{\text{h}i'}^{\ a'} \tag{3.4}$$
$$+ \sum_{\substack{i<j \\ a<b}} \sum_{\substack{i'<j' \\ a'<b'}} c_{iji'j'}^{aba'b'} G \Phi_{\text{e}ij}^{\ ab} \Phi_{\text{h}i'j'}^{\ a'b'} + \dots$$

The expansion coefficients $c_0, c_{ii'}^{aa'}, c_{iji'j'}^{aba'b'}$ are obtained variationally by solving the CI eigenvalue equations. In the above expression the indices $i, j, \dots$ are used to represent occupied orbitals and $a, b, \dots$ are used to represent the unoccupied orbitals. Primed and unprimed indices are used for holes and electrons, respectively. The determinant $\Phi_{\text{e}ij}^{\ ab}$ is obtained by replacing the occupied orbitals χ_i and χ_j by χ_a and χ_b, respectively. The XCCI wave function can be related to the conventional CI wave function by setting the geminal function to unity

$$\Psi_{\text{CI}} = \lim_{G \to 1} \Psi_{\text{XCCI}} \tag{3.5}$$

The above equation implies, that the CI energy is an upper bound to the XCCI energy

$$E_{\text{exact}} \leq E_{\text{XCCI}} \leq E_{\text{CI}} \tag{3.6}$$

where the equality relationship holds in the limit of infinite basis. The XCCI method requires evaluation of the matrix elements of the form $\langle G \Phi_k | H | G \Phi_{k'} \rangle$. The evalua-

tion of the matrix elements has been described earlier in the context of the eh-XCHF method and only the key steps are summarized here. The matrix elements are computed by performing congruent transformation on the Hamiltonian using the geminal operator

$$\langle G\Phi_k | H | G\Phi_{k'} \rangle = \langle \Phi_k | G^\dagger H G | \Phi_{k'} \rangle \tag{3.7}$$

where Φ_k and $\Phi_{k'}$ are product of electron and hole Slater determinants. The transformed Hamiltonian is expanded as a sum of 1-6 particle operators as shown below

$$G^\dagger H G = O_1 + O_2 + O_3 + O_4 + O_5 + O_6 \tag{3.8}$$

The matrix elements involving the operators $\{\langle \Phi_k | O_\alpha | \Phi_{k'} \rangle, \alpha = 1, \ldots, 6\}$ can be computed using the Slater-Condon rules for Slater determinants .[245] The integration Gaussian-type geminal function over Gaussian-type orbitals (GTOs) is well known [210] and was implemented for computation of the integrals. The exact form of the transformed Hamiltonian and the details about the operators are discussed in Ref. [9].

To test the performance of the XCCI method, benchmark calculations were performed for a parabolic quantum dot system [246, 247, 248, 188, 249, 187, 250]. The parabolic quantum dot has been used previously as a test bed for new methods and has used extensively to study various processes in quantum dots including thermodynamic properties [251], the effect of magnetic fields [252] and, more specifically the effect of electric field on the optical rectification coefficient in a GaAs parabolic QD [253]. The system consists of an electron-hole pair trapped in a three dimensional isotropic harmonic potential. The motions of the particles are correlated and the interaction between them is described by attractive Coulomb interaction . The

Table 3.1: GTO basis used for the FCI and XCCI calculations

Type	Exponent
S	2.500×10^{-1}
P	2.500×10^{-1}
D	2.500×10^{-1}
S	6.130×10^{-1}
P	6.130×10^{-1}
D	6.130×10^{-1}
S	1.176×10^{0}
P	1.176×10^{0}
D	1.176×10^{0}

Hamiltonian for the benchmark system for these calculations is as follows,

$$H = -\frac{1}{2m_\mathrm{e}}\nabla_\mathrm{e}^2 - \frac{1}{2m_\mathrm{h}}\nabla_\mathrm{h}^2 + \frac{1}{2}kr_\mathrm{e}^2 + \frac{1}{2}kr_\mathrm{h}^2 - \frac{1}{r_\mathrm{eh}} \tag{3.9}$$

where $m_\mathrm{e} = m_\mathrm{h} = 1$ and all quantities are expressed in atomic units. The force constant was set to $k = 0.25$ atomic units and was selected for direct comparison with previously reported [196] results. The XCCI method was used to calculate the ground state energy of the system and the result was compared with Hartree-Fock (HF) and full configuration interaction (FCI) calculations. Identical set of Gaussian-type orbitals (GTOs) were used for HF, FCI and XCCI and the angular momentum and exponents are presented in Table 3.1.

All the GTOs were centered at the minimum of the harmonic potential well. The exponents of the GTOs are obtained by minimizing the ground state FCI energy. In addition to the GTOs, the XCCI calculations also require the geminal coefficient and we have used the identical geminal coefficients that were used in earlier study on eh-XCHF. The list of b_k and γ_k used in the XCCI calculations is presented in Table 3.2.

Table 3.2: Parameters used in the Gaussian-type geminal function. These parameters were obtained from Ref. [9]

k	b_k	γ_k
1	1.0000	0.0000
2	1.2100	0.3500
3	0.4640	3.9600
4	0.5800	0.0900
5	0.2270	1.9000
6	0.2800	0.1000
7	0.1028	1.6700
8	-0.1020	0.3500

3.3 Results of benchmark calculations with XCCI method

The ground state energy from the XCCI calculations are compared with HF and FCI results in Table 3.3. It is seen that the XCCI energy is lower than the FCI energy by 0.228 eV. We attribute to this lowering of energy to the better description of the electron-hole wave function at r_{eh} distances. To analyze the effect of the electron-hole cusp on the quality of the eh-wave function, we compared the XCCI energy with the R12-FCI calculation reported earlier. The principle difference between the R12-FCI method with the methods presented here (XCCI and FCI) is that the R12-FCI calculation include the correct exponential form of the electron-hole cusp. The R12-FCI calculations are inherently more computationally expensive than the XCCI calculations because of the use STO basis functions . In contrast, the XCCI method uses GTG functions for approximating the eh-cusp . The integrals involving GTG functions are much easier to calculate and have been derived earlier by Boys and Persson. [210] The comparison between XCCI and R12-FCI results from Table 3.3 show that the XCCI energy is in good agreement with the R12-FCI results. These results indicate that the GTG function in the XCCI wave function provide a good approximation to the eh-cusp .

Table 3.3: Ground state energy (in Hartree) from HF, FCI, XCCI, and R12-FCI calculations

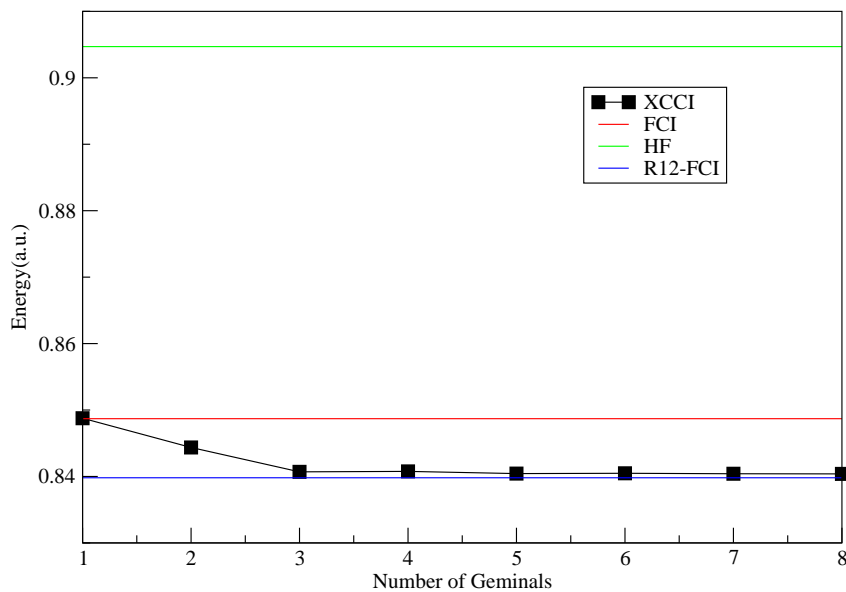| Method	Ground State Energy	$\eta(\%)$
HF	0.9047	0.0000
FCI	0.8488	86.252
XCCI	0.8403	99.156
R12-FCI [9]	0.8399	100.00

Figure 3-1: Convergence of the ground state XCCI energy as a function of number of terms in the Gaussian-type geminal function. Ground state energy from FCI, and R12-FCI calculations are also shown for comparison.

We define the electron-hole correlation energy as the energy difference between the HF and the other methods discussed here

$$E_\alpha^{\text{corr}} = E_\alpha - E_{\text{HF}} \quad \alpha = \text{FCI}, \text{XCCI}, \text{R12} - \text{FCI} \tag{3.10}$$

The percent correlation energy recovered by FCI and XCCI method is compared with the R12-FCI results by defining the following quantity

$$\eta = \frac{E_\alpha^{\text{corr}}}{E_{\text{R12}-\text{FCI}}^{\text{corr}}} \times 100 \tag{3.11}$$

and is presented in Table 3.3. It is seen that the XCCI method recovers 99.15% of the correlation energy.

To investigate the dependence of the XCCI energy on the quality of the geminal function we have performed a series of XCCI calculation by varying the number of geminal function from $N_{\text{g}} = 1, \ldots 8$ and the results are presented in Fig. 3-1. The geminal parameters used in these calculations are listed in Table 3.2. For the $N_{\text{g}} = 1$ calculations, the geminal parameters were chosen to make $G = 1$ so that the XCCI wave function becomes identical to the FCI wave function (see Eq. 3.5). As seen in Fig. 3-1 the XCCI energy coincides with the FCI energy at $N_{\text{g}} = 1$. Subsequent addition of geminal parameters makes XCCI energy lower than the FCI energy. We found that for $N_{\text{g}} \geq 4$, the XCCI energy exhibits convergence with respect to addition of geminal parameters. For comparison, the R12-FCI energy is also shown in Fig. 3-1 and it is seen that the XCCI energy approaches the R12-FCI energy with increasing number of geminal parameters . In principle, the XCCI and R12-FCI energy will be identical only in the limit of infinite basis. For any finite basis calculation, we expect XCCI energy that is converged with respect to number of GTG functions to be slightly higher than the R12-FCI calculation. We attribute this difference to approximate treatment of the electron-hole cusp by the GTG functions in the XCCI

Table 3.4: Comparison of the lowest seven eigenvalues of the Hamiltonian obtained using the FCI and XCCI method. All quantities are in atomic units

State number	FCI	XCCI
1	0.8488	0.8403
2	1.3668	1.3406
3	1.3668	1.3406
4	1.3668	1.3406
5	1.6064	1.6062
6	1.6064	1.6062
7	1.6064	1.6062

method. In addition to calculating the ground state energy, the XCCI method is also capable of calculating accurate excited state energies. The lowest seven eigenvalues of the Hamiltonian obtained using the XCCI and FCI method are presented in Table 3.4. Both XCCI and FCI methods give the expected degeneracy

of the first two excited states, however in both cases the XCCI energies are lower that FCI values.

3.4   Conclusions with respect to XCCI

In conclusion, the core concept of the XCCI method is to perform a CI from a correlated wave function as opposed to a mean-field reference wave function. The XCCI method provides a systematic procedure for improving the short-range description of the electron-hole wave function. As evident from the benchmark calculation, this significantly improves estimate of the ground and excited state energies. The use of the Gaussian-type geminal functions instead of STOs allows for fast evaluation of the integrals involving basis functions . Comparison between the XCCI and R12-FCI results indicate that the GTG functions provide a very good approximation to the eh-cusp.

Chapter 4

Congruent Transformation of the Hamiltonian and Application to the Helium Atom

4.1   Introduction and motivation for congruent transformation of the Hamiltonian

The form of the many-electron wave function in the proximity of the electron-electron and electron-nuclear coalescence point plays a critical role in accurate determination of the ground and excited state energies . Although, the precise structure of the many-electron wave function continues to be elusive, the form of the exact wave function at the coalescence point is well understood and is given by the Kato cusp condition [254, 255, 256, 257]. In the many-electron wave function, the electron-nuclear cusp condition can be incorporated by using Slater-type orbitals (STOs) . For calculations involving Gaussian-type orbitals (GTOs) , the one-electron basis can be improved iteratively by adding GTOs with increasing angular momentum quantum number [258] The subject of convergence. of single-particle basis has been analyzed extensively us-

ing both analytical and numerical techniques [259, 260, 261]. The electron-electron cusp has been the focus of intense research because of its direct relation to the electron correlation problem and accurate description of the Coulomb and Fermi hole [262, 263, 264, 214, 265]. However, unlike the electron-nuclear cusp, atom-centered basis functions are not ideal for accurate description of the many-electron wave function near the electron-electron cusp [266, 267, 268]. Indeed it has been shown that the slow convergence of a full configuration interaction (FCI) calculation with respect to the one-particle basis is related to the inadequate treatment of the electron-electron cusp [267]. The solution is to include explicit r_{12} dependence in the form of the wave function, and there is a large assortment of quantum chemical methods that have incorporated this approach. For example, in the variational Monte Carlo (VMC) method, the Jastrow function is used for including explicit r_{12} terms in the trial wave function [257, 255]. The form of the Jastrow is chosen to ensure that the electron-electron and electron-nuclear Kato cusp conditions are satisfied. The parameters in the Jastrow function are obtained by minimizing the linear combination of energy and its variance. Because of the complicated mathematical form of the Jastrow function it is not possible to evaluate the integral over the electronic coordinates analytically, and a stochastic numerical method is used for computation of the energy. Recently, Morales *et al.* performed highly accurate multi-determinant VMC calculations on water. [269] A detailed review of various applications of Quantum Monte Carlo (QMC) methods in physics and chemistry can be found in Ref. [270, 271, 159]. Explicitly correlated methods have also been developed for post Hartree-Fock schemes such as perturbation theory (MP2-R12), coupled-cluster methods (CC-R12), and multireference CI schemes (R12-MRCI) . These methods introduce the electron-electron inter-particle distance directly into the calculation in order to increase the accuracy of the calculations. The field of explicitly correlated methods for electronic structure calculation has been reviewed and a detailed description of various methods can

be found in Ref. [272, 267, 273]. A common feature of the R12 and F12 methods discussed above is that they all involve analytical computation of the r_{12} correlation function. Recently, Chinnamsetty and coworkers have presented an interesting study that compared and contrasted QMC with various F12 methods. [274]

A different strategy known as the transcorrelated method was developed by Handy and Boys in 1969. [275] The basic idea of the transcorrelated method is to remove the electron-electron Coulomb singularity by performing similarity transformation on the Hamiltonian using an explicitly correlated function. The method was later extended by Ten-no to treat the electron-electron cusp using Guassian geminal functions and was applied to chemical systems. [276, 261] The transcorrelated method has also been combined with other methods such as QMC [277] and coupled-cluster theory [278] and has been used to study electron correlation in periodic systems. [279] One of the defining characteristics of this method is that the transcorrelated Hamiltonian is not Hermitian and therefore is not required to be bounded from below by the exact ground state energy. The correlation function can be obtained either by minimizing the energy variance of the transcorrelated Hamiltonian [280, 281] or by requiring the correlation function to satisfy the electron-electron cusp condition.

The focus of the present work is to address the non-Hermitian property of the transcorrelated Hamiltonian by replacing the similarity transformation by congruent transformation . [282, 283, 284] By performing congruent transformation, we preserve the Hermitian property of the electronic Hamiltonian which allows us to use a standard electronic structure method such as configuration interaction method to minimize the total energy . The remainder of the paper describes the theoretical development and the implementation details of the method. The derivation of the congruent transformed Hamiltonian is presented in Sec. 4.2. Details of performing FCI calculations using the congruent transformed Hamiltonian and interfacing it with existing FCI methods are presented in Sec. 4.2.1 and 4.2.2. Benchmark calculations

using the congruent transformed Hamiltonian are presented in Sec. 4.3. The analysis of the results and conclusions are presented in Sec. 4.4.

4.2 Congruent transformed Hamiltonian

The congruent transformed (CT) Hamiltonian $\tilde{H}$ is defined by performing the following transformation [282, 283, 284]

$$\tilde{H} = G^{\dagger} H G, \tag{4.1}$$

where G is an explicitly correlated function which will be defined later. The expectation value of the CT Hamiltonian with respect to any trial wave function is given as

$$\tilde{E}_{\mathrm{T}}[\Psi_{\mathrm{T}}, G] = \frac{\langle \Psi_{\mathrm{T}} | \tilde{H} | \Psi_{\mathrm{T}} \rangle}{\langle \Psi_{\mathrm{T}} | \tilde{1} | \Psi_{\mathrm{T}} \rangle}, \tag{4.2}$$

where $\tilde{1} = G^{\dagger} 1 G$. The above expression is mathematically equivalent to calculating the expectation value of the electronic Hamiltonian using a correlated wave function and is bounded from below by the exact ground state energy $E_{\mathrm{exact}} \leq \tilde{E}_{\mathrm{T}}$. The optimized energy associated with the CT Hamiltonian is obtained by performing a minimization with respect to the trial wave function and explicitly correlated function,

$$E_{\mathrm{CT}} = \min_{\Psi_{\mathrm{T}}} \min_{G} \tilde{E}_{\mathrm{T}}[\Psi_{\mathrm{T}}, G]. \tag{4.3}$$

The optimization of the correlation function G and the trial wave function Ψ_{T} is conducted in two steps. In the first step, the form of the trial function is kept fixed to a single Slater determinant and the parameters of the geminal functions are determined by minimizing the geminal parameters and the molecular orbitals. In the

second step, the minimized geminal function G_{min} is kept fixed and the trial wave function Ψ_{T} is minimized. The steps involved are described by the following equation

$$\tilde{E}[G_{\mathrm{min}}] = \min_{G,\Phi_{\mathrm{SD}}} \tilde{E}_{\mathrm{T}}[\Phi_{\mathrm{SD}},G], \tag{4.4}$$

$$E_{\mathrm{CT}} = \min_{\Psi_{\mathrm{T}}} \tilde{E}_{\mathrm{T}}[\Psi_{\mathrm{T}},G_{\mathrm{min}}]. \tag{4.5}$$

The optimization of the correlation function and the trial wave function are described in the following subsections.

4.2.1   Optimization of the correlation function

The choice of the correlation function G plays an important part in the implementation of the method for practical applications. In principle, a variety of correlated functions such as two and three-body Jastrow functions can be used. However, the matrix elements associated with these functions cannot be integrated analytically and one has to use numerical techniques such as the VMC method to calculate the integrals. In the present work, Gaussian-type geminal (GTG) functions were used for the correlated functions. The GTG functions were introduced by Boys [285, 165] and Singer [286], and have been used extensively in explicitly correlated methods. [287, 288, 289, 290, 168, 291] Slater determinants augmented with GTG functions have been used to study electron-electron and electron-proton systems. The integrals involving GTG functions with GTOs can be performed analytically and have been derived earlier. [164, 210, 285, 165] The form of the correlated function used in the following calculations is defined as

$$G = \sum_{i<j}^{N} g(i,j), \tag{4.6}$$

60

$$g(i,j) = \sum_{k=1}^{N_g} b_k e^{-\gamma_k r_{ij}^2}, \qquad (4.7)$$

where N is number of electrons and N_g is the number of Gaussian functions. The geminal coefficients $\{b_k, \gamma_k\}$ in the GTG function are determined variationally. In the limit of $G \to 1$, the energy $\tilde{E}[G_{\min}]$ becomes equal to the Hartree-Fock energy.

$$E_{\text{HF}} = \lim_{G \to 1} \tilde{E}[G_{\min}], \qquad (4.8)$$

As a consequence, the HF energy is the upper bound to the geminal minimization process

$$\tilde{E}[G_{\min}] \leq E_{\text{HF}}. \qquad (4.9)$$

The transformed Hamiltonian is expanded as a sum of 2-6 particle operators as shown below

$$\tilde{H} = \sum_{i<j} \sum_{k} \sum_{m<n} g(m,n) h_1(k) g(i,j) + \sum_{i<j} \sum_{k<l} \sum_{m<n} g(i,j) r_{kl}^{-1} g(m,n), \qquad (4.10)$$

$$= O_2 + O_3 + O_4 + O_5 + O_6 \qquad (4.11)$$

where, the operators $\{O_n, n = 2, \ldots, 6\}$ are defined by collecting all two, three, four, five and six particle operators obtained by expanding the summation in Eq. (4.10).

Specifically,

$$O_2 = \sum_{i<j} h_2(i,j), \tag{4.12}$$

$$O_3 = \sum_{i<j<k} h_3(i,j,k), \tag{4.13}$$

$$O_4 = \sum_{i<j<k<l} h_4(i,j,k,l), \tag{4.14}$$

$$O_5 = \sum_{i<j<k<l<m} h_5(i,j,k,l,m), \tag{4.15}$$

$$O_6 = \sum_{i<j<k<l<m<n} h_6(i,j,k,l,m,n). \tag{4.16}$$

The exact form of the operators $\{h_n, n = 2, \ldots, 6\}$ have been derived earlier and are not duplicated here. It should be emphasized that the operators $\{h_n, n = 2, \ldots, 6\}$ are defined so that they are completely symmetric with respect to all $n!$ permutation of the indices

$$\mathcal{P}_k h_n = h_n \quad \text{where} \, \mathcal{P}_k \in S_n. \tag{4.17}$$

The operator $\mathcal{P}_k$ is the permutation operator that belongs to the complete symmetric group S_n. An important feature of this method is the availability of the analytical gradients of the total energy with respect to the geminal parameters. The gradients can be computed analytically and are given by the following expressions

$$\frac{\partial g(1,2)}{\partial b_k} = e^{-\gamma_k r_{12}^2}, \tag{4.18}$$

$$\frac{\partial g(1,2)}{\partial \gamma_k} = -b_k r_{12}^2 e^{-\gamma_k r_{12}^2}. \tag{4.19}$$

The AO integrals involving the gradients of the GTG functions are performed analytically and are computed with other AO integrals.

4.2.2   Optimization of the trial wave function

The optimization of the trial wave function Ψ_T is performed by performing a full configuration interaction (FCI) calculation on the congruent transformed Hamiltonian. The FCI wave function is constructed by performing all possible excitations from the reference wave function. [245] This can be represented by the following expression,

$$\Psi_{\text{FCI}} = C_0\Phi + \sum_a^{N_{\text{occ}}}\sum_p^{N_{\text{vir}}} C_a^p\Phi_a^p + \sum_{a<b}^{N_{\text{occ}}}\sum_{p<q}^{N_{\text{vir}}} C_{ab}^{pq}\Phi_{ab}^{pq} + \sum_{a<b<c}^{N_{\text{occ}}}\sum_{p<q<r}^{N_{\text{vir}}} C_{abc}^{pqr}\Phi_{abc}^{pqr} + \dots, \quad (4.20)$$

where we have retained N_{vir} in the expression to emphasize that only a finite number of terms are evaluated. This point will be a subject of discussion later in the derivation. The occupied and virtual orbitals are represented by $(a, b, c, \dots)$ and $(p, q, r, \dots)$, respectively, and the CI coefficients are represented by $(C_a^p, \dots)$ and are obtained variationally by minimizing the total energy . The construction of the full set of excitations and the determination of the CI coefficients are the two principle computational challenges associated with the FCI method. For very small molecules, the CI matrix can be explicitly constructed and diagonalized, however, this simple approach becomes prohibitively expensive as the system size increases. Currently, there are various computational techniques for efficient calculation of the expansion coefficients. [292, 293, 294, 295, 214, 296] The calculation requires matrix elements involving the operators $\{\langle\Phi_k|O_\alpha|\Phi_{k'}\rangle, \alpha = 2, \dots, 6\}$ which are derived below.

The matrix elements involving the 2-particle operators are evaluated as

$$\langle\Phi_0|O_2|\Phi_0\rangle = \frac{1}{2!}\sum_{k=1}^{2!}\sum_{i_1 i_2}^{N_{\text{occ}}}(-1)^{p_k}\langle i_1 i_2|h_2|P_k i_1 i_2\rangle, \quad (4.21)$$

$$\langle\Phi_0|O_2|\Phi_a^p\rangle = \frac{1}{1!}\sum_{k=1}^{2!}\sum_{i_1}^{N_{\text{occ}}}(-1)^{p_k}\langle a i_1|h_2|P_k p i_1\rangle, \quad (4.22)$$

$$\langle\Phi_0|O_2|\Phi_{ab}^{pq}\rangle = \sum_{k=1}^{2!}(-1)^{p_k}\langle ab|h_2|P_k pq\rangle. \quad (4.23)$$

The matrix elements involving the 3-particle operators are evaluated as

$$\langle\Phi_0|O_3|\Phi_0\rangle = \frac{1}{3!}\sum_{k=1}^{3!}\sum_{i_1i_2i_3}^{N_{\text{occ}}}(-1)^{p_k}\langle i_1i_2i_3|h_3|P_ki_1i_2i_3\rangle, \qquad (4.24)$$

$$\langle\Phi_0|O_3|\Phi_a^p\rangle = \frac{1}{2!}\sum_{k=1}^{3!}\sum_{i_1i_2}^{N_{\text{occ}}}(-1)^{p_k}\langle ai_1i_2|h_3|P_kpi_1i_2\rangle, \qquad (4.25)$$

$$\langle\Phi_0|O_3|\Phi_{ab}^{pq}\rangle = \sum_{k=1}^{3!}\sum_{i_1}^{N_{\text{occ}}}(-1)^{p_k}\langle abi_1|h_3|P_kpqi_1\rangle, \qquad (4.26)$$

$$\langle\Phi_0|O_3|\Phi_{abc}^{pqr}\rangle = \sum_{k=1}^{3!}(-1)^{p_k}\langle abc|h_3|P_kpqr\rangle. \qquad (4.27)$$

The matrix elements involving the 4-particle operators are evaluated as

$$\langle\Phi_0|O_4|\Phi_0\rangle = \frac{1}{4!}\sum_{k=1}^{4!}\sum_{i_1i_2i_3i_4}^{N_{\text{occ}}}(-1)^{p_k}\langle i_1i_2i_3i_4|h_4|P_ki_1i_2i_3i_4\rangle, \qquad (4.28)$$

$$\langle\Phi_0|O_4|\Phi_a^p\rangle = \frac{1}{3!}\sum_{k=1}^{4!}\sum_{i_1i_2i_3}^{N_{\text{occ}}}(-1)^{p_k}\langle ai_1i_2i_3|h_4|P_kpi_1i_2i_3\rangle, \qquad (4.29)$$

$$\langle\Phi_0|O_4|\Phi_{ab}^{pq}\rangle = \frac{1}{2!}\sum_{k=1}^{4!}\sum_{i_1i_2}^{N_{\text{occ}}}(-1)^{p_k}\langle abi_1i_2|h_4|P_kpqi_1i_2\rangle, \qquad (4.30)$$

$$\langle\Phi_0|O_4|\Phi_{abc}^{pqr}\rangle = \sum_{k=1}^{4!}\sum_{i_1}^{N_{\text{occ}}}(-1)^{p_k}\langle abci_1|h_4|P_kpqri_1\rangle, \qquad (4.31)$$

$$\langle\Phi_0|O_4|\Phi_{abcd}^{pqrs}\rangle = \sum_{k=1}^{4!}(-1)^{p_k}\langle abcd|h_4|P_kpqrs\rangle. \qquad (4.32)$$

The matrix elements involving the 5-particle operators are evaluated as

$$\langle\Phi_0|O_5|\Phi_0\rangle = \frac{1}{5!}\sum_{k=1}^{5!}\sum_{i_1i_2i_3i_4i_5}^{N_{\text{occ}}}(-1)^{p_k}\langle i_1i_2i_3i_4i_5|h_5|P_k i_1i_2i_3i_4i_5\rangle, \tag{4.33}$$

$$\langle\Phi_0|O_5|\Phi_a^p\rangle = \frac{1}{4!}\sum_{k=1}^{5!}\sum_{i_1i_2i_3i_4}^{N_{\text{occ}}}(-1)^{p_k}\langle ai_1i_2i_3i_4|h_5|P_k pi_1i_2i_3i_4\rangle, \tag{4.34}$$

$$\langle\Phi_0|O_5|\Phi_{ab}^{pq}\rangle = \frac{1}{3!}\sum_{k=1}^{5!}\sum_{i_1i_2i_3}^{N_{\text{occ}}}(-1)^{p_k}\langle abi_1i_2i_3|h_5|P_k pqi_1i_2i_3\rangle, \tag{4.35}$$

$$\langle\Phi_0|O_5|\Phi_{abc}^{pqr}\rangle = \frac{1}{2!}\sum_{k=1}^{5!}\sum_{i_1i_2}^{N_{\text{occ}}}(-1)^{p_k}\langle abci_1i_2|h_5|P_k pqri_1i_2\rangle, \tag{4.36}$$

$$\langle\Phi_0|O_5|\Phi_{abcd}^{pqrs}\rangle = \sum_{k=1}^{5!}\sum_{i_1}^{N_{\text{occ}}}(-1)^{p_k}\langle abcdi_1|h_5|P_k pqrsi_1\rangle, \tag{4.37}$$

$$\langle\Phi_0|O_5|\Phi_{abcde}^{pqrst}\rangle = \sum_{k=1}^{5!}\langle abcde|h_5|P_k pqrst\rangle. \tag{4.38}$$

The matrix elements involving the 6-particle operators are evaluated as

$$\langle\Phi_0|O_6|\Phi_0\rangle = \frac{1}{6!}\sum_{k=1}^{6!}\sum_{i_1i_2i_3i_4i_5i_6}^{N_{\text{occ}}}(-1)^{p_k}\langle i_1i_2i_3i_4i_5i_6|h_6|P_k i_1i_2i_3i_4i_5i_6\rangle, \tag{4.39}$$

$$\langle\Phi_0|O_6|\Phi_a^p\rangle = \frac{1}{5!}\sum_{k=1}^{6!}\sum_{i_1i_2i_3i_4i_5}^{N_{\text{occ}}}(-1)^{p_k}\langle ai_1i_2i_3i_4i_5|h_6|P_k pi_1i_2i_3i_4i_5\rangle, \tag{4.40}$$

$$\langle\Phi_0|O_6|\Phi_{ab}^{pq}\rangle = \frac{1}{4!}\sum_{k=1}^{6!}\sum_{i_1i_2i_3i_4}^{N_{\text{occ}}}(-1)^{p_k}\langle abi_1i_2i_3i_4|h_6|P_k pqi_1i_2i_3i_4\rangle, \tag{4.41}$$

$$\langle\Phi_0|O_6|\Phi_{abc}^{pqr}\rangle = \frac{1}{3!}\sum_{k=1}^{6!}\sum_{i_1i_2i_3}^{N_{\text{occ}}}(-1)^{p_k}\langle abci_1i_2i_3|h_6|P_k pqri_1i_2i_3\rangle, \tag{4.42}$$

$$\langle\Phi_0|O_6|\Phi_{abcd}^{pqrs}\rangle = \frac{1}{2!}\sum_{k=1}^{6!}\sum_{i_1i_2}^{N_{\text{occ}}}(-1)^{p_k}\langle abcdi_1i_2|h_6|P_k pqrsi_1i_2\rangle, \tag{4.43}$$

$$\langle\Phi_0|O_6|\Phi_{abcde}^{pqrst}\rangle = \sum_{k=1}^{6!}\sum_{i_1}^{N_{\text{occ}}}\langle abcdei_1|h_6|P_k pqrsti_1\rangle, \tag{4.44}$$

$$\langle\Phi_0|O_6|\Phi_{abcdef}^{pqrstu}\rangle = \sum_{k=1}^{6!}\langle abcdef|h_6|P_k pqrstu\rangle. \tag{4.45}$$

The computation of matrix elements in the above expression requires atomic orbital integrals involving the GTG functions. One of the advantages of using the GTG functions is that all the AO integrals needed for the CT Hamiltonian calculation can be computed analytically. Boys and Singer have derived the integrals involving GTG functions with s-type GTOs. Persson and Taylor have extended the method for higher angular momentum by using the Hermite Gaussian expansion approach. [210] Recently, Hofener and coworkers have also derived the geminal integrals by extending the Obara-Saika techniques for calculating the GTG integrals. [297]

The solution for the CI coefficients requires diagonalization of the CI Hamiltonian matrix. However, the lowest eigenvalue and eigenfunction can be obtained without explicit construction and storage of the CI matrix. There are various efficient methods such as the Davidson diagonalization to perform this task. [298] Recently, Alavi et al. have developed the FCIQMC method which allows very efficient evaluation of the FCI wave function. [299, 300, 301, 302, 303]

In the present calculation, the FCI eigenvector was obtained by performing the Nesbet update scheme and was selected because of its ease of implementation. [304] In the Nesbet method, a expansion coefficient c_μ is updated by Δc_μ

$$c_\mu = c_\mu + \Delta c_\mu, \tag{4.46}$$

where the update is calculated as

$$\Delta c_\mu = \frac{\sigma_\mu}{E\tilde{1}_{\mu\mu} - \tilde{H}_{\mu\mu}}, \tag{4.47}$$

$$\sigma_\mu = \sum_i \tilde{H}_{\mu i} c_i - E \sum_i \tilde{1}_{\mu i} c_i. \tag{4.48}$$

The energy is updated at each step using

$$\Delta E = \frac{\sigma_\mu \Delta c_\mu}{D + \Delta D}, \tag{4.49}$$

$$\Delta D = \Delta c_\mu \left[2 \sum_i S_{\mu i} c_i + S_{\mu\mu} \Delta c_\mu \right]. \tag{4.50}$$

The FCI energy can be recovered from the CT calculation by setting $G = 1$

$$E_{\text{FCI}} = \lim_{G \to 1} E_{\text{CT}}. \tag{4.51}$$

From the above relationship, we expect that the CTH energy calculated with G_{min} will be lower than the FCI results. In the following section, we perform CTH calculations on well-studied two-electron systems and compare calculated energies with reported benchmark values.

4.3   Calculations and results of benchmark systems

The Hooke's atom is one of the few correlated two-electron systems for which the Schrödinger equation can be solved analytically. This feature has made it a testing ground for a wide variety of methods. [305, 306, 307, 308] The Hooke's atom consists of two electrons in a parabolic potential. The Hamiltonian of that system can be written as

$$\hat{H} = -\frac{1}{2}\nabla_1^2 - \frac{1}{2}\nabla_2^2 + \frac{1}{2}kr_1^2 + \frac{1}{2}kr_2^2 + \frac{1}{r_{12}} \tag{4.52}$$

where, all the quantities are expressed in the atomic units. The interaction between an electron and the nucleus is described with the harmonic potential. For $k = 0.5 \, \text{a.u.}$, the Schrödinger equation can be solved exactly and the ground state energy is equal to 2.0 Hartrees. [196] The Hooke's atom provides an ideal ground for testing the
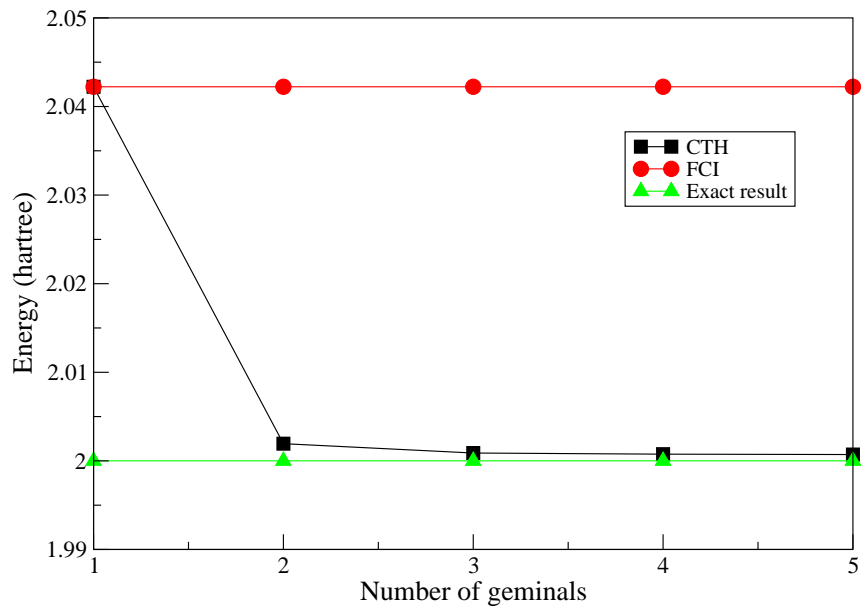
Figure 4-1: Comparison of the exact ground state energy of Hooke's atom with the results from CTH and FCI calculations.

CTH method . The CTH calculations were performed using the 6-311G basis and the geminal parameters were obtained variationally from the solution of Eq. (4.4). The energy was converged with respect to number of geminal parameters N_{g}, and the results are presented in Fig. 4-1. It is seen that the energy was converged after addition of four geminal parameters and the optimized geminal parameters are listed in Table 4.1.

Table 4.1: Geminal parameters for Hooke's atom using the 6-311G basis set

Number	b_k	γ_k
1	1.0000	0.0000
2	-0.6090	0.1050
3	-0.0709	2.350
4	0.0216	0.175
5	-0.0132	1.120

Table 4.2: Difference between exact and calculated energy Hooke's atom using the CTH method

Hartree	kcal/mol	kJ/mol	eV	cm^{-1}
0.000296	0.186	0.777	0.00805	65.0

Comparing the energy with the exact result of 2.0 Hartrees, it is seen that the $\tilde{E}[G_{\min}]$ is slightly higher by 0.770 mHartrees (or 0.483 kcal/mol) . The optimized Slater determinant Φ obtained in the previous step is used as the reference wave function for the CTH calculations and the results are summarized in Fig. 4-1. For $G = 1$, the CTH energy is identical to the FCI energy. However, inclusion of additional geminal terms makes the CTH energy lower than the energy from the FCI calculation. It is seen that the CTH energy is in good agreement with the exact analytical results and is higher by 0.000296 Hartrees, these results are provided in Table 4.2.
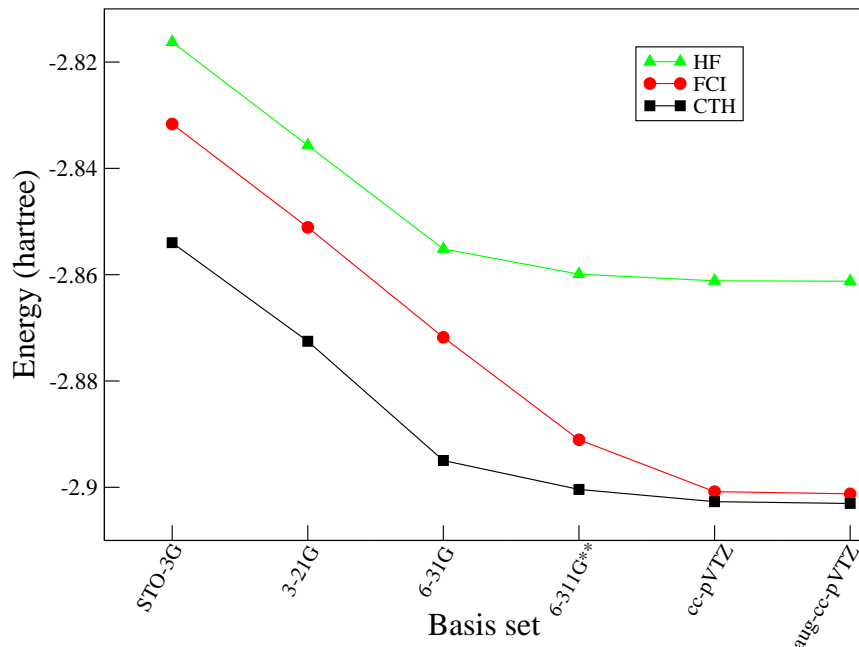
Figure 4-2: Effect of basis set on ground state energy of Helium for HF, FCI, and CTH methods.

The CTH calculations were also carried out for the helium atom and the results are presented in Fig. 4-2.

The calculations were performed using different basis functions , and the results were compared with HF and FCI values. It is seen that for small basis sets, the $\tilde{E}$ energy is lower than the FCI energy. We expect this because of the inclusion of the optimized geminal terms. The key result from Fig. 4-2 is that for small basis sets, the CTH method provides a substantial lowering of energy with respect to the corresponding FCI values. The CTH calculations with respect to a small basis provides a wave function that is comparable to the FCI wave function at much larger basis functions. Since the cost of the FCI expansion increases sharply with the size of the underlying 1-particle basis, the CTH method provides an appealing alternative for obtaining accurate results when an FCI calculation is prohibitively expensive. The dependence of the CTH energies on the number of geminal parameters is shown in
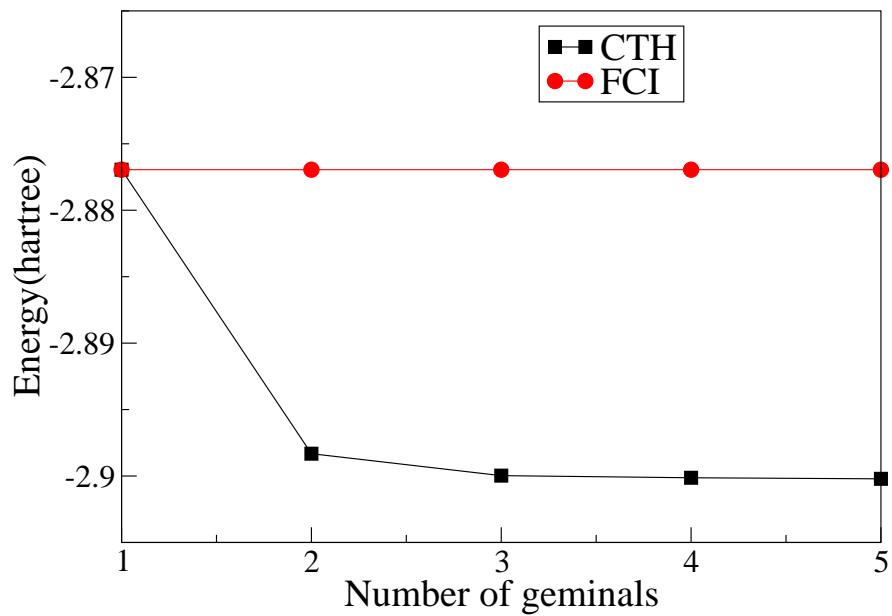
Figure 4-3: Convergence of the CT Hamiltonian energy of the Helium atom with respect to the number of geminal functions. The calculations were performed with 6-311G basis set.

Fig. 4-3 and the

optimized geminal parameters for the helium atom are listed in Table 4.3.

Table 4.3: Geminal parameters for Helium atom using 6-311G

Number	b_k	γ_k
1	1.000000	0.00000
2	-0.320260	0.57816
3	-0.063365	10.3760
4	0.020918	0.83536
5	-0.029282	0.08799

4.4 Discussion and conclusions

The first geminal parameter is always set to $b_1 = 1$ and $\gamma_1 = 0$ and is never optimized during the calculations. When all the other $N_{\mathrm{g}} - 1$ geminal parameters are set to zero, these values of b_1 and γ_1 represent the $G = 1$ limit. Geminal parameters from $b_2 \ldots b_{N_{\mathrm{g}}}$ and $\gamma_2 \ldots \gamma_{N_{\mathrm{g}}}$ are optimized to obtain $G_{\min}$ as described in Eq. (4.4). This procedure ensures that the optimized energy is always bounded from above by the HF energy. Figures 4-1 and 4-2 show the effect of inclusion of additional geminal parameters and it is seen that the second geminal parameter lowers the energy significantly. This is an important result and clearly indicates the importance of the geminal function in construction of the congruent transformed Hamiltonian. The set of $\{b_k\}$ was optimized without any constraint and it is seen from Tables 4.1 and 4.3 that the overal geminal parameter is negative. This is an expected result and is in agreement with previous work on explicitly correlated methods. [297, 309, 310] The negative values of geminal parameters indicate the role of the geminal function in providing a better description of the Coulomb hole.

The analytical forms of the GTG functions are inherently approximate and are not capable of describing the cusp correctly because their first derivative vanishes in the limit of $r_{\mathrm{ee}} = 0$

$$\left(\frac{\partial G}{\partial r_{\mathrm{ee}}} \right)_{r_{\mathrm{ee}} = 0} = 0. \tag{4.53}$$

Table 4.4: Comparison of ground state energy (in Hartrees) of the helium atom

E	function	ref
-2.900233	FCI	[320]
-2.903041	CTH	this work
-2.903724377034119598311592245194404446969	free ICI	[314, 315]

To assess the quality of the CTH energy, it is important to estimate how much of an error this feature introduces in the calculated energy. For the Hooke's atom this can be done in a a straightforward manner since the analytical solution of the Schrödinger equation is known. From Table 4.2, it is seen that the CTH energy is close to the exact ground state energy and is higher by 0.296 mHartrees or 0.186 kcal/mol. This difference between the CTH and the exact energy represents the upper bound in the error that one can expect for this system by approximating the cusp with GTG functions. For the helium atom , the situation is less straightforward because we do not have access to the exact solution. Instead, we compared the CTH energies with other high-level methods from previous studies [311, 312, 313, 314, 315, 316, 317, 318, 319] that include the exact cusp condition in the wave function. In order to achieve the best CTH energy, the calculation was performed with an aug-cc-pVTZ basis set and geminal parameters were optimized with respect to the aug-cc-pVTZ basis. Comparing the CTH method with the highly accurate ICI method by Nakatsuji [314, 315], it is seen that CTH energy is higher than the ICI energy by 0.429 kcal/mol. The comparison of the CTH calculation to the ICI method and other highly accurate results can be seen in Table 4.4.

The impact of electron-electron cusp on ground state energy was investigated in detail by Prendergast [214] and coworker using CI and QMC methods. Their study concluded that one can still expect to get mHartree level of accuracy even in situations where the exact cusp condition is not satisfied. Our study using GTG functions also confirms this observation. The use of GTG functions in the CTH

method, represents a trade-off between the implementation of exact cusp condition and analytical expression for computing the Gaussian-type geminal integrals.

One of the objectives of the CTH method is to address the factorial scaling of the FCI calculation with respect to the basis size. As discussed above, the CTH method can give results that are comparable to FCI calculation at larger basis function. As the system size increases, the computation cost of the CTH method will be dominated by the calculation and storage of the many-particle integrals. Therefore, additional optimization techniques must be used for efficient implementation of the CTH method. Some of the many-particle integrals can be factorized as products of lower dimensional integrals. For example, five and six particle integrals of the form

$$\langle i_1 i_2 i_3 i_4 i_5 i_6 | g(1,2) r_{34}^{-1} g(5,6) | j_1 j_2 j_3 j_4 j_5 j_6 \rangle = \langle i_1 i_2 | g(1,2) | j_1 j_2 \rangle \langle i_3 i_4 | r_{34}^{-1} | j_3 j_4 \rangle \quad (4.54)$$
$$\times \langle i_5 i_6 | g(5,6) | j_5 j_6 \rangle$$

can be factored exactly in term to lower dimensional integrals. The many-particle integrals that cannot be factorized exactly into lower-dimensional integrals can be approximately factorized by using the resolution of identity (RI) approach that has been used extensively in R12 and F12 methods. The RI scheme not only reduces the complexity of evaluating the integrals but also helps in reducing the memory requirement for storing the integrals. We have implemented the RI-CTH method and have performed calculation on a series of 10 isoelectronic systems. However, the implementation details are beyond the present discussion and are presented in a separation article.

In addition to the RI extension, the CTH method can also be used for computation of excited state energies . One of the key aspects of the correlation function used in the congruent transformation is that it is completely symmetric operator and belongs to the A1 irreducible representation. The congruent transformed Hamilto-

nian and identity operators retain their A1 symmetry. Consequently, eigenfunctions of different symmetry are orthogonal to each other and the CTH method can be used for computation of excited states with different symmetry that the ground state wave function. Excited states that are of same symmetry than the ground state pose additional challenges and will be investigated in future studies.

In conclusion, the congruent transformation of the electronic Hamiltonian using Gaussian type geminal function is presented as a general method for calculating accurate ground state energy. The form of the congruent transformed Hamiltonian can be systematically improved by using the geminal function. It was found that a small number of geminal functions are needed to converge the energy. Furthermore, addition of just one geminal parameter results in a substantial improvement in the accuracy of the wave function. For a given finite basis set the CTH energy was found to be lower that the FCI calculation on untransformed Hamiltonian. The results indicate that the congruent transformed Hamiltonian provides a viable alternative for obtaining FCI quality energy using a smaller underlying 1-particle basis set.

Chapter 5

Investigation of Optical Properties of CdSe Quantum Dots using XCHF Method

5.1 Introduction and motivation for using explicitly correlated Hartree-Fock for the study of CdSe quantum dots

Semiconductor quantum dots and rods have been the focus of intense theoretical and experimental research because of inherent size-dependent optical and electronic properties. Generation of bound electron-hole pairs (excitons) and their subsequent dissociation into free charge carriers are the two important factors that directly impact the light-harvesting efficiency of the semiconductor quantum dots. The dissociation of excitons is a complex process that is influenced by various factors such as shape and size of the quantum dots, [50, 46, 45, 42, 54, 321] presence of surface defects, [322, 323, 324] surface ligands, [325, 326] and coupling with phonon

modes. [148, 327, 328, 329, 330, 331, 332, 333] The energetics of the electron-hole interaction in quantum dots is quantified by the exciton dissociation energy and has been determined using both theoretical and experimental techniques [334, 58, 335]. Generation of free charge carriers by exciton dissociation has been facilitated by introducing core/shell heterojunctions [336, 62, 337], and applying external and ligand-induced electric fields . [338, 339, 340, 341, 139, 342]

One of the direct routes for enhancing exciton dissociation is by modifying the size and shape of quantum dots. Studies on CdSe and other quantum dots have shown that the exciton binding energy decreases with increasing dot size. [3, 2, 4, 36, 37, 1, 5, 6, 7] The size of the quantum dots has significant impact on the Auger recombination, [38, 39] multiple exciton generation [40, 41, 42, 43], and blinking effect in quantum dots [44, 45, 46]. In addition to exciton binding energy, the spatial distribution of electrons and holes in quantum dots also provides important insight into the exciton dissociation process. [343, 344] Electron and hole densities $\rho_e(\mathbf{r})$ and $\rho_h(\mathbf{r})$ have been widely used to investigate quasi-particle distribution in quantum dots. [336, 62] For example in core/shell quantum dots, presence of the heterojunction induces asymmetric spatial distribution of electrons and holes which, in turn, facilitates the exciton dissociation. Asymmetric electron probability density in the shell region of the core/shell quantum dots has been attributed to fast electron transfer from the quantum dots. [336, 62, 345, 64]

The central challenge in the theoretical investigation of quantum dots is efficient computational treatment of large number of electrons in the system. For small clusters where all-electron treatment is feasible, ground state and excited-state calculations have been performed using GW Bethe-Salpeter , [346, 347, 348] density functional theory (DFT) [349, 350, 351, 352, 353, 354, 355], time-dependent DFT (TDDFT) [356, 357, 68, 358, 359, 360, 147, 149], and MP2 [361]. For bigger quantum dots where all-electron treatment is computationally prohibitive, atomistic semiem-

perical pseudopotential methods have been used extensively. [3, 1, 151, 39, 362] In this approach, the one-particle Schrödinger equation incorporating the pseudopotential v_ps

$$\left[-\frac{\hbar^2}{2m} \nabla^2 + v_\mathrm{ps} \right] \phi_i = \lambda_i \phi_i, \tag{5.1}$$

is solved and the eigenfunctions are used in construction of the quasiparticle states [1, 3]. The quasiparticle states serve as a basis for both configuration interaction (CI) and perturbation theory calculations. Solution of Eq. (5.1) is generally obtained by introducing a set of basis functions (typically plane-waves), constructing the Hamiltonian matrix in that basis, and diagonalizing it. The computational efficiency of CI has been greatly improved by using only states near the band gap for construction of the CI space. [1, 363] This technique alleviates the need to compute the entire eigenspectrum of the Hamiltonian matrix, however, successful implementation of this approach requires computation of selected eigenvalues and eigenfunctions of the Hamiltonian matrix. Computation of the specific eigenvalues of large matrices is challenging and various methods such as the folded-spectrum method [364, 365], filter-diagonalization method [366, 361], and generalized Davidson method [367, 368] have been specifically developed to address this problem.

The main goal of this article is to compare the effect of dot size on exciton binding energy and electron-hole recombination probability . The central quantity of interest for the present work is the electron-hole pair density $\rho_\mathrm{eh}(\mathbf{r}_\mathrm{e}, \mathbf{r}_\mathrm{h})$. The electron-hole pair density is defined as the probability density of finding an electron and a hole in the neighborhood of $\mathbf{r}_\mathrm{e}$ and $\mathbf{r}_\mathrm{h}$, respectively. The pair density is a mathematically complicated quantity and is generally obtained from an underlying wave function . Direct construction of the pair-density is also possible as long as $N-$ representability can be enforced [369]. For an interacting electron-hole system, the pair density is not

78

equal to the product of electron and hole densities

$$\rho_{\text{eh}}(\mathbf{r}_{\text{e}}, \mathbf{r}_{\text{h}}) \neq \rho_{\text{e}}(\mathbf{r}_{\text{e}})\rho_{\text{h}}(\mathbf{r}_{\text{h}}). \tag{5.2}$$

Furthermore, the electron-hole pair density contains information about the correlated spatial distribution of the electrons and hole that cannot be obtained from the product of individual electron and hole densities. Both electron-hole recombination probability and exciton binding energy can be computed from the pair density. The electron-hole interaction energy V_{eh} is the major component of the exciton binding energy and can be calculated from the electron-hole pair density using the following expression,

$$V_{\text{eh}} = \int d\mathbf{r}_{\text{e}}d\mathbf{r}_{\text{h}} \ \rho_{\text{eh}}(\mathbf{r}_{\text{e}}, \mathbf{r}_{\text{h}})r_{\text{eh}}^{-1}\epsilon^{-1}(\mathbf{r}_{\text{e}}, \mathbf{r}_{\text{h}}), \tag{5.3}$$

where, $\epsilon^{-1}(\mathbf{r}_{\text{e}}, \mathbf{r}_{\text{h}})$ is the inverse dielectric function. The electron-hole recombination probability, P_{eh}, is related to the pair density as

$$P_{\text{eh}} = \frac{1}{N_{\text{e}}N_{\text{h}}} \int d\mathbf{r}_{\text{e}} \int_{\mathbf{r}_{\text{e}}-\frac{\Delta}{2}}^{\mathbf{r}_{\text{e}}+\frac{\Delta}{2}} d\mathbf{r}_{\text{h}} \ \rho_{\text{eh}}(\mathbf{r}_{\text{e}}, \mathbf{r}_{\text{h}}), \tag{5.4}$$

where N_{e} and N_{h} are number of electrons and holes, respectively. In the above equation, we define electron-hole recombination probability as the probability of finding a hole in a cube of volume Δ^3 centered at the electron position. The computation of the recombination probability is especially demanding because it requires evaluation of the pair density at small interparticle distances. As a consequence, the form of the electron-hole wave function near the electron-hole coalescence point is very important. [9, 140, 138, 146, 145, 370] In the present work, we address this challenge by using the electron-hole explicitly correlated Hartree-Fock (eh-XCHF) method presented in earlier chapters. The eh-XCHF method is a variational method where the wave function depends explicitly on the electron-hole interparticle distance and has

been used successfully for investigating electron-hole interaction. [9, 140, 139]

5.2 Theoretical details of eh-XCHF method for the study of CdSe quantum dots

In the eh-XCHF method the electron-hole wave function is represented by multiplying the mean-field wave function with an explicitly correlated function as shown in the following equation

$$\Psi_{\text{eh}-\text{XCHF}} = G\Phi^{\text{e}}\Phi^{\text{h}}, \tag{5.5}$$

where Φ^{e} and Φ^{h} are electron and hole Slater determinants and G is a Gaussian-type geminal (GTG) function [165] which is defined as,

$$G(\mathbf{r}^{\text{e}}, \mathbf{r}^{\text{h}}) = \sum_{i=1}^{N_{\text{e}}} \sum_{j=1}^{N_{\text{h}}} \sum_{k=1}^{N_{\text{g}}} b_k \exp[-\gamma_k r_{ij}^2]. \tag{5.6}$$

The GTG function depends on the r_{eh} term and is responsible for incorporating electron-hole inter-particle distance dependence in the eh-XCHF wave function. The coefficients b_k and γ_k are expansion coefficients which are obtained variationally. The Gaussian-type geminal functions have been used extensively in explicitly correlated methods for treating electron-electron correlation in many-electron systems. [266, 371] They have also been used successfully for treating electron-hole correlation. [9, 140] The use of Gaussian-type geminal functions offers three principle advantages. First, the variational determination of the geminal parameters $\{b_k, \gamma_k\}$ results in accurate description of the wave function near the electron-hole coalescence point. As can be seen in Eq. (6.16) the electron-hole recombination probability strongly depends on the form of the electron-hole wave function at small interparticle distances. Conse-

quently, the use of Gaussian-type geminal functions and the variational determination of the geminal parameters are crucial for accurate computation of electron-hole recombination probability. The importance of the geminal function for the present work is highlighted in Sec. 5.4.5. Second, the integrals of GTG functions with Gaussian-type orbitals (GTO) can be performed analytically and have been derived earlier by Boys[165] and Persson et al. [164] This alleviates the need to approximate the integrals using numerical methods. The third advantage of the GTG function is that it allows construction of a compact representation of an infinite-order configuration interaction expansion. This can be seen explicitly by introduction of the closure relationship,

$$G|\Psi_{\text{ref}}\rangle = \underbrace{\sum_{ii'}^{\infty} |\Phi_i^{\text{e}}\Phi_{i'}^{\text{h}}\rangle\langle\Phi_i^{\text{e}}\Phi_{i'}^{\text{h}}|}_{1} G|\Psi_{\text{ref}}\rangle. \tag{5.7}$$

The electron-hole interaction was described using the effective electron-hole Hamiltonian[137, 370, 206, 138, 205, 372, 373, 374, 375, 142, 376, 203] which is defined in the following equation

$$
\begin{aligned}
H = &\sum_{ij}\langle i|\frac{-\hbar^2}{2m_{\text{e}}}\nabla_{\text{e}}^2 + v_{\text{ext}}^{\text{e}}|j\rangle e_i^{\dagger}e_j \\
&+ \sum_{ij}\langle i|\frac{-\hbar^2}{2m_{\text{h}}}\nabla_{\text{h}}^2 + v_{\text{ext}}^{\text{h}}|j\rangle h_i^{\dagger}h_j \\
&+ \sum_{iji'j'}\langle iji'j'|\epsilon^{-1}r_{\text{eh}}^{-1}|iji'j'\rangle e_i^{\dagger}e_j h_{i'}^{\dagger}h_{j'} \\
&+ \sum_{ijkl}w_{ijkl}^{\text{ee}}e_i^{\dagger}e_j^{\dagger}e_l e_k + \sum_{ijkl}w_{ijkl}^{\text{hh}}h_i^{\dagger}h_j^{\dagger}h_l h_k.
\end{aligned} \tag{5.8}
$$

The effective electron-hole Hamiltonian provides a computationally efficient route for investigating large systems and in the present work was used for investigating CdSe clusters in the range of $Cd_{20}Se_{19}$ to $Cd_{74608}Se_{74837}$. We have also developed eh-XCHF

method using a pseudopotential [377], but the current implementation is restricted to cluster sizes of 200 atoms and cannot be applied to large dot sizes.

The effective Hamiltonian in Eq. (6.3) was used in combination with parabolic potential which has been used extensively [247, 246, 248, 188, 250, 187, 249, 252, 251, 253] for approximating the confining potential in quantum dots and wires. The electron and hole external potentials v_{ext}^{α} were expressed as

$$v_{\text{ext}}^{\alpha} = \frac{1}{2}k_{\alpha}|\mathbf{r}_{\alpha}|^2 \quad \alpha = \text{e}, \text{h}. \tag{5.9}$$

The form of the external potential directly impacts the electron-hole pair density and is important for accurate computation of the binding energy and recombination probability. In this work, we have developed a particle number based search procedure for determining the external potential. The central idea of this method is to find an external potential such that the computed 1-particle electron and hole densities are spatially confined within the volume of the quantum dot. Mathematically, this is implemented by obtaining the force constant k by the following minimization process

$$\min_{k_{\alpha}^{\min}} \left(N_{\alpha} - \int_0^{\frac{D_{\text{dot}}}{2}} dr r^2 \int d\Omega \rho_{\alpha}(\mathbf{r})[v_{\text{ext}}^{\alpha}] \right)^2, \tag{5.10}$$

where $\alpha = \text{e}, \text{h}$, $d\Omega = sin\theta d\theta d\phi$, D_{dot} is the dot diameter, and $k_{\alpha}^{\min}$ is the smallest force constant that satisfies the above minimization conditions. The single-particle density is a functional of the external potential and is denoted explicitly in the above equation.

The eh-XCHF wave function is obtained variationally by minimizing the eh-XCHF energy

$$E_{\text{eh}-\text{XCHF}} = \min_{G,\Phi^{\text{e}},\Phi^{\text{h}}} \frac{\langle \Psi_{\text{eh}-\text{XCHF}}|H|\Psi_{\text{eh}-\text{XCHF}}\rangle}{\langle \Psi_{\text{eh}-\text{XCHF}}|\Psi_{\text{eh}-\text{XCHF}}\rangle}. \tag{5.11}$$

Instead of evaluating the above equation directly, it is more efficient to first transform the operators and then perform the integration over the coordinates. The transformed operators are obtained by performing congruent transformation [141, 378] which is defined as follows

$$\tilde{H} = G^\dagger H G \tag{5.12}$$

$$\tilde{1} = G^\dagger G. \tag{5.13}$$

The eh-XCHF energy is obtained from the transformed operators using the following expression

$$E_{\text{eh−XCHF}} = \frac{\langle \Phi^e, \Phi^h | \tilde{H} | \Phi^e, \Phi^h \rangle}{\langle \Phi^e, \Phi^h | \tilde{1} | \Phi^e, \Phi^h \rangle}. \tag{5.14}$$

The above equation allows us to reduce the minimization over the electron and hole Slater determinants in terms of coupled self-consistent field (SCF) equations as shown below [167]

$$\mathbf{F}_G^e[\mathbf{C}^h]\mathbf{C}^e = \lambda^e \mathbf{S}_G^e \mathbf{C}^e \tag{5.15}$$

$$\mathbf{F}_G^h[\mathbf{C}^e]\mathbf{C}^h = \lambda^h \mathbf{S}_G^h \mathbf{C}^h. \tag{5.16}$$

This is identical to the Roothaan-Hall equation where $\mathbf{F}_G^e$ and $\mathbf{F}_G^e$ are Fock matrices for electron and holes, respectively. The subscript G in the above expression denotes that the Fock operators were obtained from the congruent transformed Hamiltonian and include contribution from the geminal operator. The functional form of the congruent transformed operators and the Fock operators have been derived earlier and can be found in previous chapters. The single-particle basis for electrons and holes

Table 5.1: Material parameters for the CdSe quantum dots used in the electron-hole Hamiltonian

Property	Value (Atomic units) [138]
m_e	0.13
m_h	0.38
ϵ	6.2

are constructed from the eigenfunctions of zeroth order single-particle Hamiltonian

$$H_0^\alpha \phi_i^\alpha = E_i^\alpha \phi_i^\alpha \quad \alpha = \mathrm{e}, \mathrm{h}. \tag{5.17}$$

where the zeroth-order Hamiltonian is obtained from H using the following limiting condition

$$H_0 = H_0^\mathrm{e} + H_0^\mathrm{h} = \lim_{\mathrm{r_{eh}} \to \infty} H. \tag{5.18}$$

The exciton binding energy is computed using the following expression

$$E_\mathrm{EB} = (E_0^\mathrm{e} + E_0^\mathrm{h}) - E_\mathrm{eh-XCHF}. \tag{5.19}$$

5.3   Computational details

The material parameters for the CdSe quantum dots used in the electron-hole Hamiltonian in Eq. (6.3) were obtained from Ref. [138] and are presented in Table 5.1. The single-particle basis was constructed using a set of ten s,p,d GTOs as shown in Eq. (5.20)

$$\phi = x^n y^m z^l e^{-\alpha r^2}. \tag{5.20}$$

Table 5.2: Parameters for the external potential and the GTOs used in the eh-XCHF calculation. All values are given in atomic units.

D_{dot}(nm)	k_e	k_h	α_e	α_h
1.24	2.66×10^{-2}	9.10×10^{-3}	2.94×10^{-2}	2.94×10^{-2}
1.79	6.22×10^{-3}	2.13×10^{-3}	1.42×10^{-2}	1.42×10^{-2}
2.76	1.10×10^{-3}	3.76×10^{-4}	5.98×10^{-3}	5.98×10^{-3}
2.98	8.10×10^{-4}	2.77×10^{-4}	5.13×10^{-3}	5.13×10^{-3}
3.28	5.52×10^{-4}	1.89×10^{-4}	4.24×10^{-3}	4.24×10^{-3}
3.79	3.09×10^{-4}	1.06×10^{-4}	3.17×10^{-3}	3.17×10^{-3}
4.80	1.20×10^{-4}	4.12×10^{-4}	1.98×10^{-3}	1.98×10^{-3}
6.60	3.38×10^{-5}	1.16×10^{-5}	1.05×10^{-3}	1.05×10^{-3}
10.0	6.41×10^{-6}	2.19×10^{-6}	4.57×10^{-4}	4.57×10^{-4}
15.0	1.26×10^{-6}	4.33×10^{-7}	2.03×10^{-4}	2.03×10^{-4}
20.0	4.01×10^{-7}	1.37×10^{-7}	1.14×10^{-4}	1.14×10^{-4}

The exponent of the GTOs and the force constants for the external potential used in the calculations are presented in Table 5.2. A set of three geminal functions were used for each dot size, where the geminal parameters were optimized variationally. The optimized parameters for all the dot sizes are presented in Table 5.3. The first set of geminal parameters were always set to $b_1 = 1$ and $\gamma_1 = 0$ to ensure that the eh-XCHF energy is always bounded from above by the mean-field energy during the geminal optimization. [9, 140]

5.4 Results of calculations

5.4.1 Exciton binding energy

The exciton binding energy was computed for a series of CdSe clusters ranging from $Cd_{20}Se_{19}$ to $Cd_{74608}Se_{74837}$. The approximate diameters of these quantum dots are in the range of 1 to 20nm, respectively and the results are presented in Table 5.4. It is seen that binding energy decreases as the size of the quantum dot increases. This trend is in agreement with earlier results. [3, 2, 4] In Figure 5-1, the computed binding energies are compared with previously reported experimental and theoretical results

Table 5.3: Optimized geminal parameters obtained by minimizing the eh-XCHF energy. The first set of geminal parameters were set to $b_1 = 1$ and $g_1 = 0$ and the details are presented in the text. All values are given in atomic units.

D_{dot}(nm)	b_2	b_3	γ_2	γ_3
1.24	3.06	2.55×10^{-1}	1.40×10^{-3}	1.79×10^{-1}
1.79	2.16	2.69×10^{-1}	1.20×10^{-3}	9.80×10^{-2}
2.76	1.79	3.49×10^{-1}	9.00×10^{-4}	4.62×10^{-2}
2.98	1.69	3.50×10^{-1}	9.00×10^{-4}	4.21×10^{-2}
3.28	2.24	4.46×10^{-1}	7.00×10^{-4}	2.04×10^{-2}
3.79	1.98	4.56×10^{-1}	7.00×10^{-4}	2.01×10^{-2}
4.80	2.43	6.34×10^{-1}	6.00×10^{-4}	1.94×10^{-2}
6.60	2.43	8.05×10^{-1}	5.00×10^{-4}	1.71×10^{-2}
10.0	2.81	9.39×10^{-1}	5.00×10^{-4}	1.83×10^{-2}
15.0	3.35	1.29	4.00×10^{-4}	2.00×10^{-4}
20.0	3.27	1.38	2.00×10^{-4}	3.00×10^{-2}

Table 5.4: Exciton binding energy calculated using eh-XCHF method as function of dot diameter.

D_{dot}(nm)	Cd_xSe_y	E_{BE}(eV)
1.24	$Cd_{20}Se_{19}$	0.855
1.79	$Cd_{47}Se_{57}$	0.595
2.76	$Cd_{199}Se_{195}$	0.389
2.98	$Cd_{232}Se_{257}$	0.360
3.28	$Cd_{311}Se_{352}$	0.329
3.79	$Cd_{513}Se_{515}$	0.285
4.80	$Cd_{1012}Se_{1063}$	0.225
6.60	$Cd_{2704}Se_{2661}$	0.167
10.0	$Cd_{9338}Se_{9363}$	0.111
15.0	$Cd_{31534}Se_{31509}$	0.078
20.0	$Cd_{74608}Se_{74837}$	0.066

[3, 2, 4, 1, 5, 6, 7]. For D_{dot} equal to 1.8, 3.32 and 4.82 nm, Franceschetti and Zunger
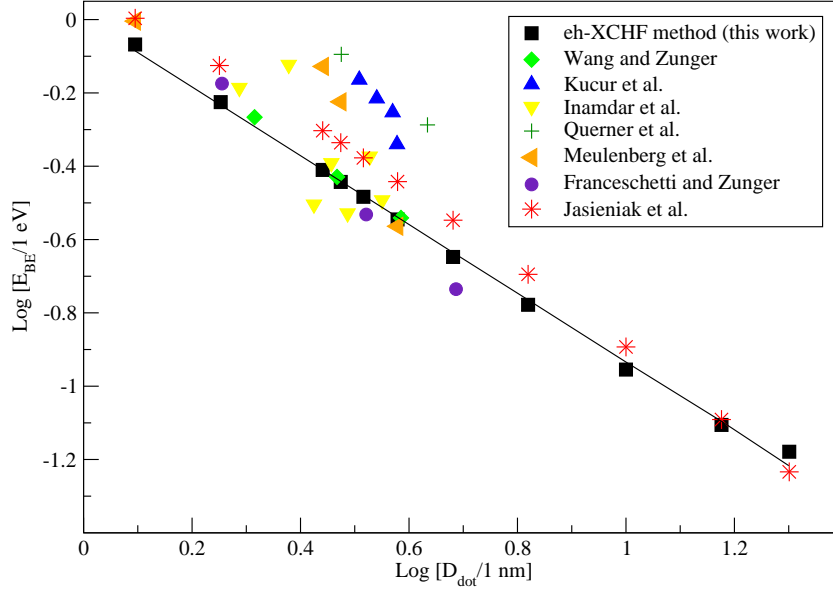
Figure 5-1: Log of binding energy (E_{BE}) versus log of diameter for CdSe quantum dots. The values from the eh-XCHF calculations are compared with results from earlier studies by Wang et al. [1], Franceschetti et al. [2], Meulenberg et al. [3], Jasieniak et al. [4], Kucur et al. [5], Inamdar et al. [6], and Querner et al. [7] The details of the comparison are presented in the text.

have computed binding energies using an atomistic pseudopotential based configuration interaction method, [3] and the exciton binding energies shown in Figure 5-1 were obtained from the tabulated values in Ref. [3]. In a recent combined experimental and theoretical investigation, Jasieniak et al. [4] have reported size-dependent valence and conduction band energies of CdSe quantum dots. The values from the Jasieniak et al. studies in Figure 5-1 were obtained from the least-square fit equation provided in Ref. [4]. The remaining data points were obtained from the plot in Ref. [4]. The log-log plot in Figure 5-1 shows that the computed binding energy is described very well by a linear-fit and the exciton binding energy scales as D^{-n} with respect to the dot

size. This observation is consistent with the trend observed in earlier studies. [3, 2, 4] We find that the exciton binding energies from the eh-XCHF calculations are in very good agreement with the atomistic pseudopotential calculations by Wang et al. [1] and Franceschetti et al. [3] Comparing between eh-XCHF and Jasieniak et al. [4] results show that the eh-XCHF values are lower than the Jasieniak et al. values for small dot sizes, but the difference becomes smaller with increasing dot size. One possible explanation for this observation is that smaller quantum dots have high surface to volume ratios and their optical properties are dominated by surface effects [379, 102] which are not currently included in the eh-XCHF calculations. The plot in Figure 5-1 highlights the ability of the eh-XCHF method to predict exciton binding energies for large quantum dots.

5.4.2   Electron-hole Coulomb energy

Another important quantity that is directly related to the electron-hole interaction is the electron-hole Coulomb energy . We have used the definition given by Franceschetti and Zunger [3] and calculated the electron-hole Coulomb energy using the following expression

$$A = \int d\mathbf{r}_\mathrm{e} d\mathbf{r}_\mathrm{h} \ \rho_\mathrm{eh}(\mathbf{r}_\mathrm{e}, \mathbf{r}_\mathrm{h}) r_\mathrm{eh}^{-1}. \tag{5.21}$$

In Figure 5-2, we have compared the electron-hole Coulomb energy with the pseudopotential+CI calculations by Franceschetti and Zunger and the results were found to be in good agreement with each other. The Coulomb energy is a very important quantity because it allows us to directly compare the quality of electron-hole pair density without introducing any additional approximation due to the choice of the dielectric function used for computation of the binding energy . The good agreement between the two methods provides important verification of the implementation of
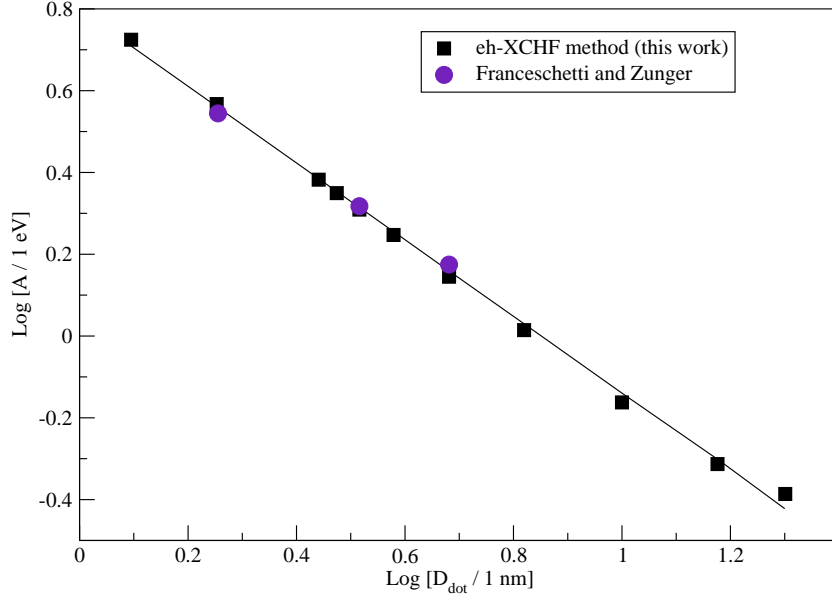
Figure 5-2: Log of Coulomb energy (A) for CdSe quantum dots versus log of diameter of quantum dot.

the eh-XCHF method.

5.4.3   Recombination probability

In addition to exciton binding energies, electron-hole recombination probabilities were also calculated. Using the expression in Eq. (6.16), the electron-hole pair density from the eh-XCHF method was used in the computation of electron-hole recombination probabilities and the results are presented in Figure 5-3. A log-log plot of P_{eh} versus D_{dot} indicates that the recombination probability also follows D_{dot}^{-n} dependence with dot diameter . One of the key results from this study is that the electron-hole recombination probability decreases at a much faster rate than the exciton binding energy with increasing dot size. This is illustrated in Figure 5-4, where comparison of the relative binding energy and recombination probability is presented with respect

89
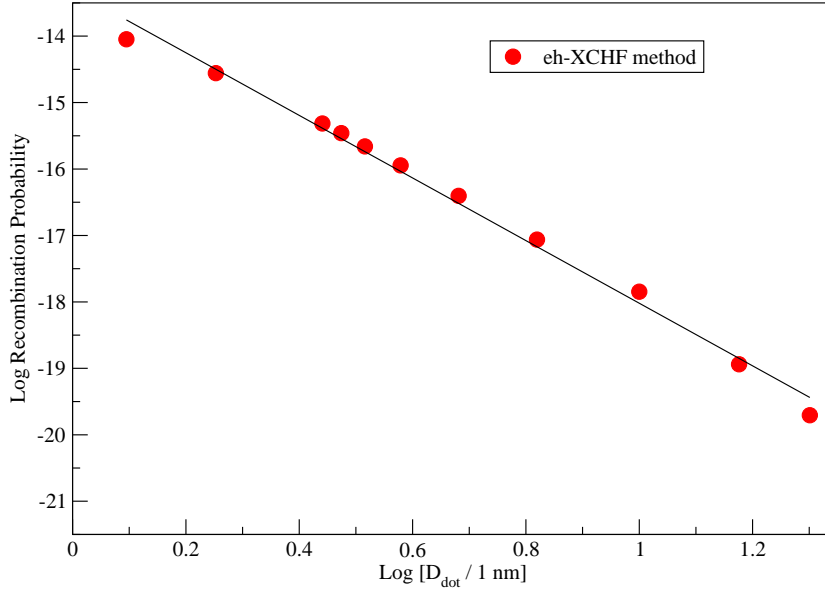
Figure 5-3: Log of recombination probability (P_{eh}) of CdSe quantum dots versus log of diameter of quantum dot.

to dot size. We see that at large dot sizes, both exciton binding energy and electron-hole recombination probability show weak dependence on the dot diameter D. This is consistent with the expected result that the both of these quantities should become asymptotically invariant to the dot size. It was found that for a factor of 16.1 change in the dot diameter, the exciton binding energy and the recombination probability decrease by a factor of 12.9 and 4.55×10^5, respectively.

The linear regression equations of the Coulomb energy , exciton binding energy and electron-hole recombination probability as function of dot diameter are summarized in Table 5.5. It is seen that the slope for the recombination is substantially higher than the binding energy . The absolute value of the slope for both Coulomb energy and exciton binding energy was found to be lower than one which indicates that both of these quantities scale sublinearly with respect to D^{-1}. This is in contrast
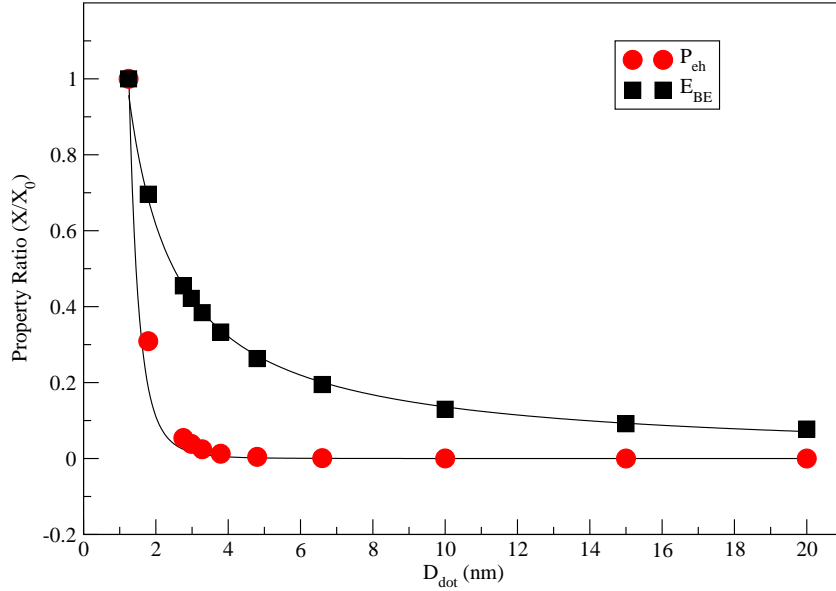
Figure 5-4: Comparison of E_{BE} and P_{eh} relative properties versus r_{dot}.

Table 5.5: Linear regression equation of Coulomb energy, exciton binding energy, and electron-hole recombination probability with respect to dot diameter

Property	Equation
$\log[A/eV]$	$-0.938 \log[D/nm] + 0.7983$
$\log[E_{BE}/eV]$	$-0.938 \log[D/nm] + 0.0039$
$\log P_{eh}$	$-4.712 \log[D/nm] - 13.308$

with the particle in a box model which predicts a slope of -1. The sublinear scaling with respect to D^{-1} obtained in this work is in agreement with the previous results by Franceschetti et al. [2] and Meulenberg et al. [3], respectively.

5.4.4 Effect of 1-particle basis size

The convergence of the computed exciton binding energy and electron-hole recombination probability with respect to the size of the 1-particle basis was investigated by

Table 5.6: Comparison of eh-XCHF binding energies and recombination probabilities obtained using s and s, p, d GTO basis functions.

$D_{dot}(nm)$	$\%\Delta E_{BE}$	$\%\Delta P_{eh}$
1.24	1	3
1.79	1	5
2.76	1	7
2.98	2	8
3.28	2	9
3.79	2	10
4.80	3	14
6.60	3	15
10.0	5	21
15.0	4	7
20.0	2	33

performing eh-XCHF calculation using two different sets of basis functions . The eh-XCHF calculations were performed using s and s, p, d GTOs and the results from the these calculations are summarized in Table 5.6. The change from s to s, p, d GTOs represents a 10-fold increase in the basis size for both electron and hole quasiparticles and it is seen from Table 5.6 that in all cases the change in the exciton binding energy is less than or equal to 5%. These results indicate that the exciton binding energies are converged with respect to the basis size. In contrast, the recombination probabilities were found to more sensitive to the change in the basis size and the maximum change in the P_{eh} was found to be 33%. Addition of another set of s,p,d, GTOs resulted in a maximum difference of 0.2% and 3% in the binding energy and recombination probability, respectively.

5.4.5   Comparison with uncorrelated wavfunction

In this section, the results from the eh-XCHF calculations are compared with the exciton binding energies and recombination probabilities obtained using the uncorrelated electron-hole wave function. The uncorrelated electron-hole wave function is a special case of the eh-XCHF wave function and can be obtained by setting the

Table 5.7: Comparison of exciton binding energy and recombination probability obtained using the uncorrelated wave function and the eh-XCHF method.

$D_{dot}(nm)$	$\%\Delta E_{BE}$	$\%\Delta P_{eh}$
1.24	1	24
1.79	1	37
2.76	2	61
2.98	2	67
3.28	2	69
3.79	2	86
4.80	2	127
6.60	4	202
10.0	5	426
15.0	12	468
20.0	28	822

geminal correlation operator to $G = 1$ as shown in the following equation

$$\Psi_0 = \Phi_0^e \Phi_0^h, \tag{5.22}$$

where $\Phi_0^\alpha, \alpha = e, h$ are eigenfunctions of the zeroth-order Hamiltonian $H_0^\alpha, \alpha = e, h$ defined in Eq. (5.18). In order to evaluate the importance of the explicitly correlated ansatz, we define the following eh-XCHF wave function

$$\Psi_{eh-XCHF}' = G_{opt} \Phi_0^e \Phi_0^h, \tag{5.23}$$

where the only difference between Eq. (5.22) and (5.23) is the presence of the G_{opt} term. The difference between the exciton binding energy and the recombination probability computed using the uncorrelated wave function and the eh-XCHF wave function in Eq. (5.23) are presented in Table 5.7. It is seen that for small dots with diameters less than 5 nm, the computed exciton binding energies are in very good agreement with each other. The eh-XCHF exciton binding energy and the electron-hole recombination probability for the smallest three quantum dots were found to scale as $D^{-1.00}$ and $D^{-5.67}$, respectively. The scaling of exciton binding

energy for the small dots is identical to the particle in a box result of D^{-1} and good agreement between the two methods indicate the dominance of the the strong confinement effect in small quantum dots . However, in contrast to the binding energies, the corresponding errors in the recombination probabilities were found to be much higher. For larger quantum dots, it is seen that the uncorrelated wave function severely underestimates the electron-hole recombination probability. For the biggest quantum dots investigated in the present work, it was found the the uncorrelated wave function underestimates the binding energy and recombination probability by 28% and 822%, respectively. The uncorrelated wave function is able to correctly predict that the recombination probability decreases at a faster rate than the binding energy with respect to size of the quantum dot. Specifically, increasing the dot size from 1.24 to 20 nm decreases the recombination probability obtained using the uncorrelated wave function by a factor of 1.7×10^7. However, this value was found to be higher by two orders of magnitude than the result of 4.6×10^5 obtained from the eh-XCHF calculation. Comparison between the two methods indicates that the accuracy of the uncorrelated wave function decreases significantly in the weak-confinement region. The results from Table 5.7 show the importance of explicitly correlated wave function for computation of electron-hole recombination probability and also highlight the limitation of using exciton binding energy as the sole criteria for characterizing the quality of the electron-hole wave function. This observation is also supported by previous study using path integral Monte Carlo (PIMC) method, where Wimmer and Shumway found that although both CI and PIMC gave comparable biexciton binding energies, the CI method can underestimate the recombination rates by a factor of two. [138]

94

5.5 Conclusions with respect to the eh-XCHF study of effect of size on CdSe quantum dots

In conclusion, we have presented a multifaceted study of the effect of dot size on electron-hole interaction in CdSe quantum dots . The electron-hole explicitly correlated Hartree-Fock method was used for computation of exciton binding energy and electron-hole recombination probability. It was found that both exciton binding energy and electron-hole recombination probability decrease with increasing dot size and both quantities scale as D_{dot}^{-n} with respect to the diameter of the quantum dot. The computed exciton binding energies were found to be in good agreement with previously reported results. One of the significant results from these calculations is that the electron-hole recombination probability decreases at a substantially higher rate than the binding energy with increasing dot size. Changing the dot size by a factor of 16.1 resulted in a decrease in the electron-hole recombination probability by a factor of 10^5. Comparison of the explicitly correlated results with independent-particle approximation showed that the independent-particle approximation seriously underestimates the recombination probability at large dot sizes. For the 20 nm dot size, the error in exciton binding energy and electron-hole recombination probability computed using the independent-particle approximation were found to be 28% and 822%, respectively. The results from this study highlight the importance of electron-hole explicitly correlated wave function and also illustrate the limitations of using exciton binding energy as the sole metric for characterization of theoretical and computational methods.

5.6 Improving the model of the CdSe system: XCHF + pseudopotential calculations

The above calculations on the CdSe quantum dot system were performed using parabolic confining potential. The parabolic quantum dot is a good approximation to the structure of the quantum dot; however, there are associated problems with the accuracy of the parabolic confinement. For smaller systems, an all electron-based treatment is feasible and can be performed using methods such as GW-BSE, DFT, and TDDFT as mentioned in the beginning of the chapter. However, for large quantum dots this treatment becomes extremely prohibitve and thus atomistic pseudopotential methods have been developed to address the issue, as mentioned above.

In the work described here, the eh-XCHF method was coupled with the empirical pseudopotential developed by Rabani et al. [363]. The form of the potential is as follows,

$$v(q) = \frac{a_1(q^2 - a_2)}{a_3 \exp(a_4 q^2) + 1} \tag{5.24}$$

Parameters for Cd and Se were used from [363].

The resulting eigenvalue problem is given as follows,

$$[\frac{-\hbar^2}{2m}\nabla^2 + v_{\mathrm{ps}}(\mathbf{r})]\phi_i = \epsilon_i \phi_i. \tag{5.25}$$

The Hamiltonian matrix was constructed using distributed Gaussian basis functions and in turn was diagonalized to obtain the spectrum of the quasiparticles . Geminal parameters were optimized with respect to the parabolic quantum dot. The eigenvalues of the resulting pseudopotential matrix were used for determination of the exciton binding energy of three specific quantum dot structures. These QD systems range in diameter from 1.78 nm to 4.8 nm and contain 104 to 2075 total atoms at

the largest dot size. The dot diameters in comparison were taken from Ref. [3]. In [3] Franceschetti et al. have performed pseudopotential calculations using configuration interaction for the dot sizes in question. This method is highly computationally
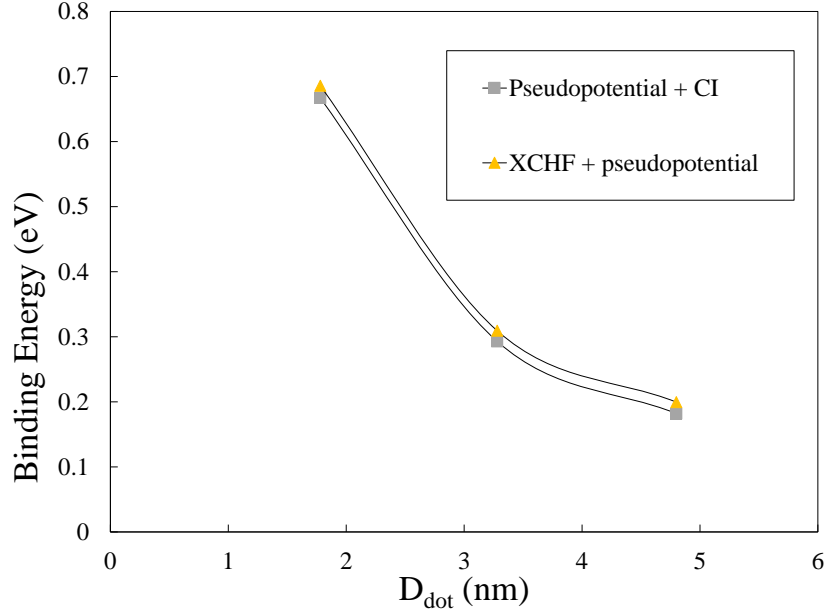
Figure 5-5: Exciton binding energy for CdSe quantum dots versus dot diameter for XCHF method with pseudopotential. Exciton binding energy computed by Franceschetti et al. using pseudopotential with configuration interaction are presented for comparison [3].

expensive due to the expense of the configuration interaction calculation. It is apparent in Figure 5-5 that the XCHF method with pseudopotential compares very well with the pseudopotential + CI method. One of the advantages of the XCHF method with pseudopotential is that it provides an infinite order expansion in configuration interaction space as described in previous chapters. This alleviates the need for large CI calculation. Therefore, the XCHF method with pseudopotential provides a much faster and accurate computational route to computation of optical properties of quantum dots.

Chapter 6

Investigation of Effect of Size versus Effect of Heterojunction on Electron-Hole Dynamics in CdSe/ZnS Core/Shell Quantum Dots

6.1 Motivation for studying effect of heterojunction on core/shell quantum dots

Controlling the particle shape [380, 381, 382], size[383, 384], and material composition[24, 149, 385, 386, 387] allow for direct manipulation of optical and electronic properties of QDs. Applications of nanoparticles include labeling and tracking of biomolecules [90, 388, 91, 95, 92, 93, 71, 94], light emitting devices [89, 389, 390, 391], hydrogen generation[85, 86, 87, 392],resonance energy transfer [393, 394, 84, 395, 396], and photovoltaics [397, 77, 78, 79, 75, 398, 399, 82, 74, 81, 76, 80, 400, 34, 73]. Electronic excitations in QDs can be represented in quasiparticle representation by formation of electron-hole (eh) pairs (excitons) . Generation and dissociation of excitons and

multiexcitons [401, 402, 41, 403, 404] have important applications in solar-to-electric and solar-to-chemical energy conversion processes [405, 406] . Theoretical investigation of these processes requires accurate treatment of electron-hole correlation in QDs. One of the metrics used for studying eh-interaction is exciton binding energy , [3, 2, 4, 1] which is the energy required to dissociate the bound eh-pair. Both exciton binding energy and finite excitonic lifetime can be modified by changing the chemical composition and dot size [3, 2, 4, 36, 37, 1, 139, 407, 408].

There is also technological interest in designing QDs for controlling charge separation which can be achieved by changing the size of the QD, modifying the shape, and introducing a heterojunction into the system [409, 410, 411]. Core/shell quantum dots are ideal for applications which require transfer of charge carriers to an outside sink for photovoltaic applications. When a shell is grown on a core material, the alignment of the band structure changes and thus introduces new features into the electronic structure of the material. Based on the band alignment between the core and shell material, the interface can be classified as a type I, type II or quasi-type II heterojunction [61]. The optical and charge transport properties can be modified significantly by changing the shell thickness of the nanoparticle and have been used in experimental studies for controlling charge separation,[412, 63, 413] hole-transfer,[64] and electron-transfer rates.[65]

In addition to experiments, theoretical approaches have been used to study the optical properties of quantum dots. For smaller quantum dots, an all-electron treatment can be used with methods like density functional theory (DFT) [349, 350, 351, 352, 353, 354, 355], GW-Bethe-Salpeter [346, 347, 348] and MP2 [361]. However, treatment of larger quantum dots becomes computationally prohibitive with all-electron theoretical methods and traditionally, atomistic semiempirical pseudopotential methods have been used to address this problem [3, 1, 151, 39, 362].

In this work, we have investigated the effect of the heterojunction on a series

of CdSe/ZnS quantum dots with diameters 6-15 nm. The excitonic wave function was obtained using the electron-hole explicitly correlated Hartree-Fock (eh-XCHF) method and the exciton binding energy , electron-hole recombination probability , and electron-hole separation distance were computed for each dot in the series. The effects of shell thickness , core-size , and dot diameter on the excitonic properties were analyzed and preferential spatial localization of the quasiparticles was investigated using the 1-particle reduced density. The results from this multi-faceted study show that the presence of the heterojunction can promote exciton dissociation and generation of free charge carriers .

The remaining sections of the chapter are organized as follows. The theoretical and computational implementation details of the eh-XCHF method are summarized in section 6.2. The results from the calculations are presented in section 6.3 and the conclusions from the investigation are discussed in section 6.4.

6.2 Theoretical method and challenges associated with studying core/shell QDs

6.2.1 Form of the electron-hole wave function

The CdSe/ZnS system was studied using the electron-hole explicitly correlated Hartree-Fock (eh-XCHF) method. The details of the eh-XCHF method have been presented earlier and only the key features of the method are highlighted here. The electron-hole wave function in the eh-XCHF method is represented by multiplying a reference wave function by an explicitly correlated function, as shown in the following expression,

$$\Psi_{\text{XCHF}} = G\Phi^{\text{e}}\Phi^{\text{h}}. \tag{6.1}$$

Where the explicitly correlated function is the Gaussian-type geminal function (GTG) is shown below,

$$G(\mathbf{r}^{\mathrm{e}}, \mathbf{r}^{\mathrm{h}}) = \sum_{i=1}^{N_{\mathrm{e}}} \sum_{j=1}^{N_{\mathrm{h}}} \sum_{k=1}^{N_{\mathrm{g}}} b_k \mathrm{exp}[-\gamma_k r_{ij}^2]. \tag{6.2}$$

The GTG includes the electron-hole interparticle distance directly in the form of the wave function and the b and γ parameters are determined variationally by minimizing the total energy.

There are two important advantages associated with using the Gaussian-type geminal function in the eh-XCHF wave function. These advantages are described in the previous chapter.

The eh-interaction was described using the electron-hole Hamiltonian which has been used successfully describe electron hole interaction in quantum dots, [137, 370, 206, 138, 205, 372, 373, 374, 375, 142, 376, 203]

$$\begin{aligned} H = &\sum_{ij} \langle i | \frac{-\hbar^2}{2m_{\mathrm{e}}} \nabla_{\mathrm{e}}^2 + v_{\mathrm{ext}}^{\mathrm{e}} | j \rangle e_i^\dagger e_j \\ &+ \sum_{ij} \langle i | \frac{-\hbar^2}{2m_{\mathrm{h}}} \nabla_{\mathrm{h}}^2 + v_{\mathrm{ext}}^{\mathrm{h}} | j \rangle h_i^\dagger h_j \\ &+ \sum_{iji'j'} \langle iji'j' | \epsilon^{-1} r_{\mathrm{eh}}^{-1} | iji'j' \rangle e_i^\dagger e_j h_{i'}^\dagger h_{j'} \\ &+ \sum_{ijkl} w_{ijkl}^{\mathrm{ee}} e_i^\dagger e_j^\dagger e_l e_k + \sum_{ijkl} w_{ijkl}^{\mathrm{hh}} h_i^\dagger h_j^\dagger h_l h_k. \end{aligned} \tag{6.3}$$

The parabolic potential has been extensively used to approximate the confining potential for quantum dot systems [247, 246, 248, 188, 250, 187, 249, 252, 251, 253] and was used as the confinement potential in the above expression. The confining potential for the electrons and holes was described as follows,

$$v_{\mathrm{ext}}^\alpha = \frac{1}{2} k_\alpha |\mathbf{r}_\alpha|^2 + v_{\mathrm{mat}}^\alpha \quad \alpha = \mathrm{e, h}. \tag{6.4}$$

The force constants, k_α, for the parabolic potential were obtained from Ref. [10]. These force constants were determined using a particle-number based search procedure. The key idea of the method is to find an external potential that ensures that the single particle electron and hole densities are confined in the volume of the quantum dot. The force constant, k_α, is obtained via the following minimization procedure,

$$\min_{k_\alpha^{\min}} \left(N_\alpha - \int_0^{\frac{D_{\mathrm{dot}}}{2}} dr r^2 \int d\Omega \rho_\alpha(\mathbf{r})[v_{\mathrm{ext}}^\alpha] \right)^2, \tag{6.5}$$

where $\alpha = \mathrm{e,h}$, $d\Omega = \sin\theta d\theta d\phi$, D_{dot} is the dot diameter, and $k_\alpha^{\min}$ is the smallest force constant that satisfies the above minimization condition.

In addition to the parabolic confinement potential, a material potential was used to describe the core and shell regions

$$v_{\mathrm{mat}}^\alpha = v_{\mathrm{CdSe}}^\alpha + m(r - r_{\mathrm{core}})(v_{\mathrm{ZnS}}^\alpha - v_{\mathrm{CdSe}}^\alpha), \tag{6.6}$$

where $\alpha = \mathrm{e,h}$. A masking function [39] $m(r)$ was used to smoothly transition between the core and shell materials. This masking function is analogous to the one developed by Franceschetti et al. for smoothly connecting regions of different dielectric functions in quantum dots [39]. The function used in the present work is given by the following expression

$$m(r) = \frac{(\tanh(\beta r) + 1)}{2}, \tag{6.7}$$

where β is a parameter used to control smoothness between core and shell region and is given in Table 6.1.

The eh-XCHF wave function was obtained from variational minimization of the

eh-XCHF energy,

$$E_{\text{eh}-\text{XCHF}} = \min_{G, \Phi^e, \Phi^h} \frac{\langle \Psi_{\text{eh}-\text{XCHF}} | H | \Psi_{\text{eh}-\text{XCHF}} \rangle}{\langle \Psi_{\text{eh}-\text{XCHF}} | \Psi_{\text{eh}-\text{XCHF}} \rangle}. \tag{6.8}$$

To facilitate the evaluation of the above equation, the operators were transformed via congruent transformation [141, 378] as shown in the following equations

$$\tilde{H} = G^\dagger H G \tag{6.9}$$

$$\tilde{1} = G^\dagger G. \tag{6.10}$$

The eh-XCHF energy was obtained using the transformed operators as shown below

$$E_{\text{eh}-\text{XCHF}} = \frac{\langle \Phi^e \Phi^h | \tilde{H} | \Phi^e \Phi^h \rangle}{\langle \Phi^e \Phi^h | \tilde{1} | \Phi^e \Phi^h \rangle}. \tag{6.11}$$

The above transformation allows us to perform the minimization over the Slater determinants using coupled self-consistent field (SCF) equations [167] as shown below,

$$\mathbf{F}_G^e[\mathbf{C}^h]\mathbf{C}^e = \lambda^e \mathbf{S}_G^e \mathbf{C}^e \tag{6.12}$$

$$\mathbf{F}_G^h[\mathbf{C}^e]\mathbf{C}^h = \lambda^h \mathbf{S}_G^h \mathbf{C}^h. \tag{6.13}$$

In the above expression, $\mathbf{F}_G^e$ and $\mathbf{F}_G^h$ are the Fock matrices for the electron and hole respectively. The subscript G denotes that the Fock operators were obtained from the congruent transformed Hamiltonian and include contribution from the geminal operator.

6.2.2 Computational Details

The material parameters for the CdSe core-only and CdSe/ZnS core/shell quantum dots used in the electron-hole Hamiltonian are summarized in Table 6.1. These pa-

Table 6.1: Material parameters for the CdSe/ZnS quantum dots used in the electron-hole Hamiltonian. All values are given in atomic units.

Property	Value CdSe	Value ZnS
m_e	0.13	0.25
m_h	0.38	1.30
ϵ	6.20	8.90
v_{mat}^e	-0.147	-0.114
v_{mat}^h	-0.209	-0.176
β	10.0	10.0

rameters were taken from Ref. [62, 1, 414]. The single particle basis for the electron and hole were constructed as a linear combination of Gaussian-type orbitals functions, as shown in the following expression,

$$\Phi^x = \sum_{i=1}^{n_b} c_i \phi_i(r) \quad x = e, h. \tag{6.14}$$

A linear combination of 11 basis functions was used for each particle with angular momentum value of $0 - 10$. The coefficients c_i and exponents α for the GTOs were found by minimizing the single-component energy for electron and hole, respectively. A set of three geminal functions were used for each dot and were determined by minimizing the eh-XCHF energy . To ensure that the eh-XCHF energy is always bounded from above by the mean-field energy, the first geminal parameters are always set to $b_1 = 1$ and $\gamma_1 = 0$.

6.3 Results from investigation of CdSe/ZnS core/shell QDs

6.3.1 Effect of Shell Thickness in CdSe/ZnS QD

The change in exciton binding energy , eh-recombination probability , and electron-hole separation distance as a function of shell thickness was calculated using the eh-XCHF method. A series of CdSe/ZnS quantum dots with diameters 6-15 nm were investigated by adding ZnS shell to a CdSe core with core-diameter of 4.8 nm. The exciton binding energy E_{BE} was calculated from the difference between the bound and the non-interacting electron-hole pair as shown the following equation,

$$E_{BE} = E_{non-interacting} - E_{exciton}. \qquad (6.15)$$

As shown in Figure 6-1, the exciton binding energy was found to decrease with increasing shell thickness . The exciton binding energy of the core-only quantum dot was found to be 0.264 eV and is in good agreement with both experimental and theoretical findings for exciton binding energy [10, 4] . For a factor of three change in the dot diameter, the exciton binding energy was found to decrease by 46% in the core/shell dot.

In addition to the exciton binding energy, the electron-hole recombination probability was calculated from the eh-XCHF wave function using the following expression

$$P_{eh} = \frac{1}{N_e N_h} \int d\mathbf{r}_e \int_{\mathbf{r}_e - \frac{\Delta}{2}}^{\mathbf{r}_e + \frac{\Delta}{2}} d\mathbf{r}_h \ \rho_{eh}(\mathbf{r}_e, \mathbf{r}_h). \qquad (6.16)$$

Analogous to the exciton binding energy, the recombination probability was found to decrease as the shell material was added to the CdSe core. As shown in Figure 6-2, the recombination probability decreased by 98% as compared to the bare CdSe QD.
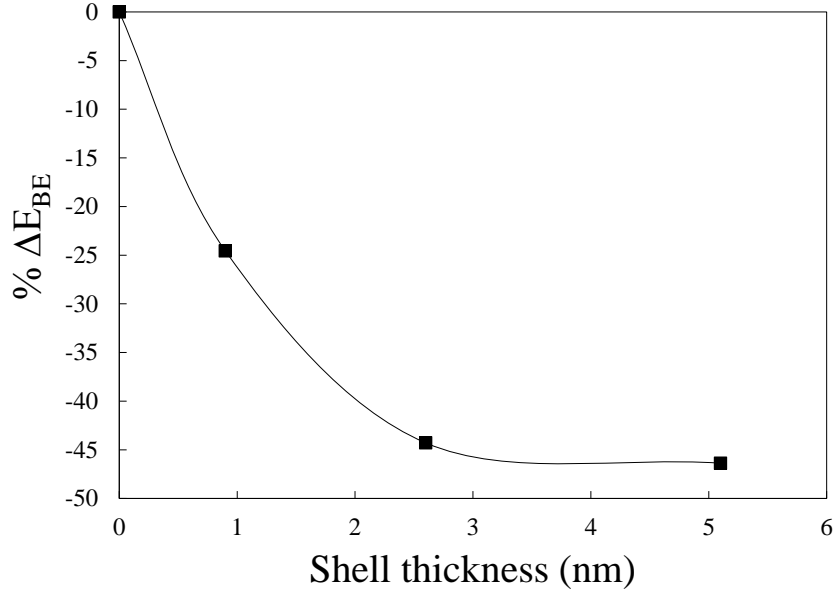
Figure 6-1: Percent change in exciton binding energy as a function of shell thickness for a CdSe/ZnS core/shell quantum dot. $E_{\mathrm{BE}}^{\mathrm{core}} = 0.264$ eV.

However, the change in the eh-recombination probability was much higher than the change in exciton binding energy.

The electron-hole separation distance r_{eh} was calculated as an additional metric for investigating the effect of shell thickness on the exciton dissociation process. The r_{eh} was calculated from the eh-XCHF wave function using the following expression

$$\langle r_{\mathrm{eh}} \rangle = \langle \Psi_{\mathrm{eh-XCHF}} || \mathbf{r}_{\mathrm{e}} - \mathbf{r}_{\mathrm{h}} || \Psi_{\mathrm{eh-XCHF}} \rangle, \tag{6.17}$$

and the results are presented in Figure 6-3 . It is seen from Figure 6-3 that the spatial separation increases by 60% with addition of ZnS shell.

The results shown in Figure 6-1-Figure 6-3 indicate that addition of ZnS can facilitate dissociation of the exciton into free charge carriers. This observation is

106
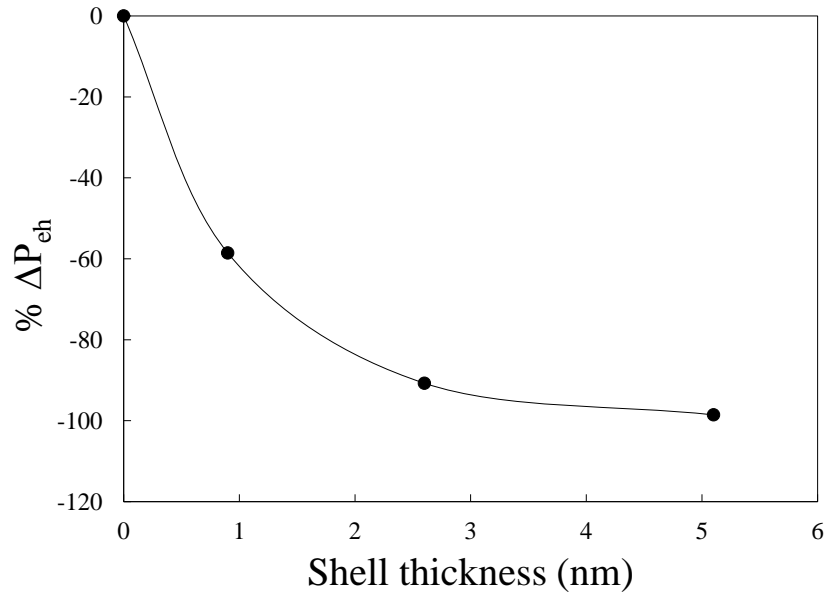
Figure 6-2: Percent change in electron-hole recombination probability as a function of shell thickness for CdSe/ZnS core/shell quantum dot.

consistent with experimental results on core/shell quantum dots. For example, in CdSe/ZnS QDs, Zhu et al. have found enhancement in the electron transfer rate from QD with increasing shell thickness [412]. This phenomenon is not restricted to CdSe/ZnS and is also seen in other core/shell quantum dots. Htoon et al. have shown an increase in multiexciton dissociation as a function of shell thickness [415]. In addition to quantum dot systems, Zhu et al. have shown that dielectric discontinuity at the surface of organic materials can strongly effect the exciton dissociation [416] .

6.3.2 Exponential scaling with respect to shell thickness

One of the interesting results in core/shell quantum dots is exponential scaling of experimentally observed quantities as a function of shell thickness. In the present work, we find that as the shell thickness is increased, the recombination probability
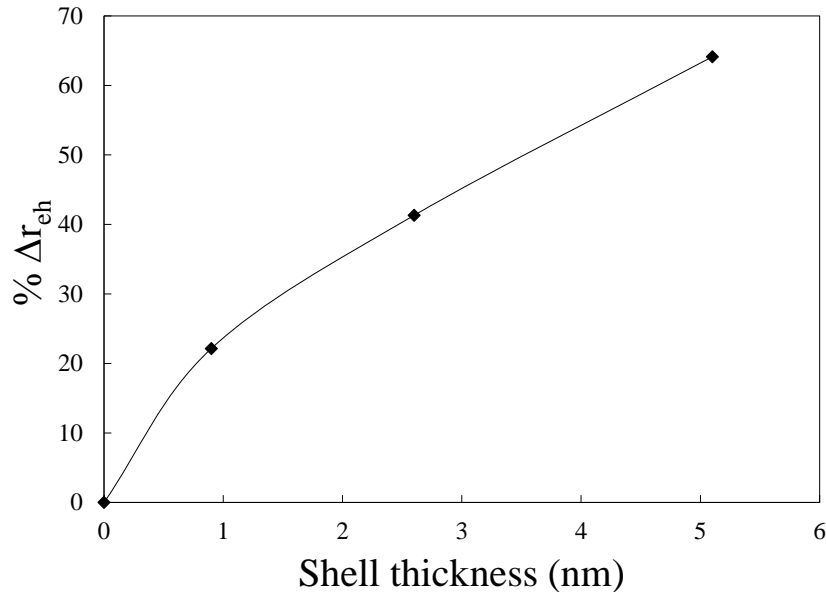
Figure 6-3: Percent change in electron-hole separation as a function of shell thickness for a CdSe/ZnS core/shell quantum dot. $r_{\mathrm{eh}}^{\mathrm{core}} = 1.18$ nm
.

decays exponentially . Exponential fit of the relative recombination probability as a function of shell thickness is shown in Figure 6-4. These results are consistent with experimentally observed trends in core/shell quantum dots. For example, in 2010 Zhu et al. have shown experimentally that there is an exponential decay associated with both charge-recombination and charge-transfer rates as a function of shell thickness [412]. Abdellah et al. have also found that the charge injection rate in core/shell quantum dots displays a very strong exponential dependence [63]. Sun et al. find that the electron transfer rates in core/shell quantum dots show strong exponential decay with respect to increasing shell thickness [417]. Although in the present calculations a direct comparison with the rates are not possible, we find that similar trends exist between computed and experimentally observed quantities.
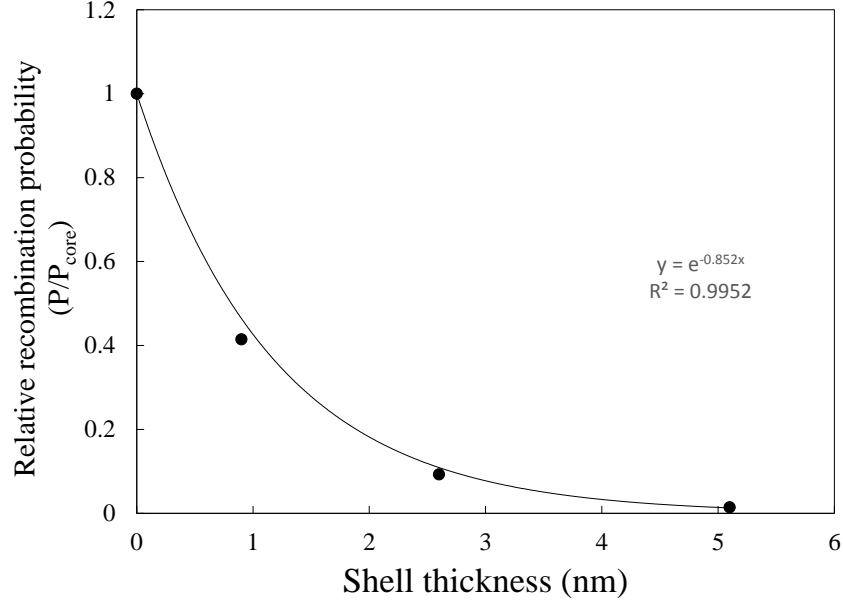
Figure 6-4: Ratio of recombination probability as a function of ZnS shell thickness. Exponential fit is given as $y = e^{-0.852x}$.

6.3.3 Preferential localization of quasiparticle density

To further evaluate the spatial separation of the quasiparticles, we have computed the probability of finding the electron or hole in the core and shell region of the QD. Starting with the 1-particle reduced density, we define the probability P_{core}^{α} of finding the quasiparticle in the core region as

$$P_{\text{core}}^{\alpha} = \frac{1}{N_\alpha} \langle \rho_\alpha(\mathbf{r})\theta(r_{\text{core}} - |\mathbf{r}|)\rangle \tag{6.18}$$

$$= 1 - P_{\text{shell}}^{\alpha} \quad \text{with} \quad \alpha = \text{e, h,} \tag{6.19}$$

where $\theta(x)$ is the Heaviside step function and the angular brackets represent integration over the spatial coordinates. The P_{shell} for both electron and hole are shown in Figure 6-5. It is seen that as compared to the hole, the electron is preferentially
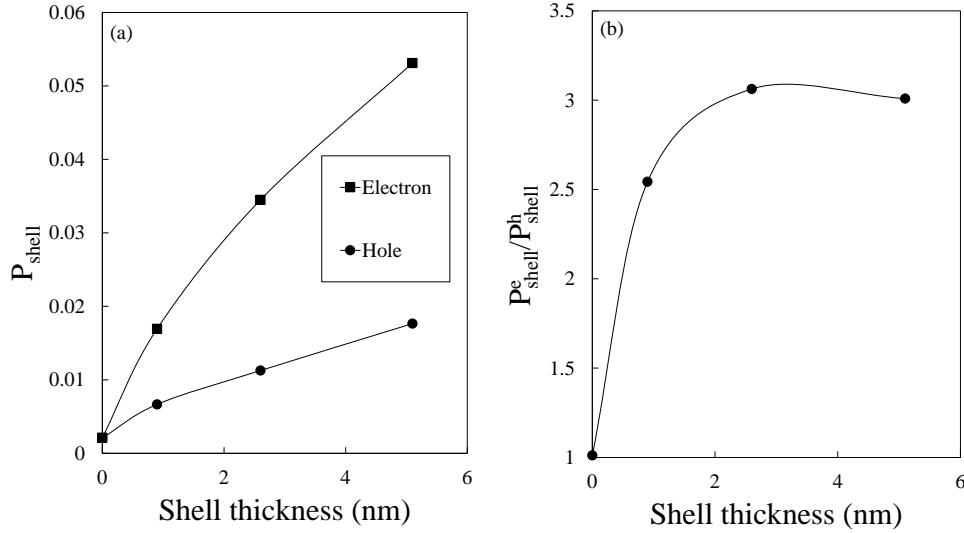
Figure 6-5: (a) Probability of finding an electron and hole within the shell region and (b) ratio of P_{shell}^e/P_{shell}^h for a CdSe/ZnS quantum dot.

localized in the shell region by a factor of three. This trend is consistent with experimental observations.[412, 61, 63, 66, 418, 419, 65, 413] For example, Zhu et al. have found that there is an optimum shell thickness for controlling the charge separation in CdSe/ZnS QDs [412]. In addition, they have also observed preferential localization of the electron in the shell material for these QDs. [61] Abdellah et al. have also found that there is an optimal shell thickness for achieving efficient charge transfer from the core/shell quantum dot system [63]. As a consequence of this, core/shell quantum dots have been coupled with materials like TiO_2 in order to modify the electron transfer rates [66, 418, 419, 65]. Zhu et al. have engineered core/shell QDs to increase the charge separation and decreasing the charge recombination. [413] The results in Figure 6-1-Figure 6-5 provide additional metrics that confirm these experimental observations.

6.3.4   Isolating the effect of heterojunction from volume

Addition of multiple monolayers of shell material not only introduces heterojunction into the quantum dot but also increases the effective volume of the nanoparticle. It is often difficult to separate the influence of these two contributing quantities on the properties of the QD system. A useful metric to analyze these effects is to compute the scaling relationship of the excitonic properties as a function of the dot diameter. In this work, we isolate the effect of heterojunction by comparing the results between core/shell and core-only quantum dots with identical dot diameter.

The scaling of the exciton binding energy as a function of dot diameters was analyzed and is presented in Figure 6-6. The exciton binding energy for the CdSe/ZnS system was found to scale as $D_{\text{dot}}^{-0.56}$ with respect to the dot diameter D. This scal-
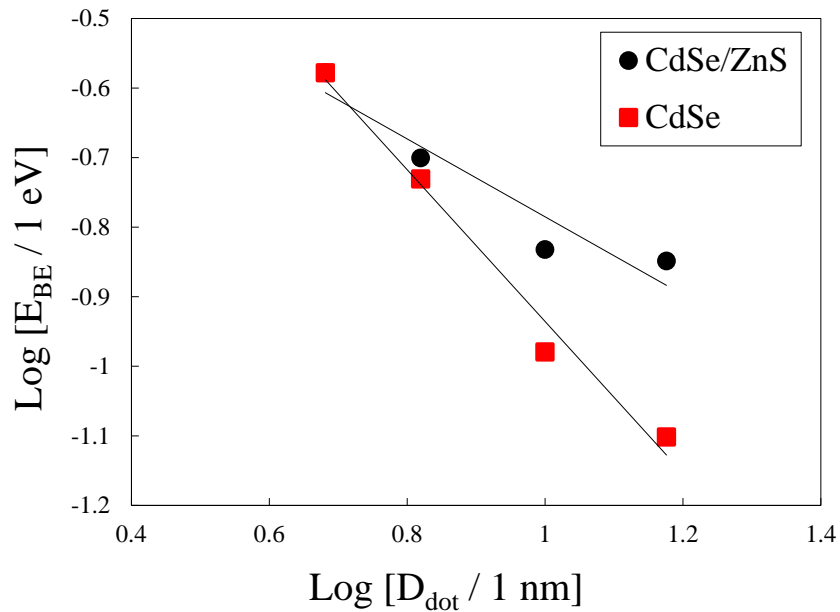
Figure 6-6: Exciton binding energy as a function of dot size for quantum dots.

ing behavior is considerably different from the scaling laws obtained in core-only

111

quantum dots where the binding energy scaled as $D_{\text{dot}}^{-0.94}$ [10, 2]. We attribute this difference in the scaling behavior to the presence of the core/shell heterojunction. The scaling comparison for the core vs. core shell system was also evaluated for the eh-recombination probability and average eh-separation distance and the results from these calculations are presented in Figure 6-7 and Figure 6-8 respectively. In both cases, the scaling of the CdSe/ZnS properties was found to be different as compared to the core-only scaling. For P_{eh}, the core/shell system was found to scale as $D_{\text{dot}}^{-3.73}$ where the core-only system scaled as $D_{\text{dot}}^{-4.71}$. The average electron hole separation r_{eh} scaled as $D_{\text{dot}}^{0.42}$ for the core/shell system as compared to the $D_{\text{dot}}^{0.81}$ scaling exhibited in the core-only system. The significant deviation in the scaling behavior from the core-
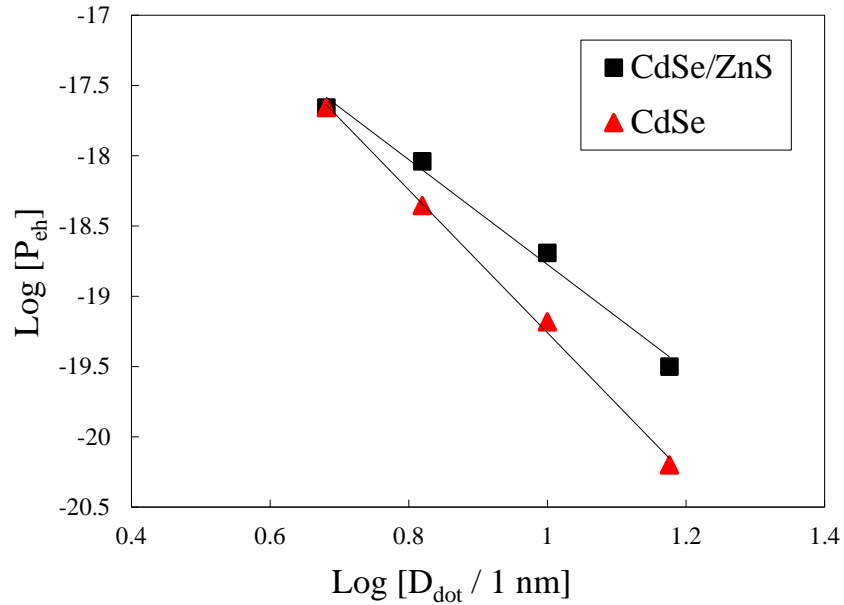
Figure 6-7: Dependence of recombination probability as a function of dot diameter for quantum dots.

only QDs is consistent with experimental results reported earlier. García-Santamaría et al. have found that core/shell quantum dots exhibit a breakdown in traditional

volume scaling laws . They have shown that for a CdSe/CdS core/shell QD system with large shell thickness, the scaling laws associated with Auger recombination differ considerably from expected scaling [420].

6.3.5   Effect of core size

To investigate the effect of the core size in core/shell QDs, we have generated a second set of CdSe/ZnS QDs with a smaller CdSe core of 2.8 nm diameter . To facilitate direct comparison of excitonic properties between the two sets as a function of dot size, the dot diameters were selected to be identical to the first set of CdSe/ZnS dots with 4.8 nm core. The probability of finding the electron in the shell region as a function of dot size is shown in 6-9. It was found that the core size can strongly influence
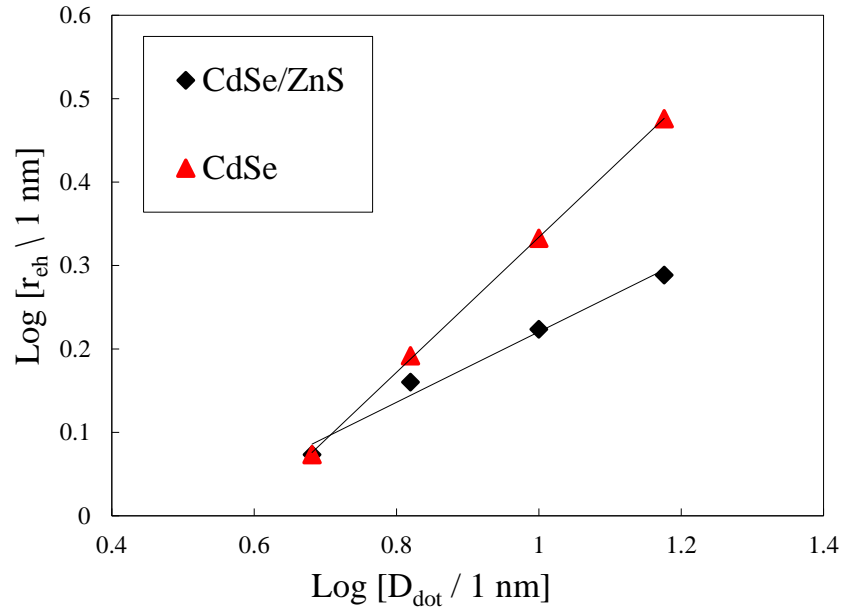
Figure 6-8: Average electron-hole separation as a function of dot diameter for quantum dots.

the quasiparticle localization in the shell region. We find that reducing the size of

the core by a factor of 1.7 increases the preferential localization of the electron in the shell region by a factor of 11.3. In contrast, the hole was found to be preferentially localized in the core with $P_{\text{core}}^{\text{h}}$ equal to 0.87 and 0.98 for the 15 nm CdSe/ZnS dot with 2.8 nm and 4.8 nm core-diameters, respectively. The results show that the hole density in the core is not substantially modified by the presence of the shell. These results are consistent with the experimental results on giant core/shell quantum dots, where dots with small cores were found to enhance multiexciton generation [415].

The scaling of exciton binding energy , eh-recombination probability, and average eh-distance as a function of dot diameter for different core sizes and core-only dots are presented in Table 6.2. We find that both of the core/shell systems display similar scaling behavior with respect to dot size. However, as discussed earlier, the excitonic properties in core-only and core/shell dots exhibit different scaling behavior with respect to dot size and we attribute the differences to the presence of heterojunction.

Table 6.2: Scaling equations for core/shell and core-only quantum dots.[*]

Log[Property]	Log[E_{BE}/eV]		Log[P_{eh}]		Log[$\langle r_{\text{eh}} \rangle$/nm]	
Scaling constants	m	c	m	c	m	c
2.8 nm core-diameter	−0.521	−0.147	−3.587	−14.875	0.487	−0.319
4.8 nm core-diameter	−0.569	−0.225	−3.730	−15.044	0.422	−0.202
Core-only CdSe	−0.938	−0.004	−4.712	−13.308	0.809	−0.476

[*] **Note:** Scaling relationships satisfy $A = m\log[\text{D/nm}] + c$, where A is the property being investigated.

6.4   Conclusion

In conclusion, the effect of shell thickness on excitonic properties in CdSe/ZnS quantum dots was investigated using the electron-hole explicitly correlated Hartree-Fock method. We found that exciton binding energy and electron-hole recombination probability decrease by 46% and 98%, respectively with an increase in the shell thickness
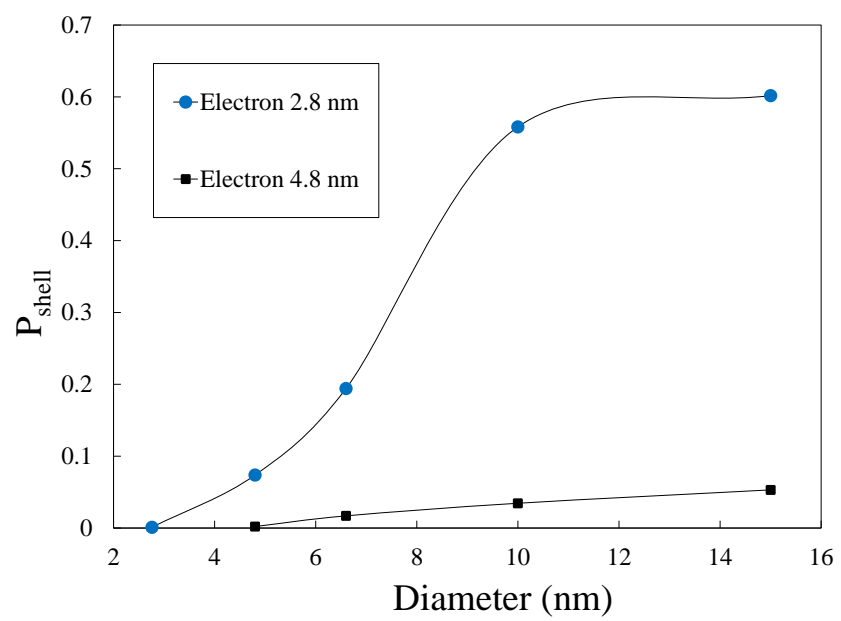
Figure 6-9: Relative probability (P_{shell}) of finding the electron in the shell region for a 2.8 nm and 4.8 nm CdSe core diameter.

of 5 nm. However, the average electron-hole separation distance was found to increase by 60% with increasing shell thickness. The electron-hole recombination probability was found to decrease exponentially with respect to shell thickness. The scaling of the three excitonic properties as a function of shell thickness illustrates the effectiveness of introducing core/shell heterojunction for promoting exciton dissociation. Electron and hole 1-particle densities were computed from the eh-XCHF wave function, and it was found that as compared to the hole, the electron is preferentially localized in the shell region by a factor of 3. Consequently, we expect that introduction of shell should increase dot-to-ligand electron-transfer rates. The core-size of the CdSe/ZnS quantum dot was found to dramatically alter the preferential localization of the electron in the shell region. We found that a decrease in CdSe core diameter by a factor of 1.7 increased the probability of electron localization in the shell by a factor of 11.3. Based on these results, we conclude that large CdSe/ZnS quantum dots with a small CdSe core have the necessary characteristics for efficient exciton dissociation and generation of free charge carrier. This observation is consistent with experimental results on other core/shell systems mentioned throughout the chapter.

Chapter 7

Effect of Shape on CdSe Nanocrystals using XCHF Method

The effect of shape on CdSe nanocrystals via isovolumetric transformation was investigated in close association with Jeremy Scher. I have contributed to this work by the development of the method used to study the isovolumetric nanocrystals. Below, a brief summary of the method and conclusions are presented on the findings of the effect of shape on transformations of CdSe nanocrystals.

7.1   Brief introduction

In the current work, the challenge associated with isolating nanoparticle shape from volume was addressed by generating a series of CdSe ellipsoids, each with identical volume. By generating these nanocrystals with an isovolumetric condition, the effect of particle shape on excitonic properties can truly be investigated. The isovolumetric series was generated by varying three semi-axes of the ellipsoid, A, B and C while keeping the product of the three constant. Generating the particles in this fashion and computing excitonic properties for each of the respective ellipsoids will allow for systematic evaluation of the optical properties of particles of different morphologies.

117

Table 7.1: System parameters used to calculate properties of CdSe nanocrystals. [10]

Parameter	Value
ϵ	6.2
m_e	0.13 m_0
m_h	0.38 m_0

In keeping with the isovolumetric conditions described above, 900 ellipsoids were generated with identical volume. Excitonic properties were computed for each. The system was studied using the explicitly correated Hartree-Fock method.

7.2 Theoretical approach to studying isovolumetric nanocrystals

The CdSe nanocrystals in this study were modeled using the electron-hole explicitly correlated Hartree Fock method. The complete details of this method are outlined in chapter 2 and chapter 5.

The effective electron-hole Hamiltonian [144, 137, 206, 138, 136] was used,

$$\hat{H} = \sum_{ij} \langle i| \frac{-\hbar^2}{2m_\text{e}} + v_\text{ext}^\text{e} |j\rangle e_i^\dagger e_j \tag{7.1}$$

$$+ \sum_{ij} \langle i| \frac{-\hbar^2}{2m_\text{h}} + v_\text{ext}^\text{h} |j\rangle h_i^\dagger h_j \tag{7.2}$$

$$+ \sum_{iji'j'} \langle iji'j'| \epsilon^{-1} r_\text{eh}^{-1} |iji'j'\rangle e_i^\dagger e_j h_{i'}^\dagger h_{j'} \tag{7.3}$$

$$+ \sum_{ijkl} w_{ijkl}^\text{ee} e_i^\dagger e_j^\dagger e_l e_k + \sum_{ijkl} w_{ijkl}^\text{hh} h_i^\dagger h_j^\dagger h_l h_k. \tag{7.4}$$

The external potential used in this investigation is a parabolic potential for both the electron and hole,

$$v_{\text{ext}}^{\alpha} = \frac{1}{2}k_{\alpha}|\mathbf{r}_{\alpha}|^2 \quad \alpha = \text{e}, \text{h}. \tag{7.5}$$

The force constants in the external potential used in the current work are impor-
tant for the accurate calculation of exciton binding energy in these nanocrystals. The
force constants are calculated such that the electron and hole are confined to within
the dot diameter,

$$\min_{k_{\alpha}^{min}} = \left(N_{\alpha} - \int_{0}^{\frac{D_{dot}}{2}} drr^2 \int d\Omega \rho_{\alpha}(\mathbf{r})[v_{ext}^{\alpha}] \right)^2, \tag{7.6}$$

where $\alpha = \text{e}, \text{h}$, $d\Omega = \sin d\theta d\varphi$, D_{dot} is the diameter of the corresponding spherical
quantum dot, and k_{α} is the smallest force constant that satisfies the above minimiza-
tion conditions. An appropriate force constant for the spherical CdSe nanocrystal
was obtained using this approach, and then the force constants corresponding to all
other semi axis lengths were scaled accordin

A force constant that satisfied the above minimization conditions was found for
the CdSe spherical quantum dot. Once this parameter was found, the remaining
force constants for the ellipsoids were found by scaling the spherical force constant as
shown in the following expression,

$$k_{\alpha a} = \frac{k_{\alpha \text{sphere}} r_{\text{sphere}}^2}{a^2}, \tag{7.7}$$

where a is the axis length, and r_{sphere} is the radius of a spherical dot with a force
constant $k_{\alpha \text{sphere}}$.

The ansatz of the eh-XCHF wave function is a product of electron and hole ref-

erence wave functions and a correlation function. The electron and hole reference wave functions are Slater determinants and the correlation function is a Gaussian type geminal operator

$$\Psi_{\text{eh--XCHF}} = \hat{G}\Phi^{\text{e}}\Phi^{\text{h}}. \tag{7.8}$$

The geminal operator $\hat{G}$ depends explicitly on electron-hole interparticle distance, as well as variational parameters b_k and γ_k as described in the previous chapters.

The eh-XCHF wave function is obtained by variational minimization of the total energy,

$$\text{E} = \min_{\hat{G},\Phi^{\text{e}},\Phi^{\text{h}}} \frac{\langle\Psi_{\text{eh--XCHF}}|\hat{H}|\Psi_{\text{eh--XCHF}}\rangle}{\langle\Psi_{\text{eh--XCHF}}|\Psi_{\text{eh--XCHF}}\rangle}. \tag{7.9}$$

Facilitation of the caculation of the minimum energy is achieved by congruent transformation of the Hamiltonian,

$$\tilde{H} = \hat{G}^{\dagger}\hat{H}\hat{G} \tag{7.10}$$

$$\tilde{1} = \hat{G}^{\dagger}1\hat{G}. \tag{7.11}$$

$$\text{E} = \frac{\langle\Phi^{\text{e}}\Phi^{\text{h}}|\tilde{H}|\Phi^{\text{e}}\Phi^{\text{h}}\rangle}{\langle\Phi^{\text{e}}\Phi^{\text{h}}|\tilde{1}|\Phi^{\text{e}}\Phi^{\text{h}}\rangle}. \tag{7.12}$$

The three optical properties of interest in this study are the exciton binding energy, the electron hole recombination probability, and the electron hole separation distance.
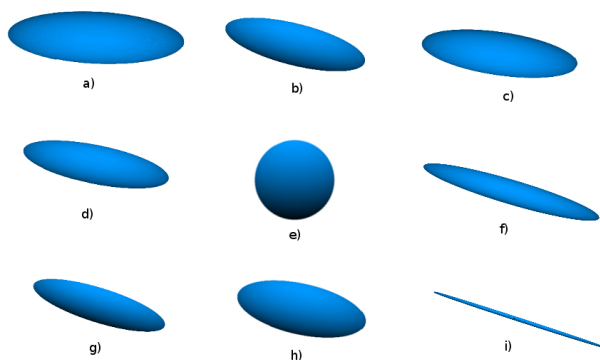
Figure 7-1: Sample set of ellipsoidal CdSe nanocrystals. Each ellipsoid has the same volume, but exhibits different optical properties. Image was made by Jeremy Scher.

A short summary of the results for exciton binding energy are presented below.

7.3   Results of the study and important conclusions

A sample grid of ellipsoids are given below. In order to investigate the effect of shape of the CdSe nanocrystals, the ellipsoids were generated isovolumetrically, therefore, all ellipsoids within the image are of the same volume.

For each of the 900 isovolumetric ellipsoids, the exciton binding energy was calculated. It is clear from these results that the particle shape has a strong effect on the binding energy. The largest binding energy was displayed by the spherical CdSe nanoparticle, at 57.154 meV. It was found that the binding energy for the wire like particle was much smaller than the spherical particle, with a magnitude of 1.279 meV. Local maxima and minima are readily apparently in Figure 7-2. The recombination probabilit and separation distance were also found to be strongly dependent one nanocrystal shape .
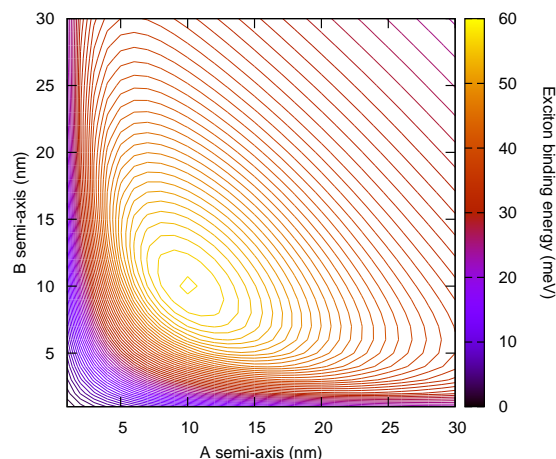
Figure 7-2: Contour plot of exciton binding energy vs. the A and B semi axes of a CdSe ellipsoid. Image made by Jeremy Scher.

7.4   Conclusions

The explicitly correlated eh-XCHF method was used to study optical properties of CdSe nanocrystal ellipsoids by performing isovolumetric transformations. It is important to keep in mind that this method is general, and can be used to study a large variety of electron-hole systems. The exciton binding energy, electron-hole separation distance, and electron-hole recombination probability of 900 isovolumetric CdSe ellipsoids. All three properties were found to have a strong dependence on ellipsoid shape. It was found that the exciton binding energy was maximized in the case of a sphere, and minimized in a wire with largest aspect ratio, and the electron-hole separation distance exhibits the opposite trend. The exciton binding energy was found to have a linear dependence on the inverse of the electron-hole separation distance.

Chapter 8

Optical signature of formation of protein corona in the firefly luciferase-CdSe quantum dot complex

8.1   Introduction and motivation for studying protein corona formation

The work described in this chapter was done in collaboration with Shikha Nangia and Flaviyan Irudayanathan. The optimization of protein structure and all molecular mechanics calculations were performed by them. I have contributed to this project by performing the quantum mechanical calculations of the QD-protein complex and interpreted the data therein.

When quantum dots (QDs) are exposed to biological media, their surfaces adsorb biomolecules , generally proteins, present in the system.[421] The formation of protein corona on the surface of quantum dots directly influences their physical, chemical,

and biochemical properties. In this work, we present theoretical investigation of the interaction of a 5 nm CdSe ($Cd_{1159}Se_{1183}$) quantum dot with firefly luciferase enzyme by analyzing the change in the optical property of the quantum dot due to corona formation. The objective of this work is to correlate the spectral shift of the QD with structure and stoichiometry of the protein corona.

Quantum dots are being used as nanoprobes for biological systems because of their nanoscale dimensions and sensitivity of their optical properties to local chemical environment. For example, CdSe quantum dots have been used for determination of local pH in cells,[422, 423, 424, 425, 426] and for detection of various biomolecules such as DNA ,[427] and glucose[428]. They have also been used for bioimaging [429] including *in vivo* imaging of tumor cells.[430] Quantum dots functionalized with bioluminescent proteins such as luciferase have been used for mapping of lymph nodes, [431] detection of nucleic acids, [432] *in vivo* imaging,[433, 434] photodynamic therapy, [435] and investigation of bioluminescence resonance energy transfer (BRET). [22, 393, 436, 437, 438] However, there is a growing body of evidence that shows that it is the QD-protein complex and not the pristine quantum dot that is important for biological activity.[439, 440, 441, 442, 443, 444]

The computational treatment of the QD-protein complex is challenging because of the size of the system. This problem is further aggravated for calculation of optical properties because it requires quantum mechanical description of both the ground and excited electronic states . For small CdSe quantum dots with 1.3 nm diameter, Anandampillai et al. [445] have investigated the effect of QD-DNA interactions using density functional theory (DFT). Kim et al. have also studied the effect of bioconjugation on a CdSe-Adenine complex utilizing DFT methodology. [355] Ligated quantum dot systems have been studied extensively using DFT based approach [325, 357, 68, 351, 326]. However, an all-electron DFT calculation is computationally prohibitive for the present system. Our system consists of a 5 nm CdSe quantum dot

($Cd_{1159}Se_{1183}$) with 2342 heavy atoms. Each luciferase enzyme molecule contributes 8423 heavy atoms. The protein corona on the surface was found to consist of seven enzyme molecules making the total number of heavy atoms in the QD-protein complex equal to 61303. Additionally, the entire QD-protein complex was solvated with explicit water molecules. The total size of the system presents an imposing challenge for computational investigation. To surmount the computational bottleneck, a multi-level approach has been developed by combining the strengths of quantum mechanics, molecular mechanics, classical molecular dynamics, and Monte Carlo techniques. The quantum dot was treated quantum mechanically, the protein was treated using molecular mechanics, and the assembly of the protein corona was performed using combined molecular dynamics/Monte Carlo procedure. The details of the individual steps of the calculations are discussed below.

8.2   Theoretical details

QM/MM description of QD-protein complex: In the current QM/MM framework, only the quantum dot was treated quantum mechanically, and the protein corona surrounding the quantum dot was treated using molecular mechanics force field. The separation between the QM and the MM region is illustrated in Figure 8-1. One of the challenging aspects of any QM/MM calculation is the treatment of the QM/MM boundary and this is a topic of ongoing research [446, 447]. For systems where the QM and MM atoms are bonded chemically by covalent bonds, the QM/MM boundary can be treated using either link-atom or frozen-orbital based approaches.[446, 447] However, the interaction between the protein corona and the quantum dot is known to be dominated by electrostatic interactions [448]. This non-bonding nature of the QD-protein interaction allows for a much simpler treatment of the QM/MM boundary. In the present work, the effect of protein environment was included by performing the
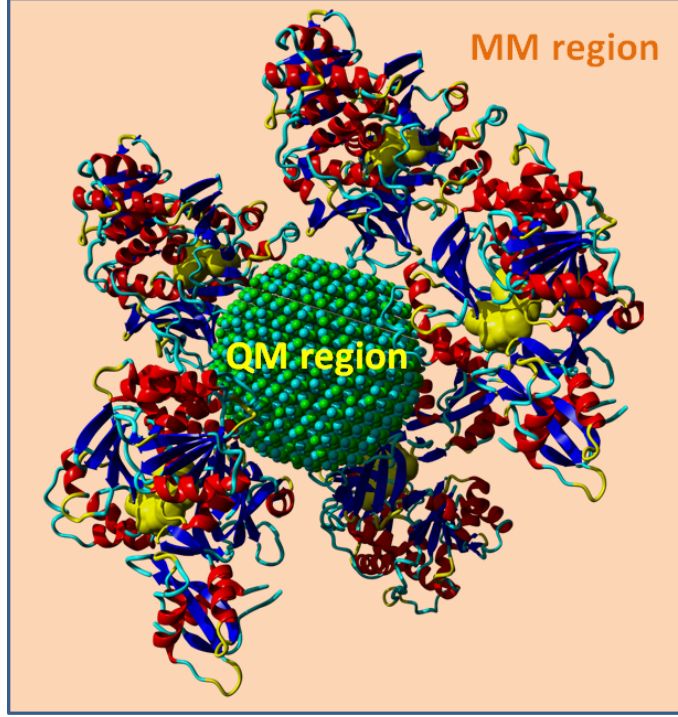
Figure 8-1: Separation of quantum mechanical and molecular mechanics region for the CdSe QD (green) + firefly luciferase protein (ribbon representation) complex.

QM calculation in presence of the electrostatic field generated by the partial charges on the proteins. The external potential in the QM calculation was modified as shown in Equation 8.1

$$v_{\text{ext}}^{\text{QM/MM}}(\mathbf{r}) = \sum_{k \in \text{protein}} \frac{q_k}{|\mathbf{R}_k - \mathbf{r}|}, \tag{8.1}$$

where, all terms in the above expression are in atomic units, and the magnitude and position of the partial charges on the protein are given by q_k and $\mathbf{R}_k$, respectively.

QM description of the quantum dot: The pseudopotential approach is a computationally efficient route for performing QM calculations on large quantum dots, and we have used the empirical CdSe pseudopotential developed by Rabani et al. for this work [363]. The surface of the quantum dot was passivated with hydrogen atoms, and the interactions with the protein corona were included in the QM calculations

126

by adding 1-body $v_{\text{ext}}^{\text{QM/MM}}$ term to the pseudopotential Hamiltonian. The resulting eigenvalue equation is shown in Equation 8.2

$$[\frac{-\hbar^2}{2m}\nabla^2 + v_{\text{ps}}(\mathbf{r}, \mathbf{R}^{\text{dot}}) \qquad (8.2)$$
$$+ v_{\text{ext}}^{\text{QM/MM}}(\mathbf{r}, \mathbf{R}^{\text{protein}})]\phi_i = \epsilon_i\phi_i.$$

The pseudopotential Hamiltonian was constructed using distributed Gaussian basis functions and was diagonalized to obtain the quasiparticle spectrum . The eigenvalues of the psedupotential matrix were used for determination of the quasiparticle energy gap (E_{qp}). The quasiparticle energy gap and the optical energy gap are related to each other via the exciton binding energy, and the relationship between these three quantities is illustrated in Figure 8-2. The optical energy gap (E_{opt}) was obtained by
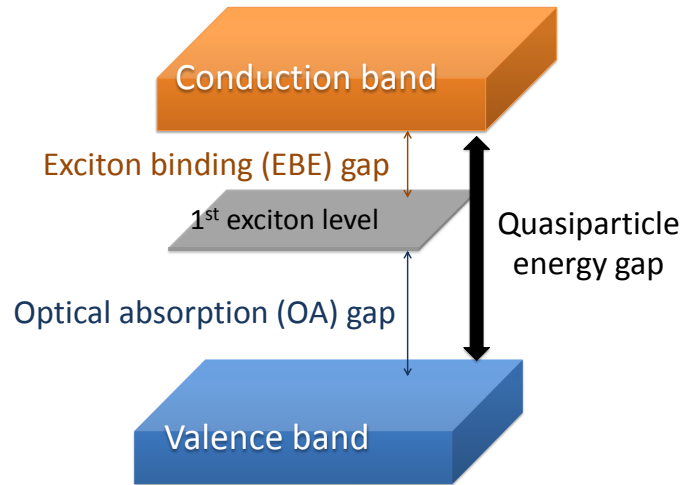
Figure 8-2: The relationship between optical energy gap, quasiparticle gap , and exciton binding energy.

first computing the exciton binding energy ($E_{\text{bind}}^{\text{eh}}$) of the system and then subtracting the exction binding energy from the quasiparticle energy gap as shown in the following

equation,

$$E_{\text{opt}} = E_{\text{qp}} - E_{\text{bind}}^{\text{eh}}. \tag{8.3}$$

The exciton binding energy was computed using the electron-hole explicitly correlated Hartree-Fock method (eh-XCHF), which uses the following ansatz for the electron-hole wave function

$$\Psi_{\text{eh-XCHF}} = G\Phi_0^{\text{e}}\Phi_0^{\text{h}}. \tag{8.4}$$

One of the key features of the eh-XCHF is that the presence of the explicitly correlated function G alleviates the need for a large CI expansion for treating electron-hole correlation [141]. In earlier studies, [10] the eh-XCHF method has been used successfully for computation of exciton binding energies in CdSe quantum dots. The electron and hole (1e-1h) basis states in the eh-XCHF wave function were obtained from the HOMO and LUMO states of the eigenspectrum of the pseudopotential Hamiltonian. The parameters used in the definition of the correlation function G were obtained from Ref. [449]. The construction of the pseudopotential Hamiltonian requires two key pieces of information; the magnitude of the partial charges $\{q_k\}$ and their location $\{\mathbf{R}_k\}$. The determination of these two quantities are discussed below.

MM description of the protein: The protein molecules on the surface of the CdSe quantum dot were treated classically using molecular mechanics force field . As shown in Equation 8.1, the QM/MM interaction term is influenced by both the partial charges and the structure of the protein molecules. We have used the CHARMM36 force field for determination of the partial charges in the firefly luciferase enzyme after assigning protonation states and explicit hydrogens using PROPKA [450]. The CHARMM suite of force fields have been designed specifically for simulating biomolecules and has been used extensively for simulating biomolecules. [451]

The initial structure of the firefly luciferase enzyme was obtained from the protein data bank (PDB:4G37) and was equilibrated at 300 K by performing molecular dynamics (MD) simulations. One of the key features of the equilibration process was the use of explicit water molecules for representing the solvent environment within the MD calculations. This is an important detail, because the solvated structure of the protein is generally different from its *in vacuo* structure. By equilibrating the protein in the presence of explicit water molecules allows us to incorporate the effect of solvation and temperature in the QM/MM calculations. The equilibration runs were performed for 10 ns using the NAMD molecular dynamics package [452]. The equilibrated structure of the single protein molecule was used as the monomeric unit for the construction of the protein corona.

Formation of luciferase corona: The two main challenges associated with protein corona formation are the QD-protein interaction and the MD simulation of the self-assembly process. Earlier studies on protein corona formation have shown that the electrostatic interaction is the dominant driving force for the corona formation [453]. For the present calculations, defining the interaction between the quantum dot and the protein is challenging because of the QM/MM separation. In principle, the QM subsystem polarizes the MM subsystem and in-turn is also polarized by the MM subsystem. Ideally, these interactions should be treated in the self-consistent procedure, however, such an approach will make the calculation impractical because of the large system size. To make the calculations feasible, we have removed the QM/MM separation and treated the entire QD-protein system classically during the corona formation. We have used the CdSe force field developed by Rabani [454] for assignment of the partial charges for Cd and Se in the quantum dot . The self-assembly of the protein corona was performed in the field of the partial charges on the quantum dot. It is very important to note that the quantum dot was treated classically *only* during formation of the protein corona and not during the optical gap calculations .

The underlying assumption of this approach is that the set of partial charges from the CdSe force field is a good approximation to the charge distribution obtained from the QM treatment of the CdSe quantum dot.

All-atom MD simulation of the self-assembly of the protein corona is challenging due to long timescales and is further exacerbated due to the presence of explicit water molecules as solvent. To make these calculations tractable, we have used a combined MD/Monte Carlo approach for this system. In the first step, the initial structure for the Monte Carlo step was obtained by arranging the protein molecules on the surface of the quantum dot. To minimize protein-protein steric interactions in the initial configuration, we have used the best-packing-on-sphere method[455] such that the center-of-mass between two protein molecules is maximized.[456] In the second step, the position of Cd and Se atoms in the quantum dot were kept fixed and the conformational degrees-of-freedom of the luciferase molecules were sampled using Monte Carlo procedure to obtain the minimum energy structure. In the third step, the minimized structure was solvated in explicit water, and the entire system was thermally equilibrated using molecular dynamics simulation at 300 K. In the final step, the optical gap of the QD-protein complex was calculated using Equation 8.2.

Results: To facilitate the discussion of the results and analysis of the simulations, we represent the single luciferase bound complex as QD-Lu$_1$. The procedure described above was repeated starting with the QD-Lu$_1$ complex to generate QD-Lu$_2$. We found that up to seven luciferase molecules were able to bind with the quantum dot and the intermediate steps of the corona formation are illustrated in Figure 8-3. Addition of more luciferase molecules on the QD-Lu$_7$ complex were found to be unfavorable due to steric crowding. The atomic position of the partial charges (denoted as $\mathbf{R}^{\text{protein}}$ in Equation 8.2) were used in the QM/MM calculations and the optical gap E_{opt} for each of the QD-Lu$_n$ (with $n = 1, \ldots, 7$) complexes were calculated.
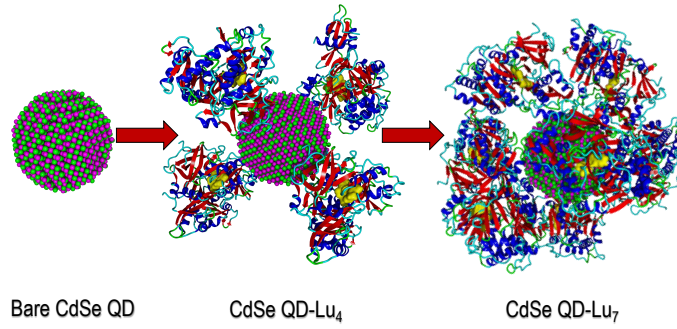
Figure 8-3: Progressive growth of CdSe-luciferase protein complex.

8.3 Results and conclusion

The change in the optical gap of the quantum dot due the presence of the protein is denoted as ΔE_{opt} and is defined as by the following equation

$$\Delta E_{\text{opt}} = E_{\text{opt}}(\text{QD-Lu}_n) - E_{\text{opt}}(\text{QD}). \tag{8.5}$$

The change in the optical gap for the series of quantum dot-protein complexes during the formation of the protein corona is presented in Table 8.1. We find that in all cases the optical gap in QD-Lu$_n$ complexes are red-shifted as compared to the bare quantum dot. The magnitude of the shift was found to increase with the increasing number of luciferase molecules. Although published experimental and computational results on CdSe-luciferase is not available, similar trends for other systems have been observed. For example, Anandampillai and coworkers have performed calculations on small CdSe-DNA clusters [445]. Their results show that the λ_{max} was red-shifted by 12 and 19 nm for dot diameters of 1.1 and 1.3 nm, respectively. Additionally, Xiong et al. have found that peptide conjugated CdTe quantum dots display a considerable redshift as compared to the bare quantum dots. [457] In the work done by Paramanik et al., a red-shift was reported for quantum dots surrounded by DNA. They concluded

131
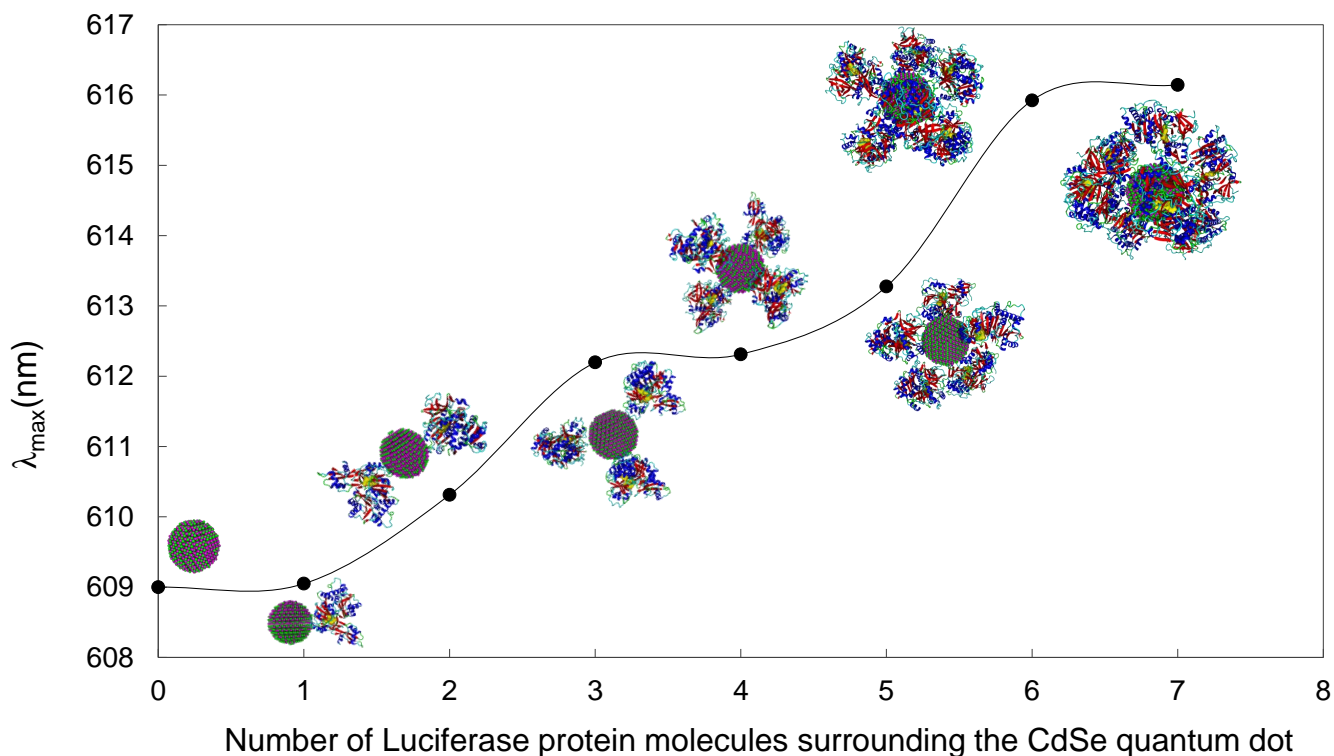
Figure 8-4: Shift in λ_{max} as a function of formation of protein corona around CdSe quantum dot.

that the shift was mainly driven by strong electrostatic interaction between the QD and DNA [458]. Based on the reported experimental results, the shift in λ_{max} calculated in the present work is consistent with experimental findings of QD-biomolecule systems.

In conclusion, a multilevel strategy for calculating optical gap of large quantum dot-protein complexes has been presented. This multilevel scheme includes techniques from quantum mechanical pseudopotential calculations, electron-hole explicitly correlated wave function, classical molecular dynamics, and Monte Carlo method and is specifically designed to address the challenges associated with treating large quantum dot-protein complexes in aqueous medium. Although the method was applied to the specific example of CdSe-luciferase complex, the computational strategy developed here is general and can be applied to other QD-protein complexes.

Table 8.1: Spectral shift associated with building protein corona around a 5nm CdSe quantum dot.

QD-protein	ΔE_{opt}(meV)	$\Delta \lambda_{\mathrm{max}}$ (nm)
Bare QD	0	0
QD-Lu$_1$	0.17	1
QD-Lu$_2$	4.38	2
QD-Lu$_3$	10.63	4
QD-Lu$_4$	11.02	4
QD-Lu$_5$	14.20	5
QD-Lu$_6$	22.89	7
QD-Lu$_7$	23.61	8

Chapter 9

Utilization of XCHF Method for Development of Adiabatic Connection Curve for Application to Electron-hole Multi-Component Density Functional Theory

9.1 Introduction and motivation for development of electron-hole adiabatic connection curve

Development of functionals within the constrains of density functional theory is often a difficult and challenging process [459, 460, 461, 462, 463, 464, 465, 466, 467, 468, 469]. One of the theoretical routes that is used towards functional development is the adiabatic connection method [470, 471, 472, 473, 474, 475, 476, 477, 353, 478, 479]. This method provides the necessary direct link between non-interacting and interacting physical systems [480]. For example, Teale and coworkers in 2009 have used an

adiabatic connection curve (AC curve) method based on full configuraton interaction densities for the construction of AC curves for the helium isoelectronic series as well as the H$_2$O molecule [480]. In 2010, Teale again used the adiabatic connection method to construct curves for several systems including helium, hydrogen, and beryllium using differing levels of electronic structure theory including HF, MP2, CCSD and CCSDT(Q) [481]. Zhang et al. presented the adiabatic connection curve for both the Hooke's atom and Helium atom benchmark systems from accurate wave function calculations [472]. Cohen et al. have also used an adiabatic connection method approach to functional development and they find that functionals resulting from the adiabatic connection method can improve upon currently widely used functionals, specifically with respect to single electron systems [482, 483]. Peach et al. have studied the adiabatic connection method for the H_2 molecule and aso the helium isoelectronic series, their work has shown that simple approximate forms of the adiabatic connection integrand can be generated and used. However, these simple forms and the parameters therein must be strongly based on accurate data for them to be feasible [484, 485].

Though it is clear that this method has been used extensively in the development of functionals for electronic structure methods, an adiabatic connection curve has not been constructed for an electron-hole system. The electron-hole adiabatic connection curve is central in the development of an accurate correlation functional for multi-component electron-hole density functional theory (eh-DFT). The construction of this curve is challenging because it requires density constrained minimization at different values of coupling constants. In the present work, the density constraint was implemented by defining an electron-hole Levy Lieb Lagrangian (eh-LLL). For a given set of input densities the eh-LLL was constructed and expressed as a functional of the coupling constant dependent external potential. Thus unconstrained minimization of the eh-LLL was then performed by varying the eh-wave function, external potential and Lagranges multipliers. Within this chapter, the electron-hole explicitly correlated

135

Hartree-Fock method is used as as the ansatz for the trial wave function towards the development of the exchange correlation functional for an electron-hole system using the adiabatic connection method. The theory is described in section 9.2, and results from this study are described in section 9.3. Though multi-component density functional theory is not at all a new concept [486, 487, 488], this is the first time that the adiabatic connection curve has been constructed for the electron-hole system.

9.2 Theoretical details

9.2.1 Electron-hole correlation functional

The central concept of the electron-hole density functional theory (eh-DFT) is that the ground state energy of the eh-Hamiltonian is a functional of electron and hole densities

$$E[\rho_e, \rho_h] = F[\rho_e, \rho_h] + \langle v_e^{ext} \rho_e \rangle + \langle v_h^{ext} \rho_h \rangle. \tag{9.1}$$

where the functional F in Equation 9.1 is the exact electron-hole universal functional. The relationship between the exact eh-functional and the eh-Hamiltonian can be obtained by the Levy constrained search procedure as shown below

$$F[\rho_e, \rho_h] = \min_{\Psi \to \rho_e, \rho_h} \langle \Psi | T_e + V_{ee} + T_h + V_{hh} + V_{eh} | \Psi \rangle \tag{9.2}$$

In addition to the eh-functional, we also define the corresponding single-component electron and hole universal functionals F_e and F_h using the Levy procedure

$$F_e[\rho_e] = \min_{\Psi \to \rho_e} \langle \Psi | T_e + V_{ee} | \Psi \rangle \tag{9.3}$$

$$F_h[\rho_h] = \min_{\Psi \to \rho_h} \langle \Psi | T_h + V_{hh} | \Psi \rangle \tag{9.4}$$

136

In addition to the single and multicomponent universal functionals, the classical electron-hole Coulomb energy J_{eh} is defined as

$$J_{eh}[\rho_e, \rho_h] = \langle \rho_e \rho_h r_{eh}^{-1} \rangle \tag{9.5}$$

Using quantities, we define the electron-hole correlation energy E_{ehc} is the component of the eh-functional can cannot be obtained by the summation of the single-component functionals with the classical eh-Coulomb energy.

$$F[\rho_e, \rho_h] = F_e[\rho_e] + F_h[\rho_h] + J_{eh}[\rho_e, \rho_h] + E_{ehc}[\rho_e, \rho_h]. \tag{9.6}$$

The definition of the E_{ehc} is very general and is independent of the specific form of the eh-Hamiltonian . As long as the single-component external potentials are expressed as a 1-body operators, the total energy can be written as a functional of the single-particle densities. One of the key differences between E_{ehc} and the exchange-correlation E_{xc} functional used in electronic structure theory is that E_{ehc} is defined using interacting single-component reference, as opposed to non-interacting reference used in the definition of E_{xc}. Specifically, in the limit of the zero eh-interaction, the system still retains full ee- and hh- interactions,

$$\lim_{V_{eh} \to 0} F[\rho_e, \rho_h] = F_e[\rho_e] + F_h[\rho_h] \tag{9.7}$$

This difference is especially relevant for construction of the adiabatic connection curve and is discussed next.

9.2.2 Adiabatic connection

To construct the AC curve, we define the coupling parameter λ that scale the eh-interaction in the Hamiltonian

$$H^\lambda = H_{\mathrm{e}} + H_{\mathrm{h}} + \lambda V_{\mathrm{eh}} = H_0 + \lambda V_{\mathrm{eh}}. \tag{9.8}$$

The energy functional associated with the coupling-constant dependent Hamiltonian is

$$F^\lambda[\rho_{\mathrm{e}}, \rho_{\mathrm{h}}] = \min_{\Psi \to \rho_{\mathrm{e}}, \rho_{\mathrm{h}}} \langle \Psi | H_\lambda | \Psi \rangle \tag{9.9}$$

$$= \langle \Psi_{\rho_{\mathrm{e}}, \rho_{\mathrm{h}}}^{\lambda, \min} | H_\lambda | \Psi_{\rho_{\mathrm{e}}, \rho_{\mathrm{h}}}^{\lambda, \min} \rangle \tag{9.10}$$

$$E_{\mathrm{ehc}}[\rho_{\mathrm{e}}, \rho_{\mathrm{h}}] = F^\lambda[\rho_{\mathrm{e}}, \rho_{\mathrm{h}}] - F^0[\rho_{\mathrm{e}}, \rho_{\mathrm{h}}] - J_{\mathrm{eh}}[\rho_{\mathrm{e}}, \rho_{\mathrm{h}}]. \tag{9.11}$$

It is apparent that the form of our approximation to the functional takes the form of an integral expression between the non-interacting and interacting limit and can therefore be written as,

$$E_{\mathrm{ehc}}[\rho_{\mathrm{e}}, \rho_{\mathrm{h}}] = \int_0^1 d\lambda \frac{\partial F^\lambda[\rho_{\mathrm{e}}, \rho_{\mathrm{h}}]}{\partial \lambda} - J_{\mathrm{eh}}[\rho_{\mathrm{e}}, \rho_{\mathrm{h}}]. \tag{9.12}$$

$$E_{\mathrm{ehc}}[\rho_{\mathrm{e}}, \rho_{\mathrm{h}}] = \int_0^1 d\lambda \langle \Psi_{\rho_{\mathrm{e}}, \rho_{\mathrm{h}}}^{\lambda, \min} | V_{\mathrm{eh}} | \Psi_{\rho_{\mathrm{e}}, \rho_{\mathrm{h}}}^{\lambda, \min} \rangle - J_{\mathrm{eh}}[\rho_{\mathrm{e}}, \rho_{\mathrm{h}}] \tag{9.13}$$

Simplification of this expression allows for the definition of the U_{xc} term. The

definition of U_{xc} is very common among electronic structure adiabatic connection methods and has been used extensively for development of these adiabatic connection curves, however, this quantity has yet to be computed for an electron-hole system.

$$U_{\text{xc}}^{\lambda}[\rho_{\text{e}}, \rho_{\text{h}}] = \langle \Psi_{\rho_{\text{e}}, \rho_{\text{h}}}^{\lambda, \min} | V_{\text{eh}} | \Psi_{\rho_{\text{e}}, \rho_{\text{h}}}^{\lambda, \min} \rangle - J_{\text{eh}}[\rho_{\text{e}}, \rho_{\text{h}}] \tag{9.14}$$

The electron-hole correlation functional can be defined in terms of U_{xc} as follows,

$$E_{\text{ehc}}[\rho_{\text{e}}, \rho_{\text{h}}] = \int_0^1 d\lambda U_{\text{xc}}^{\lambda}[\rho_{\text{e}}, \rho_{\text{h}}]. \tag{9.15}$$

And therefore, the key to constructing the adiabatic connection curve lies in the accurate computation of the U_{xc} quantity at various values of the λ coupling parameter between 0 and 1.

9.2.3   Density-constrained minimization

There are several associated challenges that are faced when constructing the adiabatic connection curve . The first of these challenges results from the density constrained minimization of the λ dependent wave function as it must be done for each value of the coupling parameter. The second challenge faced is the accurate and computationally efficient description of the wave function at small electron-hole interparticle distance.

These challenges are addressed through the use of a method that has the capability to both ease the computation of a constrained search minimization and also provide an accurate and computationally efficient description of the wave function. The solution that is presented here is to construct the electron-hole Levy-Lieb Lagrangian as shown in Equation 9.16. Using this form of the electron-hole Levy-Lieb Lagrangian allows for the unconstrained minimization of the electron-hole wave function thus alleviating the

constrained minimization problem. However, within the Lagrangian definition there are associated electron and hole density constraints $(\eta_\text{e}, \eta_\text{h})$ respectively, that ensure that the target density is achieved.

$$\mathcal{L}[\rho_\text{e}, \rho_\text{h}, \Psi_\text{T}, W_\text{e}^\lambda, W_\text{h}^\lambda] = \frac{\langle \Psi_\text{T} | H_\lambda + W_\text{e}^\lambda + W_\text{h}^\lambda | \Psi_\text{T} \rangle}{\langle \Psi_\text{T} | \Psi_\text{T} \rangle} + \\ \eta_\text{e} \langle (\rho_\text{e}^\text{T} - \rho_\text{e})^2 \rangle + \eta_\text{h} \langle (\rho_\text{h}^\text{T} - \rho_\text{h})^2 \rangle \tag{9.16}$$

where, the trial densities were obtained from the trial wave functions

$$\rho_\text{e}^\text{T}(\mathbf{r}^\text{e}) = \frac{N_\text{e}}{\langle \Psi_\text{T} | \Psi_\text{T} \rangle} \int ds_1^\text{e} d\mathbf{x}_2^\text{e} d\mathbf{x}_1^\text{h} \dots d\mathbf{x}_{N_\text{e}}^\text{e} d\mathbf{x}_{N_\text{e}}^\text{h} |\Psi_\text{T}|^2 \tag{9.17}$$

$$\min_{\Psi_\text{T}, W_\text{e}^\lambda, W_\text{h}^\lambda, \eta_\text{e}, \eta_\text{h}} \mathcal{L}[\rho_\text{e}, \rho_\text{h}, \Psi_\text{T}, W_\text{e}^\lambda, W_\text{h}^\lambda] \implies \Psi_{\rho_\text{e}, \rho_\text{h}}^{\lambda, \min} \tag{9.18}$$

9.2.4 Form of the trial eh-wave function

Within the above expression for the eh-LLL, the choice of wave function for Ψ_T is the explicitly correlated Hartree-Fock (XCHF) ansatz . The form of the XCHF ansatz is given as follows,

$$\Psi_\text{XCHF}(\mathbf{r}_\text{e}, \mathbf{r}_\text{h}) = G\Phi_\text{eh}^0. \tag{9.19}$$

Where the wave function is composed of a correlation function, G, and a reference electron-hole wave function. Here, the reference wave function is a single Slater determinant for the electrons and for the holes,

140

$$\Phi_{eh}^0 = \Phi_e \Phi_h. \tag{9.20}$$

One of the inherent advantages of the using the XCHF wave function to construct the adiabatic curve is that it alleviates the need for large CI calculation. This has been shown in benchmark calculations of the ground state energy of the Helium atom [141]. The advantage is a result of the inherent compact representation of the infinite order configuration interaction expansion, as shown below,

$$G|\Psi_{\text{ref}}\rangle = \underbrace{\sum_{ii'}^{\infty} |\Phi_i^e \Phi_{i'}^h\rangle \langle \Phi_i^e \Phi_{i'}^h|}_{1} G|\Psi_{\text{ref}}\rangle. \tag{9.21}$$

9.2.5 Steps towards the construction of the adiabatic connection curve

The explicitly correlated Hartree-Fock wave function was used for the construction of the electron-hole adiabatic connection curve. The steps for the construction of the curve are summarized below.

As the first step, a fully interacting ($\lambda = 1$) calculation was performed using the XCHF method to obtain the target electron and hole densities. Upon obtaining the target densities we are able to define the electron-hole Levy Lieb Lagrangian as shown in Equation 9.16.

$$\min_{v_{\text{ext}}, G, \eta_e, \eta_h} \mathcal{L}[\lambda, \rho_e, \rho_h] \to \langle \Psi_{\rho_e, \rho_h}^{\lambda, \min} | V_{\text{eh}} | \Psi_{\rho_e, \rho_h}^{\lambda, \min} \rangle \quad v_{\text{ext}}^\lambda \in \{Z^\lambda r^{-1}\} \tag{9.22}$$

The minimization is performed by varying the electron-hole wave function, Lagrange's multipliers and external potential. The unconstrained minimization of the eh-LLL is

performed for $0 \leq \lambda < 1$ and therefore at each value of the λ parameter, a density constrained wave function is found. Utilizing the density constrained wave functions, U_{xc} as shown in Equation 9.14 is computed for each value of λ and thus the adiabatic curve is constructed.

9.3 Results from the development of the electron-hole adiabatic connection curve

Within this work, the adiabatic connection curve has been constructed for the electron-hole system using the electron-hole explicitly correlated Hartree-Fock based adiabatic connection method. As an important benchmark, the adiabatic connection curves were constructed for the Hooke's atom system and for the Helium atom. The results are described within the following subsections.

As a verification of the ability of the XCHF explicitly correlated wave function to be used for construction of the adiabatic connection curve a benchmark curve was constructed for the Hooke's atom system. The adiabatic curve for the Hooke's atom system is well known [8]. It has been cosnstructed here for a confining potential of $\omega = 0.5$ and for $\lambda = 0 - 1$, at this value of the confining ω, the result for Hooke's atom is analytical and is often used to benchmark theoretical methods. The results of the computation of this curve are shown in Figure 9-1. It is apparent from these results that the adiabatic curve for Hooke's atom is very linear in its construction. The curve given here compares well to results shown for the Hooke's atom curve by Magyar and coworkers which was computed using a simulated scaling adiabatic connection method [8].

In addition to the Hooke's atom, the adiabatic connection curve was also computed for the Helium atom so as to compare to a realistic two-electron system. Results were compared to the Helium curve computed by Teale and coworkers [480] and were
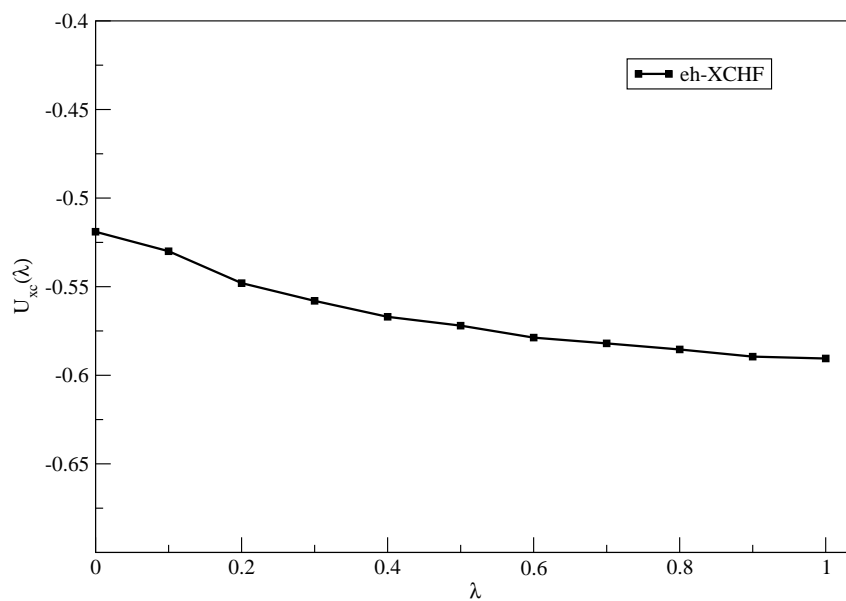
Figure 9-1: The adiabatic connection curve for Hooke's atom using the explicitly correlated Hartree-Fock method. This benchmark curve compares well with previous results for the Hooke's atom adiabatic curve from Magyar and coworkers [8].

Table 9.1: Property of helium adiabatic connection curve

λ	Total energy	T_λ	V_{ext}	V_{ee}	$U_{xc}(\lambda)$
0.0	-3.097599974	3.054810884	-6.991375975	1.095	-1.095
0.1	-3.113943181	3.041449133	-6.975423182	1.07949806	-1.11050194
0.2	-3.061846739	3.042661202	-6.971891201	1.060127436	-1.129872564
0.3	-2.983301962	3.027964203	-6.951971439	1.050092815	-1.139907185
0.4	-3.015321113	3.071601549	-6.988453512	1.030847761	-1.159152239
0.5	-3.011422847	3.07225962	-6.977377765	1.019879041	-1.170120959
0.6	-3.012898165	3.071787185	-6.97171452	1.013600981	-1.176399019
0.7	-2.923734131	3.072928564	-6.966728588	1.007614581	-1.182385419
0.8	-2.928809236	3.09828147	-6.982549247	0.998811797	-1.191188203
0.9	-2.822120327	3.099929102	-6.97461846	0.990505938	-1.199494062
1.0	-2.882953965	3.106810668	-6.976945829	0.987181196	-1.202818804

found to be in good agreement. This provides a very important verification of the capability of the XCHF method to compute the adiabatic curve. Numerical results for the energetic components are given in Table 9.1.

Upon the successful benchmarking of the Hooke's atom curve, the electron-hole adiabatic connection curve was computed for the first time for the electron hole pair in a parabolic potential. The confining $\omega = 0.5$. The electron-hole pair in a parabolic potential is often used as a benchmark system and is the multi-component analogue of a Hooke's atom system. The adiabatic connection curve for the electron-hole system is shown in 9-2. The curve has been fit using a linear least squares method and the fitting function is given as $y = -0.158x$.

As this is the first time that the adiabatic connection curve has been constructed there are no existing benchmark results to compare the curve to. However, the integration of the curve should be equivalent to the ground state energy of the electron-hole pair in a parabolic potential if the curve has been constructed correctly. The curve was integrated and thus compared to the ground state energy given by the fully interacting ($\lambda = 1$) XCHF calculation. The energy from integration of the adiabatic connection curve is given as 0.8484 Hartree and the energy from the ground state calculation using the XCHF method is 0.8402 Hartree. The energies differ by 8.4×10^{-2}
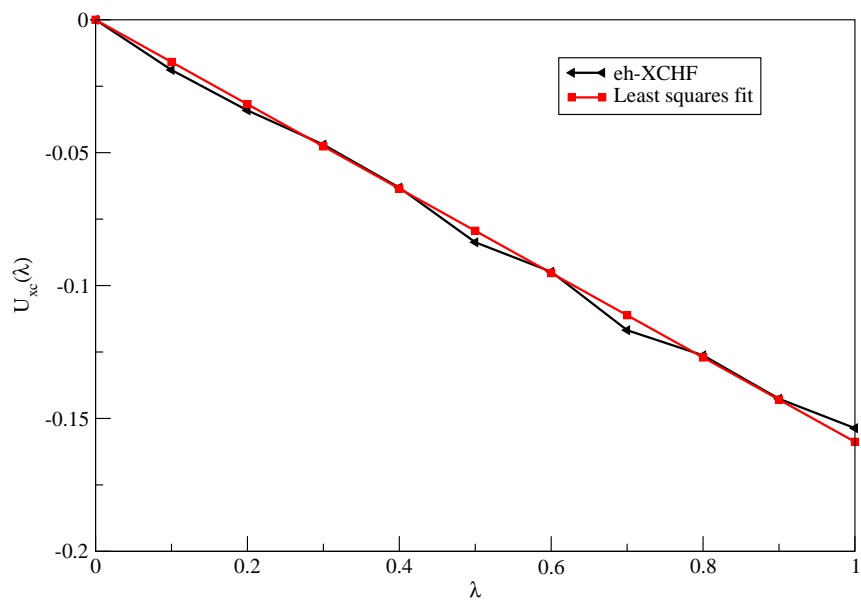
Figure 9-2: The adiabatic connection curve for an electron-hole pair in a parabolic potential, with confining $\omega = 0.5$. The curve was computed with the eh-XCHF method and is shown with a linear least squares fit. The fit equation is $y = -0.158x$.
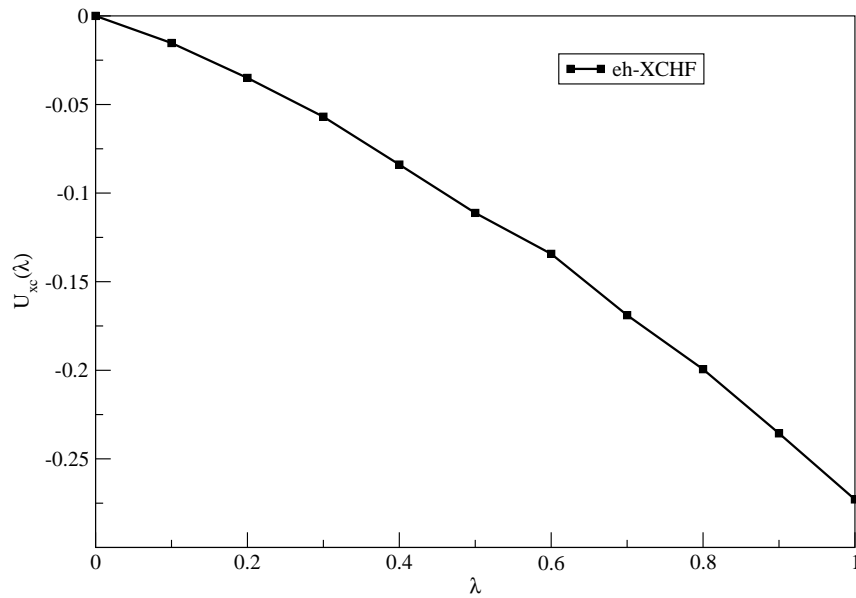
Figure 9-3: The adiabatic connection curve for an electron-hole pair in a parabolic potential, with confining $\omega = 0.05$. The weaker confining limit is shown here for confirmation of the use of the eh-XCHF method to construct the curve.

Hartree.

In addition to the computation of the curve for $\omega = 0.5$, it has also been computed for $\omega = 0.05$, the weaker confining limit. These results are shown in 9-3. It it interesting to note that the adiabatic curve for the electron-hole system is less linear in the weaker confining limit.

Chapter 10

Conclusions of the present work and future application

In conclusion, throughout the work presented here, the efficiency, importance and application of explicitly correlated wave function based methods have been demonstrated. The method developed within this work, electron-hole explicitly correlated Hartree-Fock, is a general and versatile technique for solving the electron-hole Schrodinger equation. The method has been applied to study a variety of chemical systems which include the Helium atom, CdSe quantum dots, CdSe/ZnS quantum dots and a quantum dot-protein bioconjugate system. In addition to these systems, it has been used towards the development of an electron-hole correlation functional for use within electron-hole multi-component density functional theory. The accuracy of the eh-XCHF wave function has been demonstrated through calculation of the ground state energy and recombination probability of a parabolic quantum dot system. In addition to the parabolic quantum dot, the congruent transformation of the Hamiltonian using the XCHF method has been benchmarked with respect to computing the ground state energy of the Helium atom. These calculations highlight the importance of the accuracy of the wave function at small inter-particle distances and thus the

ability of the XCHF method to be able to successfully address the problem.

Upon successful benchmarking of the method, XCHF was applied to study the effect of several influential factors on the excitonic properties of quantum dot systems. The properties studied in this work were exciton binding energy, electron-hole recombination probability and average electron hole separation distance. Each of these properties act as an efficient metric for the study of electron-hole interaction in quantum dots. In the initial study on CdSe quantum dots, using the XCHF method, the exciton binding energy and electron-hole recombination probability were found to be strongly affected by the particle size. The XCHF method compared very well to both experimental and theoretical results for exciton binding energy in quantum dots up to and including 20 nm in diameter. This provided important verification of the XCHF method to treat large quantum dot systems as current theoretical methods meet their limit at small particle size. It is essential to have a method that is both computationally efficient and flexible in treating QDs and other nanoparticles. This has been further shown with respect to the XCHF method with pseudopotential, described at the end of Chapter 5. In that implementation, XCHF was able to treat systems of up to 2075 atoms in its current form and will be able to treat even larger systems in future work. The excitonic properties in question have also been found to be strongly effected by heterojunction, shape and the formation of protein corona on the surface of a quantum dot within this work.

Theoretical methods are often used as predictive tools for the development of new materials. As in any new technology, there are limitations associated with using the XCHF method for these predictive purposes, but it is evident from this work that XCHF has the capability and generality to be applied to assist in new material development.

Bibliography

[1] Lin-Wang Wang and Alex Zunger. Pseudopotential calculations of nanoscale cdse quantum dots. *Phys. Rev. B*, 53:9579–9582, Apr 1996. doi:10.1103/PhysRevB.53.9579.

[2] Robert W. Meulenberg, Jonathan R.I. Lee, Abraham Wolcott, Jin Z. Zhang, Louis J. Terminello, and Tony van Buuren. Determination of the exciton binding energy in cdse quantum dots. *ACS Nano*, 3(2):325–330, 2009. doi:10.1021/nn8006916.

[3] Alberto Franceschetti and Alex Zunger. Direct pseudopotential calculation of exciton coulomb and exchange energies in semiconductor quantum dots. *Phys. Rev. Lett.*, 78:915–918, Feb 1997. doi:10.1103/PhysRevLett.78.915.

[4] Jacek Jasieniak, Marco Califano, and Scott E. Watkins. Size-dependent valence and conduction band-edge energies of semiconductor nanocrystals. *ACS Nano*, 5(7):5888–5902, 2011. doi:10.1021/nn201681s.

[5] Erol Kucur, Jurgen Riegler, Gerald A. Urban, and Thomas Nann. Determination of quantum confinement in cdse nanocrystals by cyclic voltammetry. *J. Chem. Phys.*, 119(4):2333–2337, 2003. doi:10.1063/1.1582834.

[6] Shaukatali N. Inamdar, Pravin P. Ingole, and Santosh K. Haram. Determination of band structure parameters and the quasi-particle gap of cdse quantum dots

by cyclic voltammetry. *ChemPhysChem*, 9(17):2574–2579, 2008. ISSN 1439-7641. doi:10.1002/cphc.200800482.

[7] Claudia Querner, Peter Reiss, Said Sadki, Malgorzata Zagorska, and Adam Pron. Size and ligand effects on the electrochemical and spectroelectrochemical responses of cdse nanocrystals. *Phys. Chem. Chem. Phys.*, 7:3204–3209, 2005. doi:10.1039/B508268B.

[8] R.J. Magyar, W. Terilla, and K. Burke. Accurate adiabatic connection curve beyond the physical interaction strength. *J. Chem. Phys.*, 119(2):696–700, 2003. doi:10.1063/1.1579465.

[9] Jennifer M. Elward, Barbara Thallinger, and Arindam Chakraborty. Calculation of electron-hole recombination probability using explicitly correlated hartree-fock method. *J. Chem. Phys.*, 136(12):124105, 2012. doi:10.1063/1.3693765.

[10] Jennifer M. Elward and Arindam Chakraborty. Effect of dot size on exciton binding energy and electron-hole recombination probability in cdse quantum dots. *J. Chem. Theory Comput.*, 9(10):4351 – 4359, 2013. doi:10.1021/ct400485s.

[11] Clemens Burda, Xiaobo Chen, Radha Narayanan, and Mostafa A. El-Sayed. Chemistry and properties of nanocrystals of different shapes. *Chem. Rev.*, 105(4):1025–1102, 2005. doi:10.1021/cr030063a.

[12] A.D. Yoffe. Semiconductor quantum dots and related systems: Electronic, optical, luminescence and related properties of low dimensional systems. *Advances in Physics*, 50(1):1–208, 2001. doi:10.1080/00018730010006608.

[13] A.P. Alivisatos. Semiconductor clusters, nanocrystals, and quan-

tum dots. *Science*, 271(5251):933–937, 1996. ISSN 00368075. doi:10.1126/science.271.5251.933.

[14] M Nirmal, BO Dabbousi, MG Bawendi, JJ Macklin, JK Trautman, TD Harris, and LE Brus. Fluorescence intermittency in single cadmium selenide nanocrystals. *Nature*, 383(6603):802–804, 1996.

[15] L Brus. Quantum crystallites and nonlinear optics. *Applied Physics A*, 53(6): 465–474, 1991.

[16] Sungjee Kim, Brent Fisher, Hans-Jürgen Eisler, and Moungi Bawendi. Type-ii quantum dots: Cdte/cdse (core/shell) and cdse/znte (core/shell) heterostructures. *J. Am. Chem. Soc.*, 125(38):11466–11467, 2003. doi:10.1021/ja0361749.

[17] Kerry J Vahala. Optical microcavities. *Nature*, 424(6950):839–846, 2003. doi:10.1038/nature01939.

[18] X. Peng. Mechanisms for the shape-control and shape-evolution of colloidal semiconductor nanocrystals. *Advanced Materials*, 15(5):459–463, 2003. ISSN 09359648. doi:10.1002/adma.200390107.

[19] Inuk Kang and Frank W Wise. Electronic structure and optical properties of pbs and pbse quantum dots. *JOSA B*, 14(7):1632–1646, 1997. doi:10.1364/JOSAB.14.001632.

[20] James E Murphy, Matthew C Beard, Andrew G Norman, S Phillip Ahrenkiel, Justin C Johnson, Pingrong Yu, Olga I Micic, Randy J Ellingson, and Arthur J Nozik. Pbte colloidal nanocrystals: synthesis, characterization, and multiple exciton generation. *Journal of the American Chemical Society*, 128(10):3241–3247, 2006. doi:10.1021/ja0574973.

[21] Z Adam Peng and Xiaogang Peng. Mechanisms of the shape evolution of cdse nanocrystals. *Journal of the American Chemical Society*, 123(7):1389–1395, 2001. doi:10.1021/ja0027766.

[22] R. Alam, D.M. Fontaine, B.R. Branchini, and M.M. Maye. Designing quantum rods for optimized energy transfer with firefly luciferase enzymes. *Nano Lett.*, 12(6):3251–3256, 2012. doi:10.1021/nl301291g.

[23] R. Alam, J. Zylstra, D.M. Fontaine, B.R. Branchini, and M.M. Maye. Novel multistep bret-fret energy transfer using nanoconjugates of firefly proteins, quantum dots, and red fluorescent proteins. *Nanoscale*, 5(12):5303–5306, 2013. doi:10.1039/c3nr01842c.

[24] L. Chen, H. Gong, X. Zheng, M. Zhu, J. Zhang, S. Yang, and B. Cao. Cds and cds/cdse sensitized zno nanorod array solar cells prepared by a solution ions exchange process. *Mater. Res. Bull.*, 48(10):4261–4266, 2013. doi:10.1016/j.materresbull.2013.06.069.

[25] P. Gallo, M. Felici, B. Dwir, K.A. Atlasov, K.F. Karlsson, A. Rudra, A. Mohan, G. Biasiol, L. Sorba, and E. Kapon. Integration of site-controlled pyramidal quantum dots and photonic crystal membrane cavities. *Appl. Phys. Lett.*, 92 (26):263101–263104, 2008. doi:10.1063/1.2952278.

[26] M. Grundmann, O. Stier, and D. Bimberg. Inas/gaas pyramidal quantum dots: Strain distribution, optical phonons, and electronic structure. *Phys. Rev. B*, 52: 11969–11981, Oct 1995. doi:10.1103/PhysRevB.52.11969.

[27] K.F. Karlsson, V. Troncale, D.Y. Oberli, A. Malko, E. Pelucchi, A. Rudra, and E. Kapon. Optical polarization anisotropy and hole states in pyramidal quantum dots. *Appl. Phys. Lett.*, 89(25):251113, 2006. doi:10.1063/1.2402241.

[28] A. Schliwa, M. Winkelnkemper, and D. Bimberg. Impact of size, shape, and composition on piezoelectric effects and electronic properties of in (ga) asgaas quantum dots. *Phys. Rev. B*, 76(20), 2007. doi:10.1103/PhysRevB.76.205324.

[29] A.S. Barnard and P. Zapol. A model for the phase stability of arbitrary nanoparticles as a function of size and shape. *J. Chem. Phys.*, 121(9):4276–4283, 2004. ISSN 00219606. doi:10.1063/1.1775770.

[30] C.R. Bealing, W.J. Baumgardner, J.J. Choi, T. Hanrath, and R.G. Hennig. Predicting nanocrystal shape through consideration of surface-ligand interactions. *ACS Nano*, 6(3):2118–2127, 2012. ISSN 19360851. doi:10.1021/nn3000466.

[31] N.J. Borys, M.J. Walter, J. Huang, D.V. Talapin, and J.M. Lupton. The role of particle morphology in interfacial energy transfer in cdse/cds heterostructure nanocrystals. *Science*, 330(6009):1371–1374, 2010. doi:10.1126/science.1198070.

[32] A. Ben Moshe, D. Szwarcman, and G. Markovich. Size dependence of chiroptical activity in colloidal quantum dots. *ACS Nano*, 5(11):9034–9043, 2011. doi:10.1021/nn203234b.

[33] L. Cademartiri, E. Montanari, G. Calestani, A. Migliori, A. Guagliardi, and G.A. Ozin. Size-dependent extinction coefficients of pbs quantum dots. *J. Am. Chem. Soc.*, 128(31):10337–10346, 2006. doi:10.1021/ja063166u.

[34] H. Choi, J.-H. Ko, Y.-H. Kim, and S. Jeong. Steric-hindrance-driven shape transition in pbs quantum dots: Understanding size-dependent stability. *J. Am. Chem. Soc.*, 135(14):5278–5281, 2013. doi:10.1021/ja400948t.

[35] http://nanocluster.mit.edu/research.php, 2014.

[36] J. C. Maan, G. Belle, A. Fasolino, M. Altarelli, and K. Ploog. Magneto-

optical determination of exciton binding energy in gaas-ga$_{1-x}$al$_x$As quantum wells. *Phys. Rev. B*, 30:2253–2256, Aug 1984. doi:10.1103/PhysRevB.30.2253.

[37] Peter Ramvall, Satoru Tanaka, Shintaro Nomura, Philippe Riblet, and Yoshinobu Aoyagi. Observation of confinement-dependent exciton binding energy of gan quantum dots. *Appl. Phys. Lett.*, 73(8):1104–1106, 1998. doi:10.1063/1.122098.

[38] Florencio García-Santamaría, Yongfen Chen, Javier Vela, Richard D. Schaller, Jennifer A. Hollingsworth, and Victor I. Klimov. Suppressed auger recombination in "giant" nanocrystals boosts optical gain performance. *Nano Lett.*, 9(10): 3482–3488, 2009. doi:10.1021/nl901681d.

[39] Lin-Wang Wang, Marco Califano, Alex Zunger, and Alberto Franceschetti. Pseudopotential theory of auger processes in cdse quantum dots. *Phys. Rev. Lett.*, 91:056404, Jul 2003. doi:10.1103/PhysRevLett.91.056404.

[40] Kim Hyeon-Deuk and Oleg V. Prezhdo. Multiple exciton generation and recombination dynamics in small si and cdse quantum dots: An ab initio time-domain study. *ACS Nano*, 6(2):1239–1250, 2012. doi:10.1021/nn2038884.

[41] Eran Rabani and Roi Baer. Theory of multiexciton generation in semiconductor nanocrystals. *Chem. Phys. Lett.*, 496(4âĂŞ6):227 – 235, 2010. ISSN 0009-2614. doi:10.1016/j.cplett.2010.07.059.

[42] Zhibin Lin, Alberto Franceschetti, and Mark T. Lusk. Size dependence of the multiple exciton generation rate in cdse quantum dots. *ACS Nano*, 5(4):2503–2511, 2011. doi:10.1021/nn200141f.

[43] Heather M. Jaeger, Kim Hyeon-Deuk, and Oleg V. Prezhdo. Exciton multiplication from first principles. *Acc. Chem. Res.*, 46(6):1280–1289, 2013. doi:10.1021/ar3002365.

[44] Javier Vela, Han Htoon, Yongfen Chen, Young-Shin Park, Yagnaseni Ghosh, Peter M. Goodwin, James H. Werner, Nathan P. Wells, Joanna L. Casson, and Jennifer A. Hollingsworth. Effect of shell thickness and composition on blinking suppression and the blinking mechanism in "giant" cdse/cds nanocrystal quantum dots. *J. Biophotonics*, 3(10-11):706–717, 2010. ISSN 1864-0648. doi:10.1002/jbio.201000058.

[45] W.K. Bae, L.A. Padilha, Y.-S. Park, H. McDaniel, I. Robel, J.M. Pietryga, and V.I. Klimov. Controlled alloying of the core-shell interface in cdse/cds quantum dots for suppression of auger recombination. *ACS Nano*, 7(4):3411–3419, 2013. doi:10.1021/nn4002825.

[46] Yagnaseni Ghosh, Benjamin D. Mangum, Joanna L. Casson, Darrick J. Williams, Han Htoon, and Jennifer A. Hollingsworth. New insights into the complexities of shell growth and the strong influence of particle volume in non-blinking "giant" core/shell nanocrystal quantum dots. *J. Am. Chem. Soc.*, 134 (23):9634–9643, 2012. doi:10.1021/ja212032q.

[47] A.P. Alivisatos. Perspectives on the physical chemistry of semiconductor nanocrystals. *J. Phys. Chem.*, 100(31):13226–13239, 1996. ISSN 00223654. doi:10.1021/jp9535506.

[48] F. Wang and W.E. Buhro. Determination of the rod-wire transition length in colloidal indium phosphide quantum rods. *J. Am. Chem. Soc.*, 129(46):14381–14387, 2007. doi:10.1021/ja075015c.

[49] J. Ristić, C. Rivera, E. Calleja, S. Fernández-Garrido, M. Povoloskyi, and A. Di Carlo. Carrier-confinement effects in nanocolumnar gan alxga1-xn quantum disks grown by molecular-beam epitaxy. *Phys. Rev. B*, 72(8):085330–085336, 2005. doi:10.1103/PhysRevB.72.085330.

[50] H. Zhu and T. Lian. Enhanced multiple exciton dissociation from cdse quantum rods: The effect of nanocrystal shape. *J. Am. Chem. Soc.*, 134(27):11289–11297, 2012. doi:10.1021/ja304724u.

[51] H. Htoon, J.A. Hollingsworth, R. Dickerson, and V.I. Klimov. Effect of zero- to one-dimensional transformation on multiparticle auger recombination in semiconductor quantum rods. *Phys. Rev. Lett.*, 91(22):227401/1–227401/4, 2003. doi:10.1103/PhysRevLett.91.227401.

[52] L.-S. Li, J. Hu, W. Yang, and A.P.Ye Alivisatos. Band gap variation of size- and shape-controlled colloidal cdse quantum rods. *Nano Lett.*, 1(7):349–351, 2001. doi:10.1021/nl015559r.

[53] C.-W. Hsu, E.S. Moskalenko, M.O. Eriksson, A. Lundskog, K. Fredrik Karlsson, U. Forsberg, E. Janzén, and P. Olof Holtz. The charged exciton in an ingan quantum dot on a gan pyramid. *Appl. Phys. Lett.*, 103(1):013109–013113, 2013. doi:10.1063/1.4812984.

[54] Rabeka Alam, Danielle M. Fontaine, Bruce R. Branchini, and Mathew M. Maye. Designing quantum rods for optimized energy transfer with firefly luciferase enzymes. *Nano Lett.*, 12(6):3251–3256, 2012. doi:10.1021/nl301291g.

[55] F. Qian, S. Gradečak, Y. Li, C.-Y. Wen, and C.M. Lieber. Core/multishell nanowire heterostructures as multicolor, high-efficiency light-emitting diodes. *Nano Lett.*, 5(11):2287–2291, 2005. doi:10.1021/nl051689e.

[56] B. O. Dabbousi, J. Rodriguez-Viejo, F. V. Mikulec, J. R. Heine, H. Mattoussi, R. Ober, K. F. Jensen, and M. G. Bawendi. (cdse)zns coreâĹŠshell quantum dots: synthesis and characterization of a size series of highly luminescent nanocrystallites. *The Journal of Physical Chemistry B*, 101(46):9463–9475, Nov 1997. ISSN 15206106. doi:10.1021/jp971091y.

[57] Farzana Aslam, David J. Binks, Mark D. Rahn, David P. West, Paul O'Brien, Nigel Pickett, and Steve Daniels. Photorefractive performance of a cdse/zns core/shell nanoparticle-sensitized polymer. *J. Chem. Phys.*, 122(18):184713, 2005. doi:10.1063/1.1896350.

[58] Bonghwan Chon, Jiwon Bang, Juwon Park, Cherlhyun Jeong, Jong Hwa Choi, Jong-Bong Lee, Taiha Joo, and Sungjee Kim. Unique temperature dependence and blinking behavior of cdte/cdse (core/shell) type-ii quantum dots. *J. Phys. Chem. C*, 115(2):436–442, 2011. doi:10.1021/jp109229u.

[59] Qi Cui, Changwen Liu, Fan Wu, Wenjin Yue, Zeliang Qiu, Hui Zhang, Feng Gao, Wei Shen, and Mingtai Wang. Performance improvement in polymer/zno nanoarray hybrid solar cells by formation of zno/cds-core/shell heterostructures. *J. Phys. Chem. C*, 117(11):5626–5637, 2013. doi:10.1021/jp312728t.

[60] Z. Deng, A. Samanta, J. Nangreave, H. Yan, and Y. Liu. Robust dna-functionalized core/shell quantum dots with fluorescent emission spanning from uv-vis to near-ir and compatible with dna-directed self-assembly. *J. Am. Chem. Soc.*, 134(42):17424–17427, 2012. doi:10.1021/ja3081023.

[61] Haiming Zhu and Tianquan Lian. Wavefunction engineering in quantum confined semiconductor nanoheterostructures for efficient charge separation and solar energy conversion. *Energy & Environmental Science*, 5(11):9406, 2012. ISSN 17545692. doi:10.1039/c2ee22679k.

[62] Haiming Zhu, Nianhui Song, and Tianquan Lian. Controlling charge separation and recombination rates in cdse/zns type i core-shell quantum dots by shell thicknesses. *J. Am. Chem. Soc.*, 132(42):15038–15045, 2010. doi:10.1021/ja106710m.

[63] Mohamed Abdellah, Karel Žídek, Kaibo Zheng, Pavel Chábera, Maria E. Mess-

ing, and To?nu Pullerits. Balancing electron transfer and surface passivation in gradient cdse/zns core-shell quantum dots attached to zno. *J. Phys. Chem. Lett.*, 4(11):1760–1765, Apr 2013. doi:10.1021/jz4006459.

[64] Zhihua Xu, Corey R. Hine, Mathew M. Maye, Qingping Meng, and Mircea Cotlet. Shell thickness dependent photoinduced hole transfer in hybrid conjugated polymer/quantum dot nanocomposites: From ensemble to single hybrid level. *ACS Nano*, 6(6):4984–4992, Jun 2012. ISSN 19360851. doi:10.1021/nn300525b.

[65] Morihiko Hamada, Shunsuke Nakanishi, Tamitake Itoh, Mitsuru Ishikawa, and Vasudevanpillai Biju. Blinking suppression in cdse/zns single quantum dots by tio2 nanoparticles. *ACS Nano*, 4(8):4445–54, 2010. ISSN 1936086X. doi:10.1021/nn100698u.

[66] Shengye Jin and Tianquan Lian. Electron transfer dynamics from single cdse/zns quantum dots to tio2 nanoparticles. *Nano Lett.*, 9(6):2448–2454, 2009. doi:10.1021/nl9011744.

[67] T. Blaudeck, E.I. Zenkevich, M. Abdel-Mottaleb, K. Szwaykowska, D. Kowerko, F. Cichos, and C. Von Borczyskowski. Formation principles and ligand dynamics of nanoassemblies of cdse quantum dots and functionalised dye molecules. *ChemPhysChem*, 13(4):959–972, 2012. doi:10.1002/cphc.201100711.

[68] Sean A. Fischer, Angela M. Crotty, Svetlana V. Kilina, Sergei A. Ivanov, and Sergei Tretiak. Passivating ligand and solvent contributions to the electronic properties of semiconductor nanocrystals. *Nanoscale*, 4:904–914, 2012. doi:10.1039/C2NR11398H.

[69] Matthew T. Frederick and Emily A. Weiss. Relaxation of exciton confinement in cdse quantum dots by modification with a conjugated dithiocarbamate ligand. *ACS Nano*, 4(6):3195–3200, 2010. doi:10.1021/nn1007435.

[70] P. Sippel, W. Albrecht, D. Mitoraj, R. Eichberger, T. Hannappel, and D. Van-maekelbergh. Two-photon photoemission study of competing auger and surface-mediated relaxation of hot electrons in cdse quantum dot solids. *Nano Lett.*, 13 (4):1655–1661, 2013. doi:10.1021/nl400113t.

[71] Y. Zhang, G. Hong, Y. Zhang, G. Chen, F. Li, H. Dai, and Q. Wang. Ag 2s quantum dot: A bright and biocompatible fluorescent nanoprobe in the second near-infrared window. *ACS Nano*, 6(5):3695–3702, 2012. doi:10.1021/nn301218z.

[72] M.T. Frederick, V.A. Amin, L.C. Cass, and E.A. Weiss. A molecule to detect and perturb the confinement of charge carriers in quantum dots. *Nano Lett.*, 11(12):5455–5460, 2011. doi:10.1021/nl203222m.

[73] S.C. Boehme, H. Wang, L.D.A. Siebbeles, D. Vanmaekelbergh, and A.J. Houtepen. Electrochemical charging of cdse quantum dot films: Dependence on void size and counterion proximity. *ACS Nano*, 7(3):2500–2508, 2013. doi:10.1021/nn3058455.

[74] L. Etgar, T. Moehl, S. Gabriel, S.G. Hickey, A. Eychmüller, and M. Grätzel. Light energy conversion by mesoscopic pbs quantum dots/tio 2 heterojunction solar cells. *ACS Nano*, 6(4):3092–3099, 2012. doi:10.1021/nn2048153.

[75] L.-Y. Chang, R.R. Lunt, P.R. Brown, V. Bulović, and M.G. Bawendi. Low-temperature solution-processed solar cells based on pbs colloidal quantum dot/cds heterojunctions. *Nano Lett.*, 13(3):994–999, 2013. doi:10.1021/nl3041417.

[76] S.M. Willis, C. Cheng, H.E. Assender, and A.A.R. Watt. The transitional heterojunction behavior of pbs/zno colloidal quantum dot solar cells. *Nano Lett.*, 12(3):1522–1526, 2012. doi:10.1021/nl204323j.

[77] P.K. Santra and P.V. Kamat. Tandem-layered quantum dot solar cells: Tuning the photovoltaic response with luminescent ternary cadmium chalcogenides. *J. Am. Chem. Soc.*, 135(2):877–885, 2013. doi:10.1021/ja310737m.

[78] P.K. Santra and P.V. Kamat. Mn-doped quantum dot sensitized solar cells: A strategy to boost efficiency over 5*J. Am. Chem. Soc.*, 134(5):2508–2511, 2012. doi:10.1021/ja211224s.

[79] M.P. Genovese, I.V. Lightcap, and P.V. Kamat. Sun-believable solar paint. a transformative one-step approach for designing nanocrystalline solar cells. *ACS Nano*, 6(1):865–872, 2012. doi:10.1021/nn204381g.

[80] B. Ehrler, M.W.B. Wilson, A. Rao, R.H. Friend, and N.C. Greenham. Singlet exciton fission-sensitized infrared quantum dot solar cells. *Nano Lett.*, 12(2): 1053–1057, 2012. doi:10.1021/nl204297u.

[81] A. Salant, M. Shalom, Z. Tachan, S. Buhbut, A. Zaban, and U. Banin. Quantum rod-sensitized solar cell: Nanocrystal shape effect on the photovoltaic proper-ties. *Nano Lett.*, 12(4):2095–2100, 2012. doi:10.1021/nl300356e.

[82] Z. Pan, H. Zhang, K. Cheng, Y. Hou, J. Hua, and X. Zhong. Highly efficient in-verted type-i cds/cdse core/shell structure qd-sensitized solar cells. *ACS Nano*, 6(5):3982–3991, 2012. doi:10.1021/nn300278z.

[83] S. Jin, H.-J. Son, O.K. Farha, G.P. Wiederrecht, and J.T. Hupp. Energy transfer from quantum dots to metal-organic frameworks for enhanced light harvesting. *J. Am. Chem. Soc.*, 135(3):955–958, 2013. doi:10.1021/ja3097114.

[84] W. Russ Algar, Mario G. Ancona, Anthony P. Malanoski, Kimihiro Susumu, and Igor L. Medintz. Assembly of a concentric forster resonance energy transfer relay on a quantum dot scaffold: Characterization and application

to multiplexed protease sensing. *ACS Nano*, 6(12):11044–11058, Dec 2012. doi:10.1021/nn304736j.

[85] J. Zhao, M.A. Holmes, and F.E. Osterloh. Quantum confinement controls photocatalysis: A free energy analysis for photocatalytic proton reduction at cdse nanocrystals. *ACS Nano*, 7(5):4316–4325, 2013. doi:10.1021/nn400826h.

[86] J. Huang, K.L. Mulfort, P. Du, and L.X. Chen. Photodriven charge separation dynamics in cdse/zns core/shell quantum dot/cobaloxime hybrid for efficient hydrogen production. *J. Am. Chem. Soc.*, 134(40):16472–16475, 2012. doi:10.1021/ja3062584.

[87] M. Ye, J. Gong, Y. Lai, C. Lin, and Z. Lin. High-efficiency photoelectrocatalytic hydrogen generation enabled by palladium quantum dots-sensitized tio 2 nanotube arrays. *J. Am. Chem. Soc.*, 134(38):15720–15723, 2012. doi:10.1021/ja307449z.

[88] Jai K Verma, Vladimir V Protasenko, SM Islam, Huili Xing, and Debdeep Jena. Boost in deep-uv electroluminescence from tunnel-injection gan/aln quantum dot leds by polarization-induced doping. In *SPIE OPTO*, pages 89861W–89861W. International Society for Optics and Photonics, 2014.

[89] S. Jun, J. Lee, and E. Jang. Highly luminescent and photostable quantum dot-silica monolith and its application to light-emitting diodes. *ACS Nano*, 7(2):1472–1477, 2013. doi:10.1021/nn3052428.

[90] Y. Zhang, X. Ke, Z. Zheng, C. Zhang, Z. Zhang, F. Zhang, Q. Hu, Z. He, and H. Wang. Encapsulating quantum dots into enveloped virus in living cells for tracking virus infection. *ACS Nano*, 7(5):3896–3904, 2013. doi:10.1021/nn305189n.

[91] G. Wang, Y. Leng, H. Dou, L. Wang, W. Li, X. Wang, K. Sun, L. Shen, X. Yuan, J. Li, K. Sun, J. Han, H. Xiao, and Y. Li. Highly efficient preparation of multiscaled quantum dot barcodes for multiplexed hepatitis b detection. *ACS Nano*, 7(1):471–481, 2013. doi:10.1021/nn3045215.

[92] M.S. Draz, B.A. Fang, L. Li, Z. Chen, Y. Wang, Y. Xu, J. Yang, K. Killeen, and F.F. Chen. Hybrid nanocluster plasmonic resonator for immunological detection of hepatitis b virus. *ACS Nano*, 6(9):7634–7643, 2012. doi:10.1021/nn3034056.

[93] B.R. Smith, P. Kempen, D. Bouley, A. Xu, Z. Liu, N. Melosh, H. Dai, R. Sinclair, and S.S. Gambhir. Shape matters: Intravital microscopy reveals surprising geometrical dependence for nanoparticles in tumor models of extravasation. *Nano Lett.*, 12(7):3369–3377, 2012. doi:10.1021/nl204175t.

[94] S.-L. Liu, Z.-L. Zhang, Z.-Q. Tian, H.-S. Zhao, H. Liu, E.-Z. Sun, G.F. Xiao, W. Zhang, H.-Z. Wang, and D.-W. Pang. Effectively and efficiently dissecting the infection of influenza virus by quantum-dot-based single-particle tracking. *ACS Nano*, 6(1):141–150, 2012. doi:10.1021/nn2031353.

[95] X. Ji, G. Palui, T. Avellini, H.B. Na, C. Yi, K.L. Knappenberger Jr., and H. Mattoussi. On the ph-dependent quenching of quantum dot photoluminescence by redox active dopamine. *J. Am. Chem. Soc.*, 134(13):6006–6017, 2012. doi:10.1021/ja300724x.

[96] Michael H. Stewart, Kimihiro Susumu, Bing C. Mei, Igor L. Medintz, James B. Delehanty, Juan B. Blanco-Canosa, Philip E. Dawson, and Hedi Mattoussi. Multidentate poly(ethylene glycol) ligands provide colloidal stability to semiconductor and metallic nanocrystals in extreme conditions. *J. Am. Chem. Soc.*, 132(28):9804–9813, 2010. doi:10.1021/ja102898d.

[97] S.A. DÃŋaz, L. Giordano, T.M. Jovin, and E.A. Jares-Erijman. Modula-

tion of a photoswitchable dual-color quantum dot containing a photochromic fret acceptor and an internal standard. *Nano Lett.*, 12(7):3537–3544, 2012. doi:10.1021/nl301093s.

[98] L.A. Padilha, W.K. Bae, V.I. Klimov, J.M. Pietryga, and R.D. Schaller. Response of semiconductor nanocrystals to extremely energetic excitation. *Nano Lett.*, 13(3):925–932, 2013. doi:10.1021/nl400141w.

[99] D. Zhou, M. Lin, X. Liu, J. Li, Z. Chen, D. Yao, H. Sun, H. Zhang, and B. Yang. Conducting the temperature-dependent conformational change of macrocyclic compounds to the lattice dilation of quantum dots for achieving an ultrasensitive nanothermometer. *ACS Nano*, 7(3):2273–2283, 2013. doi:10.1021/nn305423p.

[100] O. Schwartz, R. Tenne, J.M. Levitt, Z. Deutsch, S. Itzhakov, and D. Oron. Colloidal quantum dots as saturable fluorophores. *ACS Nano*, 6(10):8778–8782, 2012. doi:10.1021/nn302551v.

[101] S.J. Yang, S. Nam, T. Kim, J.H. Im, H. Jung, J.H. Kang, S. Wi, B. Park, and C.R. Park. Preparation and exceptional lithium anodic performance of porous carbon-coated zno quantum dots derived from a metal-organic framework. *J. Am. Chem. Soc.*, 135(20):7394–7397, 2013. doi:10.1021/ja311550t.

[102] Joseph M Luther and Jeffrey M Pietryga. Stoichiometry control in quantum dots: A viable analog to impurity doping of bulk materials. *ACS Nano*, 7(3): 1845–1849, 2013. doi:10.1021/nn401100n.

[103] Moungi G Bawendi, Michael L Steigerwald, and Louis E Brus. The quantum mechanics of larger semiconductor clusters (" quantum dots"). *Annu. Rev. Phys. Chem.*, 41(1):477–496, 1990.

[104] Garnett W Bryant. Excitons in quantum boxes: Correlation ef-

fects and quantum confinement. *Phys. Rev. B*, 37(15):8763, 1988. doi:10.1103/PhysRevB.37.8763.

[105] H. Haug and S.W. Koch. *Quantum Theory of the Optical and Electronic Properties of Semiconductors*. World Scientific Publishing Company, Incorporated, 2009. ISBN 9789812838834.

[106] S. Glutsch. *Excitons in Low-Dimensional Semiconductors: Theory, Numerical Methods, Applications*. Springer Series in Solid-State Sciences. Springer, 2004. ISBN 9783540202400.

[107] K. Barnham and D. Vvedensky. *Low-Dimensional Semiconductor Structures: Fundamentals and Device Applications*. Cambridge University Press, 2008. ISBN 9780521599047.

[108] Lixin He, Gabriel Bester, and Alex Zunger. Prediction of an excitonic ground state in i n a s/i n s b quantum dots. *Phys. Rev. Lett.*, 94(1):016801, 2005. doi:10.1103/PhysRevLett.94.016801.

[109] Francesco Tassone and Carlo Piermarocchi. Electron-hole correlation effects in the emission of light from quantum wires. *Phys. Rev. Lett.*, 82(4):843, 1999. doi:10.1103/PhysRevLett.82.843.

[110] Fausto Rossi and Elisa Molinari. Coulomb-induced suppression of band-edge singularities in the optical spectra of realistic quantum-wire structures. *Phys. Rev. Lett.*, 76(19):3642, 1996. doi:10.1103/PhysRevLett.76.3642.

[111] George Pal, Georgios Lefkidis, Hans Christian Schneider, and Wolfgang Hübner. Optical response of small closed-shell sodium clusters. *J. Chem. Phys.*, 133(15): 154309, 2010. doi:10.1063/1.3494093.

[112] Dong-Hun Chae, Tobias Utikal, Siegfried Weisenburger, Harald Giessen, Klaus v Klitzing, Markus Lippitz, and Jurgen Smet. Excitonic fano resonance in free-standing graphene. *Nano Lett.*, 11(3):1379–1382, 2011. doi:10.1021/nl200040q.

[113] Vasili Perebeinos, J Tersoff, and Phaedon Avouris. Radiative lifetime of excitons in carbon nanotubes. *Nano Lett.*, 5(12):2495–2499, 2005. doi:10.1021/nl051828s.

[114] Peter Puschnig and Claudia Ambrosch-Draxl. Suppression of electron-hole correlations in 3d polymer materials. *Phys. Rev. Lett.*, 89(5):056405, 2002. doi:10.1103/PhysRevLett.89.056405.

[115] CW Tang, SA VanSlyke, and CH Chen. Electroluminescence of doped organic thin films. *J. Appl. Phys.*, 65(9):3610–3616, 1989. doi:10.1063/1.343409.

[116] Jessica Krüger, Robert Plass, Michael Grätzel, Petra J Cameron, and Laurence M Peter. Charge transport and back reaction in solid-state dye-sensitized solar cells: a study using intensity-modulated photovoltage and photocurrent spectroscopy. *The Journal of Physical Chemistry B*, 107(31):7536–7539, 2003. doi:10.1021/jp0348777.

[117] Marc Achermann, Melissa A Petruska, Simon Kos, Darryl L Smith, Daniel D Koleske, and Victor I Klimov. Energy-transfer pumping of semiconductor nanocrystals using an epitaxial quantum well. *Nature*, 429(6992):642–646, 2004. doi:10.1038/nature02571.

[118] MJ Hetzer, YM Strzhemechny, M Gao, MA Contreras, A Zunger, and LJ Brillson. Direct observation of copper depletion and potential changes at copper indium gallium diselenide grain boundaries. *Appl. Phys. Lett.*, 86(16):162105, 2005. doi:10.1063/1.1906331.

[119] Sasa Lacic and Olle Inganäs. Modeling electrical transport in blend heterojunction organic solar cells. *J. Appl. Phys.*, 97(12):124901, 2005. doi:10.1063/1.1931038.

[120] C-Y Chen, S-J Wu, J-Y Li, C-G Wu, J-G Chen, and K-C Ho. A new route to enhance the light-harvesting capability of ruthenium complexes for dye-sensitized solar cells. *Advanced materials*, 19(22):3888–3891, 2007. doi:10.1002/adma.200701111.

[121] RR King, DC Law, KM Edmondson, CM Fetzer, GS Kinsey, H Yoon, RA Sherif, and NH Karam. 40% efficient metamorphic gainp/gainas/ge multijunction solar cells. *Appl. Phys. Lett.*, 90(18):183516–183516, 2007. doi:10.1063/1.2734507.

[122] Chong Mou Wang, Adam Heller, and Heinz Gerischer. Palladium catalysis of o2 reduction by electrons accumulated on tio2 particles during photoassisted oxidation of organic compounds. *J. Am. Chem. Soc.*, 114(13):5230–5234, 1992. doi:10.1021/ja00039a039.

[123] Junwang Tang, James R Durrant, and David R Klug. Mechanism of photocatalytic water splitting in tio2. reaction of water with photoholes, importance of charge carrier dynamics, and evidence for four-hole chemistry. *J. Am. Chem. Soc.*, 130(42):13885–13891, 2008. doi:10.1021/ja8034637.

[124] Neeruganti O Gopal, Hsin-Hsi Lo, Shiann-Cherng Sheu, and Shyue-Chu Ke. A potential site for trapping photogenerated holes on rutile tio2 surface as revealed by epr spectroscopy: an avenue for enhancing photocatalytic activity. *J. Am. Chem. Soc.*, 132(32):10982–10983, 2010. doi:10.1021/ja909901f.

[125] Nianqiang Wu, Jin Wang, De Nyago Tafen, Hong Wang, Jian-Guo Zheng, James P Lewis, Xiaogang Liu, Stephen S Leonard, and Ayyakkannu Manivannan. Shape-enhanced photocatalytic activity of single-crystalline

anatase tio2 (101) nanobelts. *J. Am. Chem. Soc.*, 132(19):6679–6685, 2010. doi:10.1021/ja909456f.

[126] CW Tang and SA VanSlyke. Organic electroluminescent diodes. *Appl. Phys. Lett.*, 51(12):913–915, 1987. doi:10.1063/1.98799.

[127] Jessica E Kroeze, Narukuni Hirata, Sara Koops, Md K Nazeeruddin, Lukas Schmidt-Mende, Michael Grätzel, and James R Durrant. Alkyl chain barriers for kinetic optimization in dye-sensitized solar cells. *J. Am. Chem. Soc.*, 128 (50):16376–16383, 2006. doi:10.1021/ja065653f.

[128] LV Butov, CW Lai, AL Ivanov, AC Gossard, and DS Chemla. Towards bose–einstein condensation of excitons in potential traps. *Nature*, 417(6884):47–52, 2002. doi:10.1038/417047a.

[129] Sergei A Ivanov, Andrei Piryatinski, Jagjit Nanda, Sergei Tretiak, Kevin R Zavadil, William O Wallace, Don Werder, and Victor I Klimov. Type-ii core/shell cds/znse nanocrystals: synthesis, electronic structures, and spectroscopic properties. *J. Am. Chem. Soc.*, 129(38):11708–11719, 2007. doi:10.1021/ja068351m.

[130] Peter Reiss, Myriam Protiere, and Liang Li. Core/shell semiconductor nanocrystals. *Small*, 5(2):154–168, 2009. doi:10.1002/smll.200800841.

[131] Victor I Klimov, Sergei A Ivanov, Jagjit Nanda, Marc Achermann, Ilya Bezel, John A McGuire, and Andrei Piryatinski. Single-exciton optical gain in semiconductor nanocrystals. *Nature*, 447(7143):441–446, 2007. doi:10.1038/nature05839.

[132] Giovanni Onida, Lucia Reining, and Angel Rubio. Electronic excitations: density-functional versus many-body green's-function approaches. *Rev. Mod. Phys.*, 74:601–659, Jun 2002. doi:10.1103/RevModPhys.74.601.

[133] Michael Rohlfing and Steven G. Louie. Electron-hole excitations and optical spectra from first principles. *Phys. Rev. B*, 62:4927–4944, Aug 2000. doi:10.1103/PhysRevB.62.4927.

[134] L S Cederbaum. One-body green's function for atoms and molecules: theory and application. *Journal of Physics B: Atomic and Molecular Physics*, 8(2): 290, 1975. doi:10.1088/0022-3700/8/2/018.

[135] L. E. Brus. Electron-electron and electron-hole interactions in small semiconductor crystallites: The size dependence of the lowest excited electronic state. *J. Chem. Phys.*, 80(9):4403–4409, 1984. doi:http://dx.doi.org/10.1063/1.447218.

[136] M. Braskén, M. Lindberg, D. Sundholm, and J. Olsen. Full configuration interaction calculations of electron-hole correlation effects in strain-induced quantum dots. *Phys. Rev. B*, 61:7652–7655, Mar 2000. doi:10.1103/PhysRevB.61.7652.

[137] Y. Z. Hu, M. Lindberg, and S. W. Koch. Theory of optically excited intrinsic semiconductor quantum dots. *Phys. Rev. B*, 42:1713–1723, Jul 1990. doi:10.1103/PhysRevB.42.1713.

[138] Michael Wimmer, S. V. Nair, and J. Shumway. Biexciton recombination rates in self-assembled quantum dots. *Phys. Rev. B*, 73:165305, Apr 2006. doi:10.1103/PhysRevB.73.165305.

[139] C.J. Blanton, C. Brenon, and A. Chakraborty. Development of polaron-transformed explicitly correlated full configuration interaction method for investigation of quantum-confined stark effect in gaas quantum dots. *J. Chem. Phys.*, 138(5):054114, 2013. doi:10.1063/1.4789540.

[140] Jennifer M. Elward, Jacob Hoffman, and Arindam Chakraborty. Investigation of electron-hole correlation using explicitly correlated configuration inter-

action method. *Chem. Phys. Lett.*, 535(0):182 – 186, 2012. ISSN 0009-2614. doi:10.1016/j.cplett.2012.03.050.

[141] Jennifer M. Elward, Johannes Hoja, and Arindam Chakraborty. Variational solution of the congruently transformed hamiltonian for many-electron systems using a full-configuration-interaction calculation. *Phys. Rev. A*, 86:062504, Dec 2012. doi:10.1103/PhysRevA.86.062504.

[142] T. Vänskä, M. Lindberg, J. Olsen, and D. Sundholm. Computational methods for studies of multiexciton complexes. *Phys. Status Solidi B*, 243(15):4035–4045, 2006. doi:10.1002/pssb.200642169.

[143] J. Shumway. Quantum monte carlo simulation of exciton-exciton scattering in a gaas/algaas quantum well. *Phys. E*, 32(12):273 – 276, 2006. ISSN 1386-9477. doi:http://dx.doi.org/10.1016/j.physe.2005.12.052. Proceedings of the 12th International Conference on Modulated Semiconductor Structures Proceedings of the 12th International Conference on Modulated Semiconductor Structures.

[144] Xuejun Zhu, Mark S. Hybertsen, and P. B. Littlewood. Electron-hole system revisited: A variational quantum monte carlo study. *Phys. Rev. B*, 54:13575–13580, Nov 1996. doi:10.1103/PhysRevB.54.13575.

[145] A.C. Cancio and Y.-C. Chang. Quantum monte carlo studies of binding energy and radiative lifetime of bound excitons in direct-gap semiconductors. *Phys. Rev. B*, 47(20):13246–13259, 1993. doi:10.1103/PhysRevB.47.13246.

[146] A.C. Cancio and Y.-C. Chang. Quantum monte carlo study of polyexcitons in semiconductors. *Phys. Rev. B*, 42(17):11317–11324, 1990. doi:10.1103/PhysRevB.42.11317.

[147] Z.-H. Yang, Y. Li, and C.A. Ullrich. A minimal model for excitons within

time-dependent density-functional theory. *J. Chem. Phys.*, 137(1):014513, 2012. doi:10.1063/1.4730031.

[148] Svetlana V. Kilina, Dmitri S. Kilin, and Oleg V. Prezhdo. Breaking the phonon bottleneck in pbse and cdse quantum dots: Time-domain density functional theory of charge carrier relaxation. *ACS Nano*, 3(1):93–99, 2009. doi:10.1021/nn800674n.

[149] Z.-H. Yang and C.A. Ullrich. Direct calculation of exciton binding energies with time-dependent density-functional theory. *Phys. Rev. B*, 87(19):195204, 2013. doi:10.1103/PhysRevB.87.195204.

[150] Olli Lehtonen, Dage Sundholm, and Tommy Vanska. Computational studies of semiconductor quantum dots. *Phys. Chem. Chem. Phys.*, 10:4535–4550, 2008. doi:10.1039/B804212H.

[151] A. Franceschetti, H. Fu, L. W. Wang, and A. Zunger. Many-body pseudopotential theory of excitons in inp and cdse quantum dots. *Phys. Rev. B*, 60:1819–1829, Jul 1999. doi:10.1103/PhysRevB.60.1819.

[152] Jun-Wei Luo, Alberto Franceschetti, and Alex Zunger. Carrier multiplication in semiconductor nanocrystals: theoretical screening of candidate materials based on band-structure effects. *Nano Lett.*, 8(10):3174–3181, 2008. doi:10.1021/nl801459h.

[153] Marco Califano, Alberto Franceschetti, and Alex Zunger. Lifetime and polarization of the radiative decay of excitons, biexcitons, and trions in cdse nanocrystal quantum dots. *Phys. Rev. B*, 75(11):115401, 2007. doi:10.1103/PhysRevB.75.115401.

[154] Gustavo A. Narvaez, Gabriel Bester, and Alex Zunger. Excitons, biexcitons, and trions in self-assembled (In,Ga)AsGaAs quantum dots: Recombination energies,

polarization, and radiative lifetimes versus dot height. *Phys. Rev. B*, 72:245318, Dec 2005. doi:10.1103/PhysRevB.72.245318.

[155] Marco Califano, Alex Zunger, and Alberto Franceschetti. Efficient inverse auger recombination at threshold in cdse nanocrystals. *Nano Lett.*, 4(3):525–531, 2004. doi:10.1021/nl049869w.

[156] S. Corni, M. Braskén, M. Lindberg, J. Olsen, and D. Sundholm. Electron-hole recombination density matrices obtained from large configuration-interaction expansions. *Phys. Rev. B*, 67:085314, Feb 2003. doi:10.1103/PhysRevB.67.085314.

[157] S. Corni, M. Braskén, M. Lindberg, J. Olsen, and D. Sundholm. Stabilization energies of charged multiexciton complexes calculated at configuration interaction level. *Phys. E*, 18(4):436 – 442, 2003. ISSN 1386-9477. doi:http://dx.doi.org/10.1016/S1386-9477(03)00146-2.

[158] William A Lester Jr and Brian L Hammond. Quantum monte carlo for the electronic structure of atoms and molecules. *Annu. Rev. Phys. Chem.*, 41(1): 283–311, 1990. doi:10.1146/annurev.pc.41.100190.001435.

[159] W. M. C. Foulkes, L. Mitas, R. J. Needs, and G. Rajagopal. Quantum monte carlo simulations of solids. *Rev. Mod. Phys.*, 73:33–83, Jan 2001. doi:10.1103/RevModPhys.73.33.

[160] Wim Klopper, Frederick R Manby, Seiichiro Ten-No, and Edward F Valeev. R12 methods in explicitly correlated molecular electronic structure theory. *Int. Rev. Phys. Chem.*, 25(3):427–468, 2006. doi:10.1080/01442350600799921.

[161] Wolfgang von der Linden. A quantum monte carlo approach to many-body physics. *Phys. Rep.*, 220(2):53–162, 1992. doi:10.1016/0370-1573(92)90029-Y.

[162] S Corni, M Brasken, M Lindberg, J Olsen, and D Sundholm. Size dependence of the electron-hole recombination rates in semiconductor quantum dots. *Phys. Rev. B*, 67(4):045313, 2003.

[163] J Shumway and DM Ceperley. Quantum monte carlo treatment of elastic exciton-exciton scattering. *Phys. Rev. B*, 63(16):165209, 2001. doi:10.1103/PhysRevB.63.165209.

[164] B. Joakim Persson and Peter R. Taylor. Accurate quantum-chemical calculations: The use of gaussian-type geminal functions in the treatment of electron correlation. *J. Chem. Phys.*, 105(14):5915–5926, 1996. doi:10.1063/1.472432.

[165] S. F. Boys. The integral formulae for the variational solution of the molecular many-electron wave equations in terms of gaussian functions with direct electronic correlation. *Proc. R. Soc. A.*, 258(1294):402–411, 1960. doi:10.1098/rspa.1960.0195.

[166] Sergey A. Varganov and Todd J. MartÃČÂŋnez. Variational geminal-augmented multireference self-consistent field theory: Two-electron systems. *The Journal of Chemical Physics*, 132(5):054103, 2010. doi:http://dx.doi.org/10.1063/1.3303203.

[167] Chet Swalina, Michael V. Pak, Arindam Chakraborty, and Sharon Hammes-Schiffer. Explicit dynamical electron-proton correlation in the nuclear-electronic orbital framework. *J. Phys. Chem. A*, 110(33):9983–9987, 2006. doi:10.1021/jp0634297.

[168] Arindam Chakraborty, Michael V Pak, and Sharon Hammes-Schiffer. Inclusion of explicit electron-proton correlation in the nuclear-electronic orbital approach using gaussian-type geminal functions. *J. Chem. Phys.*, 129(1):014101, 2008. doi:10.1063/1.2943144.

[169] Arindam Chakraborty and Sharon Hammes-Schiffer. Density matrix formulation of the nuclear-electronic orbital approach with explicit electron-proton correlation. *J. Chem. Phys.*, 129(20):204101, 2008. doi:10.1063/1.2998312.

[170] Michael V Pak, Arindam Chakraborty, and Sharon Hammes-Schiffer. Calculation of the positron annihilation rate in psh with the positronic extension of the explicitly correlated nuclear- electronic orbital methodâĂă. *The Journal of Physical Chemistry A*, 113(16):4004–4008, 2009. doi:10.1021/jp810410y.

[171] M Chamarro, C Gourdon, Ph Lavallard, O Lublinskaya, and AI Ekimov. Enhancement of electron-hole exchange interaction in cdse nanocrystals: A quantum confinement effect. *Phys. Rev. B*, 53(3):1336, 1996. doi:10.1103/PhysRevB.53.1336.

[172] Al L Efros and M Rosen. The electronic structure of semiconductor nanocrystals 1. *Annu. Rev. Mater. Sci.*, 30(1):475–521, 2000. doi:10.1146/annurev.matsci.30.1.475.

[173] T Takagahara. Electron-phonon interactions in semiconductor nanocrystals. *J. Lumin.*, 70(1):129–143, 1996. doi:10.1016/0022-2313(96)00050-6.

[174] Toshihide Takagahara and Kyozaburo Takeda. Theory of the quantum confinement effect on excitons in quantum dots of indirect-gap materials. *Phys. Rev. B*, 46:15578–15581, Dec 1992. doi:10.1103/PhysRevB.46.15578.

[175] B Delley and EF Steigmeier. Quantum confinement in si nanocrystals. *Phys. Rev. B*, 47(3):1397, 1993. doi:10.1103/PhysRevB.47.1397.

[176] Sarah H Tolbert, Amy B Herhold, Christopher S Johnson, and AP Alivisatos. Comparison of quantum confinement effects on the electronic absorption spectra of direct and indirect gap semiconductor nanocrystals. *Phys. Rev. Lett.*, 73(24): 3266, 1994. doi:10.1103/PhysRevLett.73.3266.

[177] G Ledoux, J Gong, F Huisken, O Guillois, and C Reynaud. Photoluminescence of size-separated silicon nanocrystals: Confirmation of quantum confinement. *Appl. Phys. Lett.*, 80(25):4834–4836, 2002. doi:10.1063/1.1485302.

[178] Jun-Wei Luo, Alberto Franceschetti, and Alex Zunger. Direct-bandgap inas quantum-dots have long-range electron- hole exchange whereas indirect gap si dots have short-range exchange. *Nano Lett.*, 9(7):2648–2653, 2009. doi:10.1021/nl901000x.

[179] FA Reboredo, A Franceschetti, and A Zunger. Dark excitons due to direct coulomb interactions in silicon quantum dots. *Phys. Rev. B*, 61(19):13073, 2000. doi:10.1103/PhysRevB.61.13073.

[180] S Brovelli, RD Schaller, SA Crooker, F Garcia-Santamaria, Y Chen, R Viswanatha, JA Hollingsworth, H Htoon, and VI Klimov. Nano-engineered electron–hole exchange interaction controls exciton dynamics in core–shell semiconductor nanocrystals. *Nature communications*, 2:280, 2011. doi:10.1038/ncomms1281.

[181] Gabriel Bester, Selvakumar Nair, and Alex Zunger. Pseudopotential calculation of the excitonic fine structure of million-atom self-assembled in 1-x ga x a s/g a a s quantum dots. *Phys. Rev. B*, 67(16):161306, 2003. doi:10.1103/PhysRevB.67.161306.

[182] IA Akimov, KV Kavokin, A Hundt, and F Henneberger. Electron-hole exchange interaction in a negatively charged quantum dot. *Phys. Rev. B*, 71(7):075326, 2005. doi:10.1103/PhysRevB.71.075326.

[183] GV Astakhov, AV Koudinov, KV Kavokin, IS Gagis, Yu G Kusrayev, W Ossau, and LW Molenkamp. Exciton spin decay modified by strong

electron-hole exchange interaction. *Phys. Rev. Lett.*, 99(1):016601, 2007. doi:10.1103/PhysRevLett.99.016601.

[184] Jun He, Haizheng Zhong, and Gregory D Scholes. Electron-hole overlap dictates the hole spin relaxation rate in nanocrystal heterostructures. *Phys. Rev. Lett.*, 105(4):046601, 2010. doi:10.1103/PhysRevLett.105.046601.

[185] Silvia M Santos, Bertrand Yuma, Stéphane Berciaud, Jonah Shaver, Mathieu Gallart, Pierre Gilliot, Laurent Cognet, and Brahim Lounis. All-optical trion generation in single-walled carbon nanotubes. *Phys. Rev. Lett.*, 107(18):187401, 2011. doi:10.1103/PhysRevLett.107.187401.

[186] Ryusuke Matsunaga, Kazunari Matsuda, and Yoshihiko Kanemitsu. Observation of charged excitons in hole-doped carbon nanotubes using photoluminescence and absorption spectroscopy. *Phys. Rev. Lett.*, 106(3):037404, 2011. doi:10.1103/PhysRevLett.106.037404.

[187] W. Xie. Exciton states trapped by a parabolic quantum dot. *Phys. B (Amsterdam, Neth.)*, 358(1-4):109–113, 2005. doi:10.1016/j.physb.2004.12.035.

[188] G. Lamouche and G. Fishman. Two interacting electrons in a three-dimensional parabolic quantum dot: A simple solution. *J. Phys.: Condens. Matter*, 10(35):7857–7867, 1998. doi:10.1088/0953-8984/10/35/018.

[189] Mohammad El-Said. The ground-state energy of an exciton in a parabolic quantum dot. *Semicond. Sci. Technol.*, 9(3):272, 1994. doi:10.1088/0268-1242/9/3/006.

[190] Shi-Hua Chen. Hydrogenic impurity bound polaron in a parabolic quantum dot with arbitrary electron–phonon coupling strength. *Physica B: Condensed Matter*, 406(10):2033–2037, 2011. doi:10.1016/j.physb.2011.03.014.

[191] CM Duque, ME Mora-Ramos, and CA Duque. Simultaneous effects of electron-hole correlation, hydrostatic pressure, and temperature on the third harmonic generation in parabolic gaas quantum dots. *J. Nanopart. Res.*, 13(11):6103–6112, 2011. doi:10.1007/s11051-011-0348-5.

[192] E Sadeghi and A Avazpour. Binding energy of an off-center donor impurity in ellipsoidal quantum dot with parabolic confinement potential. *Physica B: Condensed Matter*, 406(2):241–244, 2011. doi:10.1016/j.physb.2010.10.051.

[193] Wenfang Xie. Diploe-allowed optical absorption of an exciton in a spherical parabolic quantum dot. *Opt. Commun.*, 282(13):2604–2607, 2009. doi:10.1016/j.optcom.2009.03.013.

[194] Michio Ikezawa, Selvakumar V Nair, Hong-Wen Ren, Yasuaki Masumoto, and Harry Ruda. Biexciton binding energy in parabolic gaas quantum dots. *Phys. Rev. B*, 73(12):125321, 2006. doi:10.1103/PhysRevB.73.125321.

[195] Tapash Chakraborty and Pekka Pietiläinen. Optical signatures of spin-orbit interaction effects in a parabolic quantum dot. *Phys. Rev. Lett.*, 95(13):136603, 2005. doi:10.1103/PhysRevLett.95.136603.

[196] Eduard Matito, Jerzy Cioslowski, and Sergei F Vyboishchikov. Properties of harmonium atoms from fci calculations: Calibration and benchmarks for the ground state of the two-electron species. *Phys. Chem. Chem. Phys.*, 12(25):6712–6716, 2010. doi:10.1039/b926389f.

[197] JP Coe, A Sudbery, and I DâĂŹamico. Entanglement and density-functional theory: Testing approximations on hookeâĂŹs atom. *Phys. Rev. B*, 77(20):205122, 2008. doi:10.1103/PhysRevB.77.205122.

[198] Norman H March and Angel Rubio. Change in analytic structure of first-order density matrix as a functional of electron density due to inter-particle

correlation: a two-electron model example. *Chem. Phys. Lett.*, 398(4):445–448, 2004. doi:10.1016/j.cplett.2004.08.043.

[199] David Hestenes. Vectors, spinors, and complex numbers in classical and quantum physics. *Am. J. Phys*, 39(1013), 1971. doi:10.1119/1.1986363.

[200] P Cassam-Chenaï. Variational spaces of electronic calculations in quantum chemistry. *J. Math. Chem.*, 15(1):303–321, 1994. doi:10.1007/BF01277567.

[201] Kleber C Mundim, Mario Giambiagi, and Myriam S de Giambiagi. Multicenter bond index: Grassmann algebra and n-order density functional. *J. Phys. Chem.*, 98(24):6118–6119, 1994. doi:10.1021/j100075a013.

[202] Patrick Cassam-ChenaıĬĹ and Frederic Patras. The hopf algebra of identical, fermionic particle systemsâĂŤfundamental concepts and properties. *Journal of Mathematical Physics*, 44(11):4884–4906, 2003. doi:10.1063/1.1611266.

[203] D. Sundholm and T. Vänskä. Computational methods for studies of semiconductor quantum dots and rings. *Annu. Rep. Prog. Chem., Sect. C: Phys. Chem.*, 108:96–125, 2012. doi:10.1039/C2PC90004A.

[204] E. A. Chekhovich, A. S. Brichkin, A. V. Chernenko, V. D. Kulakovskii, I. V. Sedova, S. V. Sorokin, and S. V. Ivanov. Effect of sp-d exchange interaction on excitonic states in cdse/znse/zn/mn/se quantum dots. *Phys. Rev. B*, 76: 165305, Oct 2007. doi:10.1103/PhysRevB.76.165305.

[205] U. Woggon. *Optical Properties of Semiconductor Quantum Dots.* Number v. 136 in Springer Tracts in Modern Physics. Springer-Verlag., 1997.

[206] EA Burovski, AS Mishchenko, NV Prokof'ev, and BV Svistunov. Diagrammatic quantum monte carlo for two-body problems: applied to excitons. *Phys. Rev. Lett.*, 87(18):186402, 2001. doi:10.1103/PhysRevLett.87.186402.

[207] *Methods of matrix algebra.* Mathematics in Science and Engineering. Elsevier Science, 1964. ISBN 9780080955223.

[208] R.C. James and G. James. *The Mathematics Dictionary.* Springer Netherlands, 1992. ISBN 9780412990410.

[209] T. Helgaker, J. Olsen, and P. Jorgensen. *Molecular Electronic-Structure Theory.* Wiley, 2000. ISBN 9781118531471.

[210] B Joakim Persson and Peter R Taylor. Molecular integrals over gaussian-type geminal basis functions. *Theor. Chem. Acc.*, 97(1-4):240–250, 1997. doi:10.1007/s002140050258.

[211] Jacek Karwowski and Lech Cyrnek. A class of exactly solvable schrödinger equations. *Collect. Czech. Chem. Commun.*, 70(7):864–880, 2005. doi:10.1135/cccc20050864.

[212] Jacek Karwowski. Inverse problems in quantum chemistry. *Int. J. Quantum Chem.*, 109(11):2456–2463, 2009. doi:10.1002/qua.22048.

[213] Christopher R Myers, Cyrus J Umrigar, James P Sethna, and John D Morgan III. Focks expansion, katos cusp conditions, and the exponential ansatz. *Phys. Rev. A*, 44(9):5537, 1991. doi:10.1103/PhysRevA.44.5537.

[214] David Prendergast, M. Nolan, Claudia Filippi, Stephen Fahy, and J. C. Greer. Impact of electron–electron cusp on configuration interaction energies. *J. Chem. Phys.*, 115(4):1626–1634, 2001. doi:10.1063/1.1383585.

[215] Warren J Hehre, Robert F Stewart, and John A Pople. Self-consistent molecular-orbital methods. i. use of gaussian expansions of slater-type atomic orbitals. *J. Chem. Phys.*, 51(6):2657–2664, 1969. doi:10.1063/1.1672392.

[216] Seiichiro Ten-no. Initiation of explicitly correlated slater-type geminal theory. *Chem. Phys. Lett.*, 398(1):56–61, 2004. doi:10.1016/j.cplett.2004.09.041.

[217] J-W Van der Horst, PA Bobbert, MAJ Michels, and Heinz Bässler. Calculation of excitonic properties of conjugated polymers using the bethe–salpeter equation. *The Journal of Chemical Physics*, 114(15):6950–6957, 2001. doi:10.1063/1.1356015.

[218] Rick A Kendall and Herbert A Früchtl. The impact of the resolution of the identity approximate integral method on modern ab initio algorithm development. *Theor. Chem. Acc.*, 97(1-4):158–163, 1997. doi:10.1007/s002140050249.

[219] Frank Neese. An improvement of the resolution of the identity approximation for the formation of the coulomb matrix. *J. Comput. Chem.*, 24(14):1740–1747, 2003. doi:10.1002/jcc.10318.

[220] Edward F Valeev. Improving on the resolution of the identity in linear r12 ab initio theories. *Chem. Phys. Lett.*, 395(4):190–195, 2004. doi:10.1016/j.cplett.2004.07.061.

[221] David P Tew, Wim Klopper, and Frederick R Manby. The weak orthogonality functional in explicitly correlated pair theories. *J. Chem. Phys.*, 127(17):174105, 2007. doi:10.1063/1.2795702.

[222] Hans-Joachim Werner, Thomas B Adler, and Frederick R Manby. General orbital invariant mp2-f12 theory. *The Journal of chemical physics*, 126(16):164102, 2007. doi:10.1063/1.2712434.

[223] Edward F Valeev. Combining explicitly correlated r12 and gaussian geminal electronic structure theories. *The Journal of chemical physics*, 125(24):244106, 2006. doi:10.1063/1.2403852.

[224] D. Timmerman, J. Valenta, K. DohnalovÃą, W.D.A.M. De Boer, and T. Gregorkiewicz. Step-like enhancement of luminescence quantum yield of silicon nanocrystals. *Nat. Nanotechnol.*, 6(11):710–713, 2011. ISSN 17483387. doi:10.1038/nnano.2011.167.

[225] T. Berstermann, T. Auer, H. Kurtze, M. Schwab, D. R. Yakovlev, M. Bayer, J. Wiersig, C. Gies, F. Jahnke, D. Reuter, and A. D. Wieck. Systematic study of carrier correlations in the electron-hole recombination dynamics of quantum dots. *Phys. Rev. B*, 76(16):1653181–1653188, 2007. doi:10.1103/PhysRevB.76.165318.

[226] J. J. Crochet, J. D. Sau, J. G. Duque, S. K. Doorn, and M. L. Cohen. Electrodynamic and excitonic intertube interactions in semiconducting carbon nanotube aggregates. *ACS Nano*, 5(4):2611–2618, 2011. doi:0.1021/nn200427r.

[227] Z. Li, B. Gao, G. Z. Chen, R. Mokaya, S. Sotiropoulos, and G. Li Puma. Carbon nanotube/titanium dioxide (cnt/tio2) core-shell nanocomposites with tailored shell thickness, cnt content and photocatalytic/photoelectrocatalytic properties. *Applied Catalysis B: Environmental*, 110:50–57, 2011. doi:10.1016/j.apcatb.2011.08.023.

[228] Z. Liu, A. Bushmaker, M. Aykol, and S. B. Cronin. Thermal emission spectra from individual suspended carbon nanotubes. *ACS Nano*, 5(6):4634–4640, 2011. doi:10.1021/nn200444x.

[229] S. Uryu and T. Ando. Effect of electron-hole asymmetry on cross-polarized excitons in carbon nanotubes. *Phys. Rev. B*, 83(8):085404, 2011. doi:10.1103/PhysRevB.83.085404.

[230] G. Jolley, H. F. Lu, L. Fu, H. H. Tan, and C. Jagadish. Electron-hole recombination properties of in0.5 ga0.5 as/gaas quantum dot solar cells and the

influence on the open circuit voltage. *Appl. Phys. Lett.*, 97(12):1235051, 2010. doi:10.1063/1.3492836.

[231] Z. Yang, C. Chen, P. Roy, and H. Chang. Quantum dot-sensitized solar cells incorporating nanomaterials. *Chem. Commun.*, 47(34):9561–9571, 2011. doi:10.1039/C1CC11317H.

[232] G. Rosenman, D. Aronov, L. Oster, J. Haddad, G. Mezinskis, I. Pavlovska, M. Chaikina, and A. Karlov. Photoluminescence and surface photovoltage spectroscopy studies of hydroxyapatite nano-bio-ceramics. *J. Lumin.*, 122-123(1-2): 936–938, 2007. doi:10.1016/j.jlumin.2006.01.331.

[233] T. V. Torchynska. Cdse/zns quantum dots with interface states as biosensors. In *Biosensing and Nanomedicine IV*, volume 8099. Affiliation: ESFM, National Polytechnic Institute, Mexico DF 07738, Mexico; Correspondence Address: Torchynska, T.V.; ESFM, National Polytechnic Institute, Mexico DF 07738, Mexico, 21 August 2011 through 23 August 2011 2011. ISBN 0277786X; 9780819487094 (ISBN).

[234] T. V. Torchynska, A. L. Quintos Vazquez, R. Sierra, K. Gazarian, and L. Shcherbyna. Modification of optical properties at bioconjugation of core-shell cdse/zns quantum dots. *J. Phys: Conf. Ser.*, 244, 26 April 2010 through 30 April 2010 2010. doi:10.1088/1742-6596/245/1/012013.

[235] L. Wang, X. Zhang, Y. Fu, B. Li, and Y. Liu. Bioinspired preparation of ultrathin sio2 shell on zno nanowire array for ultraviolet-durable superhydrophobicity. *Langmuir*, 25(23):13619–13624, 2009. doi:10.1021/la901998p.

[236] C. A. Castro, A. Centeno, and S. A. Giraldo. Iron promotion of the tio2 photosensitization process towards the photocatalytic oxidation of azo dyes under

solar-simulated light irradiation. *Mater. Chem. Phys.*, 129(3):1176–1183, 2011. doi:10.1016/j.matchemphys.2011.05.082.

[237] C. B. Mendive, D. Hansmann, T. Bredow, and D. Bahnemann. New insights into the mechanism of tio2 photocatalysis: Thermal processes beyond the electron-hole creation. *J. Phys. Chem. C*, 115(40):19676–19685, 2011. doi:10.1021/jp112243q.

[238] A. Franceschetti and M. C. Troparevsky. Pseudopotential theory of electronic excitations in semiconductor nanostructures. *J. Comput. Theor. Nanosci.*, 6 (6):1272–1276, 2009. doi:10.1166/jctn.2009.1175.

[239] M. Casula and S. Sorella. Geminal wave functions with jastrow correlation: A first application to atoms. *J. Chem. Phys.*, 119(13):6500–6511, 2003. doi:10.1063/1.1604379.

[240] T. Offermans, S. C. J. Meskers, and R. A. J. Janssen. Monte-carlo simulations of geminate electron-hole pair dissociation in a molecular heterojunction: A two-step dissociation mechanism. *Chem. Phys.*, 308(1-2):125–133, 2005. doi:10.1016/j.chemphys.2004.08.015.

[241] H. E. Song and I. Zacharia. Fixed-node monte carlo studies of excitons in confined geometries. *Physica Status Solidi (A) Applied Research*, 164(1):149–154, 1997. doi:10.1002/1521-396X.

[242] En-Ge Wang. Excitons in novel quantum materials: a monte carlo study. *Proc. SPIE-Int. Soc. Opt. Eng.*, 2897:68–74, 6 November 1996 through 7 November 1996 1996. doi:10.1117/12.252936.

[243] A. V. Filinov, M. Bonitz, and Y. E. Lozovik. Excitonic clusters in coupled quantum dots. *J. Phys. A: Math. Gen.*, 36(22 SPEC.ISS.):5899–5904, 2003. doi:10.1088/0305-4470/36/22/310.

[244] A. Chakraborty, M. V. Pak, and S. Hammes-Schiffer. Development of electron-proton density functionals for multicomponent density functional theory. *Phys. Rev. Lett.*, 101(15), 2008. ISSN 00319007. doi:10.1103/PhysRevLett.101.153001.

[245] Attila Szabo and Neil Ostlund. *Modern Quantum Chemistry: Introduction to Advanced Electronic Structure Theory.* Dover Publications, 1989.

[246] Mohammad El-Said. Ground-state energy of an exciton in a parabolic quantum dot. *Semicond. Sci. Technol.*, 9(3):272–274, 1994.

[247] V. Halonen, T. Chakraborty, and P. Pietiläinen. Excitons in a parabolic quantum dot in magnetic fields. *Phys. Rev. B*, 45(11):5980–5985, 1992. doi:10.1103/PhysRevB.45.5980.

[248] S. Jaziri and R. Bennaceur. Excitons in parabolic quantum dots in electric and magnetic fields. *Semicond. Sci. Technol.*, 9(10):1775–1780, 1994. doi:10.1088/0268-1242/9/10/003.

[249] W. Xie. Effect of an electric field and nonlinear optical rectification of confined excitons in quantum dots. *Phys. Status Solidi B*, 246(10):2257–2262, 2009. doi:10.1002/pssb.201248167.

[250] W. Xie and J. Gu. Exciton bound to a neutral donor in parabolic quantum dots. *Phys. Lett. A*, 312(5-6):385–390, 2003. doi:10.1016/S0375-9601(03)00651-0.

[251] F.S. Nammas, A.S. Sandouqa, H.B. Ghassib, and M.K. Al-Sugheir. Thermodynamic properties of two-dimensional few-electrons quantum dot using the static fluctuation approximation (sfa). *Phys. B (Amsterdam, Neth.)*, 406(24):4671 – 4677, 2011. ISSN 0921-4526. doi:10.1016/j.physb.2011.09.058.

[252] M.J. Karimi and G. Rezaei. Effects of external electric and magnetic fields on the linear and nonlinear intersubband optical properties of finite semi-parabolic quantum dots. *Phys. B (Amsterdam, Neth.)*, 406(23):4423 – 4428, 2011. ISSN 0921-4526. doi:10.1016/j.physb.2011.08.105.

[253] G. Rezaei, B. Vaseghi, and M. Sadri. External electric field effect on the optical rectification coefficient of an exciton in a spherical parabolic quantum dot. *Phys. B (Amsterdam, Neth.)*, 406(24):4596 – 4599, 2011. ISSN 0921-4526. doi:10.1016/j.physb.2011.09.032.

[254] Tosio Kato. On the eigenfunctions of many-particle systems in quantum mechanics. *Communications on Pure and Applied Mathematics*, 10(2):151–177, 1957. ISSN 1097-0312. doi:10.1002/cpa.3160100201.

[255] B.L. Hammond, W.A. Lester, and P.J. Reynolds. *Monte Carlo Methods in Ab Initio Quantum Chemistry*. World Scientific lecture and course notes in chemistry. World Scientific, 1994. ISBN 9789810203221.

[256] W.A. Lester. *Recent Advances in Quantum Monte Carlo Methods*. Number pt. 1 in Recent Advances in Computational Chemistry. World Scientific, 1997. ISBN 9789810230098.

[257] P. Nightingale and C.J. Umrigar. *Quantum Monte Carlo Methods in Physics and Chemistry*. NATO ASI series: Mathematical and physical sciences. Kluwer Academic, 1999. ISBN 9780792355519.

[258] Wim Klopper and Werner Kutzelnigg. Gaussian basis sets and the nuclear cusp problem. *Journal of Molecular Structure: THEOCHEM*, 135(0):339 – 356, 1986. ISSN 0166-1280. doi:10.1016/0166-1280(86)80068-9.

[259] Rogelio Cuevas-Saavedra and Paul W. Ayers. Addressing the coulomb potential singularity in exchange-correlation energy integrals with one-electron and two-

electron basis sets. *Chem. Phys. Lett.*, 539âĂŞ540(0):163 – 167, 2012. ISSN 0009-2614. doi:10.1016/j.cplett.2012.04.037.

[260] Ewa Papajak and Donald G. Truhlar. What are the most efficient basis set strategies for correlated wave function calculations of reaction energies and barrier heights? *J. Chem. Phys.*, 137(6):064110, 2012. doi:10.1063/1.4738980.

[261] Takeshi Yanai and Toru Shiozaki. Canonical transcorrelated theory with projected slater-type geminals. *The Journal of Chemical Physics*, 136(8):084107, 2012. doi:10.1063/1.3688225.

[262] A.M. Frolov and D.M. Wardlaw. On highly accurate calculations of the excited n 1s(l = 0)-states in helium atoms. *European Physical Journal D*, 61(2):305–313, 2011. doi:10.1140/epjd/e2010-100500-9.

[263] Yusaku Kurokawa, Hiroyuki Nakashima, and Hiroshi Nakatsuji. Free iterative-complement-interaction calculations of the hydrogen molecule. *Phys. Rev. A*, 72:062502, Dec 2005. doi:10.1103/PhysRevA.72.062502.

[264] Hiroshi Nakatsuji and Hiroyuki Nakashima. How does the free complement wave function become accurate and exact finally for the hydrogen atom starting from the slater and gaussian initial functions and for the helium atom on the cusp conditions? *Int. J. Quantum Chem.*, 109(10):2248âĂŞ2262, 2009. ISSN 1097-461X. doi:10.1002/qua.22109.

[265] Toru Shiozaki and Hans-Joachim Werner. Communication: Second-order multireference perturbation theory with explicit correlation: Caspt2-f12. *J. Chem. Phys.*, 133(14):141103, 2010. doi:10.1063/1.3489000.

[266] L. Kong, F.A. Bischoff, and E.F. Valeev. Explicitly correlated r12/f12 methods for electronic structure. *Chem. Rev.*, 112(1):75–107, 2012. doi:10.1021/cr200204r.

[267] Christof Hättig, Wim Klopper, Andreas Köhn, and David P. Tew. Explicitly correlated electrons in molecules. *Chem. Rev.*, 112(1):4–74, 2012. doi:10.1021/cr200168z.

[268] Bryan K. Clark, Miguel A. Morales, Jeremy McMinis, Jeongnim Kim, and Gustavo E. Scuseria. Computing the energy of a water molecule using multi-determinants: A simple, efficient algorithm. *J. Chem. Phys.*, 135(24):244105, 2011. doi:10.1063/1.3665391.

[269] Miguel A. Morales, Jeremy McMinis, Bryan K. Clark, Jeongnim Kim, and Gustavo E. Scuseria. Multideterminant wave functions in quantum monte carlo. *J. Chem. Theory Comput.*, 8(7):2181–2188, 2012. doi:10.1021/ct3003404.

[270] Brian M. Austin, Dmitry Yu. Zubarev, and William A. Lester. Quantum monte carlo and related approaches. *Chem. Rev.*, 112(1):263–288, 2012. doi:10.1021/cr2001564.

[271] David M. Ceperley. An overview of quantum monte carlo methods. *Reviews in Mineralogy and Geochemistry*, 71(1):129–135, 2010. doi:10.1.1.306.4671.

[272] Liguo Kong, Florian A. Bischoff, and Edward F. Valeev. Explicitly correlated r12/f12 methods for electronic structure. *Chem. Rev.*, 112(1):75–107, 2012. doi:10.1021/cr200204r.

[273] Seiichiro Ten-no. Explicitly correlated wave functions: summary and perspective. *Theoretical Chemistry Accounts: Theory, Computation, and Modeling (Theoretica Chimica Acta)*, 131:1–11, 2012. ISSN 1432-881X. doi:10.1007/s00214-011-1070-1.

[274] Sambasiva Rao Chinnamsetty, Hongjun Luo, Wolfgang Hackbusch, Heinz-Jürgen Flad, and André Uschmajew. Bridging the gap between quantum

monte carlo and f12-methods. *Chem. Phys.*, 401(0):36 – 44, 2012. ISSN 0301-0104. doi:10.1016/j.chemphys.2011.09.019.

[275] S. F. Boys and N. C. Handy. The determination of energies and wavefunctions with full electronic correlation. *Proceedings of the Royal Society of London. A. Mathematical and Physical Sciences*, 310(1500):43–61, 1969. doi:10.1098/rspa.1969.0061.

[276] Seiichiro Ten-no. A feasible transcorrelated method for treating electronic cusps using a frozen gaussian geminal. *Chem. Phys. Lett.*, 330(1âĂŞ2):169 – 174, 2000. ISSN 0009-2614. doi:10.1016/S0009-2614(00)01066-6.

[277] Naoto Umezawa and Shinji Tsuneyuki. Transcorrelated self-consistent calculation for electronic systems with variational monte carlo method. *Int. J. Quantum Chem.*, 91(2):184–190, 2003. ISSN 1097-461X. doi:10.1002/qua.10455.

[278] Osamu Hino, Yoshitaka Tanimura, and Seiichiro Ten-no. Application of the transcorrelated hamiltonian to the linearized coupled cluster singles and doubles model. *Chem. Phys. Lett.*, 353(3âĂŞ4):317 – 323, 2002. ISSN 0009-2614. doi:10.1016/S0009-2614(02)00042-8.

[279] Naoto Umezawa and Shinji Tsuneyuki. Ground-state correlation energy for the homogeneous electron gas calculated by the transcorrelated method. *Phys. Rev. B*, 69:165102, Apr 2004. doi:10.1103/PhysRevB.69.165102.

[280] N.C. Handy. On the minimization of the variance of the transcorrelated hamiltonian. *Mol. Phys.*, 21(5):817–828, 1971. doi:10.1080/00268977100101961.

[281] N.C. Handy. The transcorrelated method for accurate correlation energies using gaussian-type functions: examples on he, h2, lih and h2o. *Mol. Phys.*, 23(1): 1–27, 1972. doi:10.1080/00268977200100011.

[282] G. James, R.C. James, and A.A. Alchian. *Mathematics dictionary.* Van Nostrand, 1968.

[283] K.B. Datta. *Matrix and Linear Algebra.* Prentice-Hall Of India Pvt. Ltd., 2004. ISBN 9788120306363.

[284] D.S. Watkins. *Fundamentals of Matrix Computations.* Pure and Applied Mathematics. John Wiley & Sons, 2002. ISBN 9780471213949.

[285] S. F. Boys. Electronic wave functions. i. a general method of calculation for the stationary states of any molecular system. *Proceedings of the Royal Society of London. Series A. Mathematical and Physical Sciences*, 200(1063):542–554, 1950. doi:10.1098/rspa.1950.0036.

[286] K. Singer. The use of gaussian (exponential quadratic) wave functions in molecular problems. i. general formulae for the evaluation of integrals. *Proceedings of the Royal Society of London. Series A. Mathematical and Physical Sciences*, 258(1294):412–420, 1960. doi:10.1098/rspa.1960.0196.

[287] Andrew Komornicki and Harry F. King. A general formulation for the efficient evaluation of n-electron integrals over products of gaussian charge distributions with gaussian geminal functions. *J. Chem. Phys.*, 134(24):244115, 2011. doi:10.1063/1.3600745.

[288] Tatiana Korona, Hayes L. Williams, Robert Bukowski, Bogumil Jeziorski, and Krzysztof Szalewicz. Helium dimer potential from symmetry-adapted perturbation theory calculations using large gaussian geminal and orbital basis sets. *J. Chem. Phys.*, 106(12):5109–5122, 1997. doi:10.1063/1.473556.

[289] Robert Bukowski, Bogumil Jeziorski, and Krzysztof Szalewicz. Basis set superposition problem in interaction energy calculations with explicitly correlated

bases: Saturated second- and third-order energies for he[sub 2]. *J. Chem. Phys.*, 104(9):3306–3319, 1996.

[290] Robert Bukowski, Bogumil Jeziorski, and Krzysztof Szalewicz. Gaussian geminals in explicitly correlated coupled cluster theory including single and double excitations. *J. Chem. Phys.*, 110(9):4165–4183, 1999. doi:10.1063/1.479109.

[291] P. Dahle, T. Helgaker, D. Jonsson, and P. R. Taylor. Accurate quantum-chemical calculations using gaussian-type geminal and gaussian-type orbital basis sets: Applications to atoms and diatomics. *Phys. Chem. Chem. Phys.*, 9 (24):3112–3126, 2007.

[292] K.L Bak, A Halkier, P JÃÿrgensen, J Olsen, T Helgaker, and W Klopper. Chemical accuracy from âĂŸcoulomb holeâĂŹ extrapolated molecular quantum-mechanical calculations. *J. Mol. Struct.*, 567âĂŞ568(0):375 – 384, 2001. ISSN 0022-2860. doi:10.1016/S0022-2860(01)00566-X.

[293] S. A. Blundell and K. Joshi. Precise correlation energies in small parabolic quantum dots from configuration interaction. *Phys. Rev. B*, 81:115323, Mar 2010. doi:10.1103/PhysRevB.81.115323.

[294] Katharina Boguslawski, Konrad H. Marti, and Markus Reiher. Construction of casci-type wave functions for very large active spaces. *J. Chem. Phys.*, 134(22): 224101, 2011. doi:10.1063/1.3596482.

[295] S. Corni, M. Braskén, M. Lindberg, J. Olsen, and D. Sundholm. Electron-hole recombination density matrices obtained from large configuration-interaction expansions. *Phys. Rev. B*, 67:085314, Feb 2003.

[296] Massimo Rontani, Carlo Cavazzoni, Devis Bellucci, and Guido Goldoni. Full configuration interaction approach to the few-electron problem in artificial atoms. *J. Chem. Phys.*, 124(12):124102, 2006. doi:10.1063/1.2179418.

[297] Sebastian HÃűfener, David P. Tew, Wim Klopper, and Trygve Helgaker. The geminal basis in explicitly correlated wave functions. *Chem. Phys.*, 356(1âĂŞ3): 25 – 30, 2009. ISSN 0301-0104. doi:DOI: 10.1016/j.chemphys.2008.10.022.

[298] Ernest R. Davidson. The iterative calculation of a few of the lowest eigenvalues and corresponding eigenvectors of large real-symmetric matrices. *J. Comput. Phys.*, 17(1):87 – 94, 1975. ISSN 0021-9991. doi:10.1016/0021-9991(75)90065-0.

[299] George H. Booth, Alex J. W. Thom, and Ali Alavi. Fermion monte carlo without fixed nodes: A game of life, death, and annihilation in slater determinant space. *J. Chem. Phys.*, 131(5):054106, 2009. doi:10.1063/1.3193710.

[300] George H. Booth and Ali Alavi. Approaching chemical accuracy using full configuration-interaction quantum monte carlo: A study of ionization potentials. *J. Chem. Phys.*, 132(17):174104, 2010. doi:10.1063/1.3407895.

[301] George H. Booth, Deidre Cleland, Alex J. W. Thom, and Ali Alavi. Breaking the carbon dimer: The challenges of multiple bond dissociation with full configuration interaction quantum monte carlo methods. *J. Chem. Phys.*, 135(8): 084104, 2011. doi:10.1063/1.3624383.

[302] D. M. Cleland, George H. Booth, and Ali Alavi. A study of electron affinities using the initiator approach to full configuration interaction quantum monte carlo. *J. Chem. Phys.*, 134(2):024112, 2011. doi:10.1063/1.3525712.

[303] James J. Shepherd, George H. Booth, and Ali Alavi. Investigation of the full configuration interaction quantum monte carlo method using homogeneous electron gas models. *J. Chem. Phys.*, 136(24):244101, 2012. doi:10.1063/1.4720076.

[304] R. K. Nesbet. Algorithm for diagonalization of large matrices. *J. Chem. Phys.*, 43(1):311–312, 1965. doi:10.1063/1.1696477.

[305] Daniel P. Joubert. Functional relations for the density-functional exchange and correlation functionals connecting functionals at three densities. *Phys. Rev. A*, 85:032511, Mar 2012. doi:10.1103/PhysRevA.85.032511.

[306] Hiroshi Nakatsuji. General method of solving the schrödinger equation of atoms and molecules. *Phys. Rev. A*, 72:062110, Dec 2005. doi:10.1103/PhysRevA.72.062110.

[307] Tao Yang, Xiao-Yin Pan, and Viraht Sahni. Quantal density-functional theory in the presence of a magnetic field. *Phys. Rev. A*, 83:042518, Apr 2011. doi:10.1103/PhysRevA.83.042518.

[308] Cai Liang, Zhang Ping, Yang Tao, and Pan Xiao-Yin. Hooke's atom in an arbitrary external electric field: Analytical solutions of two-electron problem by path integral approach. *Commun. Theor. Phys.*, 55(4):565, 2011. doi:10.1088/0253-6102/55/4/06.

[309] Toru Shiozaki, Gerald Knizia, and Hans-Joachim Werner. Explicitly correlated multireference configuration interaction: Mrci-f12. *J. Chem. Phys.*, 134(3): 034113, 2011. doi:10.1063/1.3528720.

[310] Seiichiro Ten-no and Jozef Noga. Explicitly correlated electronic structure theory from r12/f12 ansätze. *Wiley Interdisciplinary Reviews: Computational Molecular Science*, 2(1):114–125, 2012. ISSN 1759-0884. doi:10.1002/wcms.68.

[311] E.A. Hylleraas. Neue berechnung der energie des heliums im grundzustande, sowie des tiefsten terms von ortho-helium. *Z. Phys.*, 54(5-6):347–366, 1929. doi:10.1007/BF01375457.

[312] T. Kinoshita. Ground state of the helium atom. ii. *Physical Review*, 115(2): 366–374, 1959. doi:10.1103/PhysRev.115.366.

[313] T. Kinoshita. Ground state of the helium atom. *Physical Review*, 105(5):1490–1502, 1957.

[314] H. Nakashima and H. Nakatsuji. Solving the electron-nuclear schrÃűdinger equation of helium atom and its isoelectronic ions with the free iterative-complement-interaction method. *J. Chem. Phys.*, 128(15), 2008. doi:10.1063/1.2904562.

[315] H. Nakashima and H. Nakatsuji. Solving the schrÃűdinger equation for helium atom and its isoelectronic ions with the free iterative complement interaction (ici) method. *J. Chem. Phys.*, 127(22), 2007. doi:10.1039/B806979B.

[316] S. Rosendorff and H. G. Schlaile. Logarithmic mean excitation energies: Hydrogen and helium. *Phys. Rev. A*, 40(12):6892–6896, 1989. doi:10.1103/PhysRevA.40.6892.

[317] A. J. May, E. Valeev, R. Polly, and F. R. Manby. Analysis of the errors in explicitly correlated electronic structure theory. *Phys. Chem. Chem. Phys.*, 7(14):2710–2713, 2005. doi:10.1039/b507781h.

[318] S. Rosendorff and H. G. Schlaile. Logarithmic mean excitation energies: Ii. helium, lithium, beryllium, and the 2s state of hydrogen. *Phys. Rev. A*, 48(4):2798–2810, 1993. doi:10.1103/PhysRevA.48.2798.

[319] J. D. Morgan. The validity of kinoshita's expansion for s-state eigenfunctions of the helium atom. *J. Phys. A: Math. Gen.*, 11(1):221–224, 1978. doi:10.1088/0305-4470/11/1/023.

[320] Russel D. III Johnson. Nist 101. computational chemistry comparison and benchmark database, August 2011. Release 15b.

[321] Hyunjoo Han, Gianna Di Francesco, and Mathew M. Maye. Size control and photophysical properties of quantum dots prepared via a novel tunable hydrothermal route. *J. Phys. Chem. C*, 114(45):19270–19277, 2010. doi:10.1021/jp107702b.

[322] B L Williams, D P Halliday, B G Mendis, and K Durose. Microstructure and point defects in cdte nanowires for photovoltaic applications. *Nanotechnology*, 24(13):135703, 2013. doi:10.1088/0957-4484/24/13/135703.

[323] Jun Yin, Chuang Yue, Yashu Zang, Ching-Hsueh Chiu, Jinchai Li, Hao-Chung Kuo, Zhihao Wu, Jing Li, Yanyan Fang, and Changqing Chen. Effect of the surface-plasmon-exciton coupling and charge transfer process on the photoluminescence of metal-semiconductor nanostructures. *Nanoscale*, 5:4436–4442, 2013. doi:10.1039/C3NR00920C.

[324] Heather M. Jaeger, Sean Fischer, and Oleg V. Prezhdo. The role of surface defects in multi-exciton generation of lead selenide and silicon semiconductor quantum dots. *J. Chem. Phys.*, 136(6):064701, 2012. doi:10.1063/1.3682559.

[325] Svetlana Kilina, Kirill A. Velizhanin, Sergei Ivanov, Oleg V. Prezhdo, and Sergei Tretiak. Surface ligands increase photoexcitation relaxation rates in cdse quantum dots. *ACS Nano*, 6(7):6515–6524, 2012. doi:10.1021/nn302371q.

[326] Svetlana Kilina, Sergei Ivanov, and Sergei Tretiak. Effect of surface ligands on optical and electronic spectra of semiconductor nanoclusters. *J. Am. Chem. Soc.*, 131(22):7717–7726, 2009. doi:10.1021/ja9005749.

[327] A.M. Kelley. Electron-phonon coupling in cdse nanocrystals. *J. Phys. Chem. Lett.*, 1(9):1296–1300, 2010. doi:10.1021/jz100123b.

[328] A.M. Kelley. Electron-phonon coupling in cdse nanocrystals from an atomistic phonon model. *ACS Nano*, 5(6):5254–5262, 2011. doi:10.1021/nn201475d.

[329] A.M. Kelley, Q. Dai, Z.-j. Jiang, J.A. Baker, and D.F. Kelley. Resonance raman spectra of wurtzite and zincblende cdse nanocrystals. *Chem. Phys.*, Article in press, 2012. doi:10.1016/j.chemphys.2012.09.029.

[330] S.V. Kilina, D.S. Kilin, V.V. Prezhdo, and O.V. Prezhdo. Theoretical study of electron-phonon relaxation in pbse and cdse quantum dots: Evidence for phonon memory. *J. Phys. Chem. C*, 115(44):21641–21651, 2011. doi:Publi.

[331] K. Hyeon-Deuk and O.V. Prezhdo. Time-domain ab initio study of auger and phonon-assisted auger processes in a semiconductor quantum dot. *Nano Lett.*, 11(4):1845–1850, 2011. doi:10.1021/nl200651p.

[332] K. Hyeon-Deuk and O.V. Prezhdo. Photoexcited electron and hole dynamics in semiconductor quantum dots: Phonon-induced relaxation, dephasing, multiple exciton generation and recombination. *J. Phys.: Condens. Matter*, 24(36): 363201, 2012. doi:10.1088/0953-8984/24/36/363201.

[333] S.V. Kilina, A.J. Neukirch, B.F. Habenicht, D.S. Kilin, and O.V. Prezhdo. Quantum zeno effect rationalizes the phonon bottleneck in semiconductor quantum dots. *Phys. Rev. Lett.*, 110(18):180404, 2013.

[334] I. Musa, F. Massuyeau, L. Cario, J. L. Duvail, S. Jobic, P. Deniard, and E. Faulques. Temperature and size dependence of time-resolved exciton recombination in zno quantum dots. *Appl. Phys. Lett.*, 99(24):243107, 2011. doi:10.1063/1.3669511.

[335] Alberto Franceschetti and Alex Zunger. Exciton dissociation and interdot transport in cdse quantum-dot molecules. *Phys. Rev. B*, 63:153304, Mar 2001. doi:10.1103/PhysRevB.63.153304.

[336] Haiming Zhu, Nianhui Song, and Tianquan Lian. Wave function engineering for ultrafast charge separation and slow charge recombination in type

ii core/shell quantum dots. *J. Am. Chem. Soc.*, 133(22):8762–8771, 2011. doi:10.1021/ja202752s.

[337] Jessica Hoy, Paul J. Morrison, Lindsey K. Steinberg, William E. Buhro, and Richard A. Loomis. Excitation energy dependence of the photoluminescence quantum yields of core and core/shell quantum dots. *J. Phys. Chem. C*, 4(0): 2053–2060, 2013. doi:10.1021/jz4004735.

[338] Dehui Li, Jun Zhang, Qing Zhang, and Qihua Xiong. Electric-field-dependent photoconductivity in cds nanowires and nanobelts: Exciton ionization, franz-keldysh, and stark effects. *Nano Lett.*, 12(6):2993–2999, 2012. doi:10.1021/nl300749z.

[339] Nir Yaacobi-Gross, Michal Soreni-Harari, Marina Zimin, Shifi Kababya, Asher Schmidt, and Nir Tessler. Molecular control of quantum-dot internal electric field and its application to cdse-based solar cells. *Nat. Mater.*, 10(12):974–979, 2011. doi:10.1038/nmat3133.

[340] Su Liu, Nicholas J. Borys, Jing Huang, Dmitri V. Talapin, and John M. Lupton. Exciton storage in cdse/cds tetrapod semiconductor nanocrystals: Electric field effects on exciton and multiexciton states. *Phys. Rev. B*, 86:045303, Jul 2012. doi:10.1103/PhysRevB.86.045303.

[341] Vasili Perebeinos and Phaedon Avouris. Exciton ionization, franz-keldysh, and stark effects in carbon nanotubes. *Nano Lett.*, 7(3):609–613, 2007. doi:10.1021/nl0625022.

[342] KyoungWon Park, Zvicka Deutsch, J. Jack Li, Dan Oron, and Shimon Weiss. Single molecule quantum-confined stark effect measurements of semiconductor nanoparticles at room temperature. *ACS Nano*, 6(11):10013–10023, 2012. doi:10.1021/nn303719m.

[343] Sachin Rawalekar, Sreejith Kaniyankandy, Sandeep Verma, and Hirendra N. Ghosh. Ultrafast charge carrier relaxation and charge transfer dynamics of cdte/cds core-shell quantum dots as studied by femtosecond transient absorption spectroscopy. *J. Phys. Chem. C*, 114(3):1460–1466, 2010. doi:10.1021/jp909118c.

[344] Alexander Nemchinov, Maria Kirsanova, Nishshanka N. Hewa-Kasakarage, and Mikhail Zamkov. Synthesis and characterization of type ii znse/cds core/shell nanocrystals. *J. Phys. Chem. C*, 112(25):9301–9307, 2008. doi:10.1021/jp801523m.

[345] Yueran Yan, Gang Chen, and P. Gregory Van Patten. Ultrafast exciton dynamics in cdte nanocrystals and core/shell cdte/cds nanocrystals. *J. Phys. Chem. C*, 115(46):22717–22728, 2011. doi:10.1021/jp204420q.

[346] Y. Noguchi, O. Sugino, M. Nagaoka, S. Ishii, and K. Ohno. A gwbethe-salpeter calculation on photoabsorption spectra of (cdse) 3 and (cdse) 6 clusters. *J. Chem. Phys.*, 137(2):024306, 2012. ISSN 00219606. doi:10.1063/1.4732123.

[347] M. Lopez Del Puerto, M.L. Tiago, and J.R. Chelikowsky. Ab initio methods for the optical properties of cdse clusters. *Phys. Rev. B*, 77(4):045404, 2008. ISSN 10980121. doi:10.1103/PhysRevB.77.045404.

[348] M.L. Del Puerto, M.L. Tiago, and J.R. Chelikowsky. Excitonic effects and optical properties of passivated cdse clusters. *Phys. Rev. Lett.*, 97(9):096401, 2006. ISSN 00319007. doi:10.1103/PhysRevLett.97.096401.

[349] K.A. Nguyen, P.N. Day, and Pachte. Understanding structural and optical properties of nanoscale cdse magic-size quantum dots: Insight from computational prediction. *J. Phys. Chem. C*, 114(39):16197–16209, 2010. doi:10.1021/jp103763d.

[350] P. Yang, S. Tretiak, and S. Ivanov. Influence of surfactants and charges on cdse quantum dots. *J. Cluster Sci.*, 22(3):405–431, 2011. doi:10.1007/s10876-011-0398-y.

[351] Victor V. Albert, Sergei A. Ivanov, Sergei Tretiak, and Svetlana V. Kilina. Electronic structure of ligated cdse clusters: Dependence on dft methodology. *The Journal of Physical Chemistry C*, 115(32):15793–15800, 2011. doi:10.1021/jp202510z.

[352] D.S. Kilin, K. Tsemekhman, O.V. Prezhdo, E.I. Zenkevich, and C. von Borczyskowski. Ab initio study of exciton transfer dynamics from a core-shell semiconductor quantum dot to a porphyrin-sensitizer. *J. Photochem. Photobiol., A*, 190(2-3):342–351, 2007. doi:10.1016/j.jphotochem.2007.02.017.

[353] C. Liu, S.-Y. Chung, S. Lee, S. Weiss, and D. Neuhauser. Adsorbate-induced absorption redshift in an organic-inorganic cluster conjugate: Electronic effects of surfactants and organic adsorbates on the lowest excited states of a methanethiol-cdse conjugate. *J. Chem. Phys.*, 131(17):174705, 2009. doi:10.1063/1.3251774.

[354] S.-Y. Chung, S. Lee, C. Liu, and D. Neuhauser. Structures and electronic spectra of cdse-cys complexes: Density functional theory study of a simple peptide-coated nanocluster. *J. Phys. Chem. B*, 113(1):292–301, 2009. doi:10.1021/jp8062299.

[355] H.S. Kim, S.-W. Jang, S.Y. Chung, S. Lee, Y. Lee, B. Kim, C. Liu, and D. Neuhauser. Effects of bioconjugation on the structures and electronic spectra of cdse: Density functional theory study of cdse - adenine complexes. *J. Phys. Chem. B*, 114(1):471–479, 2010. doi:10.1021/jp907725f.

[356] R. Nadler and J.F. Sanz. Simulating the optical properties of cdse clus-

ters using the rt-tddft approach. *Theor. Chem. Acc.*, 132(4):1–9, 2013. doi:10.1007/s00214-013-1342-z.

[357] Ahmed M. Abuelela, Tarek A. Mohamed, and Oleg V. Prezhdo. Dft simulation and vibrational analysis of the ir and raman spectra of a cdse quantum dot capped by methylamine and trimethylphosphine oxide ligands. *The Journal of Physical Chemistry C*, 116(27):14674–14681, 2012. doi:10.1021/jp303275v.

[358] M. Del Ben, R.W.A. Havenith, R. Broer, and M. Stener. Density functional study on the morphology and photoabsorption of cdse nanoclusters. *J. Phys. Chem. C*, 115(34):16782–16796, 2011. doi:10.1021/jp203686a.

[359] V. Turkowski, A. Leonardo, and C.A. Ullrich. Time-dependent density-functional approach for exciton binding energies. *Phys. Rev. B*, 79(23):233201, 2009. doi:10.1103/PhysRevB.79.233201.

[360] Y. Li and C.A. Ullrich. Time-dependent transition density matrix. *Chem. Phys.*, 391(1):157–163, 2011. doi:10.1016/j.chemphys.2011.02.001.

[361] D. Neuhauser, E. Rabani, and R. Baer. Expeditious stochastic calculation of random-phase approximation energies for thousands of electrons in three dimensions. *J. Phys. Chem. Lett.*, 4(7):1172–1176, 2013. doi:10.1021/jz3021606.

[362] Roi Baer and Eran Rabani. Communication: Biexciton generation rates in cdse nanorods are length independent. *J. Chem. Phys.*, 138(5):051102, 2013. doi:10.1063/1.4790600.

[363] Eran Rabani, Balazs Hetenyi, B. J. Berne, and L. E. Brus. Electronic properties of cdse nanocrystals in the absence and presence of a dielectric medium. *J. Chem. Phys.*, 110(11):5355–5369, 1999. doi:10.1063/1.478431.

[364] L.-W. Wang and A. Zunger. Solving schrödinger's equation around a desired energy: Application to silicon quantum dots. *J. Chem. Phys.*, 100(3):2394–2397, 1994. doi:10.1063/1.466486.

[365] A. Canning, L.W. Wang, A. Williamson, and A. Zunger. Parallel empirical pseudopotential electronic structure calculations for million atom systems. *J. Comput. Phys.*, 160(1):29–41, 2000. doi:10.1006/jcph.2000.6440.

[366] S. Toledo and E. Rabani. Verly large electronic structure calculations using an out-of-core filter-diagonalization method. *J. Comput. Phys.*, 180(1):256–269, 2002. doi:10.1006/jcph.2002.7090.

[367] C. Vömel, S.Z. Tomov, O.A. Marques, A. Canning, L.-W. Wang, and J.J. Dongarra. State-of-the-art eigensolvers for electronic structure calculations of large scale nano-systems. *J. Comput. Phys.*, 227(15):7113–7124, 2008. doi:10.1016/j.jcp.2008.01.018.

[368] G. Jordan, M. Marsman, Y.-S. Kim, and G. Kresse. Fast iterative interior eigensolver for millions of atoms. *J. Comput. Phys.*, 231(14):4836–4847, 2012. doi:10.1016/j.jcp.2012.04.010.

[369] D.A. Mazziotti. *Advances in Chemical Physics, Reduced-Density-Matrix Mechanics: With Application to Many-Electron Atoms and Molecules.* Advances in Chemical Physics. Wiley, 2007. ISBN 9780470106594.

[370] Xuejun Zhu, Mark S. Hybertsen, and P. B. Littlewood. Electron-hole system revisited: A variational quantum monte carlo study. *Phys. Rev. B*, 54:13575–13580, Nov 1996. doi:10.1103/PhysRevB.54.13575.

[371] C. Höttig, W. Klopper, A. Köhn, and D.P. Tew. Explicitly correlated electrons in molecules. *Chem. Rev.*, 112(1):4–74, 2012. doi:10.1021/cr200168z.

[372] M. Braskén, M. Lindberg, D. Sundholm, and J. Olsen. Full configuration interaction calculations of electron-hole correlation effects in strain-induced quantum dots. *Phys. Status Solidi B*, 224(3):775–779, 2001. doi:10.1103/PhysRevB.61.7652.

[373] S. Corni, M. Braskén, M. Lindberg, J. Olsen, and D. Sundholm. Stabilization energies of charged multiexciton complexes calculated at configuration interaction level. *Phys. E*, 18(4):436–442, 2003.

[374] S. Corni, M. Braskén, M. Lindberg, J. Olsen, and D. Sundholm. Electron-hole recombination density matrices obtained from large configuration-interaction expansions. *Phys. Rev. B*, 67(8):853141–853147, 2003.

[375] S. Corni, M. Braskén, M. Lindberg, J. Olsen, and D. Sundholm. Size dependence of the electron-hole recombination rates in semiconductor quantum dots. *Phys. Rev. B*, 67(4):453131–453139, 2003. doi:10.1103/PhysRevB.67.045313.

[376] T. Vänskä and D. Sundholm. Interpretation of the photoluminescence spectrum of double quantum rings. *Phys. Rev. B*, 82(8):085306, 2010. doi:10.1103/PhysRevB.82.085306.

[377] Jennifer M. Elward and Arindam Chakraborty. Atomistic pseudopotential calculation on cdse quantum dots using electron-hole explicitly correlated hartree-fock method. *(to be submitted)*.

[378] Michael G. Bayne, John Drogo, and Arindam Chakraborty. Infinite-order diagrammatic summation approach to the explicitly correlated congruent transformed hamiltonian. *Phys. Rev. A*, 89:032515, Mar 2014. doi:10.1103/PhysRevA.89.032515.

[379] Jacek Jasieniak and Paul Mulvaney. From cd-rich to se-rich-the manipulation of

cdse nanocrystal surface stoichiometry. *J. Am. Chem. Soc.*, 129(10):2841–2848, 2007. doi:10.1021/ja066205a.

[380] A.G. Midgett, J.M. Luther, J.T. Stewart, D.K. Smith, L.A. Padilha, V.I. Klimov, A.J. Nozik, and M.C. Beard. Size and composition dependent multiple exciton generation efficiency in pbs, pbse, and pbsxse1-x alloyed quantum dots. *Nano Lett.*, 13(7):3078–3085, 2013. doi:10.1021/nl4009748.

[381] N.S.A. Eom, T.-S. Kim, Y.-H. Choa, W.-B. Kim, and B.S. Kim. Core-size-dependent properties of cdse/cds core/shell qds. *Mater. Lett.*, 99:14–17, 2013. doi:10.1016/j.matlet.2013.02.065.

[382] C.C. Yang and Y.-W. Mai. Size-dependent absorption properties of cdx (x = s, se, te) quantum dots. *Chem. Phys. Lett.*, 535:91–93, 2012. doi:10.1016/j.cplett.2012.03.048.

[383] H. Li, R. Brescia, M. Povia, M. Prato, G. Bertoni, L. Manna, and I. Moreels. Synthesis of uniform disk-shaped copper telluride nanocrystals and cation exchange to cadmium telluride quantum disks with stable red emission. *J. Am. Chem. Soc.*, 135(33):12270–12278, 2013. doi:10.1021/ja404694k.

[384] P. Ren, J. Xu, Y. Wang, X. Zhuang, Q. Zhang, H. Zhou, Q. Wan, Z. Shan, X. Zhu, and A. Pan. Synthesis and optical properties of inp quantum dot/nanowire heterostructures. *Phys. Status Solidi A*, pages 1898–1902, 2013. doi:10.1002/pssa.201329060.

[385] K.B. Subila, G. Kishore Kumar, S.M. Shivaprasad, and K. George Thomas. Luminescence properties of cdse quantum dots: Role of crystal structure and surface composition. *J. Phys. Chem. Lett.*, 4(16):2774–2779, 2013. doi:10.1021/jz401198e.

[386] X. Liu, Y. Jiang, F. Fu, W. Guo, W. Huang, and L. Li. Facile synthesis of high-quality zns, cds, cdzns, and cdzns/zns core/shell quantum dots: Characterization and diffusion mechanism. *Mater. Sci. Semicond. Process.*, 16(6): 1723–1729, 2013. doi:10.1016/j.mssp.2013.06.007.

[387] M.C. Beard, J.M. Luther, O.E. Semonin, and A.J. Nozik. Third generation photovoltaics based on multiple exciton generation in quantum confined semiconductors. *Acc. Chem. Res.*, 46(6):1252–1260, 2013. doi:10.1021/ar3001958.

[388] A. Rakovich, I. Nabiev, A. Sukhanova, V. Lesnyak, N. Gaponik, Y.P. Rakovich, and J.F. Donegan. Large enhancement of nonlinear optical response in a hybrid nanobiomaterial consisting of bacteriorhodopsin and cadmium telluride quantum dots. *ACS Nano*, 7(3):2154–2160, 2013. doi:10.1021/nn3049939.

[389] F. Maier-Flaig, J. Rinck, M. Stephan, T. Bocksrocker, M. Bruns, C. Kübel, A.K. Powell, G.A. Ozin, and U. Lemmer. Multicolor silicon light-emitting diodes (sileds). *Nano Lett.*, 13(2):475–480, 2013. doi:10.1021/nl3038689.

[390] J. Kwak, W.K. Bae, D. Lee, I. Park, J. Lim, M. Park, H. Cho, H. Woo, D.Y. Yoon, K. Char, S. Lee, and C. Lee. Bright and efficient full-color colloidal quantum dot light-emitting diodes using an inverted device structure. *Nano Lett.*, 12(5):2362–2366, 2012. doi:10.1021/nl3003254.

[391] B.N. Pal, Y. Ghosh, S. Brovelli, R. Laocharoensuk, V.I. Klimov, J.A. Hollingsworth, and H. Htoon. Giant cdse/cds core/shell nanocrystal quantum dots as efficient electroluminescent materials: Strong influence of shell thickness on light-emitting diode performance. *Nano Lett.*, 12(1):331–336, 2012. doi:10.1021/nl203620f.

[392] G. Wang, X. Yang, F. Qian, J.Z. Zhang, and Y. Li. Double-sided cds and cdse

quantum dot co-sensitized zno nanowire arrays for photoelectrochemical hydrogen generation. *Nano Lett.*, 10(3):1088–1092, 2010. doi:10.1021/nl100250z.

[393] Rabeka Alam, Joshua Zylstra, Danielle M. Fontaine, Bruce R. Branchini, and Mathew M. Maye. Novel multistep bret-fret energy transfer using nanoconjugates of firefly proteins, quantum dots, and red fluorescent proteins. *Nanoscale*, 5:5303–5306, 2013. doi:10.1039/C3NR01842C.

[394] Preston T. Snee, Rebecca C. Somers, Gautham Nair, John P. Zimmer, Moungi G. Bawendi, and Daniel G. Nocera. A ratiometric cdse/zns nanocrystal ph sensor. *J. Am. Chem. Soc.*, 128(41):13320–13321, Sep 2006. ISSN 00027863. doi:10.1021/ja0618999.

[395] Michael H. Stewart, Alan L. Huston, Amy M. Scott, Alexander L. Efros, Joseph S. Melinger, Kelly Boeneman Gemmill, Scott A. Trammell, Juan B. Blanco-Canosa, Philip E. Dawson, and Igor L. Medintz. Complex foÌĹrster energy transfer interactions between semiconductor quantum dots and a redox-active osmium assembly. *ACS Nano*, 6(6):5330–5347, Jun 2012. ISSN 19360851. doi:10.1021/nn301177h.

[396] Sedat Nizamoglu, Burak Guzelturk, Dae-Woo Jeon, In-Hwan Lee, and Hilmi Volkan Demir. Efficient nonradiative energy transfer from ingan/gan nanopillars to cdse/zns core/shell nanocrystals. *Appl. Phys. Lett.*, 98(16): 163108, 2011. doi:10.1063/1.3562035.

[397] B. Ehrler, K.P. Musselman, M.L. Böhm, F.S.F. Morgenstern, Y. Vaynzof, B.J. Walker, J.L. MacManus-Driscoll, and N.C. Greenham. Preventing interfacial recombination in colloidal quantum dot solar cells by doping the metal oxide. *ACS Nano*, 7(5):4210–4220, 2013. doi:10.1021/nn400656n.

[398] K. Žídek, K. Zheng, M. Abdellah, N. Lenngren, P. Chäbera, and T. Pullerits.

Ultrafast dynamics of multiple exciton harvesting in the cdse-zno system: Electron injection versus auger recombination. *Nano Lett.*, 12(12):6393–6399, 2012. doi:10.1021/nl303746d.

[399] J. Tang, H. Liu, D. Zhitomirsky, S. Hoogland, X. Wang, M. Furukawa, L. Levina, and E.H. Sargent. Quantum junction solar cells. *Nano Lett.*, 12(9):4889–4894, 2012. doi:10.1021/nl302436r.

[400] A. Salant, M. Shalom, I. Hod, A. Faust, A. Zaban, and U. Banin. Quantum dot sensitized solar cells with improved efficiency prepared using electrophoretic deposition. *ACS Nano*, 4(10):5962–5968, 2010. doi:10.1021/nn1018208.

[401] Y. Yang, W. Rodríguez-Córdoba, and T. Lian. Multiple exciton generation and dissociation in pbs quantum dot-electron acceptor complexes. *Nano Lett.*, 12(8):4235–4241, 2012. doi:10.1021/nl301847r.

[402] A.F. Cihan, P.L. Hernandez Martinez, Y. Kelestemur, E. Mutlugun, and H.V. Demir. Observation of biexcitons in nanocrystal solids in the presence of photocharging. *ACS Nano*, 7(6):4799–4809, 2013. doi:10.1021/nn305259g.

[403] V. Sukhovatkin, S. Hinds, L. Brzozowski, and E.H. Sargent. Colloidal quantum-dot photodetectors exploiting multiexciton generation. *Science*, 324(5934):1542–1544, 2009. doi:10.1126/science.1173812.

[404] E. Rabani and R. Baer. Distribution of multiexciton generation rates in cdse and inas nanocrystals. *Nano Lett.*, 8(12):4488–4492, 2008. doi:10.1021/nl802443c.

[405] Jier Huang, Zhuangqun Huang, Ye Yang, Haiming Zhu, and Tianquan Lian. Multiple exciton dissociation in cdse quantum dots by ultrafast electron transfer to adsorbed methylene blue. *J. Am. Chem. Soc.*, 132(13):4858–4864, 2010. doi:10.1021/ja100106z.

[406] Jiangtian Li, Scott K. Cushing, Peng Zheng, Tess Senty, Fanke Meng, Alan D. Bristow, Ayyakkannu Manivannan, and Nianqiang Wu. Solar hydrogen generation by a cds-au-tio2 sandwich nanorod array enhanced with au nanoparticle as electron relay and plasmonic photosensitizer. *J. Am. Chem. Soc.*, 0(0):null, 0. doi:10.1021/ja503508g.

[407] F. Rajadell, J.I. Climente, J. Planelles, and A. Bertoni. Excitons, biexcitons, and trions in cdse nanorods. *J. Phys. Chem. C*, 113(26):11268–11272, 2009. doi:10.1021/jp902652z.

[408] W. Qin, R.A. Shah, and P. Guyot-Sionnest. Cdses/zns alloyed nanocrystal lifetime and blinking studies under electrochemical control. *ACS Nano*, 6(1): 912–918, 2012. doi:10.1021/nn2044388.

[409] S. Verma, S. Kaniyankandy, and H.N. Ghosh. Charge separation by indirect bandgap transitions in cds/znse type-ii core/shell quantum dots. *J. Phys. Chem. C*, 117(21):10901–10908, 2013. doi:10.1021/jp400014j.

[410] Kaifeng Wu, Zheng Liu, Haiming Zhu, and Tianquan Lian. Exciton annihilation and dissociation dynamics in group ii-v cd3p2 quantum dots. *J. Phys. Chem. A*, 2013. doi:10.1021/jp402511m.

[411] Y.-L. Xie. Enhanced photovoltaic performance of hybrid solar cell using highly oriented cds/cdse-modified tio2 nanorods. *Electrochim. Acta*, 105:137–141, 2013. doi:10.1016/j.electacta.2013.04.157.

[412] Haiming Zhu, Nianhui Song, and Tianquan Lian. Controlling charge separation and recombination rates in cdse/zns type i coreâĹŠshell quantum dots by shell thicknesses. *J. Am. Chem. Soc.*, 132(42):15038–15045, 2010. doi:10.1021/ja106710m.

[413] Haiming Zhu, Nianhui Song, William RodrÃŋguez-CÃşrdoba, and Tianquan Lian. Wave function engineering for efficient extraction of up to nineteen electrons from one cdse/cds quasi-type ii quantum dot. *J. Am. Chem. Soc.*, 134 (9):4250–4257, 2012. doi:10.1021/ja210312s.

[414] P.K. Ghosh, A. Ghosal, and D. Chattopadhyay. Magnetoelectronic transport of the two-dimensional electron gas in cdse single quantum wells. *Pramana*, 72 (2):399–405, 2009. ISSN 0304-4289. doi:10.1007/s12043-009-0035-6.

[415] H. Htoon, A. V. Malko, D. Bussian, J. Vela, Y. Chen, J. A. Hollingsworth, and V. I. Klimov. Highly emissive multiexcitons in steady-state photoluminescence of individual "giant" cdse/cds core/shell nanocrystals. *Nano Lett.*, 10(7):2401–2407, 2010. doi:10.1021/nl1004652.

[416] X.-Y. Zhu, Q. Yang, and M. Muntwiler. Charge-transfer excitons at organic semiconductor surfaces and interfaces. *Acc. Chem. Res.*, 42(11):1779–1787, 2009. doi:10.1021/ar800269u. PMID: 19378979.

[417] Jianhui Sun, Jialong Zhao, and Yasuaki Masumoto. Shell-thickness-dependent photoinduced electron transfer from cuins2/zns quantum dots to tio2 films. *Appl. Phys. Lett.*, 102(5), 2013. doi:http://dx.doi.org/10.1063/1.4790603.

[418] Chun-Li Chang, Po-Yu Tsai, Yu-pin Chang, and King-Chuen Lin. Interfacial electron transfer from cdse/zns quantum dots to tio2 nanoparticles: Size dependence at the single-molecule level. *ChemPhysChem*, 13(11):2711–2720, 2012. ISSN 1439-7641. doi:10.1002/cphc.201200037.

[419] Hyunbong Choi, Pralay K. Santra, and Prashant V. Kamat. Synchronized energy and electron transfer processes in covalently linked cdse–squaraine dye–tio2 light harvesting assembly. *ACS Nano*, 6(6):5718–5726, Jun 2012. doi:10.1021/nn301982e.

[420] Florencio García-Santamaría, Sergio Brovelli, Ranjani Viswanatha, Jennifer A. Hollingsworth, Han Htoon, Scott A. Crooker, and Victor I. Klimov. Breakdown of volume scaling in auger recombination in cdse/cds heteronanocrystals: The role of the core-shell interface. *Nano Lett.*, 11(2):687–693, 2011. doi:10.1021/nl103801e.

[421] A.E. Nel, L. Madler, D. Velegol, T. Xia, E.M.V. Hoek, P. Somasundaran, F. Klaessig, V. Castranova, and M. Thompson. Understanding biophysico-chemical interactions at the nano-bio interface. *Nat. Mater.*, 8(7):543–557, 2009. doi:10.1038/nmat2442.

[422] Z. Chen and D. Wu. Colloidal znse quantum dot as ph probes for study of enzyme reaction kinetics by fluorescence spectroscopic technique. *Colloids and Surfaces A: Physicochemical and Engineering Aspects*, 414:174–179, 2012. doi:10.1016/j.colsurfa.2012.08.021.

[423] I.C. Serrano, Q. Ma, and E. Palomares. Qd-onion-multicode silica nanospheres with remarkable stability as ph sensors. *J. Mater. Chem.*, 21(44):17673–17679, 2011. doi:10.1039/c1jm13125g.

[424] I.L. Medintz, M.H. Stewart, S.A. Trammell, K. Susumu, J.B. Delehanty, B.C. Mei, J.S. Melinger, J.B. Blanco-Canosa, P.E. Dawson, and H. Mattoussi. Quantum-dot/dopamine bioconjugates function as redox coupled assemblies for in vitro and intracellular ph sensing. *Nat. Mater.*, 9(8):676–684, 2010. doi:10.1038/nmat2811.

[425] Y.-Q. Wang, C. Ye, Z.-H. Zhu, and Y.-Z. Hu. Cadmium telluride quantum dots as ph-sensitive probes for tiopronin determination. *Anal. Chim. Acta*, 610(1): 50–56, 2008. doi:10.1016/j.aca.2008.01.015.

[426] Y. S. Liu, Y. Sun, P.T. Vernier, C. H. Liang, S.Y.C. Chong, and M.A.

Gundersen. ph-sensitive photoluminescence of cdse/znse/zns quantum dots in human ovarian cancer cells. *J. Phys. Chem. C*, 111(7):2872–2878, 2007. doi:10.1021/jp0654718.

[427] Q. Ma, F. Yang, X. Ai, and X. Su. Dual-color quantum dot-encoded nanoprobe for dna assays and cell imaging. *Spectrosc. Lett.*, 47(4):324–332, 2014. doi:10.1080/00387010.2013.791993.

[428] W. Wu, T. Zhou, J. Shen, and S. Zhou. Optical detection of glucose by cds quantum dots immobilized in smart microgels. *Chem. Commun.*, 0(29):4390–4392, 2009. doi:10.1039/b907348e.

[429] M. Nurunnabi, K.J. Cho, J.S. Choi, K.M. Huh, and Y.K. Lee. Targeted near-ir qds-loaded micelles for cancer therapy and imaging. *Biomaterials*, 31(20):5436–5444, 2010. doi:10.1016/j.biomaterials.2010.03.057.

[430] X. Sun, X. Huang, J. Guo, W. Zhu, Y. Ding, G. Niu, A. Wang, D.O. Kiesewetter, Z.L. Wang, S. Sun, and X. Chen. Self-illuminating 64cu-doped cdse/zns nanocrystals for in vivo tumor imaging. *J. Am. Chem. Soc.*, 136(5):1706–1709, 2014. doi:10.1021/ja410438n.

[431] Q. Wu and M. Chu. Self-illuminating quantum dots for highly sensitive in vivo real-time luminescent mapping of sentinel lymph nodes. *International Journal of Nanomedicine*, 7:3433–3443, 2012. doi:10.2147/IJN.S30709.

[432] M. Kumar, D. Zhang, D. Broyles, and S.K. Deo. A rapid, sensitive, and selective bioluminescence resonance energy transfer (bret)-based nucleic acid sensing system. *Biosensors and Bioelectronics*, 30(1):133–139, 2011. doi:10.1016/j.bios.2011.08.043.

[433] R. Kojima, H. Takakura, T. Ozawa, Y. Tada, T. Nagano, and Y. Urano. Rational design and development of near-infrared-emitting firefly luciferins available

in vivo. *Angewandte Chemie - International Edition*, 52(4):1175–1179, 2013. doi:10.1002/anie.201205151.

[434] M. Hasegawa, Y. Tsukasaki, T. Ohyanagi, and T. Jin. Bioluminescence resonance energy transfer coupled near-infrared quantum dots using gst-tagged luciferase for in vivo imaging. *Chem. Commun.*, 49(3):228–230, 2013. doi:10.1039/c2cc36870f.

[435] C.-Y. Hsu, C.-W. Chen, H.-P. Yu, Y.-F. Lin, and P.-S. Lai. Bioluminescence resonance energy transfer using luciferase-immobilized quantum dots for self-illuminated photodynamic therapy. *Biomaterials*, 34(4):1204–1212, 2013. doi:10.1016/j.biomaterials.2012.08.044.

[436] N. Ma, A.F. Marshall, and J. Rao. Near-infrared light emitting luciferase via biomineralization. *J. Am. Chem. Soc.*, 132(20):6884–6885, 2010. doi:10.1021/ja101378g.

[437] Y. Xing, M.-K. So, A.L. Koh, R. Sinclair, and J. Rao. Improved qd-bret conjugates for detection and imaging. *Biochem. Biophys. Res. Commun.*, 372(3): 388–394, 2008. doi:10.1016/j.bbrc.2008.04.159.

[438] M.-K. So, C. Xu, A.M. Loening, S.S. Gambhir, and J. Rao. Self-illuminating quantum dot conjugates for in vivo imaging. *Nat. Biotechnol.*, 24(3):339–343, 2006. doi:10.1038/nbt1188.

[439] L. Treuel, S. Brandholt, P. Maffre, S. Wiegele, L. Shang, and G.U. Nienhaus. Impact of protein modification on the protein corona on nanoparticles and nanoparticle-cell interactions. *ACS Nano*, 8(1):503–513, 2014. doi:10.1021/nn405019v.

[440] C.C. Fleischer, U. Kumar, and C.K. Payne. Cellular binding of anionic nanopar-

ticles is inhibited by serum proteins independent of nanoparticle composition. *Biomaterials Science*, 1(9):975–982, 2013. doi:10.1039/c3bm60121h.

[441] C. A.J. Lin, W. K. Chuang, Z. Y. Huang, S. T. Kang, C. Y. Chang, C. T. Chen, J. L. Li, J.K. Li, H.H. Wang, F.C. Kung, J.L. Shen, W. H. Chan, C.K. Yeh, H. Yeh, W. F.T. Lai, and W.H. Chang. Rapid transformation of protein-caged nanomaterials into microbubbles as bimodal imaging agents. *ACS Nano*, 6(6): 5111–5121, 2012. doi:10.1021/nn300768d.

[442] K. Prapainop, D.P. Witter, and P. Wentworth Jr. A chemical approach for cell-specific targeting of nanomaterials: Small-molecule-initiated misfolding of nanoparticle corona proteins. *J. Am. Chem. Soc.*, 134(9):4100–4103, 2012. doi:10.1021/ja300537u.

[443] Shikha Nangia and Radhakrishna Sureshkumar. Effects of nanoparticle charge and shape anisotropy on translocation through cell membranes. *Langmuir*, 28 (51):17666–17671, 2012. doi:10.1021/la303449d.

[444] L.F. Pease, J.I. Feldblyum, S.H. Depaoli Lacaerda, Y. Liu, A.R. Hight Walker, R. Anumolu, P.B. Yim, M.L. Clarke, H.G. Kang, and J. Hwang. Structural analysis of soft multicomponent nanoparticle clusters. *ACS Nano*, 4(11):6982–6988, 2010. doi:10.1021/nn102106f.

[445] S. Anandampillai, X. Zhang, P. Sharma, Gillian C. Lynch, M.A. Franchek, and K.V. Larin. Quantum dot-dna interaction: Computational issues and pre-liminary insights on use of quantum dots as biosensors. *Computer Methods in Applied Mechanics and Engineering*, 197(41-42):3378 – 3385, 2008. ISSN 0045-7825. doi:http://dx.doi.org/10.1016/j.cma.2008.02.032.

[446] Hans Martin Senn and Walter Thiel. Qm/mm methods for biomolecular sys-

tems. *Angewandte Chemie International Edition*, 48(7):1198–1229, 2009. ISSN 1521-3773. doi:10.1002/anie.200802019.

[447] Hai Lin and DonaldG. Truhlar. Qm/mm: what have we learned, where are we, and where do we go from here? *Theor. Chem. Acc.*, 117(2):185–199, 2007. ISSN 1432-881X. doi:10.1007/s00214-006-0143-z.

[448] Hedi Mattoussi, J. Matthew Mauro, Ellen R. Goldman, George P. Anderson, Vikram C. Sundar, Frederic V. Mikulec, and Moungi G. Bawendi. Self-assembly of cdse-zns quantum dot bioconjugates using an engineered recombinant protein. *J. Am. Chem. Soc.*, 122(49):12142–12150, 2000. doi:10.1021/ja002535y.

[449] Jennifer M. Elward and Arindam Chakraborty. Effect of dot size on exciton binding energy and electron-hole recombination probability in cdse quantum dots. *J. Chem. Theory Comput.*, 9(10):4351–4359, 2013. doi:10.1021/ct400485s.

[450] Mats H. M. Olsson, Chresten R. Sondergaard, Michal Rostkowski, and Jan H. Jensen. Propka3: Consistent treatment of internal and surface residues in empirical pka predictions. *J. Chem. Theory Comput.*, 7(2):525–537, 2011. doi:10.1021/ct100578z.

[451] Robert B. Best, Xiao Zhu, Jihyun Shim, Pedro E. M. Lopes, Jeetain Mittal, Michael Feig, and Alexander D. MacKerell. Optimization of the additive charmm all-atom protein force field targeting improved sampling of the backbone ϕ, ψ and side-chain x_1 and x_2 dihedral angles. *J. Chem. Theory Comput.*, 8(9):3257–3273, 2012. doi:10.1021/ct300400x.

[452] James C. Phillips, Rosemary Braun, Wei Wang, James Gumbart, Emad Tajkhorshid, Elizabeth Villa, Christophe Chipot, Robert D. Skeel, Laxmikant KalÃľ, and Klaus Schulten. Scalable molecular dynamics with namd. *J. Comput. Chem.*, 26(16):1781–1802, 2005. ISSN 1096-987X. doi:10.1002/jcc.20289.

[453] Eudald Casals, Tobias Pfaller, Albert Duschl, Gertie Janneke Oostingh, and Victor Puntes. Time evolution of the nanoparticle protein corona. *ACS Nano*, 4(7):3623–3632, 2010. doi:10.1021/nn901372t.

[454] Eran Rabani. Structure and electrostatic properties of passivated cdse nanocrystals. *J. Chem. Phys.*, 115(3):1493–1497, 2001. doi:http://dx.doi.org/10.1063/1.1380748.

[455] E.B.a c Saff and A.B.J.b Kuijlaars. Distributing many points on a sphere. *Mathematical Intelligencer*, 19(1):5–11, 1997. doi:10.1007/BF03024331.

[456] Neil P. King, B. Bale, Jacob, William Sheffler, Dan E. McNamara, Shane Gonen, Tamir Gonen, Todd O. Yeates, and David Baker. Accurate design of co-assembling multi-component protein nanomaterials. *Nat. Mater.*, May 2014. doi:doi:10.1038/nature13404.

[457] Rongling Xiong, Zheng Li, Lan Mi, Pei-Nan Wang, Ji-Yao Chen, Lixin Wang, and Wu-Li Yang. Study on the intracellular fate of tat peptide-conjugated quantum dots by spectroscopic investigation. *Journal of Fluorescence*, 20(2): 551–556, 2010. ISSN 1053-0509. doi:10.1007/s10895-009-0579-3.

[458] Bipattaran Paramanik, Santanu Bhattacharyya, and Amitava Patra. Steady state and time resolved spectroscopic study of qd-dna interaction. *Journal of Luminescence*, 134:401–407, 2013. ISSN 0022-2313. doi:http://dx.doi.org/10.1016/j.jlumin.2012.08.013.

[459] M. Levy, N.H. March, and N.C. Handy. On the adiabatic connection method, and scaling of electron-electron interactions in the thomas-fermi limit. *J. Chem. Phys.*, 104(5):1989–1992, 1996.

[460] K. Burke, M. Ernzerhof, and J.P. Perdew. The adiabatic connection

method: A non-empirical hybrid. *Chem. Phys. Lett.*, 265(1-2):115–120, 1997. doi:10.1016/S0009-2614(96)01373-5.

[461] W. Yang. Generalized adiabatic connection in density functional theory. *J. Chem. Phys.*, 109(23):10107–10110, 1998. doi:10.1063/1.477701.

[462] M. Nekovee, W.M.C. Foulkes, A.J. Williamson, G. Rajagopal, and R.J. Needs. A quantum monte carlo approach to the adiabatic connection method. *Adv. Quantum Chem.*, 33(C):189–207, 1998. doi:10.1016/S0065-3276(08)60436-0.

[463] F. Colonna and A. Savin. Correlation energies for some two- and four-electron systems along the adiabatic connection in density functional theory. *J. Chem. Phys.*, 110(2-12):2828–2835, 1999.

[464] A. Savin, F. Colonna, and M. Allavena. Analysis of the linear response function along the adiabatic connection from the kohn-sham to the correlated system. *J. Chem. Phys.*, 115(15):6827–6833, 2001. doi:10.1063/1.1405011.

[465] M. Nekovee, W.M.C. Foulkes, and R.J. Needs. Quantum monte carlo investigations of density functional theory of the strongly inhomogeneous electron gas. *Phys. Rev. B*, 68(23):2351081–23510816, 2003.

[466] R. Pollet, F. Colonna, T. Leininger, H. Stoll, H.-J. Werner, and A. Savin. Exchange-correlation energies and correlation holes for some two- and four-electron atoms along a nonlinear adiabatic connection in density functional theory. *Int. J. Quantum Chem.*, 91(2 SPEC):84–93, 2003. doi:10.1002/qua.10395.

[467] Z.-F. Liu and K. Burke. Adiabatic connection in the low-density limit. *Physical Review A - Atomic, Molecular, and Optical Physics*, 79(6), 2009. doi:10.1103/PhysRevA.79.064503.

[468] A. Chakraborty, M.V. Pak, and S. Hammes-Schiffer. Properties of the exact universal functional in multicomponent density functional theory. *J. Chem. Phys.*, 131(12), 2009. doi:10.1063/1.3236844.

[469] A. Savin, C.J. Umrigar, and X. Gonze. Relationship of kohn-sham eigenvalues to excitation energies. *Chem. Phys. Lett.*, 288(2-4):391–395, 1998.

[470] D. Frydel, W.M. Terilla, and K. Burke. Adiabatic connection from accurate wave-function calculations. *J. Chem. Phys.*, 112(12):5292–5297, 2000.

[471] A. Savin, F. Colonna, and R. Pollet. Adiabatic connection approach to density functional theory of electronic systems. *Int. J. Quantum Chem.*, 93(3):166–190, 2003. doi:10.1002/qua.10551.

[472] F. Zhang and K. Burke. Adiabatic connection for near degenerate excited states. *Phys. Rev. A*, 69(5 A):052510–1, 2004. doi:10.1103/PhysRevA.69.052510.

[473] J. Toulouse, F. Colonna, and A. Savin. Exchange-correlation potentials and local energies per particle along nonlinear adiabatic connections. *Mol. Phys.*, 103(20):2725–2734, 2005. doi:10.1080/00268970500134615.

[474] A.M. Teale, S. Coriani, and T. Helgaker. Range-dependent adiabatic connections. *J. Chem. Phys.*, 133(16), 2010. doi:10.1063/1.3488100.

[475] M.-E. Pistol and C.-O. Almbladh. Adiabatic connections and properties of coupling-integrated exchange-correlation holes and pair densities in density functional theory. *Chem. Phys. Lett.*, 480(1-3):136–139, 2009. doi:10.1016/j.cplett.2009.08.047.

[476] S. Pittalis, C.R. Proetto, A. Floris, A. Sanna, C. Bersier, K. Burke, and E.K.U. Gross. Exact conditions in finite-temperature density-functional theory. *Phys. Rev. Lett.*, 107(16), 2011. doi:10.1103/PhysRevLett.107.163001.

[477] M. Seidl and P. Gori-Giorgi. Adiabatic connection at negative coupling strengths. *Phys. Rev. A*, 81(1), 2010. doi:10.1103/PhysRevA.81.012508.

[478] A. Sirjoosingh, M.V. Pak, and S. Hammes-Schiffer. Multicomponent density functional theory study of the interplay between electron-electron and electron-proton correlation. *J. Chem. Phys.*, 136(17), 2012. doi:10.1063/1.4709609.

[479] Y. Cornaton, O. Franck, A.M. Teale, and E. Fromager. Analysis of double-hybrid density functionals along the adiabatic connection. *Mol. Phys.*, 111 (9-11):1275–1294, 2013. doi:10.1080/00268976.2013.783640.

[480] A.M. Teale, S. Coriani, and T. Helgaker. The calculation of adiabatic-connection curves from full configuration-interaction densities: Two-electron systems. *J. Chem. Phys.*, 130(10), 2009. doi:10.1063/1.3082285.

[481] A.M. Teale, S. Coriani, and T. Helgaker. Accurate calculation and modeling of the adiabatic connection in density functional theory. *J. Chem. Phys.*, 132(16), 2010. doi:10.1063/1.3380834.

[482] A.J. Cohen, P. Mori-SÃČÂ ąnchez, and W. Yang. Assessment and formal properties of exchange-correlation functionals constructed from the adiabatic connection. *J. Chem. Phys.*, 127(3), 2007. doi:10.1063/1.2749510.

[483] A.J. Cohen, P. Mori-Sanchez, and W. Yang. Development of exchange-correlation functionals with minimal many-electron self-interaction error. *J. Chem. Phys.*, 126(19), 2007. doi:10.1063/1.2741248.

[484] M.J.G. Peach, A.M. Miller, A.M. Teale, and D.J. Tozer. Adiabatic connection forms in density functional theory: H2 and the he isoelectronic series. *J. Chem. Phys.*, 129(6), 2008. doi:10.1063/1.2965531.

[485] M.J.G. Peach, A.M. Teale, and D.J. Tozer. Modeling the adiabatic connection in h2. *J. Chem. Phys.*, 126(24), 2007. doi:10.1063/1.2747248.

[486] Leonard M. Sander, Herbert B. Shore, and L. J. Sham. Surface structure of electron-hole droplets. *Phys. Rev. Lett.*, 31:533–536, Aug 1973. doi:10.1103/PhysRevLett.31.533.

[487] T. Kreibich and E. K. U. Gross. Multicomponent density-functional theory for electrons and nuclei. *Phys. Rev. Lett.*, 86:2984–2987, Apr 2001. doi:10.1103/PhysRevLett.86.2984.

[488] Arindam Chakraborty, Michael V. Pak, and Sharon Hammes-Schiffer. Development of electron-proton density functionals for multicomponent density functional theory. *Phys. Rev. Lett.*, 101:153001, Oct 2008. doi:10.1103/PhysRevLett.101.153001.

Index

Curriculum vitae

jennifer **elward**

130 Remington Ave Apt D • Syracuse, NY • 13210

PHONE (570) 709-0089 • **E-MAIL** jmelward@syr.edu

EDUCATION

- **Doctor of Philosophy, Chemistry**   **July 2014**

  Title: "Development of Explicitly Correlated Wavefunction Based Methods for the Study of Optical Properties of Semiconductor Nanomaterials"
  Institution: Syracuse University Syracuse, NY 13244

- **Master of Philosophy, Chemistry**   **April 2011**

  Title: "Investigation of electron-hole interaction in quantum dots using explicitly correlated wavefunction based methods"
  Institution: Syracuse University Syracuse, NY 13244

- **Bachelor of Science, Chemistry**   **May 2009**

  Institution: Misericordia University Dallas, PA 18655

RESEARCH EXPERIENCE

- **Doctoral Dissertation Focus**
  - Doctoral research was based on the investigation of light with nanomaterials. Specific interest was in interaction between electron and hole particles and how the interaction is effected by different influential factors, including size, shape, material, heterojunction etc. The overall goal was to computationally explore these types of chemical systems for application in solar cells and other light harvesting materials. I have developed and maintained large scale codes to study these nanosystems.

- **Areas of Research Interest**
  - Development of multi-component methods for description of chemical systems.
  - Development of explicitly correlated wavefunction based methods for studies of nanomaterials.
  - Development of explicitly correlated adiabatic connection curve for development of electron-hole functional for density functional theory.

- **Technical Skills and Areas of Proficiency**
  - Method development and application in the following areas (hyperlinked to publication):
    - Hartree Fock
    - Explicitly Correlated Hartree-Fock
    - Perturbation Theory
    - Configuration Interaction
    - Explicitly Correlated Configuration Interaction
    - Density Functional Theory

- Quantum Monte Carlo, Variational Monte Carlo
  - Development and maintenance of large scale codes for scientific computing, languages involved include:
    - Fortran 90, Fortran 77
    - C++
    - Bash scripting
    - Python
  - Algorithm development for improving speed and sustainability of codes.
  - Proficiency in running calculations with ab initio quantum chemistry software packages.
    - Gaussian software
    - GAMESS software
  - Knowledge of multiple computing platforms including:
    - Linux OS
    - Windows OS including 8, 7, Vista, XP
    - Mac OSx
  - Experience developing, debugging and maintaining massively parallel codes for calculations on supercomputing systems
    - MPI
    - OpenMP
  - Experience running parallel calculations on supercomputer systems, including experience with:
    - XSEDE interface and allocation
    - Stampede supercomputer, Texas Advanced Computing Center
    - Brookhaven National Lab
  - Proficiency in document preparation with TeX/LaTeX
    - Preparing articles for journal submission
    - Designing templates and formatting for document preparation
  - Preparation of documents for journal submission for: ACS, APS, AIP, Arxiv
  - Knowledge of Microsoft Office suite of software

PUBLICATIONS

1. **Jennifer M. Elward** and Arindam Chakraborty, Effect of Heterojunction on exciton binding energy and electron-hole recombination probability in CdSe/ZnS quantum dots, *submitted* (2014).
2. **Jennifer M. Elward**, Flavyian J. Irudayanathan, Shikha Nangia and Arindam Chakraborty, Optical signature of protein corona in the firefly Luciferase-CdSe quantum dot complex, *submitted* (2014).
3. **Jennifer M. Elward** and Arindam Chakraborty, Investigation of CdSe quantum dots using explicitly correlated pseudopotential method, *to be submitted* (2014).
4. **Jennifer M. Elward**, Benjamin S. Kaplan, Jeremy A. Scher and Arindam Chakraborty, Construction of adiabatic connection curve for electron-hole system using multicomponent Levy-Lieb Lagrangian, *to be submitted,* (2014).
5. Jeremy A. Scher, **Jennifer M. Elward** and Arindam Chakraborty, Shape Matters: Isovolumetric Transformations of CdSe Nanocrystals, *to be submitted,* (2014).
6. **Jennifer M. Elward** and Arindam Chakraborty, Effect of Dot Size on Exciton Binding Energy and Electron–Hole Recombination Probability in CdSe Quantum Dots**,** *Journal of Chemical Theory and Computation* 9 (10), 4351–4359 (2013). **DOI:** 10.1021/ct400485s
7. **Jennifer M. Elward**, Johannes Hoja, and Arindam Chakraborty, Variational solution of the congruently transformed Hamiltonian for many-electron systems using a full-configuration-interaction calculation, *Physical Review A*, 86, 062504 (2012). **DOI:** 10.1103/PhysRevA.86.062504

8. **Jennifer M. Elward**, Jacob Hoffman, Arindam Chakraborty, Investigation of electron–hole correlation using explicitly correlated configuration interaction method, *Chemical Physics Letters*, 535, 182-186 (2012). **DOI:** 10.1016/j.cplett.2012.03.050
9. **Jennifer M. Elward**, Barbara Thallinger, and Arindam Chakraborty, Calculation of electron-hole recombination probability using explicitly correlated Hartree-Fock method *Journal of Chemical Physics* 136, 124105 (2012). **DOI:** 10.1063/1.3693765

PRESENTATIONS

1. **Jennifer M. Elward** and Arindam Chakraborty, Investigating the Effect of Volume versus Effect of Heterojunction on CdSe/ZnS Quantum Dots, Session Q27, Electron-Hole Interaction in Nanoparticles, American Physical Society March Meeting, March 2014, Denver, CO.
2. **Jennifer M. Elward** and Arindam Chakraborty, Investigation of the effect of core/shell interface on exciton binding energy and electron-hole recombination probability in CdSe/ZnS quantum dots, Session R25: Focus Session: Computational Studies of Heterostructures, American Physical Society March Meeting, March 2013, Baltimore, MD.
3. **Jennifer M. Elward,** Benjamin Kaplan and Arindam Chakraborty, Construction of adiabatic connection curve for electron-hole system using multicomponent Levy-Lieb Lagrangian**.** American Physical Society March Meeting, March 2013, Baltimore, MD.
4. Abhinanden Sambasivam, **Jennifer M. Elward** and Arindam Chakraborty**,** Multi-determinant electron-nuclear quantum Monte Carlo method for ground state solution of molecular Hamiltonian. Session J25: Focus Session: Explicitly correlated Methods and Quantum Few-Body Systems, American Physical Society March Meeting, March 2013, Baltimore, MD.
5. **Jennifer M. Elward** and Arindam Chakraborty, Investigation of Electron-Hole Correlation in CdSe Quantum Dots using Explicitly Correlated Wavefunction Based Methods, Buffalo Graduate Student Symposium, University of Buffalo, Spring 2012, Buffalo, NY.

AWARDS & RECOGNITION

- **Graduate Assistance in Areas of National Need Fellowship** (GAANN) P200A090277 sponsored by the United States Department of Education

---

MENTORING EXPERIENCE

- **Mentored summer research experience undergraduates (REU) (*2010-2012*).**
- **Mentored Syracuse University undergraduate students for research experience (*2010-2013*).**
- **Mentored local high school student (*2013-2014*).**

PROFESSIONAL EXPERIENCE

- **Research assistantship**   **Fall 2010**
- **Research assistantship**   **Fall 2013-Present**

TEACHING EXPERIENCE

- **CHE 106 –** General Chemistry Recitation   **Fall 2009**
- **CHE 346 –** Physical Chemistry Recitation   **Fall 2010-Spring 2011**
- **CHE 347 –** Physical-Analytical Chemistry Lab   **Fall 2010-Spring 2011**

REFERENCES

- Available on request.